Understanding of chemical reactions involved in pigment discoloration, in particular in mercury sulfide (HgS) blackening

Marie Radepont

Universiteit Antwerpen
City Campus
Prinsstraat 13
2000 Antwerpen
BELGIUM

LAMS – UMR 8220 CNRS
UPMC – Site « Le Raphaël »
3 rue Galilée
94200 Ivry-sur-Seine
FRANCE

Université Pierre et Marie Curie
4 place Jussieu
75005 Paris Cedex 05
FRANCE

Understanding of chemical reactions involved in pigment discoloration, in particular in mercury sulfide (HgS) blackening

PhD defended by

Marie RADEPONT

Antwerp, 2013

To obtain the degree of:
Doctor in de wetenschappen: chemie (Universiteit Antwerpen)
Docteur de l'Université Pierre et Marie Curie (Ecole doctorale ED397 – Physique et chimie des matériaux)

Promoters :

Prof. Koen JANSSENS

Professor of Analytical Chemistry
University of Antwerp, Belgium

Dr. Marine COTTE

Beamline scientist
ESRF, Grenoble, France
CNRS Researcher
LAMS UMR8220, Ivry-sur-Seine, France

Composition of the jury :

Dr. Pauline MARTINETTO, *Maître de Conférence, Institut Néel*	Reporter
Dr. Jana SANYOVA, *Conservation scientist, IRPA*	Reporter
Prof. Koen JANSSENS, *Professor, University of Antwerp*	Examiner
Dr. Marine COTTE, *Chargée de Recherche, LAMS CNRS* *Beamline scientist, ESRF*	Examiner
Prof. Vera MEYNEN, *Professor, University of Antwerp*	Examiner
Dr. Philippe WALTER, *Directeur de Recherche, LAMS CNRS*	Examiner
Dr. Yvan COQUINOT, *Ingénieur de Recherche, C2RMF*	Examiner

“It is not the mountain we conquer but ourselves”

Edmond Percival Hillary (1919-2008)

Acknowledgements

These years of research to obtain the grade of Doctor formed a rewarding and pleasant experience for me. I would like to thank here all the persons that trusted me and followed me during this period.

First of all, I would like to express my deep gratitude to my promoters and advisors Prof. Koen Janssens, Dr. Marine Cotte and Dr. Yvan Coquinot. They shared with me the quality of their reflections, their scientific rigor and skills. It was a great honor for me to work with them. I would like to thank them for trusting me all these years. I hope that my future career will allow me to cross their roads again…

Thanks to all the eminent scientists who accepted to read this manuscript and be part of my jury.

I would like to thank Philippe Walter for letting me be a part of the LAMS family. This young and already strong laboratory is composed of multiple skilled persons who played a role at different moment of my master and PhD and were of great support, especially during the last months: Marie Albéric, Rémi Brageu, Jacques Castaing, Fabienne Decuq, Laurence De Viguerie, Agnès Genevey, Thiéry Guillou, Muriel Labonnelie, Catherine Lavier, Katharina Muller, Ina Reiche, Hélène Rousselière, Elsa Van Elslande.

The first years of the present study took place at the C2RMF, and I am thankful for all the moments I spent there, the persons I met who gave to these years a particular colorful meaning. I cannot cite here all of them but I would like to express a particular gratitude to the ones that provided a technical and efficient support for the different experiments I performed (Michel Dubus, Eric Laval, Brice Moignard, Laurent Pichon), the ones who provided me with all the advices, knowledge and listening I needed (Yves Adda, Dominique Bagaud, Gilles Bastian, Michel Dubus, Jean-Jacques Ezrati, Roland Février, Maria Guerra, Juliette Langlois, François Mirambet, Abdelkader Ouahrani, Elisabeth Ravaud, and especially Myriam Eveno who accepted to read part of this manuscript and allowed me to see what was going on behind the scenes in the restoration of painting world), and the ones who welcomed me every morning with a smile and a kind word (Marie Alexandrine, Marcelle

Buatois, Eric Drouin, René Duverger, Nathalie Grambin, Rachel Sammarcelli, Richard Simb, Carounindirane Vauban). I would like to end this paragraph with a special thought to Claire Pacheco, who is behind the best memories I have with all the members of the theater group who will recognize themselves.

The present study shows many experiments and I would like to thank the persons from other laboratories and institutes, for providing me original and precious samples, state-of-the-art analytical instruments and valuable advices: the first word goes to the ID21 team at the ESRF, Hiram Castillo-Michel, Barbara Fayard, Murielle Salome, Giulia Veronesi, and especially Emeline Pouyet who made long overnight synchrotron measurements unforgettable; Ludovic Bellot-Gurlet and Céline Paris at the LADIR who trusted us enough to let the Raman HR spectrometer in our hands for multiple experiments; and all the others, Francesca Alberghina, Lucile Beck, Fabiana Da Pieve, Jean-Michel Le Cléac'h, Maite Maguregui, Christophe Methivier, Sakura Pascarelli, Jana Sanyova.

During these years, I was surrounded by colleagues who became even more over time: Marie Albéric, Matthias Alfeld, Willemien Anaf, Esther Avril, Simone Cagno, Céline Chadefaux, Wout De Nolf, Laurence De Viguerie, Chloé Duhamel, Nathalie Gandolfo, Agnès Genevey, Anita Guez-Hayem, Julien Labaune, Sophia Lahlil, Matthieu Lebon, Gaia Ligovich, Letizia Monico, Gert Nuyts, Ruven Pillay, Solène Pistre, Emeline Pouyet, Johanna Salvant, Carlotta Santoro, Geert Van Der Snickt, Frederik Vanmeert. Among these important names, two persons were the sunshine of these years and I would like to express here my kind gratitude to them, thank you Aurélia Azéma and Sophie Cersoy.

My family was, as always in my life, my support, my ears, my fresh air, and I would like to thank them, especially my parents and my brother, for being there whatever the personal and professional choices I made.

Finally, I would like to end this long list by telling to the one thanks to whom I was able to conquer this mountain and some others, David, that I am very grateful for the love and comfort he gave me.

Abstracts

Pigments form a family of compounds of which the visual stability represents the most important characteristic. Their color can sometimes evolve, unexpectedly, from the painter's or curator's point of view. This evolution is an important part of investigations in the cultural heritage field and the state-of-the-art analytical techniques are used to help preserving artworks for next generations.

Red mercury sulfide is a mineral compound that has frequently been used since Antiquity for its vivid color in different parts of the world such as South-America, China, Greece or Roman Empire. The ore, extracted with other minerals from mercury deposits, called cinnabar, was used for its aesthetic qualities, during burial ceremonies, or even as a medicine despite its toxicity. For some civilizations, this rare and expensive natural pigment was used to demonstrate social success. As examples, the use by rich Pompeian villa owners of cinnabar in the frescoes to ornate their houses can be mentioned. In the 8^{th} century, a synthetic process was developed to produce artificial α-HgS, called vermilion; this process was improved from the 17^{th} century onwards. In addition to its powerful color, this pigment is also well known for its instability.

For a long time, the complex alteration of red mercury sulfide was studied. Indeed, this compound was known to suffer from degradation under the influence of sunlight and humidity. Nonetheless, this phenomenon is rather capricious and does not take place systematically. Up to recently, the most advanced hypothesis to explain the discoloration was the phase transformation of red hexagonal cinnabar into black cubic metacinnabar by action of light. Yet, chlorine was shown to be possibly involved in the darkening of natural cinnabar and in the formation of superficial white and gray crusts. However, previous studies showed that the degradation process was far from being completely understood.

During this study, analyses performed on original artworks (six panels and two wall paintings from French and Belgium collections mainly) helped identifying degradation compounds formed at the surface of red mercury sulfide layers: calomel (Hg_2Cl_2), corderoite (α-$Hg_3S_2Cl_2$) and for the first time on patrimonial objects, β-$Hg_3S_2Cl_2$ and kenhsuite (γ-$Hg_3S_2Cl_2$). Thanks to cross-sections prepared from micro-sized fragments taken to these artworks, it was observed that these compounds were localized on top of pictorial layer according to a multi-layered structure similar for all samples. Sulfates (such as gypsum $CaSO_4.2H_2O$) were also identified at the surfaces of some altered samples. The chemical characterization of these alteration products was rather challenging mainly because of the micrometric size of the alteration (multi-)layers. Beyond the different analytical techniques available, synchrotron-based micro X-ray diffraction, micro- X-ray fluorescence and micro- X-ray absorption spectroscopy proved to be very helpful for the identification and localization of both original and altered compounds.

Assessing the effects of several environmental parameters (light, humidity, exogenous chemicals such as chlorine…) was an important aim of this study in order to identify factors influencing the degradation and to propose better conservation methods for artworks. Artificial ageing experiments were performed on red mercury sulfide (cinnabar and vermilion) in order to reproduce its degradation. The pigment was used in pure form or mixed with a binder or another pigment and was put into contact with different chemical solutions while exposed to light or in darkness. These experiments confirmed light as being a necessary parameter to obtain any color change and showed that the presence of chlorine also induced visual evolutions on model samples. When samples were in contact with a very active chlorine containing solution (sodium hypochlorite), calomel (Hg_2Cl_2) and corderoite (α-$Hg_3S_2Cl_2$) were identified on their surface. These two compounds always seemed to appear simultaneously and it was not possible to distinguish them despite the different visual aspects of the samples. Indeed, this specific degradation process showed an evolution from the formation of crystals (different from samples, small or large, white or translucent, homogeneously scattered or not) which give to the sample a purple color, to the formation of a thick and homogeneous white-grey layer. Sulfates were also identified on degraded model samples, and for some cases sulfur seemed to originate from mercury sulfide.

Results obtained with all these experiments on original artworks and model samples allowed a reflection on the factors influencing the formation of different phases during the degradation of red mercury sulfide. The origin of chlorine, which seems to play an important role in this degradation, was discussed, and next to environment (sea salts, pollution), products used during restoration processes were also part of our concern. Thanks to a simulation software, the α-HgS degradation by a NaOCl solution have been modeled and Pourbaix diagrams of different systems were drawn up. These figures helped us discuss the conditions of formation and the stability of degradation products. Different chemical reactions were proposed to understand the transformation of mercury sulfide into mercury chloride compounds as well as formation of sulfates. The contribution of degradation products to visual changes was also discussed even if the natural color of each of them could not explain, the black areas seen on some altered artworks. Different hypotheses were proposed and a special interest to the possible production of metallic mercury during the degradation process was detailed. Nevertheless this element had not been identified on darkened fragments.

These investigations confirmed preliminary hypothesis on the factors influencing the alteration of mercury sulfide and explained the conditions in which these degradations occur. The results allowed establishing an analytical protocol which could be implemented when artworks containing degraded mercury sulfide are subject to study or restoration. Moreover, help could be proposed to restorers to better identify the degradation from the original layers and to avoid the use of products dangerous for this pigment during restoration.

Résumé

Les pigments forment une famille de composés dont la stabilité visuelle représente la caractéristique la plus importante. Leur couleur peut parfois évoluer, de façon imprévisible, du point de vue du peintre ou du conservateur. Cette évolution est une part importante des recherches dans le domaine du patrimoine et les meilleures avancées techniques sont utilisées afin de pouvoir préserver les œuvres d'art pour les prochaines générations.

Le sulfure de mercure rouge est un composé minéral fréquemment utilisé depuis l'Antiquité pour sa couleur vive dans différentes parties du monde telles que l'Amérique du Sud, la Chine, la Grèce ou l'Empire Romain. Le minerai, extrait avec d'autres composés des mines de mercure et appelé cinabre, était utilisé pour ses qualités esthétiques, lors de cérémonies funéraires, ou bien encore comme médicament malgré sa toxicité. Pour certaines civilisations, la rareté et le coût élevé de ce pigment naturel en firent un marqueur social. Parmi les exemples classiques, certains riches propriétaires de Pompéi ont utilisé du cinabre pour les fresques ornant leur villa. Au cours du 8^{ième} siècle, un procédé de synthèse du α-HgS artificiel, appelé vermillon, a été découvert puis amélioré à partir du 17^{ième} siècle. En plus de sa couleur vive, ce pigment est également connu pour son instabilité.

L'altération complexe du sulfure de mercure rouge a été étudiée depuis de nombreuses années. En effet, ce composé est connu pour sa sensibilité à l'irradiation solaire et à l'humidité. Néanmoins ce phénomène est assez capricieux et n'apparait pas systématiquement. Jusqu'à récemment, l'hypothèse la plus utilisée pour expliquer la décoloration était la transformation de phase du cinabre hexagonal rouge en métacinabre cubique noir par l'action de la lumière. Il a déjà été montré que le chlore pouvait être impliqué dans le noircissement du cinabre naturel et la formation de cristaux superficiels blancs et gris. Cependant, les études précédentes ont montré que le processus de dégradation n'est pas encore complètement compris.

Pendant cette étude, les analyses réalisées sur des œuvres originales (six tableaux et deux peintures murales provenant principalement de collections françaises et belges) ont permis l'identification de composés de dégradation formés à la surface du sulfure de mercure rouge : le calomel (Hg_2Cl_2), la corderoite (α-$Hg_3S_2Cl_2$), et pour la première fois sur des objets patrimoniaux, du β-$Hg_3S_2Cl_2$ et de la kenhsuite (γ-$Hg_3S_2Cl_2$). Lorsque des coupes polies furent réalisées à partir de micro-fragments prélevés sur les œuvres, il a été possible d'observer que ces composés étaient localisés au-dessus de la couche picturale selon une stratigraphie similaire pour tous les échantillons. Des sulfates (tels que le gypse $CaSO_4.2H_2O$) ont été également identifiés à la surface de certains échantillons altérés. La caractérisation chimique de ces produits d'altération est assez délicate étant donné la taille micrométrique des (multi-)couches d'altération. Au-delà des différentes techniques analytiques disponibles, la micro-diffraction X, la micro-fluorescence X et la micro-spectroscopie d'absorption X avec source synchrotron ont récemment prouvé leur intérêt dans l'identification et la localisation des composants à la fois originaux et altérés.

Estimer les effets de plusieurs paramètres environnementaux (lumière, humidité, produits chimiques exogènes tels que le chlore…) fut un important objectif de cette étude afin d'identifier les facteurs influençant la dégradation et de proposer de meilleures méthodes de conservation des œuvres. Des expériences de vieillissements artificiels ont été réalisées à partir de sulfure de mercure rouge (cinabre et vermillon) dans le but de reproduire sa dégradation. Le pigment a été utilisé pur ou avec un liant ou encore un autre pigment et a été mis en contact avec différentes solutions chimiques et exposé à la lumière ou gardé dans l'obscurité. Ces expériences ont confirmé que la lumière est un paramètre nécessaire pour obtenir un changement de couleur et ont montré que la présence de chlore provoquait certaines évolutions visuelles sur les échantillons modèles. Lorsque les échantillons furent au contact d'une solution contenant du chlore très actif (hypochlorure de sodium), du calomel (Hg_2Cl_2) et de la corderoite (α-$Hg_3S_2Cl_2$) ont été identifiés à leur surface. Ces deux composés ont toujours semblé apparaitre de façon simultanée et il ne fut pas possible de les distinguer l'un de l'autre malgré les différents aspects visuels pris par les échantillons. En effet, ce processus de dégradation a montré une évolution partant de la formation de cristaux (différents selon les échantillons, petits ou grands, blancs ou

transparents, dispersés de façon homogène ou non) qui donnait à l'échantillon une couleur violette, jusqu'à la formation d'une couche épaisse, homogène et blanche-grise à la surface. Des sulfates ont également été identifiés sur des échantillons modèles dégradés, dont le soufre semble parfois provenir du sulfure de mercure.

Les résultats obtenus lors de ces expériences sur œuvres originales et échantillons modèles permirent une réflexion sur les facteurs influençant la formation de différentes phases lors de la dégradation du sulfure de mercure rouge. L'origine du chlore, qui semble jouer un rôle primordiale dans cette dégradation, a été discutée, et en plus de l'environnement (sels marins, pollution), certains produits utilisés lors de restaurations ont suscité notre intérêt. Par l'utilisation d'un logiciel de simulation, la dégradation de α-HgS par une solution de NaOCl a été modélisée et des diagrammes de Pourbaix de différents systèmes ont été dessinés. Ces graphiques ont servi de support à une discussion autour des conditions de formation et de la stabilité des produits de dégradation. Différentes réactions chimiques ont été proposées afin de comprendre la transformation du sulfure de mercure en chlorure de mercure ainsi que la formation de sulfates. La contribution des produits de dégradation aux changements visuels observés a également été discutée bien que la couleur naturelle de chacun d'entre eux ne permette pas d'expliquer le noircissement vu sur certaines œuvres altérées. Différentes hypothèses ont été proposées et un intérêt particulier a été apporté à la possible production de mercure métallique pendant le processus de dégradation. Néanmoins cet élément n'a pas été identifié sur les échantillons noircis.

Ces recherches ont confirmé les hypothèses préliminaires sur les facteurs influençant l'altération du sulfure de mercure et ont indiqué les conditions dans lesquelles ces dégradations se réalisent. Ces résultats ont permis l'élaboration d'un protocole analytique pouvant être mis en place lorsqu'une œuvre contenant du sulfure de mercure dégradé est soumise à étude ou restauration. De plus, une aide peut être proposée aux restaurateurs afin de mieux identifier la dégradation de la couche picturale originelle et éviter l'utilisation de produits dangereux pour ce pigment lors de restaurations.

Overzicht

Pigmenten vormen een familie van verbindingen waarvoor visuele stabiliteit een belangrijke eigenschap is. Pigmenten kunnen soms onverwacht verkleuren, zeker voor het oog van de schilder of curator die de schildering vaak door en door kennen. Deze kleurveranderingen zijn een belangrijk studiedomein binnen het erfgoedonderzoek. De best ontwikkelde analytische technieken worden aangewend om kunstwerken voor de volgende generaties te bewaren.

Sinds de oudheid werd het rode mineraal 'kwiksulfide' in verschillende delen van de wereld, zoals Zuid-Amerika, China, Griekenland en het Romeinse Rijk gebruikt voor zijn levendige kleur. De erts, samen met andere (kwik)mineralen ontgonnen, wordt 'cinnaber' genoemd. Dit mineraal werd gebruikt voor zijn esthetische kwaliteiten, tijdens uitvaartceremonies, of zelfs –ondanks de toxiciteit- als geneesmiddel. In sommige beschavingen was dit zeldzame en dure natuurlijke pigment zelfs een statussymbool. Een mooi voorbeeld hiervan is het gebruik van cinnaber in fresco's in enkele luxueuze villa's te Pompeji. In de 8ste eeuw werd een synthetisch proces ontwikkeld om α-HgS te produceren. Dit synthetische pigment wordt vermiljoen genoemd. Het productieproces werd verder geoptimaliseerd vanaf de 17de eeuw. Naast zijn krachtige kleur staat het kwiksulfidepigment ook gekend om zijn instabiliteit.

De complexe veroudering van kwiksulfide, gekarakteriseerd door een kleurverandering van rood naar zwart, wordt al verschillende jaren bestudeerd. Het pigment staat gekend om zijn gevoeligheid voor zonlicht en vocht. Toch is de degradatie onvoorspelbaar en gebeurt deze niet systematisch. Tot voor kort werd de kleurverandering meestal toegeschreven aan de faseverandering van rood zeshoekige cinnaber in zwart kubisch metacinnaber onder invloed van licht. Bovendien werd aangetoond dat chloor mogelijk betrokken is bij de verdonkering van natuurlijk cinnaber en bij de vorming van oppervlakkige witte en grijze korsten. Uit eerdere studies is echter gebleken dat het degradatieproces nog niet volledig begrepen is.

Tijdens deze studie zijn analyses uitgevoerd op originele kunstwerken (zes panelen en twee muurschilderingen, voornamelijk uit Franse en Belgische collecties). Vanuit deze analyses zijn de degradatieproducten geïdentificeerd die gevormd worden aan het oppervlak van de rode kwiksulfidelagen: kalomel (Hg_2Cl_2), corderoite (α-$Hg_3S_2Cl_2$) en voor de eerste keer op erfgoedobjecten, β-$Hg_3S_2Cl_2$ en kenhsuite (γ-$Hg_3S_2Cl_2$). Van enkele microfragmenten van deze kunstwerken is een dwarsdoorsnede gemaakt. Aan de hand hiervan is vastgesteld dat de degradatieproducten bovenop de verflaag gelokaliseerd zijn volgens een gelaagde structuur die voor alle monsters sterk gelijkend is. Buiten bovenvermelde producten zijn ook sulfaten (zoals gips $CaSO_4.2H_2O$) geïdentificeerd aan het oppervlak van sommige gedegradeerde monsters. De chemische karakterisering van de degradatieproducten is uitdagend, vooral door de micrometrische omvang van de verschillende degradatielagen. Naast de verschillende analytische technieken beschikbaar, bleken synchrotron-gebaseerde technieken zoals micro X-stralen diffractie, micro-X-stralen fluorescentie en micro-röntgen absorptie spectroscopie zeer nuttig voor de identificatie en lokalisatie van zowel originele als verouderde componenten.

Het beoordelen van de invloed van verschillende omgevingsparameters (licht, vocht, exogene chemicaliën zoals chloor...) was een belangrijk doel van deze studie om de factoren die de degradatie in de hand werken te identificeren en om geschikte conservatiemethoden voor te stellen. Om de degradatie te reproduceren zijn versnelde verouderingstesten uitgevoerd op rood kwiksulfide (cinnaber en vermiljoen). Het pigment werd zuiver of gemengd met een bindmiddel of een ander pigment in contact gebracht met verschillende chemische oplossingen, zowel in het donker als blootgesteld aan licht. Deze experimenten bevestigen dat licht een noodzakelijke parameter is om een kleurverandering te veroorzaken en tonen aan dat de aanwezigheid van chloor ook visuele veranderingen induceert in de modelmonsters. Wanneer de monsters in contact gebracht werden met een actieve chloorhoudende oplossing (natriumhypochloriet), werden zowel kalomel (Hg_2Cl_2) als corderoite (α-$Hg_3S_2Cl_2$) geïdentificeerd aan het oppervlak. Deze verbindingen leken steeds gelijktijdig te verschijnen en het was niet mogelijk beide producten van elkaar te onderscheiden ondanks de visuele verschillen tussen monsters. De degradatie vertoont inderdaad een verandering vertrekkende van de vorming van kristallen (verschillend

naargelang de monsters, klein of groot, wit of doorschijnend, homogeen verspreid of niet) die aan het monster een paarse kleur geven, tot de vorming van een dikke en homogen witte -grijze laag. Op de verouderde modelmonsters zijn ook sulfaten geïdentificeerd, waarvan het zwavel in sommige gevallen afkomstig leek van kwiksulfide.

De resultaten verkregen met de analyse van originele kunstwerken en de experimenten met modelmonsters geven een beter inzicht in de factoren die de vorming van de verschillende fasen beïnvloeden tijdens de degradatie van rood kwiksulfide. De oorsprong van het chloor, dat een belangrijke rol lijkt te spelen in de degradatie, wordt besproken. Naast chloor uit de omgeving (zeezouten, vervuiling), is chloor gebruikt tijdens de restauratiebehandelingen ook een deel van onze zorg. Dankzij een simulatiesoftware is de degradatie van α-HgS door NaOCl-oplossing gemodelleerd en zijn Pourbaix-diagrammen van de verschillende systemen opgesteld. De verkregen grafieken en diagrammen ondersteunen de discussie rond de vormingscondities en stabiliteit van de degradatieproducten. Verschillende chemische reacties worden voorgesteld om de omzetting van kwiksulfide in kwik-chloorverbindingen en de vorming van sulfaten te begrijpen. Ook de bijdrage van de degradatieproducten in de visuele verandering wordt besproken. Desondanks kon de natuurlijke kleur van elk van deze degradatieproducten de zwarte gebieden in de verouderde kunstwerken niet verklaren. Verschillende hypothesen worden voorgesteld waarbij bijzonder belang wordt gehecht aan de mogelijke vorming van metallisch kwik tijdens de degradatie. Toch is deze component nog niet vastgesteld in de donkere fragmenten.

Dit onderzoek bevestigt de voorlopige hypothese over de invloedfactoren in de degradatie van kwiksulfide en verklaart de omstandigheden waarin deze degradaties ontstaan. De resultaten hebben geleid tot de ontwikkeling van een analytisch protocol dat kan worden toegepast wanneer kunstwerken met gedegradeerd kwiksulfide worden onderworpen aan onderzoek of restauratie. Bovendien kan het restauratoren helpen om degradatie beter te onderscheiden van originele verflagen en het gebruik van ongeschikte producten tijdens restauratie te voorkomen.

SUMMARY

Introduction

The word “pigment” corresponds to an extensive family of compounds, from natural or artificial origin, that were or are still used to color different materials. Pigments are usually powders, ground to obtain a specific grain size; these are mixed with binders to allow an easier application on supports. The visual aspects and chemical stability are important properties for pigments. Pigments discoloration is a topic that raises a lot of interest in the world of conservators, curators, and also scientists. Scientific advances such as the improvement in analytical technologies are currently exploited to allow us to transmit cultural heritage artifacts to the following generations in the best possible conditions and to ensure the preservation of artworks and archaeological objets.

Cinnabar, the natural form of red mercury sulfide, is a vivid compound known since Neolithic times that has mainly been used since Antiquity in Europe, China or South-America. From the 17th century, a chemical process to synthesize red mercury sulfide, then called vermilion, has frequently been employed to obtain this sought-after red color. It has been used to paint walls, statues, panels and other artifacts; famous examples of the use of this pigment can be found on Pompeian wall paintings, in paintings from Brueghel, Rubens, or Van Gogh. Red mercury sulfide also was used for ceremonial or medicinal purposes. Since the 20th century, its use has strongly declined due to its toxicity.

However, red mercury sulfide is also well known for centuries for its complex alteration characteristics. Indeed, since Antiquity, dark areas were observed on works of art that comprise this pigment that appears to have formed under the influence of sunlight and humidity. Usually, white and gray crusts are formed in these areas, but their presence is not systematic. The phase transformation of red hexagonal cinnabar into black cubic metacinnabar has been long the most accepted hypothesis for the blackening of the mercury sulfide pigment. Recently, studies suggested that chlorine could play a role in this alteration and that mercury chlorine compounds seemed to be formed at the surface of works of art. Previous investigations demonstrated that the degradation process of red mercury sulfide is far from being completely understood. Therefore, the use of more powerful analytical techniques would help to identify these degradation compounds of HgS and assess the

conditions in which artworks containing cinnabar/vermilion could be altered. The present study was undertaken in order to achieve these aims.

Next to general information concerning the ways of production and the uses of this pigment, **Chapter 1** describes the properties of the compounds and phases associated with its formation or degradation. Assets and drawbacks of different analytical techniques in this context are also discussed, based on reference analyses and previous studies.

The first step of the present study, described in **Chapter 2**, was to analyze original works of art containing red mercury sulfide, in unaltered or in degraded form, where this material was naturally aged under atmospheric conditions outside or in museums. Some of these analyses were performed directly on the works of art, leaving the latter untouched. In other cases presented in this chapter, small fragments of paint were taken in order to perform analyses at laboratories or synchrotron facilities. The five main cases analyzed during this study were oil paintings from Rubens, Brueghel, Giotto, and two wall paintings from Pedralbes (Spain) and Torre del Greco, near Pompeii (Italy).

Following the identification of specific degradation compounds, our interest became focused on the possible factors influencing the degradation. Model samples were prepared, using vermilion powder, pure or mixed with a binder or another pigment. These samples were artificially aged in different conditions to investigate which ones provoke the color alteration. As predicted from previous studies, the most interesting environment turned out to be the one containing chlorine solutions or compounds (**Chapter 3**).

Combining the results obtained within all experiments allowed a reflection on the conditions inducing the formation of different phases during the degradation of red mercury sulfide. Some hypotheses to explain the black color of the altered surface of works of art were also examined and discussed. The stability of these compounds was investigated by means of thermochemical calculations; these yielded diagrams and simulations that help to understand the presence of particular secondary phases in certain conditions and the evolution of the system during ageing (**Chapter 4**).

The aim of this research was to confirm a number of hypotheses regarding the factors influencing the alteration and to gain a better insight into the conditions in which these degradations occur. This information will be useful to avoid such degradation in the future.

Chapter 1: Context

Content

Abstract

Red mercury sulfide is a mineral compound of which the vivid color made it one of the most used pigments since Antiquity. Cinnabar, the ore that is found with other minerals in different deposits in the world, and vermilion, the synthetic form, were also used in contexts different from the Arts, for example for medicine purposes or funeral practices. Its color instability has already been studied for years with different techniques. After the formation and use of red mercury sulfide, assets and drawbacks of different methods will be discussed in this Chapter to identify and study this compound and the associated phases.

1.1. An appreciated ore called cinnabar

Red mercury sulfide, called cinnabar in its natural form, is extracted from deposits present in different parts of the world. The most favourable conditions for the formation of α-HgS are the following: an anaerobic environment, pH between 7.5 and 10.5, and S(0) as a sulfur source *[M. Svensson, 2006]*. In many deposits, cinnabar occurs in veins and impregnation near recent volcanic rocks and hotspring deposits. Ores extracted are crushed in an iron mortar, heated and washed until impurities are gone. This process gives to the powder a powerful vivid red color (see Section 1.3) *[R.J. Gettens, 1972].*

When found in deposits, cinnabar is associated with different phases such as metacinnabar, native mercury or mercury chlorine compounds, and the gangue of this mineral also shows different compositions (see phases given by literature in Table 1.1., sorted by the localization of the deposits studied).

Table 1.1.: *Summary of previous studies performed on cinnabar ores giving the gangue and phases associated according to the localization of the deposit.* ***(+)*** *indicate high frequency and* ***(-)*** *low frequency.*

Area	Deposit	Gangue	Phases associated	Reference
USA,California	New Idria	**(+)** Quartz,dolomite **(-)** Marcasite, pyrite, stibnite	β-HgS	*N.Z. Boctor, 1987*
	Turkey Run	Quartz	β-HgS	*C.S. Kim, 2000*
	Oat Hill	Quartz, kaolinite, muscovite	$HgCl_2$, $Hg_3S_2Cl_2$, Hg_2OCl	
	Corona	Quartz, hematite	β-HgS, $HgSO_4$	
	Sulfur Bank	Quartz	β-HgS, $Hg_3S_2Cl_2$	
	Gambonini	Quartz, montmorillonite	β-HgS	
	Not known	Quartz, SiO_2, deweylite	β-HgS	*C.S. Kim, 2003*
	Not known	Quartz, SiO_2, deweylite, clinochrysotile	β-HgS, $Hg_3O_2SO_4$	
USA,Texas	El Paso	Anglesite	β-HgS, HgSe	
Slovenia	Bay of Trieste	Calcite	β-HgS	
	Idria	Pyrite, marcasite, dolomite, calcite, kaolinite, epsomite, melanterite	**(+)** $HgSO_4$ **(-)** β-HgS, $Hg_3O_2SO_4$, HgO	*J.M. Esbri, 2010*
Spain	Almadén	Quartz, chlorite, illite, kaolinite, pyrophillite	**(+)** β-HgS, $Hg_3O_2SO_4$, Hg_2Cl_2, **(-)** $HgCl_2$	
	Asturias	Orpiment, réalgar, melnikovite, chalcopyrite, arsenopyrite, stibnite, galena	**(+)** β-HgS, $HgCl_2$ **(-)** α-$Hg_3S_2Cl_2$, HgO, $HgSO_4$	

The gangues identified in all deposits from California (USA) and from Almadén (Spain) contained quartz whereas the others (from Texas-USA, Slovenia and Asturias-Spain) did not. Almost all samples analyzed contained metacinnabar (β-HgS) associated to cinnabar. Other phases were also identified, however this information does not seem to be sufficient to establish the origin of the ore studied. Next to mineral phases associated with mercury compounds, host rocks are indicating the context of formation of ores. Cinnabar ores coming from California deposits (Coast Range), Slovenia (Idria) and Spain (Almadén) seem to be all hosted in carbonate host rocks, whereas ores from Nevada (Humboldt County, Esmeralda County, Goldbanks deposit, Steamboat Springs) and Oregon (Opalite mine) are disseminated through hydrothermal silica *[R.M. Dreyer, 1939; E.E. Foord, 1974; F. Saupé, 1992; J.K. McCormack, 1998; C.S. Kim, 2000; J.V. Lavric, 2003; J.M. Esbri, 2010]*.

The determination of impurities in α-HgS ores could also be a discriminative parameter corresponding to specific studied deposits. In the context of obsidian provenance, Bellot-Gurlet et al. compared different methods and showed that even if PIXE analyses are non-destructive, the number of attainable elements is not sufficient for a source discrimination and can be completed by ICP-AES and ICP-MS *[L. Bellot-Gurlet, 2005]*. Mass-spectrometry is indeed one of the most used methods for this purpose. In a study made in Japan by Yamada et al., cosmetics found in different burials and composed of cinnabar and ferric oxide showed different ratios of iron compared to mercury *[M. Yamada, 1997]*. But even materials from the same burials showed different Hg/Fe ratios. Among all trace elements found in the samples, the amount of zinc seemed to be a good marker for local differences and allowed the identification of groups corresponding to each burial studied. In another study, antimony was also shown to be an indicator element in geochemical prospecting because even if cinnabar in deposits usually contains between 4 and 16 ppm of Sb, differences can be found between deposits enriched in Sb (as Ukraine, Russia, Turkey, Alaska) and with low Sb contents (Spain, British Columbia, California, Italy) *[R.W. Boyle, 1984]*. Identifying trace elements and their ratio could be a good method to determine the origin of cinnabar ores.

Another type of analysis is the study of isotopes ratios in ores coming from different areas. In the case of cinnabar, mercury and sulfur isotopes were previously studied by several research groups in order to define correspondences between isotopic averages and localization of deposits. The most studied element for the isotopic analyses of cinnabar is sulfur. The abundance in nature of each isotope was measured by Spangenberg et al.: 95.02% for ^{32}S, 0.75% for ^{33}S, 4.21% for ^{34}S and 0.02% for ^{35}S *[J.E. Spangenberg, 2010]*. The results of isotopic analyses are given as $\delta^{34}S$ average, which is the deviation of the isotope ratio (of the heavy to light most abundant isotopes, here $^{34}S/^{32}S$) relative to known standards. In Almadén areas, Saupé et al. showed that this average is different according to deposits (8.1 ± 0.7‰ for San Francisco, 5.9 ± 1.0‰ for San Pedro and 0.2 ± 1.1‰ for San Nicolas) *[F. Saupé, 1992]*. Another research group went even further showing that this average allowed to make the distinction between cinnabar coming from Japan and from China, as Japanese mines have a lower value of $\delta^{34}S$ (7.3 ± 1.9 to -2.1 ± 1.6‰ for Japanese mines compared to +22.6 ± 3.6‰ for Chinese ones) because ^{32}S is abundant from volcanic activity *[T. Minami, 2005]*. This group was then able to identify the origin of ores found in different Japanese burials by comparing $\delta^{34}S$ calculated to the ones of Japanese and Chinese mines. In another study made in Europe, $\delta^{34}S$ averages measured were the following *[J.E. Spangenberg, 2010]*:

- Almadén (Spain): 5.6 ± 2.0‰
- Idria (Slovenia): 4.4 ± 3.5‰
- Monte Amiata (Italy): -1.0 ± 3.2‰
- Moschellandsberg (Germany): -17.6 ± 2.8‰
- Genepy (France): -2.9 ± 0.9‰

This group also measured this $\delta^{34}S$ average on a painting from the Roman city of Aventicum (Switzerland), and showed that, within all the origins they studied, results obtained (9.9 ± 0.7‰) were near to the composition of Almadén cinnabar. Another hope for finding a new tracer of mercury source was given by Blum et al., with ratios in mercury standard solutions *[J.D. Blum, 2007]*, and measurements were also made to obtain data on carbonates ($\delta^{13}C$, $\delta^{18}O$) and sulfates ($\delta^{34}S$, $\delta^{18}O$) of cinnabar gangues to determine the mineralization of the ore *[J.V. Lavric, 2003]*. The reliability of all these analyses depends on the contribution of databases to compare results between ores coming from different deposits.

1.2. Apparition of the synthetic pigment, vermilion

From the 8th century, a synthetic process (called the "dry process") was established by heating mercury together with sulfur; this forms the same component as cinnabar, mercury sulfide, however it is then called vermilion. This process was used in Greece, Arabia, China and started to be commonly used in Europe in the 14th century. A description of the different steps is given by Gettens: 100 parts by weight of Hg^0 are added to 20 parts of molten S; a black amorphous mercury sulfide is obtained (called α'-HgS in some studies) and heated to 580°C; a strong alkali is added after the condensation to remove the free sulfur from the product; after washing and grinding, a red vivid powder is obtained. Amsterdam was the principal center of manufacture of "dry-processed" vermilion in the early 17th century. *[R.J. Gettens, 1972]*

Since the 17th century, the "wet process" was used in manufacture, consisting in putting the previously mentioned black product in an ammonium or potassium sulfide solution. This enables decreasing the heating temperature *[R.J. Gettens, 1972].* As for other syntheses, the pH of the solution where the formation of vermilion takes place is a crucial parameter. Indeed, when letting $Hg(CH_3COO)_2.2H_2O$ react with sodium thiosulfate in distilled water at 70°C, if triethanolamine is added (pH = 10), a red precipitate is formed (α-HgS) whereas if acetic acid is added to the solution (pH = 4), a black precipitate is obtained (β-HgS) *[H. Wang, 2003]*.

So far, it is not possible to scientifically assess the natural or synthetic origin of red mercury sulfide when found in works of art; however, sometimes, the grain sizes allow determining some information: if large grains are observed, the pigment is probably natural; if only very fine grains are seen, the powder might be synthesized by one of the two processes described above. Identification of trace elements was also used to try to differentiate natural cinnabar from synthetic vermilion, the latest being purer before mixing with binders or other pigments. Furthermore, according to Grout et al., next to the multiple elements found in cinnabar, the elements found in vermilion are different depending on the process used to make it: As, Sr and Zn for the "dry process" and Ba, Pb and Zn for the "wet process" *[R. Grout, 2000]*.

1.3. Uses of the red vivid compound

The first known use of red mercury sulfide dates from Neolithic period, ca. 3000 BC. Hundreds of kilograms of ground cinnabar were found on bones of ca. 100 individuals in a dolmenic burial of Palencia, Spain *[J. Martin-Gil, 1995]*. Indeed, before decorating walls or artefacts, cinnabar was used as a cosmetic and applied on mummies or bones during burial ceremonies. In the study of a mummy found in a tomb in Hunan Province, China, XRD showed that the reddish fluid covering the body contained cinnabar (α-HgS), whereas in both natural and wig hairs of this cadaver, metacinnabar (β-HgS) was found *[D. Kennedy, 1981]*. The origin of the last compound was attributed to the slow sorption of the fluid and its reaction with the keratin's disulfide groups, rather than to medicinal ingestion. Analyses of hairs from persons having absorbed mercury or mercury compounds show the same type of diffractogram as the one of the red fluid. Next to this early use, red mercury sulfide was also used in China for the manufacture of famous lacquer wares.

In South-America, cinnabar was used by different civilizations, such as the Mayas, and for a long period. The compound mixed to natural binders was used as a cosmetic and found in small purses or as pigment on wall paintings. As an example it was identified on bones in a 900-1000 AD tomb in Peru *[J. Martin-Gil, 1995]*.

In Ancient Egypt, red mercury sulfide was used only from the Late Period (664-332 BC) *[D. Le Fur, 1990]*.

In Europe, from Antiquity onwards, the production of the pigment from the extraction of red mercury sulfide was very important and the most famous and important deposit of cinnabar in the world is situated in Almadén, Spain, which accounts for about one third of the total Hg world production. Other deposits were present in Europe, as in Yugoslavia or Kosovo. Cinnabar was a precious pigment and one of the most expensive colors of the Roman world but its vivid and unique color made it appreciated. It was used in rich villas and palaces as for example the Domus Aurea in Rome *[C. Clementi, 2011]*, and in tombs as the 2nd century AD necropolis of Boccone d'Aste in Rome where α-HgS was identified on beads *[C. Aurisicchio, 2002]*. The ancient Greeks also used cinnabar, as in Macedonia where it was frequently used between the 4th and the 3rd century BC, and the ore was probably extracted

from Axios area or Serbian territory *[H. Brécoulaki, 2000]*. Its intensive use in Gaul started with the conquest of the Provence by the Romans (123 BC) and became more rare from the middle of the 1st century AD *[A. Barbet, 1990]*. At this period, cinnabar was replaced or mixed with other pigments, such as hematite, in order to decrease the price of producing a painting. During Middle Ages, cinnabar was used to prepared red ink for medieval parchments *[E. Devezeaux de Lavergne, 1990]* and sometimes for illuminations. Red mercury sulfide was used all along the centuries on classical works of art, such as paintings, frescoes and statues, or to decorate more original materials such as the pieces of furniture from the French famous cabinet maker André-Charles Boulle. The use of the natural form of the pigment, cinnabar, appears to end around 1880 in Europe.

For thousands of years, red mercury sulfide was not only known for its esthetic qualities, but also for its medical ones, for example to treat syphilis (a dermatological disease), and was sometimes ingested to give strength and to lengthen life. The beneficial effects of α-HgS were associated to its color, similar to blood, and thought to contain the soul concentrate. Indeed, about 10-30% of the Chinese patent medicines contain cinnabar, according to the Pharmacopoeia of China (2005) *[X. Zhou, 2010]*. As an example, An-Gong-Niu-Huang Wan (AGNH), one of the traditional medicines used for brain disorders such as viral encephalitis, cerebral stroke, cerebral hemorrhage or cranio-cerebral trauma, contains 10% of cinnabar *[Y.F. Lu, 2011]*.

As this red compound is composed of mercury, it is considered to be a global pollutant. Nowadays, the toxicity of medicines such as AGNH is a cause for concern for the public health. Some studies showed that after ingestion of α-HgS during 44 days, the liver presents traces of Hg, which are much lower than in the case of $HgCl_2$ ingestion *[Y.F. Lu, 2011]*. But the major risk associated with cinnabar is the volatilization of mercury (under heat, photo or laser irradiation) which can enter the lungs and can be distributed from there throughout the body, and its conversion to methyl mercury, the most toxic form of mercury; however, this conversion is not likely to happen in the human body *[J. Liu, 2008]*.

1.4. Darkening of red mercury sulfide

Mercury sulfide is also well-known for its sporadic instability, going from a red color to a black, violet or grayish one. This phenomenon was described since Antiquity: "*Exposure to the light, either of sun or the moon, is injurious to the colour*" *[Pliny the Elder, Naturalis Historia]* and still studied by research groups as it is not yet fully understood. The photosensitivity of this ore was observed many centuries ago and forces some mineralogical galleries to store α-HgS ores in closed cabinets to keep them from light. More recently, chlorine was shown to be possibly involved in the darkening of red mercury sulfide and the formation of grey or black compounds from cinnabar was studied *[J.K. McCormack, 2000]*. Moreover, in this last study, McCormack established that among the tested samples, traces of chlorine are visible only on photosensitive cinnabar ores. The presence of stable mercury chloride compounds next to cinnabar in deposits could also be caused by the action of chlorine on the natural red mercury sulfide. A soil polluted by the dumping of Hg-containing wastes from a chlor-alkali plant showed the presence of cinnabar (α-HgS), metacinnabar (β-HgS), corderoite (α-$Hg_3S_2Cl_2$) and amorphous Hg, S and Cl-containing species *[A. Santoro, 2010; R. Terzano, 2010]*. Moreover, the last study proposed a chain reaction to explain the evolution of these mercury containing compounds *[R. Terzano, 2010]*:

metacinnabar (β-HgS) → cinnabar (α-HgS) → corderoite (α-$Hg_3S_2Cl_2$)

Degradation of red mercury sulfide seen on works of art presents two kinds of aspects: one with a "moderate" level of alteration with a grey color, heterogeneous, and a second one with a darker color, closer to black, more homogeneous (see examples of these two types of degradation respectively in Figure 1.1a and b). When preparing transversal cross-sections from an altered area, a thin grey or black layer is present above the red mercury sulfide one. In most cases seen in literature, the thickness of this layer is around or below 10 µm (see examples of cross-sections in Figure 1.1c and d).

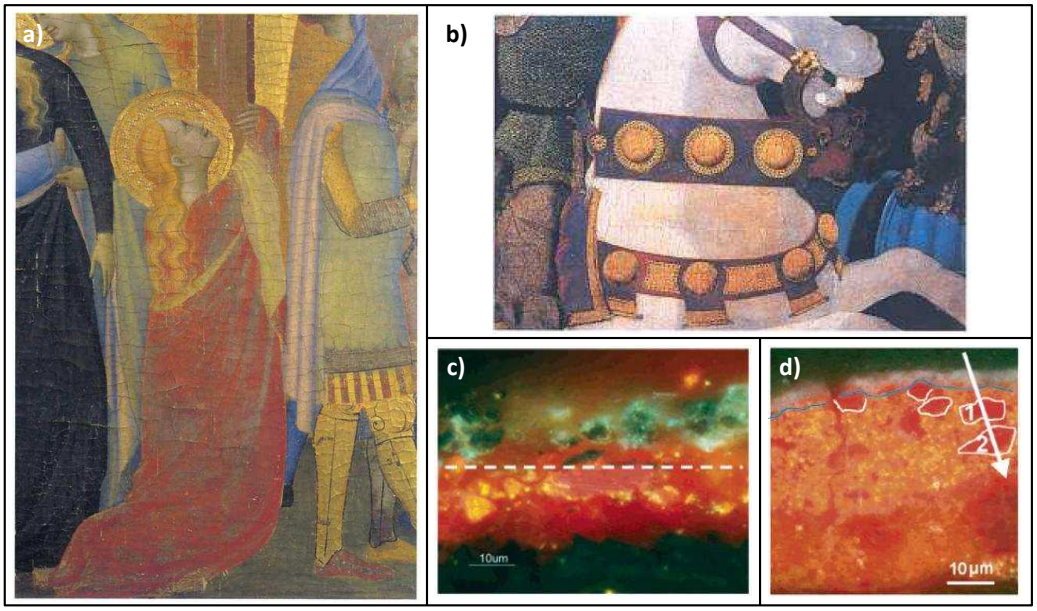

Figure 1.1.: *Visible images of altered red mercury sulfide from the literature:* ***a)*** *Detail from the polyptych The Crucifixion and Saints by B. Daddi (ca. 1280-1348) [R. Grout, 2000];* ***b)*** *Detail from the painting Niccolo Mauruzi da Tolentino at the Battle of San Romano by P. Uccello (ca. 1440) [M. Spring, 2002];* ***c)*** *Paint cross-section from Portrait of a Lady by P.P. Rubens (ca. 1625) [K. Keune, 2005];* ***d)*** *Paint cross-section from Minerva and Hercules Opening the Doors for Victory by C. van Couwenberg (1651) [K. Keune, 2005].*

Studying the origin of ores in cultural heritage domains leads to the determination of provenance of materials used and thus of exchange roads and markets between different areas and countries all over the world. Furthermore, in the case of the darkening of red mercury sulfide, it was already shown that the origin of the natural ore of cinnabar could change the kinetics of the alteration: α-HgS from the Opalite mine (McDermitt, Nevada-Oregon), the Goldbanks deposit (Winnemucca, Nevada), Steamboat Springs (Nevada) and the B&B mine (Esmeralda County, Nevada) blackens rapidly whereas α-HgS from the Aurora mine (San Benito County, California) and the Mazatzal Mountains (Arizona) did not blacken after 6 months of sun irradiation *[R.M. Dreyer, 1939]*. McCormack also explained that photosensitive cinnabar found in deposits (which darkens with exposure to light) is commonly spatially associated with mercury halide minerals such as calomel (Hg_2Cl_2), terlinguaite (Hg_2OCl), corderoite (α-$Hg_3S_2Cl_2$) or kenhsuite (γ-$Hg_3S_2Cl_2$) *[J.K. McCormack, 2000]*. There appears to be an indirect relationship between the host rocks and the photosensitivity of cinnabar as all ores from previously named deposits in Nevada and

Oregon present different host rocks from the ones from Californian deposits (see Section 1.1). The same study showed then that all known naturally occurring cinnabar that darkens rapidly occurs in a matrix of hydrothermal silica *[R.M. Dreyer, 1939]*. So the provenance of the pigment could play a role in the degradation process.

Moreover, if formations of the ore and its host rocks are contemporary, they should contain the same elements (originally contained in the geological fluids from which the ore and rocks precipitated). If the ore was formed after its host rocks, pollution could be considered to explain the presence of certain trace elements in the ore. As multiple types of host rocks can be found together with cinnabar, the proportion of traces elements can change from one deposit to another (see Section 1.1), the study of this parameter could yield new insights into the factors influencing the alteration of red mercury sulfide. Indeed Pal et al. suggested that the photosensitivity of natural cinnabar can be influenced by the impurities contained in the crystals such as sodium, magnesium, aluminum, calcium, titanium, copper, selenium, antimony and lead, which differs from the deposit of origin: "*the synthesized HgS powder is expected to be optically inactive overall and natural mineral specimens of cinnabar, though they are optically active single crystals, contain impurities reducing the photosensitizing activity of HgS*" *[B. Pal, 2003]*. Concerning the pigment, Spring et al. noted that even if the presence of impurities in red mercury sulfide can accelerate its blackening, dry-process vermilion which is considered as very pure HgS still exhibits severe blackening *[M. Spring, 2002]*.

As described in Section 1.1, multiple analytical protocols are available to answer the question of the cinnabar origin. In this study, observations and analyses were made on different cinnabar ores to determine discrimination parameters for the origin of this mineral and to link this with the kinetics of the degradation of α-HgS. First, visual observations of the rocks showed us that cinnabar can present different colors and can crystallize with different morphologies (see Appendix C.a). Then, XRD analyses of ores were performed to identify the phases associated to natural cinnabar and PIXE-PIGE analyses gave the elemental composition of each corresponding gangue (see Appendix C.b). But all results did not seem to show any statistical correlation between the composition of ores or gangue and the provenance of the samples studied.

1.5. Properties of α-HgS and other mercury compounds

Red mercury sulfide is found and studied in relation with other phases that are often associated with its formation or degradation. So next to α-HgS, properties of associated phases were examined.

Cinnabar/vermilion (α-HgS)

The hexagonal form of mercury sulfide, α-HgS, with the lattice parameters a = 4.149 Å and c = 9.495 Å *[B.K. Patel, 2007]*, has a distorted NaCl structure (space group $P3_121$ or $P3_221$); its coordination number is 6 *[A. San Miguel, 1995]*. This compound belongs to the II-VI family of semiconductors *[M.J. Peters, 1996]*.

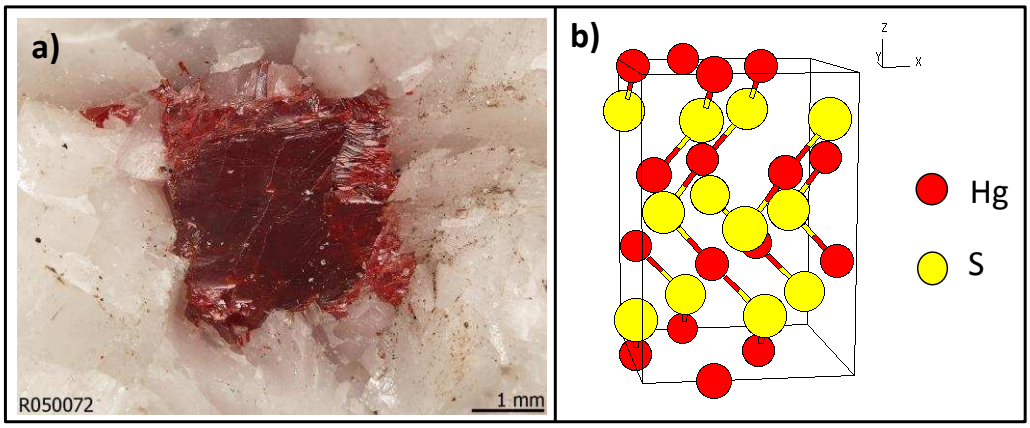

Figure 1.2.: a) *Visible image of a cinnabar ore [http://rruff.info/];* ***b)*** *crystal structure of α-HgS [http://cst-www.nrl.navy.mil].*

The color of α-HgS, vivid red, is referenced in the Munsell color system as 5R-7.5R *[R.J. Gettens, 1972].*

Metacinnabar (β-HgS)

Metacinnabar is the cubic form of mercury sulfide (zinc blende structure; a = 5.851 Å *[B.K. Patel, 2007]*), in the $F\bar{4}3m$ space group *[http://www.mindat.org]*, and presents a black color. This specificity gave it in early studies the reputation of being responsible for the transformation of the red HgS pigment into black *[R.S. Davidson, 1981; R.J. Gettens, 1993]*.

The relation between cinnabar and metacinnabar will be discussed in greater detail in Chapter 3.1.

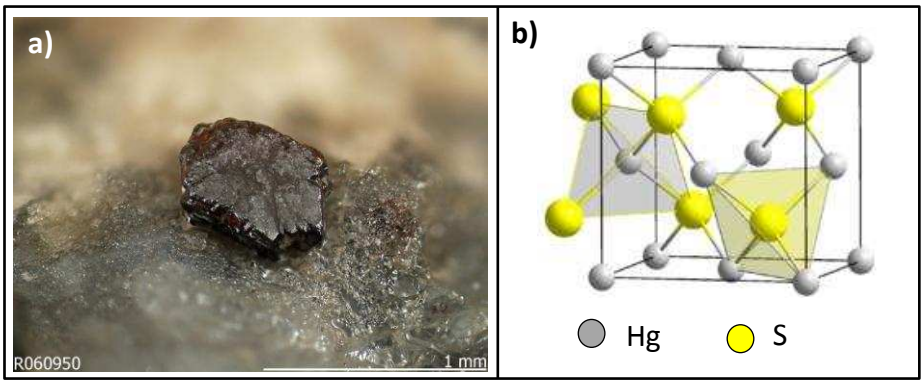

Figure 1.3.: a) *Visible image of a metacinnabar ore [http://rruff.info/];* ***b)*** *crystal structure of β-HgS [http://fr.wikipedia.org/wiki/].*

Hypercinnabar (γ-HgS)

Hypercinnabar is the third variety of mercury sulfide but is incompletely characterized; it is found within natural metacinnabar from the Mount Diablo Mine (California, USA) and was assessed as being the "high-temperature polymorph of mercury sulfide". It also has a hexagonal structure but has longer lattice parameters than α-HgS (a = 7.01 Å, c = 14.13 Å) and has a black color with purple cast *[R.W. Potter, 1978]*.

Native mercury (Hg^0)

Red mercury sulfide is commonly found in deposits where native mercury is extracted. Under normal temperature and pressure conditions, this compound is the only metal with a liquid state, forming silvery droplets. Mercury is used to form amalgams with gold, silver and other metals.

Figure 1.4.: *Visible image of native mercury [http://rruff.info/].*

Calomel (Hg_2Cl_2)

Calomel is on its natural form a rare white ore, essentially found in association with cinnabar. The Hg_2Cl_2 molecule is linear and crystallizes in the tetragonal system, with space group I4/m2/m2/m and cell parameters a = 4.4795 Å and c = 10.9054 Å *[http://www.mindat.org/min-869.html]*.

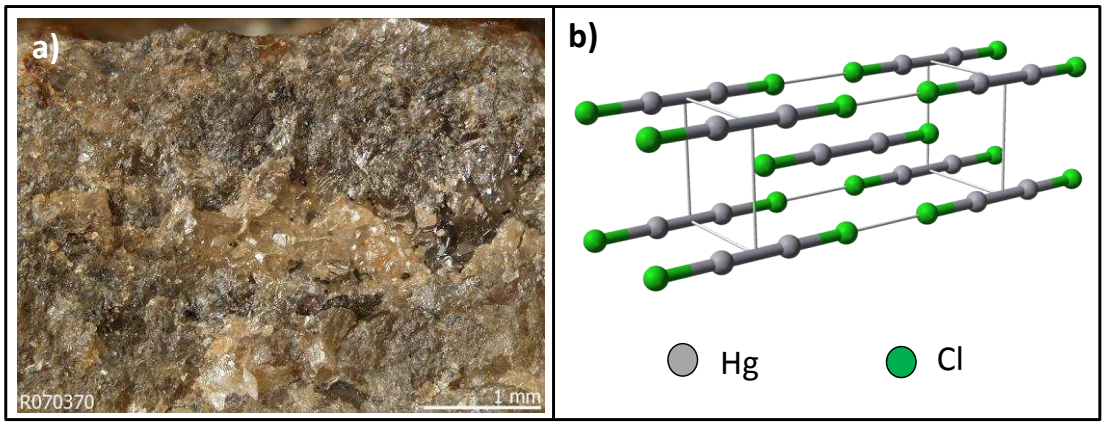

Figure 1.5.: a) *Visible image of a calomel ore [http://rruff.info/];* ***b)*** *crystal structure of Hg_2Cl_2 [http://en.wikipedia.org/wiki/].*

Mercuric chloride ($HgCl_2$)

This mercury (II) chloride compound is known for its highly toxic effects and is one of the phases often associated with cinnabar. Carlson took this phase into consideration when studying the synthesis of $Hg_3S_2Cl_2$ compounds via reaction of HCl gas with α-HgS *[E.H. Carlson, 1967]*.

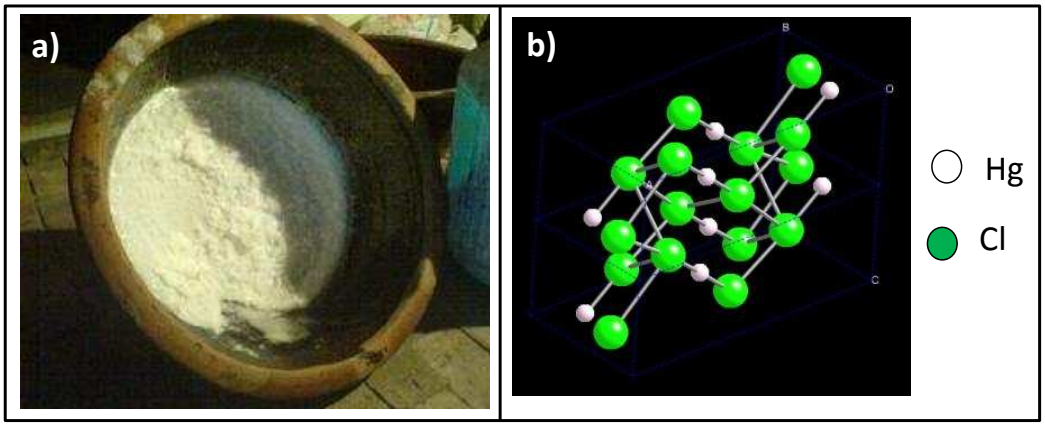

Figure 1.6.: a) *Visible image of mercury (II) chloride [http://www.hudong.com/wiki/];* ***b)*** *crystal structure of $HgCl_2$ [R.E. Taylor, 2009].*

Corderoite (α-$Hg_3S_2Cl_2$)

Corderoite is a light orange-pink mineral turning grayish-black when exposed to light *[E.E. Foord, 1974]*. This ore crystallizes in a body-centered cubic system (space group $I2_13$ *[E.E. Foord, 1974]*) with a = 9.968 Å *[J.K. McCormack, 1998]*. The sulfur atoms center the cubes of the Cl sublattice and mercury atoms center three (of six) faces *[S.V. Borisov, 2001]*. Carlson synthesized this product by letting HCl gas react with solid α-HgS between 300 and 400°C *[E.H. Carlson, 1967]*.

Figure 1.7.: *Visible image of corderoite [http://www.mindat.org].*

β-$Hg_3S_2Cl_2$

This rare and not well documented phase crystallizes in a primitive cubic system (space group Pm3n) with a = 17.93 Å *[Y.V. Voroshilov, 1996; J.K. McCormack, 1998]*. The S

atoms are equally ordered at the centers of the Cl sublattices and the Hg atoms substantially depart from the face centers of the Cl subcell *[S.V. Borisov, 2001]*.

Kenhsuite (γ-$Hg_3S_2Cl_2$)

The rare mineral kenhsuite is naturally associated with cinnabar and corderoite and was recently found in a Nevada deposit (McDermitt). This ore forms straw-yellow crystals exhibiting an orthorhombic symmetry (space group A2/mmm) with the following parameters: a = 9.328 Å, b = 16.82 Å, c = 9.081 Å *[S. Durovic, 1968]*. This yellow ore was observed as being photosensitive: it blackens on exposure to light *[J.K. McCormack, 1998]*. During the same study, McCormack et al. synthesized this compound by letting stoichiometric mixtures of α-HgS and $HgCl_2$ (2:1) react in sealed evacuated glass tubes at 400°C, following the same protocols that Carlson used previously *[E.H. Carlson, 1968]*.

Figure 1.8.: *Visible image of kenhsuite [http://webmineral.com].*

1.6. Advantages and drawbacks of different analytical techniques for the study of mercury sulfide

To study red mercury sulfide and its degradation, different analytical techniques are available and each one has its own assets and drawbacks. All information concerning the instruments used during this study and the basic principles of each one of these techniques can be found in the Appendix B.

Spectro-colorimetry

Spectro-colorimetric analysis is used to quantify the human color perception by measuring intensities of incident and reflected radiations. As for all researches based evolution of materials, this technique is very useful to follow color changes (for example during artificial ageing) in a quantitative way. Grout et al. had already proven that the use of spectrophotometry allows comparing the appearance of different red mercury sulfides (natural and synthetic) by measuring the loss of reflectance of the samples after the same ageing experiments *[R. Grout, 2000]*.

However, the spectra obtained depend partly on the light intensity surrounding the experiment and of the roughness of the surface, so that in order to be reproducible, measurements have to be performed in constant conditions. Moreover, surfaces analyzed have to be homogeneous in the area of the light spot (usually in the millimetric range), which is not always the case for degraded samples.

In Figure 1.9, two spectra acquired on the same α-HgS sample but in areas with two different colors are shown. This figure shows that these analyses allow distinguishing two areas with different colors even on the same crystal.

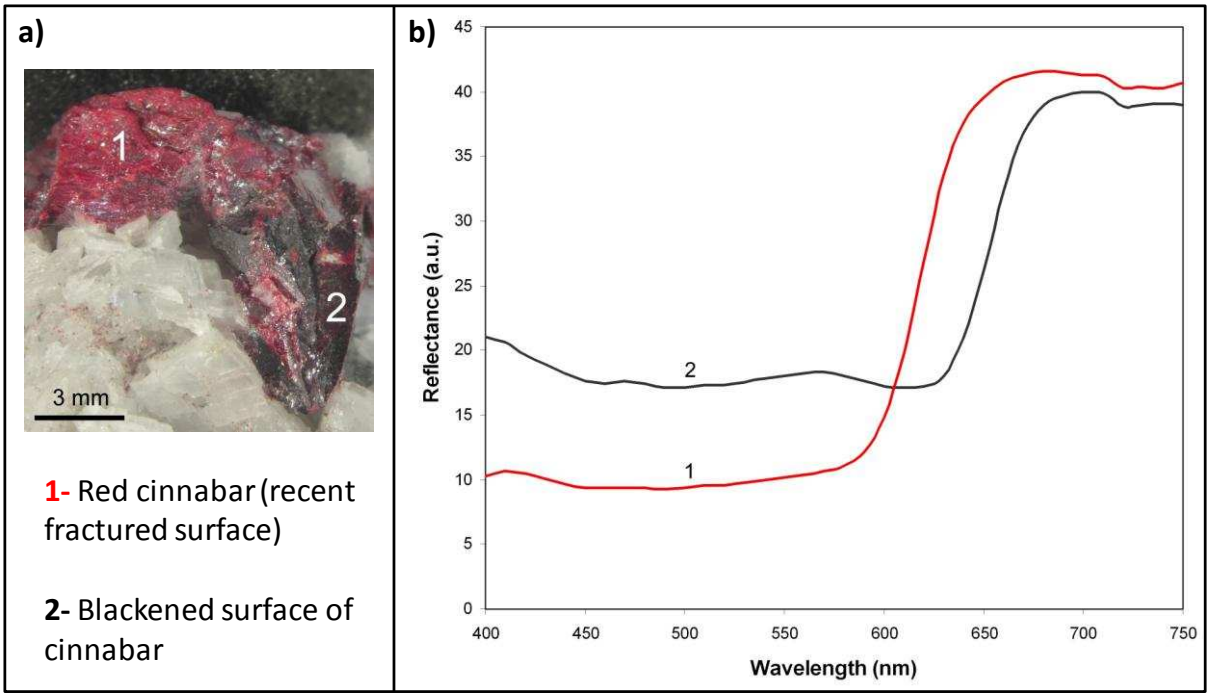

Figure 1.9.: a) *Visible image of cinnabar ore coming from China, with 2 parts: 1-recent fractured surface which appears red, 2-blackened untouched surface;* ***b)*** *Reflectance spectra acquired with the spectro-colorimeter at C2RMF on the two areas indicated in (a).*

SEM-EDX

Scanning electron microscopy (SEM) is a very valuable technique which provides high resolution images (which can go to the submicrometric range) of suitably prepared samples. Coupled to an energy dispersive X-ray probe (EDX), it determines the qualitative and/or quantitative composition of a sample from the energy of photons emitted by the irradiated area. This technique is interesting to provide a preliminary description of the samples as it is easily available in laboratories; in the cultural heritage domain SEM-EDX analyses usually compose the first step of the common protocol used to study works of art.

However, these techniques do not provide any structural information; so in the case of mercury sulfide study, they will not allow distinguishing cinnabar (α-HgS) from metacinnabar (β-HgS). By analyzing samples of a 15th century degraded painting of the National Gallery (London, UK) by SEM-EDX Spring and Grout *[M. Spring, 2002]* found chlorine next to mercury and sulfur coming from the original pigment. But only a spectroscopic

analysis was able to really identify the alteration compound coming from red mercury sulfide (see “Raman spectroscopy”).

The main issues when studying mercury sulfide by SEM-EDX is, first, the sensitivity of α-HgS. Indeed, under vacuum mercury could volatilize and pollute the detectors and radiation damages can be visible at the surface of the sample analyzed.

Another drawback is that with some instruments and without adapted software distinction between Hg and S could be delicate (see Figure 1.10). A deconvolution is necessary to separate the contribution of each element. As an example, when comparing spectra obtained for synthetic vermilion (α-HgS) (Figure 1.10a) and a rock of corderoite (α-$Hg_3S_2Cl_2$) (Figure 1.10b), the presence of chlorine allows distinguishing these two compounds. But the presence of sulfur could only be assessed by a deconvolution of the peak at 2.3 keV, and if it is not present, this spectrum could then be the one of mercury chlorine compounds such as calomel (Hg_2Cl_2).

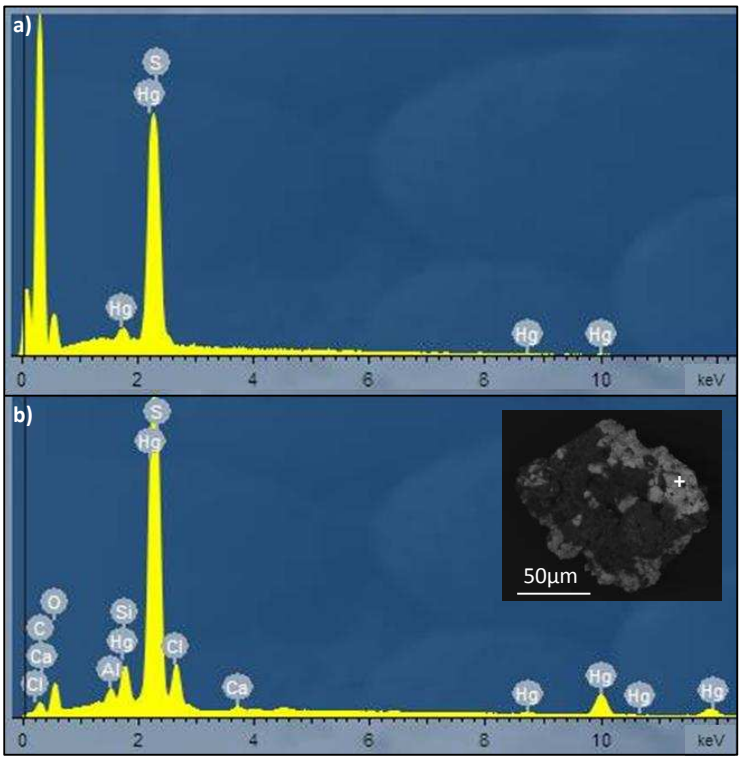

Figure 1.10.: *SEM-EDX analyses of few microns resolution showing spectra of* ***(a)*** *vermilion (α-HgS, Prolabo) and* ***(b)*** *a corderoite rock (α-$Hg_3S_2Cl_2$, Gallerie Minéralogique de L’Ecole des Mines) (the BSE image shows the localization of the point where the analysis was made).*

XPS

X-ray photoelectron spectroscopy (XPS) studies the chemical environment and electronic state of the elements composing a large area (in the millimetric range) but only the first ten nanometers of the surface of materials. As degradations sometimes consist in layers of few micrometers thick, this technique allows analyzing only the superficial compounds of an altered sample without having signals induced by the high concentrated matrix.

XPS analyses require ultra-high vacuum conditions and therefore working with mercury is delicate in order not to pollute the instrument. An important parameter of these analyses is the quality of the surface, as, for example, only by handling the sample, carbon deposited by hands will be visible in the spectra. An important quantity of material is needed to perform this analysis as the beam is in the millimetric range.

In the mercury sulfide context, Zeng et al. used XPS to identify the ratio of mercury to sulfur in the product of the synthesis of α-HgS by employing the Hg_{4f} peak of mercury and the S_{2p} peak of sulfur *[J.H. Zeng, 2001]*, such as the ones obtained from cinnabar ore shown in Figure 1.11.

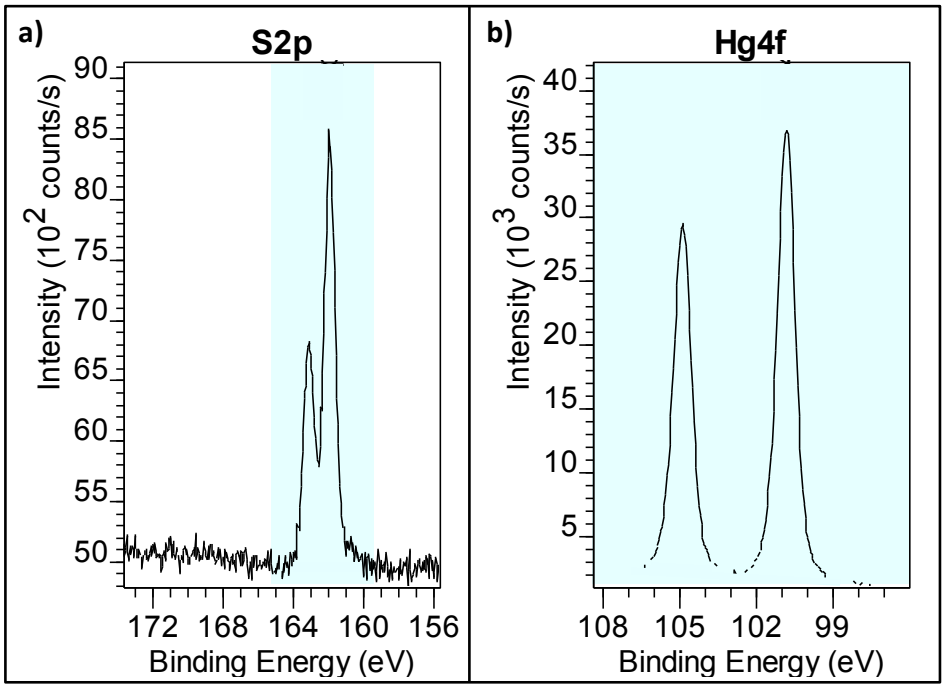

Figure 1.11.: *XPS results obtained by analyzing a cinnabar ore from China at the LRS for:* ***a)*** *sulfur S_{2p} and* ***b)*** *Hg_{4f} intensities.*

Raman spectroscopy

Raman spectroscopy allows studying the structural composition of materials analyzed in the micrometric range and distinguishing products containing the same elements, as for this study Hg, S and Cl. After analyzing a sample from an altered painting by SEM-EDX, Spring and Grout performed Raman spectroscopy analyses and identified calomel (Hg_2Cl_2) as a degradation compound of red mercury sulfide *[M. Spring, 2002]*. Classical Raman spectra range from 150 to 4000 cm^{-1}, whereas High Resolution instruments (as the one available at LADIR), despite its lower availability, allow low frequency spectra recording (<10 cm^{-1}). This capability does not allow to make a clear distinction between cinnabar and metacinnabar (see Figure 1.12b and c), but gives very interesting results for other mercury compounds such as corderoite or calomel (see Figure 1.12a).

With this valuable technique the laser flux needs to be controlled (as with other laser-based instruments) as cinnabar can blacken under the beam and the Raman spectra are then modified. Another frequent problem during spectra acquisition is the high fluorescence of some samples (this is frequently the case for archaeological samples, heated samples or samples containing organic binders or glazes for example). This phenomenon induces a noisy background masking the Raman signal of the sample.

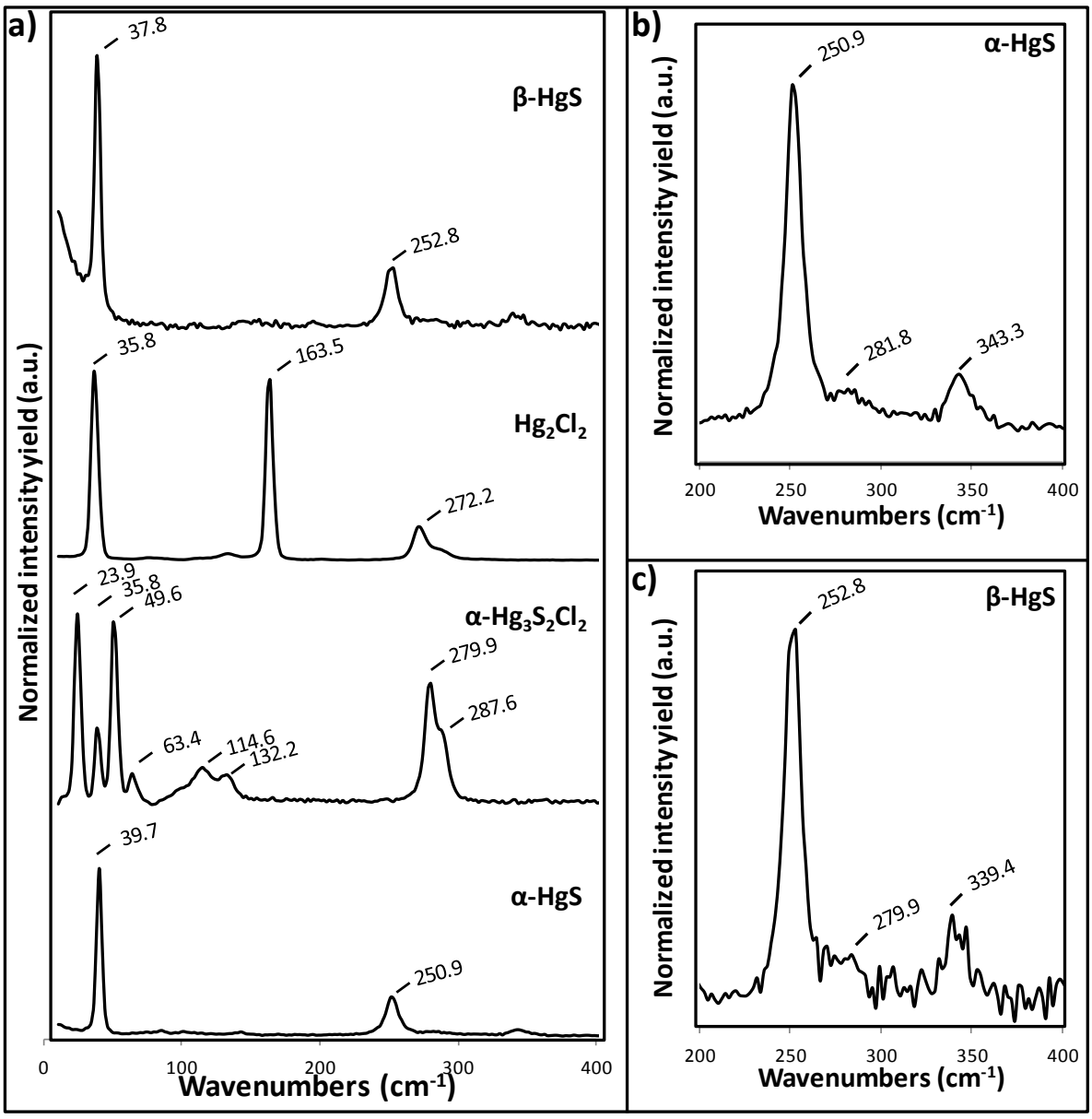

Figure 1.12.: a) *Raman spectra of vermilion (α-HgS, Prolabo), corderoite (α-$Hg_3S_2Cl_2$, Gallerie Minéralogique de l'Ecole des Mines), calomel (Hg_2Cl_2, Aldrich) and metacinnabar (β-HgS, Gallerie Minéralogique de Jussieu);* ***b)*** *Enlargement of the Raman spectrum of vermilion (α-HgS);* ***c)*** *Enlargement of the Raman spectrum of metacinnabar (β-HgS).*

μ-XRF/μ-XANES

X-ray absorption near edge spectroscopy (XANES) provides chemical information on the compounds analyzed and is employed to determine the chemical environment and the valence state of relevant elements. Contrarily to XRD analyses, the material does not need to be in crystalline form to be analyzed by XANES. When spectra are acquired in X-ray fluorescence mode, this method is sensitive to minor and trace compounds and is then a clear asset for the analysis of the alteration of materials. In addition to energy tunability, the high resolution of synchrotron radiation allows reaching submicrometric resolution which is necessary to analyze complex and micrometric degradation layers. Thanks to this technique, Cotte et al. identified different sulfur and chlorine compounds on altered α-HgS containing works of art *[M. Cotte, 2006; M. Cotte, 2008]*.

Contrary to XRD or Raman spectroscopy, databases available for XANES are quite limited and in the case of complex mixtures, it is sometimes difficult to clearly identify the phases that are present. Spectra obtained on references encountered in the study of red mercury sulfide show that, next to the most intensive peak that provides information on the chemical environment of the element considered, features on spectra will help distinguishing the different compounds (see Figure 1.13).

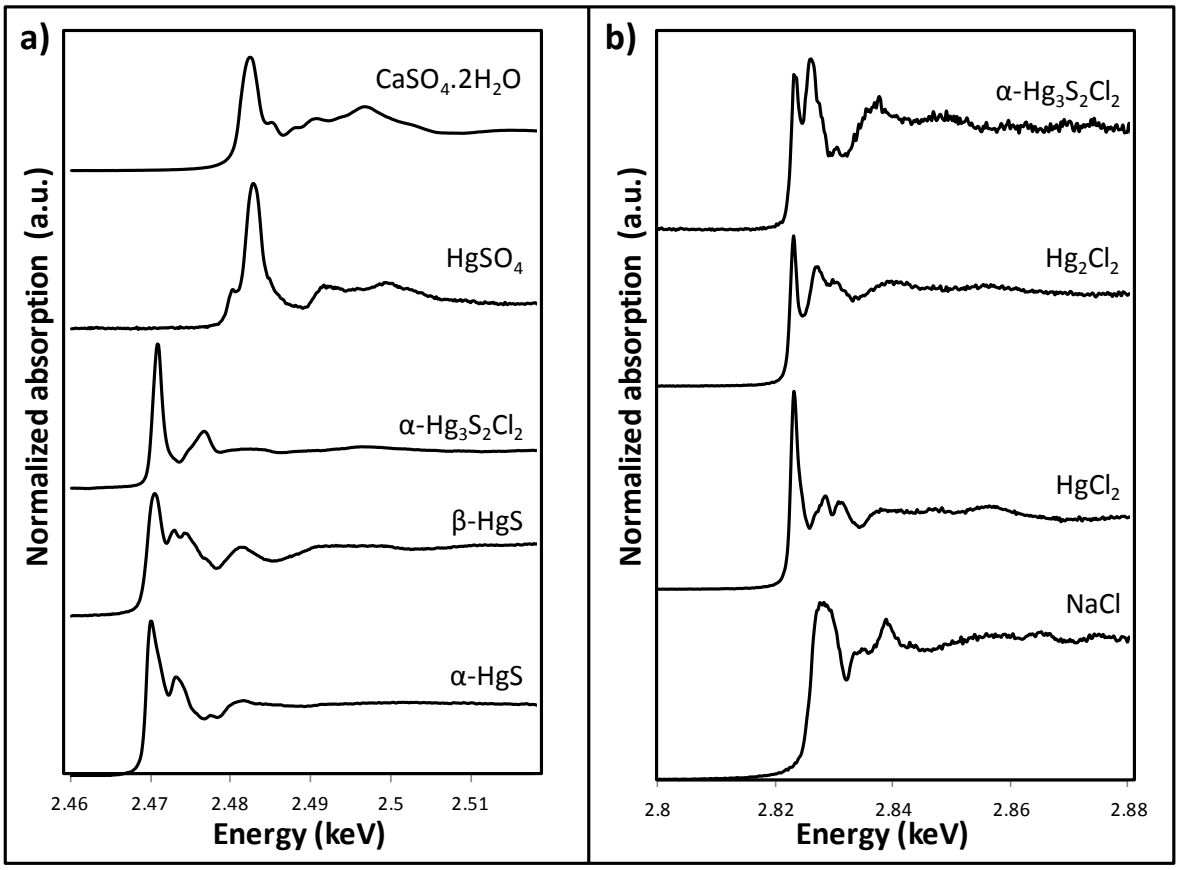

Figure 1.13.: *XANES spectra at* ***(a)*** *sulfur K-edge and* ***(b)*** *chlorine K-edge of references compounds (see origin of the references in Table B.1. of Appendix B.g): $CaSO_4.2H_2O$, $HgSO_4$, α-$Hg_3S_2Cl_2$, β-HgS, α-HgS, Hg_2Cl_2, $HgCl_2$ and NaCl.*

XRD/μ-XRD

Concerning the structural analyses, one of the most efficient techniques is X-ray diffraction (XRD) as it allows finding the crystal structure of an unknown material. As for multiple other techniques, XRD is a non destructive technique which can be adapted to portable instruments and then be directly used in museum or archeological sites.

However, to allow identification by XRD, compounds have to be in crystalline form. When studying micrometric sized layers, as for the degradation of red mercury sulfide, performing XRD with a beam larger than 10 μm (which is usually the case when laboratory equipment is being used), does not allow to distinguish the different layers and thus localize the different phases. The use of synchrotron radiation based μ-XRD is very relevant in these

cases of thin alteration layers and with complex mixtures, as demonstrated by Salvado et al. *[S. Salvado, 2009; S. Salvado, 2010]*.

Next to elemental analytical methods such as X-ray fluorescence that reveal the presence of mercury and sulfur, XRD will differentiate polymorphous minerals, such as mercury sulfide with the hexagonal form (cinnabar, red) from its cubic one (metacinnabar, black) (see Figure 1.14b) or corderoite (α-$Hg_3S_2Cl_2$) from β-$Hg_3S_2Cl_2$ and kenhsuite (γ-$Hg_3S_2Cl_2$). This is useful as metacinnabar has been thought to be responsible for the transformation of the red pigment into black *[R.S. Davidson, 1981; R.J. Gettens, 1993]*.

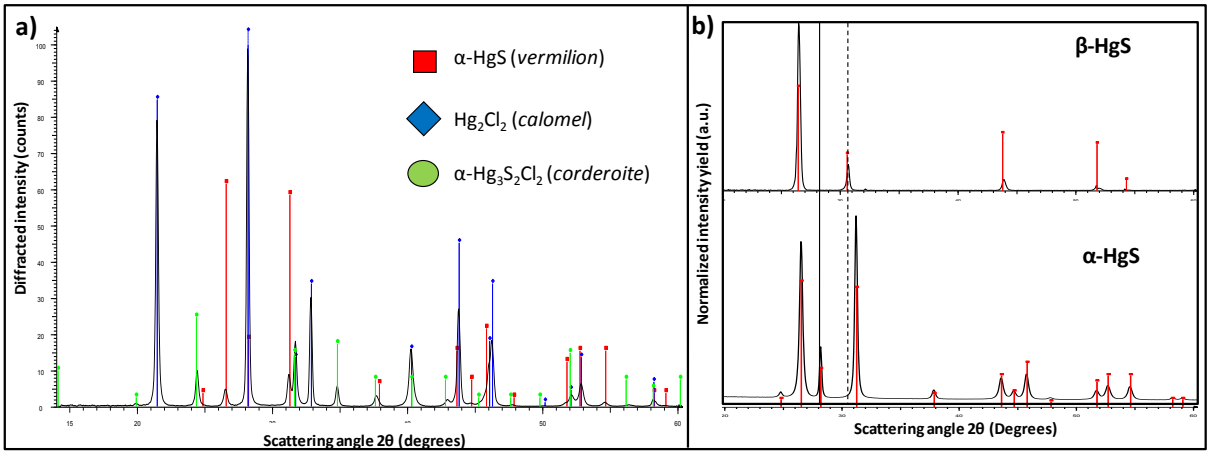

Figure 1.14.: a) *Diffractogram showing different phases (vermilion α-HgS –Prolabo-, calomel Hg_2Cl_2 – Aldrich- and corderoite α-$Hg_3S_2Cl_2$ –Gallerie minéralogique de l'Ecole des Mines);* ***b)*** *Comparison of cinnabar (α-HgS, Gallerie minéralogique de l'Ecole des Mines) and metacinnabar (β-HgS, Gallerie minéralogique de Jussieu) diffractograms.*

Other techniques

Other techniques were used by different research groups to study red mercury sulfide and its degradation.

Particle induced X-ray and gamma-ray emission (PIXE-PIGE) offers a powerful microscopic beam that allows analyzing major and minor elements of materials studied. In the study of mercury sulfide, the sensitivity of this compound induced the volatilization of

mercury under the beam and the pollution of detectors. Thus, this technique was only used to analyze the surrounding rocks of mercury containing ore crystals.

Time Of Flight Secondary Ion Mass Spectrometry (TOF-SIMS) is a very sensitive method which uses a primary ion beam at the surface of the sample and collects ejected secondary ions to determine its composition. It is a less common method of analysis for works of art but which allows high lateral resolution chemical imaging (in the submicrometric range). The critical part of these analyses lies in the sample preparation, and especially, as for XPS, the quality of the surface which can affect the results obtained. The data interpretation is also challenging due to the formation of cluster anions during the ion beam analysis that can deform the results. This phenomenon consists in the recombination of different groups of molecules that can give rise to compounds that were not necessarily present in the original material. So the analyses of pure references and of mixtures of them are essential. The interpretation of SIMS data can therefore be difficult with very complex materials as the ones encountered in cultural heritage *[S. Cersoy, 2012]*. Keune and Boon used SIMS to analyze an altered sample from a 17th century painting containing red mercury sulfide and observed Hg_2Cl_2-Cl clusters in the spectra *[K. Keune, 2005]*, which could suggest the presence of mercury chloride ($HgCl_2$) or calomel (Hg_2Cl_2) in degraded α-HgS paint samples. Therefore TOF-SIMS was not one of the techniques selected for this study.

Fourier Transform Infra-Red spectroscopy (FTIR) identifies molecular groups by analyzing infrared light transmitted through the sample. In the cultural heritage field, this technique is especially appropriate for organic components such as binders. To the best of our knowledge, only one report on FTIR analysis of mercury sulfide has been published. In that publication, Fuchs showed that FTIR allows differentiating cinnabar from metacinnabar thanks to structures in the spectrum of the latter compound around 400 cm^{-1} *[R. Fuchs, 2002]*. Despite this example, no valuable identification of mercury containing compounds by FTIR was obtained during this study.

The following table (Table 1.2) gives information concerning all techniques previously named to compare their assets and drawbacks in the context of the red mercury sulfide study.

Table 1.2.: *Comparison of assets and drawbacks of different analytical techniques in the context of the red mercury sulfide study.*

Technique	Spatial Resolution	Advantages	Limitations
Spectro-colorimetry	Millimetric	- Quantification of color - Identification of visual changes during artificial ageing	- Constant conditions of use needed - Homogenous area needed
SEM-EDX	Submicrometric	- Easily available - High resolution imaging	- Elemental analyses - Possible induction of mercury pollution and radiation damage - Sometimes no distinction between Hg and S - Sampling needed
XPS	Millimetric	- Superficial analyses	- Sensitive to pollution - Possible induction of mercury pollution - Sampling needed
Raman Spectroscopy	Micrometric	- Structural analyses - High resolution analyses and imaging	- Possible induction of radiation damage - Possible noisy background due to fluorescence
μ-XANES	Submicrometric	- Structural analyses - High resolution analyses - Sensibility to minor and trace compounds	- Low availability - Databases limited - Sampling needed
XRD/μ-XRD	Submillimetric/ Submicrometric	- Structural analyses - Distinction between α-HgS/β-HgS	- Only crystallized compounds
PIXE-PIGE	Micrometric	- Sensibility to minor and trace elements	- Induction of mercury pollution and radiation damage
TOF-SIMS	Submicrometric	- High resolution imaging	- Sensitive to pollution - Difficult interpretation - Sampling needed
FTIR	Micrometric	- Structural analyses	- Difficult distinction between α-HgS/β-HgS - Sampling needed

Chapter 2: Study of fragments from works of art

Content

Abstract

In this Chapter, the results obtained by analyses performed on samples taken from eight works of art (6 panels and 2 wall paintings) are presented. Different types of degradation compounds were identified and a similar multi-layered structure for the degradation products was observed on cross-sections prepared from these fragments. Some of these results (from a painting by Rubens and the fresco from the Spanish Monastery of Pedralbes) were published in the Journal of Analytical Atomic Spectrometry *[M. Radepont, 2011]*.

2.1. Previous studies of works of art

Since the beginning of the use of analytical instruments in the field of cultural heritage, degraded works of art were studied with the intention that the identification of the degradation compounds would lead scientists to a better understanding of the alteration processes of the materials involved.

The degradation of red mercury sulfide has been observed on several types of support, but the phenomenon seems more rare on panels than on wall paintings. On objects, very few alterations have been reported. Despite these episodic changes, different research groups studied this form of degradation and published their results. Some of these previous reports are presented below.

Before understanding the reactions responsible for the degradation of red mercury sulfide, Pliny the Elder gave in his *Naturalis Historia* advice to improve the protection of works of art against alteration: "*the remedy is to cover the wall, when it has become dry, with a mixture of Punic wax and oil, which is to be laid on while hot with hair brushes. It is to be heated again by burning gall nuts, until the surface melts; it is then smoothed down with tapers, and afterwards rubbed with linen cloths, as marbles are cleaned and polished*" *[Pliny the Elder, Naturalis Historia].*

Even if the degradation of red mercury sulfide has been observed centuries ago, analyses of this alteration in works of art are challenging and do not systematically allow the clear identification of the degradation compounds. As an example, on a stone statue from the 14th century in Bourges (France) which presents black crusts on the red area, only mercury and sulfur were identified by SEM-EDX *[C2RMF report n°3143]*. Several paintings from the Courtauld Gallery (United Kingdom) also presents this degradation, but nothing more than copper impurities were found in a sample taken from the "Estouteville Triptych" (ca 1360-1367) containing blackened vermilion *[R. Grout, 2000]*. With the use of analytical techniques allowing identification of several elements or structures, different hypotheses appeared in publications to explain the degradation of red mercury sulfide.

2.1.1. Metacinnabar

Degraded works of art often appear black and elemental analyses most of the time only identified Hg and S in altered vermilion areas. Thus, the transformation of cinnabar into metacinnabar (β-HgS) was often considered as being responsible for this alteration. This diagnosis is still present in recent publications. Baraldi et al. analyzed black dots on the surface of cinnabar on a fresco from the 1st century AD in Reggio Emilia (Italy), and specified their results as follows: "*None of these attempts* [Raman spectroscopy, XRD] *could reveal the sure presence of metacinnabarite […]. Metacinnabarite can so be attributed, into these matrixes, just for the dark color*" *[P. Baraldi, 2007]*. Indeed, in the Raman spectra they published, the background difference between the red and black spots is so important that it is difficult to differentiate these areas and clear identify α- or β-HgS. Gettens et al., when introducing mercury sulfide and its properties, also said *"Both rubbing (trituration) and exposure to light promote the conversion* [of vermilion] *to metacinnabar" [R.J. Gettens, 1993].* This transformation was also referred to in another recent book : *"Le cinabre est un matériau stable dans l'huile, mais, utilisé avec un liant aqueux ou à l'œuf, il peut noircir : le cinabre rouge devient alors du métacinabre noir" [S. Bergeon, 2009]*. The confusion is still present in multiple minds, but metacinnabar was only identified in a few cases *e.g.* by XRD on mural paintings from the 16th century in the church of Sucevita (Romania) *[I. Istudor, 2007]*. To our knowledge, no other sign of the presence of metacinnabar on degraded works of art have been reported.

2.1.2. Chlorine-based compounds

The first clues on the factors responsible for the degradation of mercury sulfide in works of art came from element analysis techniques. Indeed, SEM-EDX and XRF allowed identifying chlorine on paintings from the 14th to the 17th century such as those of Bernardo Daddi from the Courtauld Gallery (1348, United Kingdom) *[M. Spring, 2002]*, Giovanni A. Boltraffio from the Louvre (1500, France) *[M. Cotte, 2009]* or Pieter de Grebber from Huis Ten Bosch Palace (1650, Netherlands) *[K. Keune, 2005]*. Next to element analysis techniques, Raman spectroscopy clearly allowed the identification of calomel on a 15th century panel

from the National Gallery London (UK) by Benozzo Gozzoli, which also seemed to be protected from degradation in some areas by the presence of red lake *[M. Spring, 2002]*. SIMS allowed Keune et al. to presume the presence of $HgCl_2$, corderoite and calomel on two paintings from the 17th century by Peter Paul Rubens and Christiaan van Couwenberg *[K. Keune, 2005]*. Degradation of wall paintings from the Pompeian area was also studied by several research groups and gave interesting results concerning chlorine containing compounds. Next to cinnabar (α-HgS), calomel (Hg_2Cl_2) was identified by Raman spectroscopy and XRF on a fresco from 80-40 BC buried until 2006 and which began to deteriorate after a few years in contact with the atmosphere *[M. Maguregui, 2009]*. With µ-XANES, Cotte et al. identified chlorine compounds on grey altered regions of Pompeian wall paintings *[M. Cotte, 2006]*, on Catalan alterpieces of the Gothic period *[M. Cotte, 2008]* and on a 16th century painting by Boltraffio *[M. Cotte, 2009]*; these compounds appeared to be calomel (Hg_2Cl_2) and corderoite (α-$Hg_3S_2Cl_2$).

2.1.3. Sulfate-based compounds

Next to chlorine compounds, another phase that is commonly identified on degraded works of art is gypsum ($CaSO_4.2H_2O$); it is composed of white crystals in its natural form. Below are presented few of the numerous examples of identification of this product on buildings or wall paintings.

On Pompeian frescoes painted before 79AD, gypsum was identified by µ-XANES *[M. Cotte, 2006]*. The same compound was also found on frescoes in a church from the 15th century in Asturias (Spain) analyzed by Raman spectroscopy *[M. Perez-Alonso, 2004]*. Anhydrite ($CaSO_4$) was observed next to the original pigments by Raman spectroscopy on a 16th century fresco from Lemoniz (Spain) *[M. Perez-Alonso, 2006]*. It has to be noted that some of the sulfates found at the surface of frescoes could originate from the intentional application of plaster to (re)cover the wall paintings.

2.2. Results of analyses performed on works of art

In order to understand the chemical processes responsible for the alteration of mercury sulfide, original works of art containing this pigment were studied and degradation compounds were analyzed.

2.2.1. "The Adoration of the Magi", P.P. Rubens

The first original artwork studied was "The Adoration of the Magi" by Peter Paul Rubens (1577-1640). This masterpiece, exhibited in the Royal Museum of Fine Arts (KMSKA) of Antwerp (Belgium), is an oil painting executed on a wood panel (447 x 336 cm^2) in 1624. On the left part of the painting, the King Melchior in his red coat with golden embroidery is offering gold to Maria (Figure 2.1a).

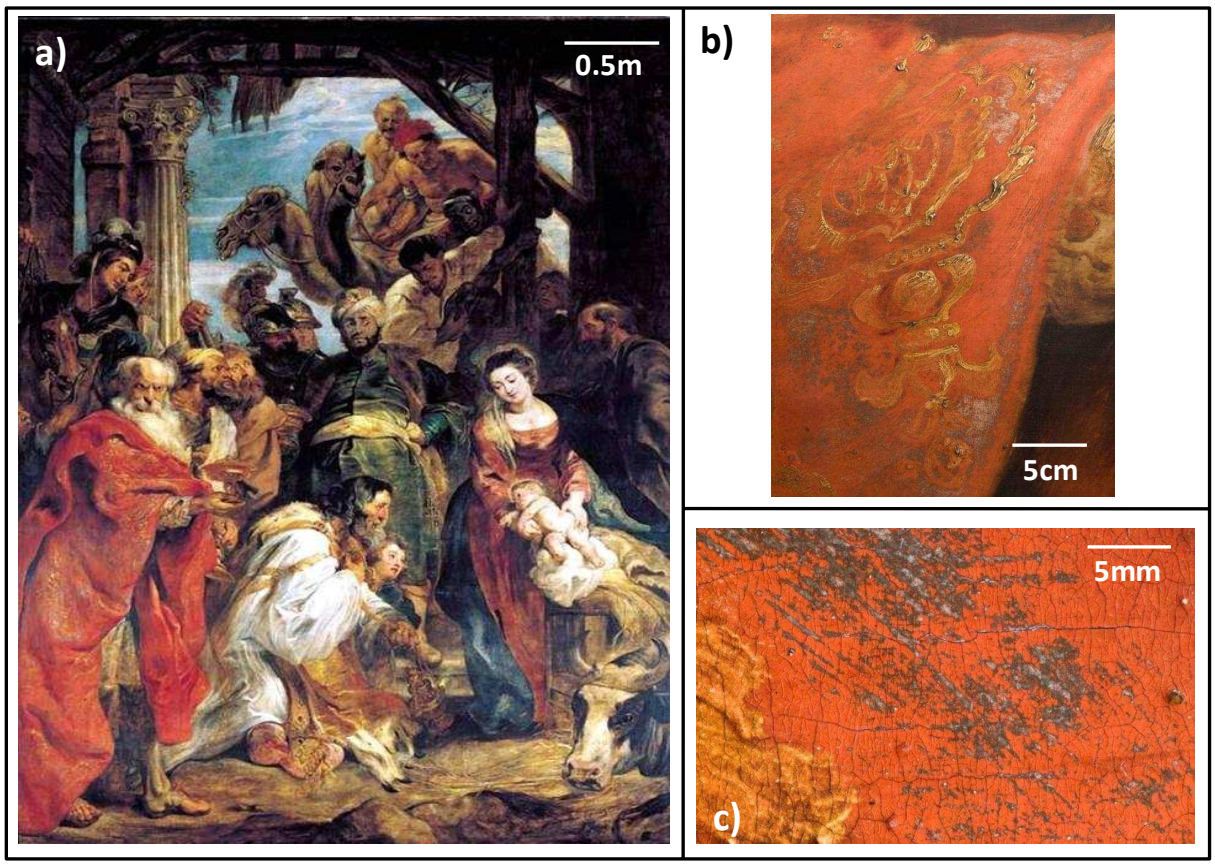

Figure 2.1.: a) *"The Adoration of the Magi", Peter Paul Rubens;* ***b)*** *and* ***c)*** *are enlargements of grey areas from the red coat.*

When carefully observing the painting, it is possible to notice that the red vivid color of this coat is soiled by grey spots in some areas (see enlargements of one of these areas in Figure 2.1b and c). Degraded areas of this panel show well defined parallel lines, similar to the ones made by brushes.

In order to perform micro-analyses of the superficial and internal layers, sampling of two fragments from degraded areas in the sleeve of the red coat on the left of the painting was allowed and performed thanks to Lizet Klaassen and Geert Van der Snickt, respectively conservator from the KMSKA and conservation scientist at the University of Antwerp. As degradation layers in these samples appeared to be micrometer-sized, synchrotron radiation based analytical techniques were chosen to study the alteration. These fragments (named below **Ru-A** and **Ru-B**) were observed and analyzed by micro-X-ray fluorescence/micro-X-ray absorption near edge spectroscopy (μ-XRF/μ-XANES) and micro-X-ray diffraction (μ-XRD) at the European Synchrotron Radiation Facilities (ESRF, Grenoble, France), respectively at beamlines ID21 and ID18F, as part of experiment n°EC442, and some of these results are published *[M. Radepont, 2011]*.

First sample: Ru-A

This sample has a triangular form and its surface is purple-light grey with some intact pigment visible on the edge (Figure 2.2a). This sample was not embedded in order to analyze its surface. Its multi-layered structure shows preparation layers consisting of calcite and lead white, and above, the red original pigment, mercury sulfide, which seems to be finely ground. Above this layer, a fine purple-grey layer is assumed to contain degradation product derived from α-HgS (Figure 2.2b).

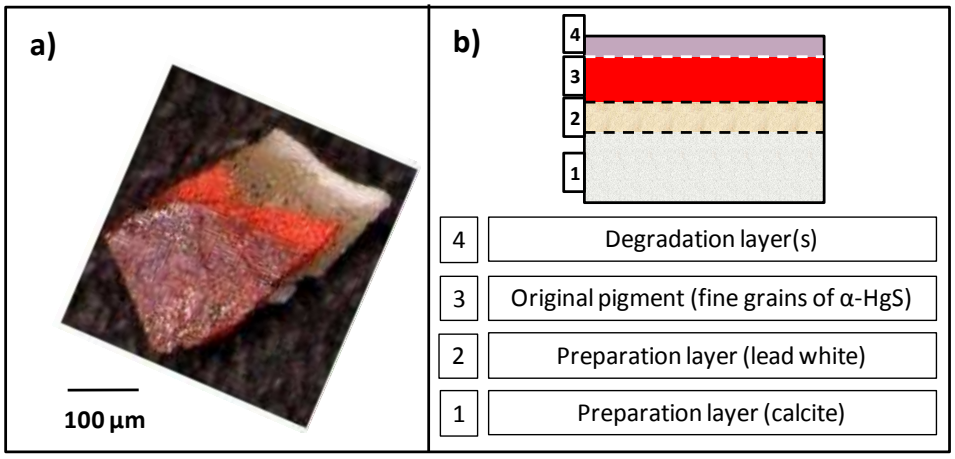

Figure 2.2.: a) *Visible picture of sample Ru- A taken from "The Adoration of the Magi", Peter Paul Rubens;* ***b)*** *Schematic representation of the multi-layered structure of sample Ru-A.*

First, elemental maps were acquired by µ-XRF at 2.85 keV in order to obtain a global view of the distribution of different elements present, and especially for chlorine and sulfur, which, according to the literature, seem to play a role in the α-HgS degradation. Among different elements, maps of mercury, sulfur and chlorine were obtained (Figure 2.3c). When compared to the visible image of the sample, the map of mercury shows that the area with a higher intensity (in black) of Hg corresponds to the edge where the red unaltered pigment is visible. But contrarily to what could be presumed on the mercury sulfide area, sulfur does not present the same distribution as mercury. Sulfur is present in higher concentration in the bottom left area of the map, corresponding to the purple-grey area of the sample. Concerning chlorine, the highest intensity for this element is visible in the intermediate area between the "high mercury" and the "high sulfur" zones. These three areas can also be discerned in the RGB composite map (Figure 2.3b); that shows in the top part a red area, corresponding to the original pigment, then a purple area which represents a mixture between mercury and chlorine maps, and finally at the bottom left of the image a green area with more sulfur than mercury or chlorine. To identify the different compounds present in each area, µ-XANES analyses were carried out as this technique allows obtaining structural information.

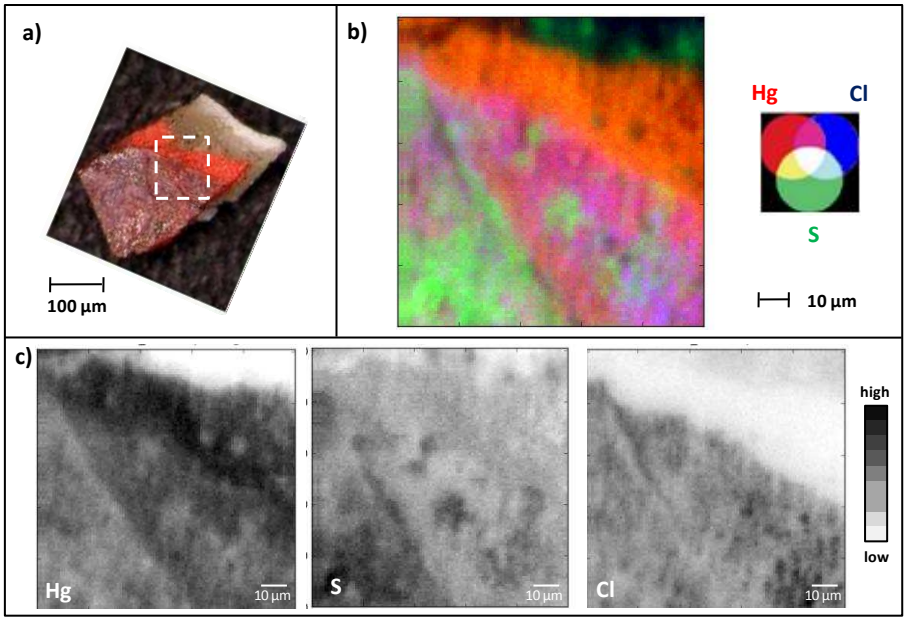

Figure 2.3.: a) *Visible image of sample Ru-A;* ***b)*** *Combination of three elemental maps obtained via µ-XRF by scanning the area represented in a) by the dashed white rectangle;* ***c)*** *Elemental maps of Hg, S and Cl giving the combination b).*

µ-XANES analyses at the sulfur K-edge were performed at twelve locations on the fragment along a horizontal line going from the right (intact pigment) to the left (purple-grey area) (cf. Figure 2.4a). By comparing the unknown XANES spectra to reference data (acquired during the same experiment) and via the calculation of linear combinations, it is possible to obtain the composition of the area analyzed. The control of the fit given by these calculations will help to identify missing compounds and to validate the results. In this case, spectra of these points were compared to S-containing reference compounds; three seemed to correspond to the composition of the analyzed points. Indeed, for points 1 and 2, spectra similar to the one of α-HgS (white line at 2.4716 keV represented by a full line in Figure 2.4b) are obtained, corresponding to the fact that these points are situated in the area of the original pigment. In the point 2, a small additional peak shows a correspondence with the spectrum of a sulfate ($CaSO_4.2H_2O$). The peak intensity of the sulfate peak (white line at 2.4825 keV, represented by a dashed line in Figure 2.4b) is increasing when going from point 3 to point 12. Among these ten points, the position of the peak of reduced sulfur is shifting from 2.4716 to 2.4726 keV; the latter can be interpreted as the white line of α-$Hg_3S_2Cl_2$, the reference compound, corderoite (see position of the lowest peak for spectra of points 5, 9 and 12 on Figure 2.4b).

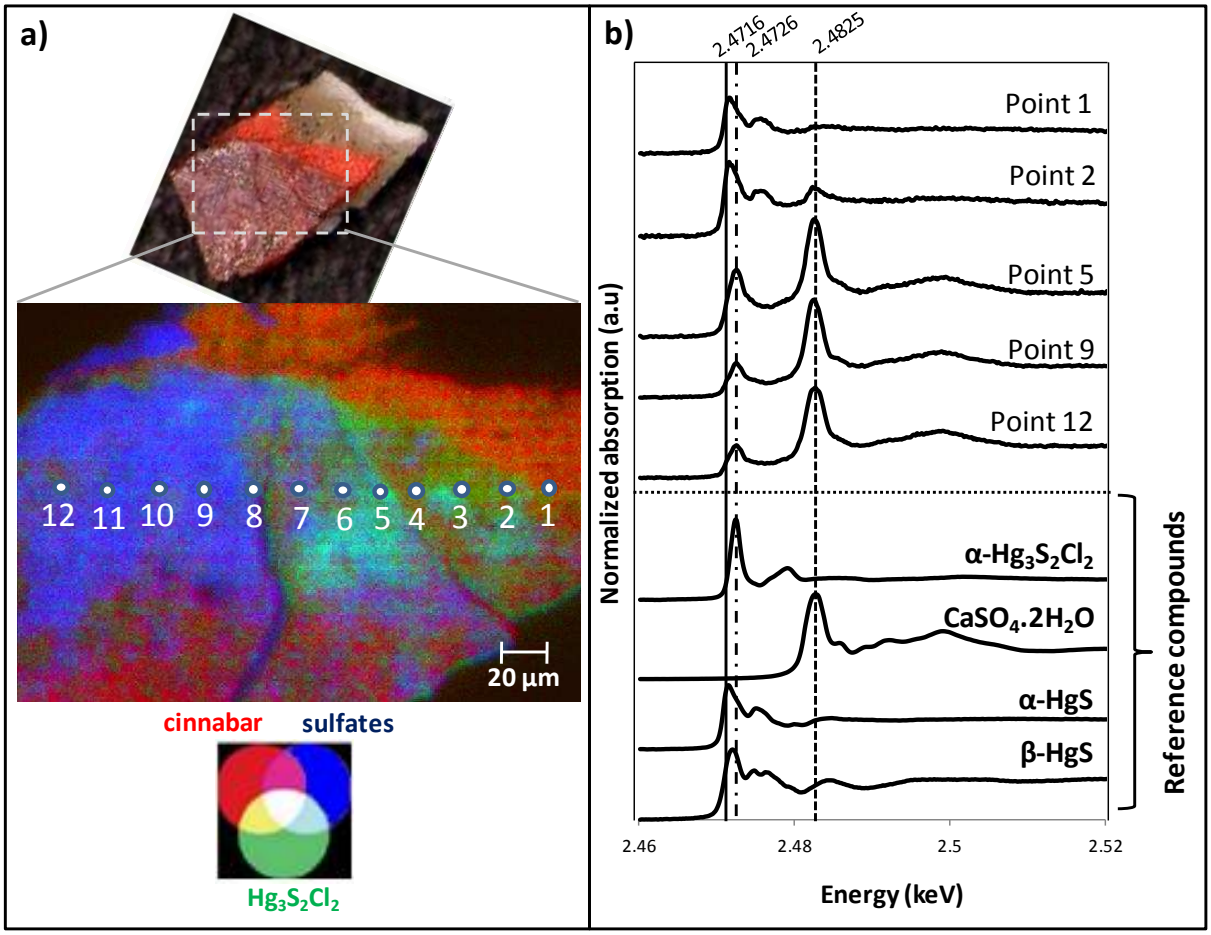

Figure 2.4.: a) *RGB composite of three S-K_α intensity maps representing sulfur acquired at 2.4716 keV (cinnabar, red), 2.4726 keV ($Hg_3S_2Cl_2$ compounds, green) and 2.4825 keV (sulfates, blue), corresponding to the dashed rectangle in the visible image of sample Ru-A;* ***b)*** *µ-XANES spectra of some of the twelve points in the map in a) compared to spectra of reference compounds (metacinnabar, cinnabar, gypsum, corderoite).*

From these considerations, it appears that sample Ru-A contains at least three different sulfur-based species having a maximum absorption at 2.4716, 2.4726 and 2.4825 keV, respectively for cinnabar, $Hg_3S_2Cl_2$ compounds and sulfates. From this hypothesis, µ-XRF mapping of sample A was performed at the three relevant energies to obtain their localization. The resulting image presents the three presumed areas with the original cinnabar pigment in red, an intermediate area with chlorine containing compounds in green, and on the left a sulfate-rich area in blue (Figure 2.4a). See Appendix B.g. for the complete calculations employed to obtain this type of image.

Second sample: Ru-B

The second sample taken from the same Rubens' painting is a rectangle with black areas at the surface (Figure 2.5a). This sample was not embedded in order to be able to analyze its surface. As for the sample Ru-A, the multi-layered structure presents preparation layers consisting of calcite and lead white, and on top of these the red original pigment. Above this layer, again a black layer (Figure 2.5b).

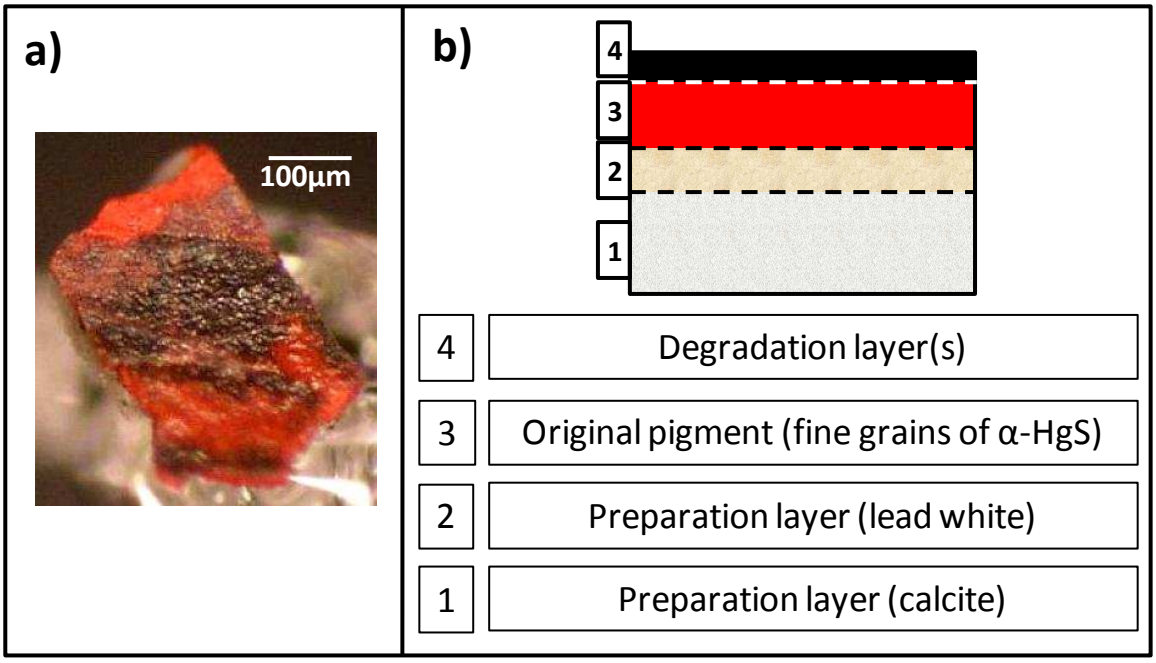

Figure 2.5.: a) *Visible picture of the sample Ru-B taken from "The Adoration of the Magi", Peter Paul Rubens;* ***b)*** *Representation of the multi-layered structure of the sample Ru-B.*

As for the sample Ru-A, first, elemental maps were acquired at 2.85 keV showing the distribution of different elements, and especially the three relevant ones, mercury, sulfur and chlorine (respectively in red, green and blue in Figure 2.6b). In the RGB composite of these three maps, next to the mercury sulfide area (in yellow), which corresponds to an area where the original pigment is not altered, a very light blue corner is visible, corresponding to the presence of chlorine, sulfur and mercury. In order to verify the composition of this area, µ-XANES spectra were acquired at the chlorine K-edge at 5 locations along a horizontal line going from the right to the left (see Figure 2.6b). When comparing them with spectra of

reference compounds, it is possible to see that the first peak of each spectrum is at the energy corresponding to the white line of all mercury chlorine containing compounds (Figure 2.6c). But the lack of features after the principal peak makes the identification of specific phases hard and the fit not reliable. It is possible to see that from the point 1 to the point 5, as the analyses are going from the extremity of the sample towards the unaltered pigment, the intensity of this first peak is decreasing. This suggests that mercury chlorine containing compounds are more concentrated at the extremity of the sample than in the center (corresponding to an unaltered area); this is coherent with the visual aspect of this area of the sample.

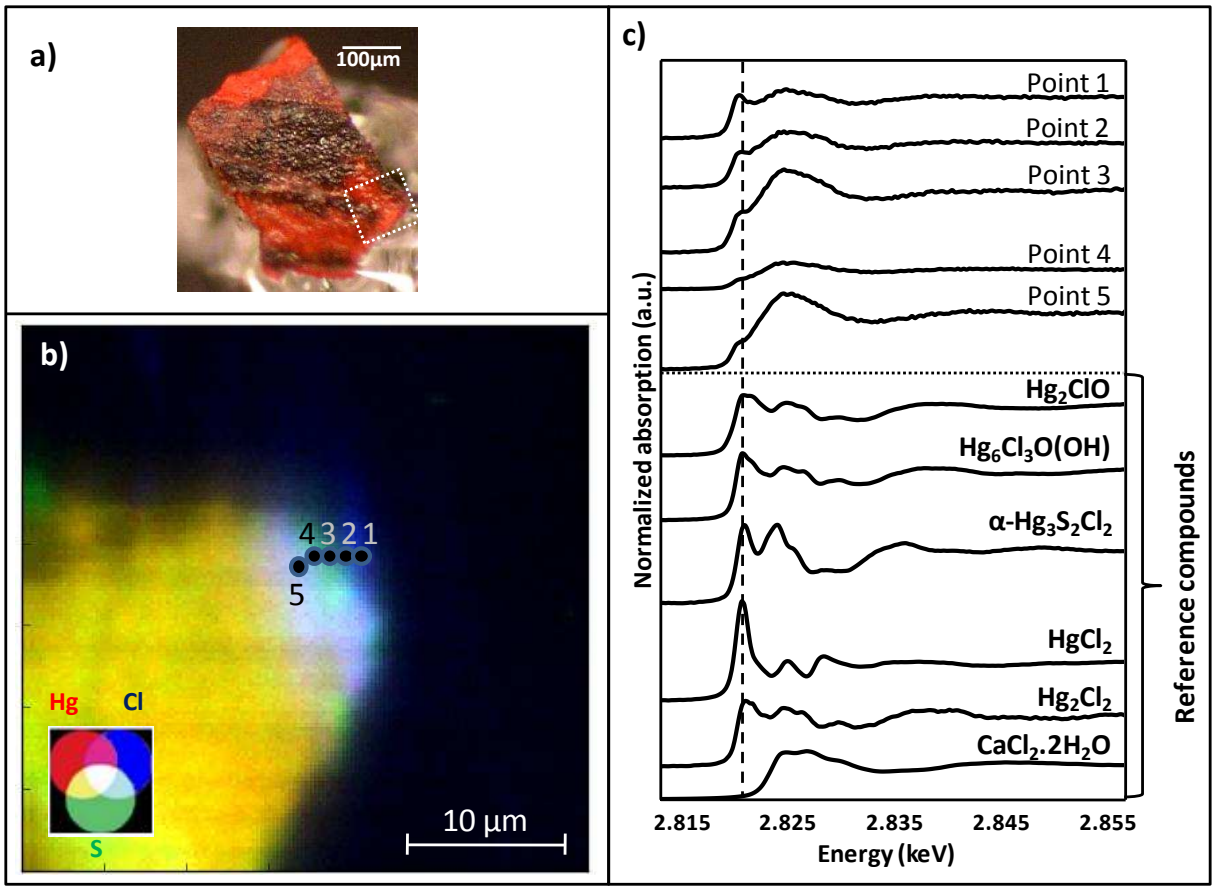

Figure 2.6.: a) *Visible image of sample Ru-B;* ***b)*** *RGB composite of three µ-XRF maps of mercury (red), sulfur (green) and chlorine (blue) of the area represented in a) by the white dashed square;* ***c)*** *µ-XANES spectra of five points indicated in b) compared to spectra of reference compounds ($CaCl_2.2H_2O$, Hg_2Cl_2, $HgCl_2$, α-$Hg_3S_2Cl_2$, $Hg_6Cl_3O(OH)$ and Hg_2ClO). The dashed line corresponds to the white line of Hg-Cl containing compounds (2.8232 keV).*

To better identify the phases present in the degradation seen at the surface of this painting, µ-XRD experiments in transmission mode were performed on sample Ru-B. Via to these analyses, next to preparation layers and original pigment, two compounds were identified: calomel (Hg_2Cl_2) and a new one, never found in works of art before, kenhsuite (γ-$Hg_3S_2Cl_2$) (see d-spacing values in Appendix B.h). These phases appear to be part of the alteration of mercury sulfide. Concerning the localization of the different phases, maps are obtained by fitting data from diffractograms using reference files, and considering the intensity distribution of the various phases identified. First, the sample was oriented in such a manner that the primary beam (28 keV) was perpendicular to the original paint surface, allowing to record the depth distribution of chlorine containing compounds, calomel (Hg_2Cl_2) and kenhsuite (γ-$Hg_3S_2Cl_2$), of the original pigment, cinnabar (α-HgS), and of preparation and ground layers, hydrocerussite ($(PbCO_3)_2.Pb(OH)_2$) and calcite ($CaCO_3$) (Figure 2.7a). Next to these phases, another crystalline compound, still unidentified, presented diffraction intensity barely discernable above the background level. In order to have a better view of the localization of each phase, the side of the same fragment was scanned by the same beam to obtain the relative in depth abundance of these phases after fitting data with reference files. In the figure obtained, the three degradation products (calomel, kenhsuite and the unknown phase) were co-localized in a layer above the cinnabar one. Next to these layers, the distribution of hydrocerussite and calcite is also clearly represented in this plot (Figure 2.7b).

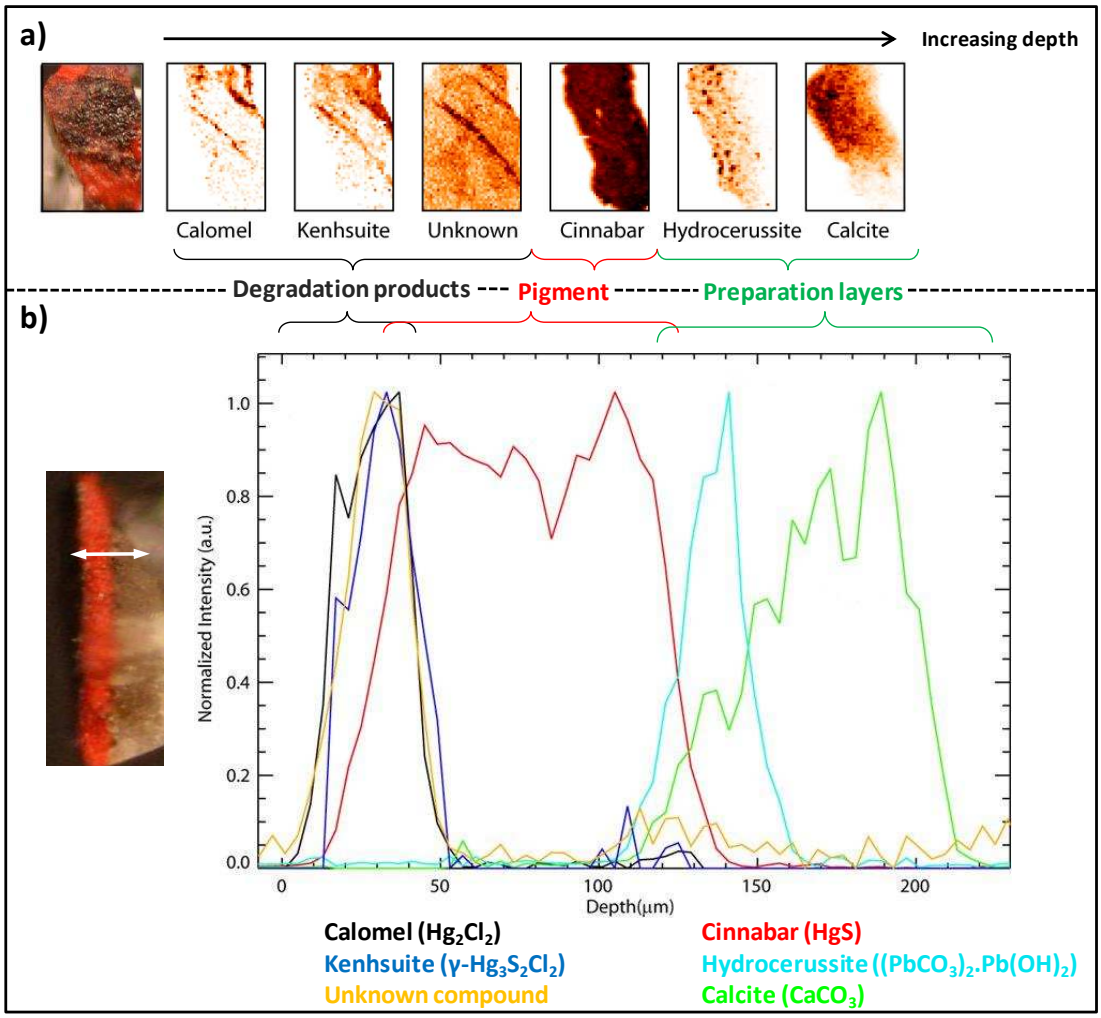

Figure 2.7.: a) *μ-XRD maps (280 x 300 μm²) of the surface of sample Ru-B (visible image on the left) showing the distribution of calomel (Hg_2Cl_2), kenhsuite (γ-$Hg_3S_2Cl_2$), an unknown phase (d = 7.1438 Å; d = 2.1922 Å), cinnabar (α-HgS), calcite ($CaCO_3$) and hydrocerussite ($(PbCO_3)_2.Pb(OH)_2$);* ***b)*** *Plot of the relative abundance of each compound identified in maps a) by analyzing the cross-section of sample Ru-B (visible image on the left indicating beam scanning path) – with maximum of each component normalized to unity.*

These results represent the first identification of kenhsuite (γ-$Hg_3S_2Cl_2$) in a degraded work of art. In previous studies, $Hg_3S_2Cl_2$ compounds were already detected but systematically identified as corderoite (the α-form of $Hg_3S_2Cl_2$). Kenhsuite is considered to be a metastable polymorph of corderoite and is not a commonly encountered material. Unfortunately, we could not find any reference mineral which would have allowed the acquisition of reference XANES or Raman spectra.

2.2.2. Gothic wall painting in Pedralbes

The second artwork analyzed is a wall painting in the Gothic church of the monastery of Pedralbes (Barcelona, Spain), a community founded in 1326 by Queen Elisenda de Montcada. In a later period, the walls were covered with plaster, to hide painting alteration or to follow new fashion, which was later again partially removed, resulting in areas of the painting covered with traces of gypsum. When the restoration of the church began in 2007, a damaged flower decoration appeared from under the residual whitewash, with a red background covered by a grey black superficial layer (Figure 2.8).

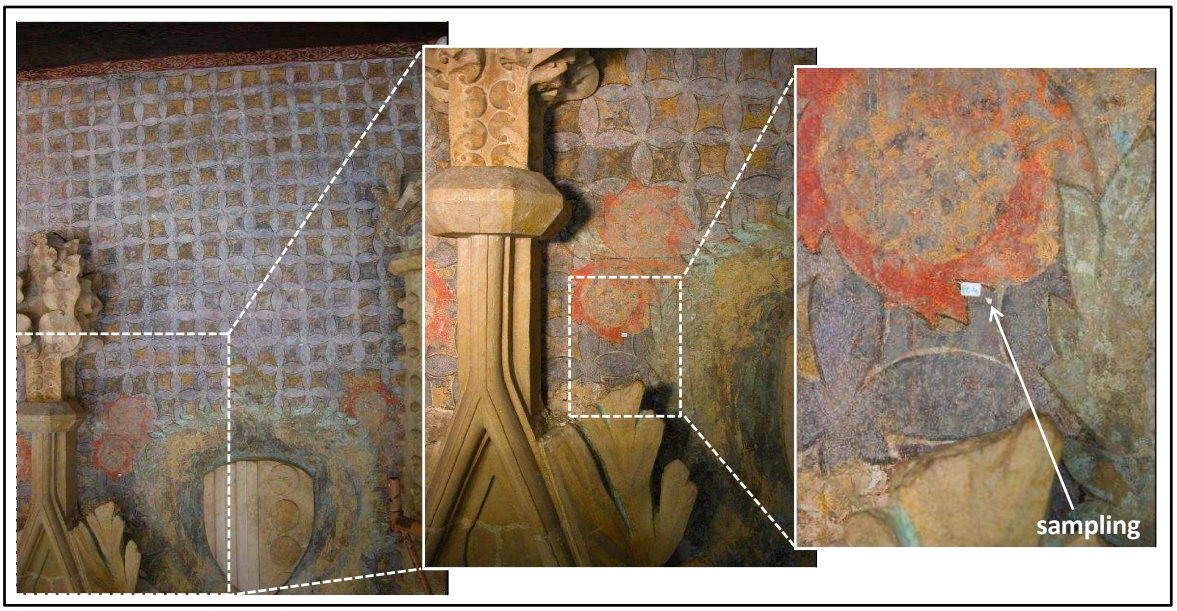

Figure 2.8.: *Visible pictures of the wall painting from Pedralbes (Spain) with different enlargements showing on the right image the localization of one the sampling made.*

Multiple samples were taken from this degraded painting and gently provided by Javier Chillida, private curator in Spain. Previous results of analyses performed on these fragments were published by Cotte et al. *[M. Cotte, 2008]*. The results obtained on Rubens' samples encouraged us to reconsider results from these first analyses and complete them with µ-XRD studies. The sample chosen **(Pe-W)** originates from a black area of the painting (see the sampling localization on the right image of Figure 2.8).

After embedding and preparing a cross-section from sample Pe-W, the multi-layered structure of the painting was observed. On the optical image of these cross-sections (Figure 2.9a), it is possible to observe a thick preparation layer consisting in calcite, and above, the red original pigment, mercury sulfide. Above this layer, a thick black layer is assumed to result from degradation of α-HgS. On top of the sample, a white layer is present that is possibly composed of rests of the plaster that was intentionally applied on the wall painting (Figure 2.9b).

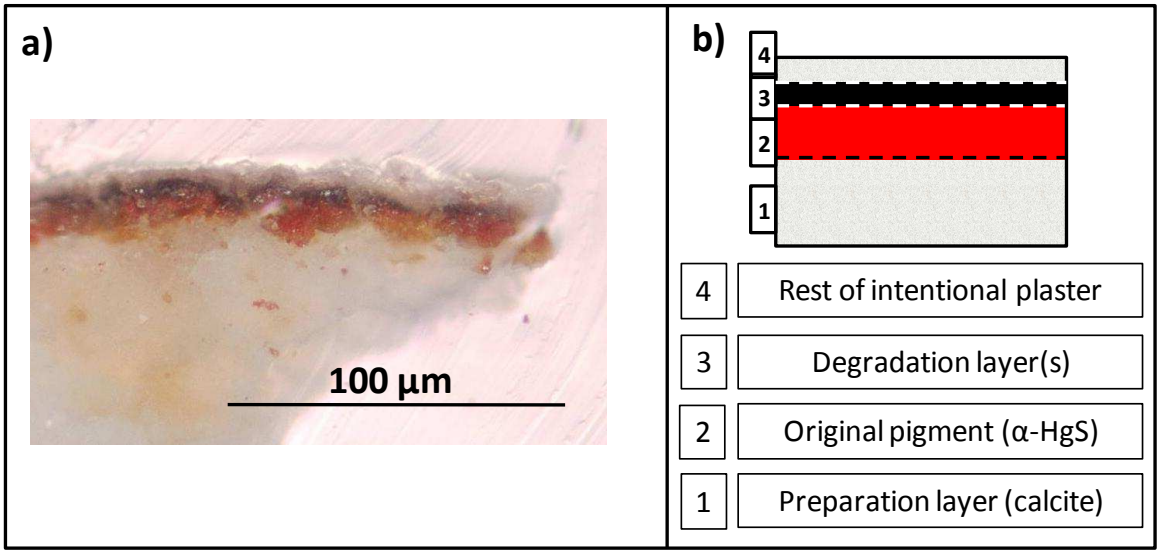

Figure 2.9.: a) *Visible picture of the cross-section from sample Pe-W taken from a wall painting in the Monastery of Pedralbes, Spain;* ***b)*** *Representation of the multi-layered structure of the sample.*

As for the Rubens' samples, first, elemental maps were acquired by µ-XRF at ID21 (ESRF, Grenoble) at 2.86 keV, showing the distribution of mercury, sulfur and chlorine (Figure 2.10b). In these maps, sulfur appears to be present in higher concentration in the top part of the sample, which could correspond to the sulfates of the residual plaster while areas with a higher chlorine content are situated in the middle of the map, in the same area as mercury. To verify these localizations, a composite map of these three maps was prepared, with mercury in red, sulfur in green and chlorine in blue (Figure 2.10c). On this image, sulfur is clearly present without any mercury or chlorine at the top of the sample. Between this thick layer and the one of cinnabar (in light orange), a thin pink layer is discernible, which

corresponds to the co-localization of mercury and chlorine. Below, some blue areas show chlorine without any mercury or sulfur.

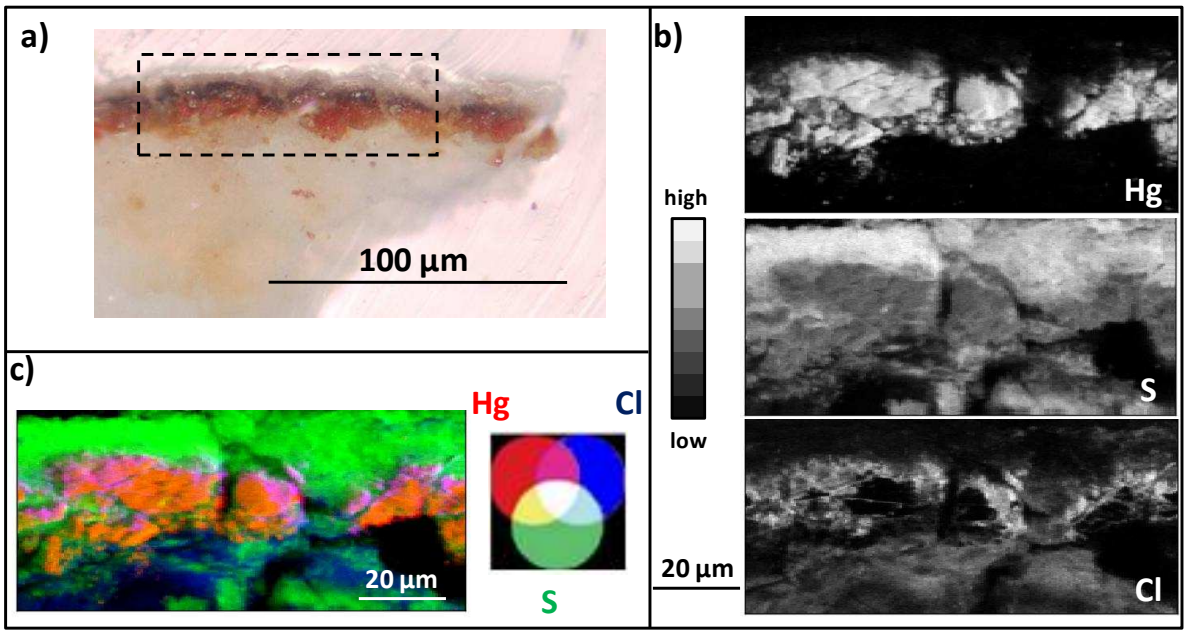

Figure 2.10.: a) *Visible picture of the cross-section prepared from sample Pe-W;* ***b)*** *µ-XRF elemental maps acquired at 2.86 keV showing the distribution of mercury, sulfur and chlorine on the area represented by a dashed rectangle on a);* ***c)*** *Composite RGB image of the three maps shown in b): mercury (red), sulfur (green) and chlorine (blue).*

µ-XANES analyses at the sulfur K-edge were performed on six locations of the sample following a vertical line going from the top (plaster) to the bottom (intact pigment) (cf. Figure 2.11a). The spectra of these locations were compared to sulfur containing reference spectra (Figure 2.11b). In these references, as for the Rubens samples, three seemed to correspond to some of the analyzed points. For the point A, the spectrum is similar to that of gypsum $CaSO_4.2H_2O$ (white line at 2.4825 keV represented by the third dotted line in Figure 2.11c), which corresponds to the residual plaster present remaining on some areas at the surface of the painting. In the point B, a small peak with a lower energy is showing a possible correspondence with the spectrum of corderoite (white line at 2.4726 keV represented by the second dashed line in the Figure 2.11c). This peak is present in the next 14 µm. At point F, the peak at a lower energy appears to be more related to the presence of cinnabar (α-HgS) (white line at 2.4716 keV represented by the first dashed line in Figure 2.11c), which is relevant since point F is in the red layer.

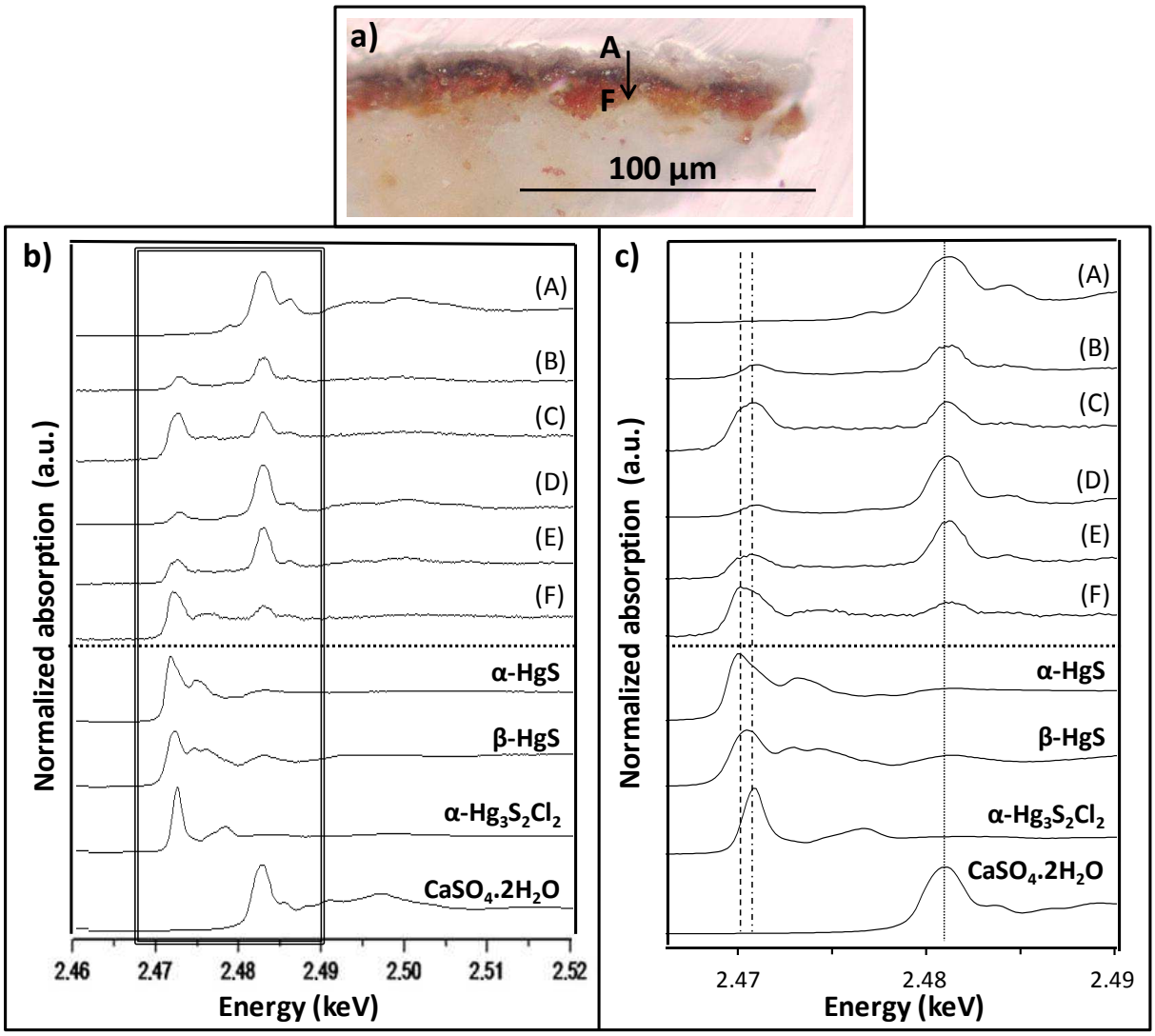

Figure 2.11.: a) *Visible picture of the cross-section prepared from sample Pe-W;* ***b)*** *µ-XANES spectra at the sulfur K-edge (2.46 to 2.52 keV) of six points analyzed along the arrow indicated in a);* ***c)*** *Enlargement of the spectra shown in b) from 2.467 keV to 2.49 keV with three lines indicating the white lines of cinnabar (α-HgS), corderoite (α-$Hg_3S_2Cl_2$) and gypsum ($CaSO_4.2H_2O$).*

After studying these XANES spectra, µ-XRF imaging of the sample was performed at four relevant energies: 2.4716, 2.4726, 2.4825 and 2.8232 keV, corresponding respectively to the energy of maximum absorption of sulfur in cinnabar, in $Hg_3S_2Cl_2$ compounds, in sulfates, and of chlorine in mercury chlorine containing compounds (Figure 2.12a). First, the combination of the three maps of cinnabar (red), mercury chloride compounds (green) and $Hg_3S_2Cl_2$ compounds (blue) was calculated. In the image shown in Figure 2.12b, and even better in the enlargement of the area represented by the white rectangle, a stratigraphy of

the degradation is clearly visible. Indeed, above the cinnabar layer, a thin layer of $Hg_3S_2Cl_2$ compounds is present, and on top of the sample, a thicker layer of mercury chloride compounds. A second combination is shown in Figure 2.12c, with the three maps of cinnabar (red), $Hg_3S_2Cl_2$ compounds (green) and sulfates (blue). Here, the $Hg_3S_2Cl_2$ layer is still visible, below a very thick layer containing a high amount of sulfates, which probably correspond to the residual plaster.

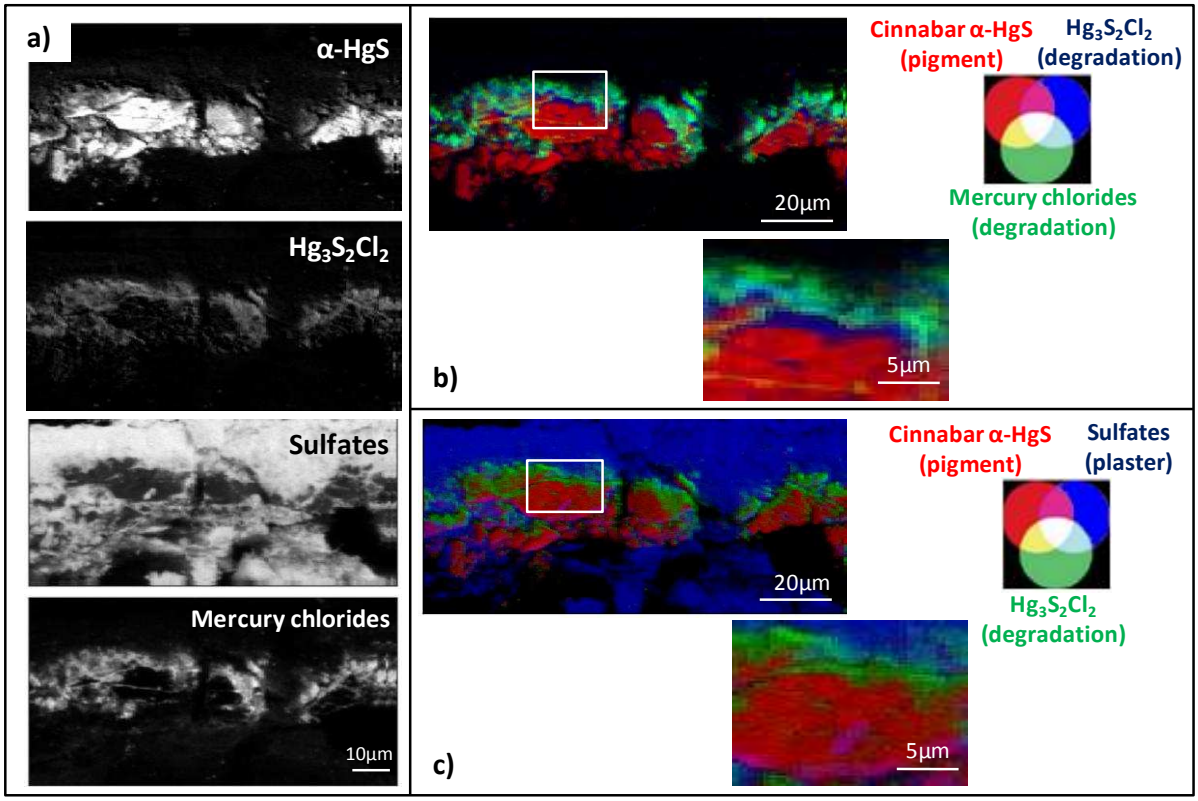

Figure 2.12.: a) *µ-XRF maps corresponding to sulfur at 2.4716 keV (cinnabar α-HgS), at 2.4726 keV ($Hg_3S_2Cl_2$ compounds), at 2.4825 keV (sulfates) and chlorine at 2.8232 keV (mercury chlorine containing compounds);* ***b)*** *RGB composite of maps of α-HgS (red), mercury,chlorine compounds (green) and $Hg_3S_2Cl_2$ (blue) with an enlargement corresponding to the white rectangle;* ***c)*** *RGB composite map of α-HgS (red), $Hg_3S_2Cl_2$ (green) and sulfates (blue) distributions with an enlargement corresponding to the white rectangle.*

To arrive at a better identification and localization of the phases present in the different degradation layers seen in the µ-XRF maps, µ-XRD experiments in transmission mode were performed at ID18F (ESRF, Grenoble) and P06 (PETRA III, Hamburg). Mapping some parts of the cross-section by µ-XRD (see selected areas in Figure 2.13) allows a more specific identification of the phases present in the different layers while also localizing each

phase in relation to the others. Maps are obtained by fitting data from diffractograms recorded at each location in the map using reference files (see d-spacings in Appendix B.h). The maps obtained during the ID18F measurements (Figure 2.13a) show the presence, next to cinnabar (α-HgS), of three chlorine containing compounds, kenhsuite (γ-$Hg_3S_2Cl_2$), corderoite (α-$Hg_3S_2Cl_2$) and calomel (Hg_2Cl_2). Kenhsuite and corderoite appear to be co-localized in a superficial layer above cinnabar. Similar to the μ-XRF results, in Figure 2.13a the combination of three maps shows that, a multi-layered structure is present in the degradation crust, with kenhsuite above the cinnabar layer, and calomel on top of these. A second experiment at P06, Petra III allowed to identify another phase: β-$Hg_3S_2Cl_2$. It is relevant to note that this polymorphous phase of $Hg_3S_2Cl_2$ is present deeper in the original pictorial layer (Figure 2.13b). Furthermore, the preparation layer made of calcite was identified while additionally goethite and weddellite were detected in the cinnabar layer and the presence of sulfates (gypsum and anhydrite) above all these layers, on the top of the cross-section, is clearly visible (Figure 2.13a).

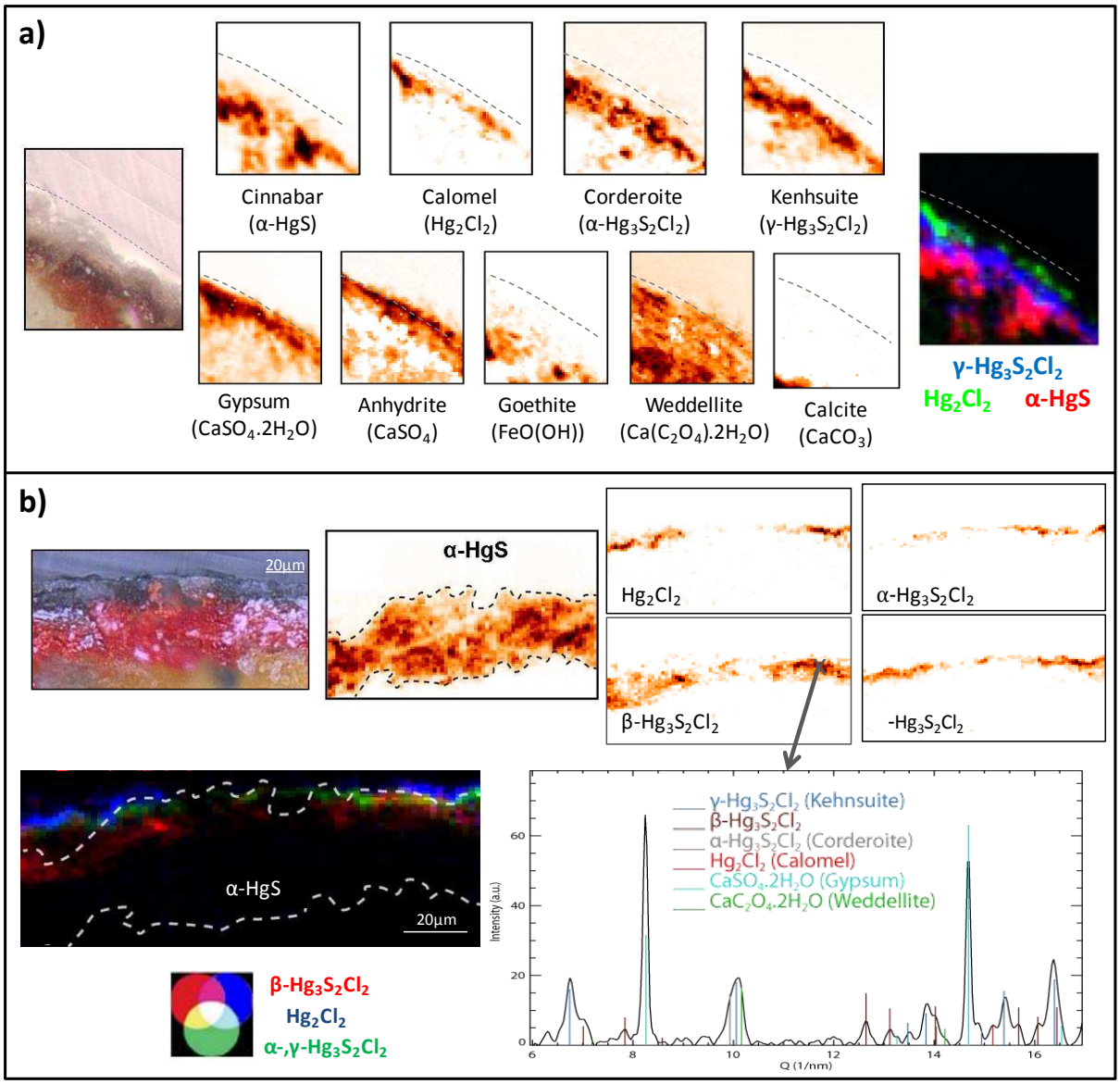

Figure 2.13.: *Results obtained during µ-XRD experiments performed on sample Pe-W:* ***a)*** *ID18F results showing in the area analyzed (visible image shown on the left) the distributions of the phases identified and (on the right) the combination of maps of kenhsuite (γ-$Hg_3S_2Cl_2$) in blue, calomel (Hg_2Cl_2) in green and cinnabar (α-HgS) in red;* ***b)*** *P06 results showing (visible image on the left) the distribution of* some of the phases identified *with (bottom right) the diffractogram corresponding to one pixel of the β-$Hg_3S_2Cl_2$ map (indicated by a grey cross) and (bottom left) the combination of maps of β-$Hg_3S_2Cl_2$ in red, calomel in blue and both corderoite and kenhsuite in green. The dashed lines in this combination correspond to the limitation of the cinnabar layer.*

2.2.3. Pompeian fresco

Pompeian paintings are very famous for their intense colors, but the red pigment used for some frescoes is suffering from darkening. In this study, two fragments coming from a fresco of “Villa Sora” in Torre del Greco, near Pompeii (Italy), were studied. The house was buried during the eruption of the Vesuvius in 79 AD, but some years after their excavation, the cinnabar areas of the frescoes began to darken. The samples studied were important in this study as they represent the two types of degradation seen on works of art: one sample shows predominantly a grey aspect **(Po-G)** while the other acquired a black color **(Po-B)**. These two, large area samples were gently provided by Mario Pagano (Soprintendenza per i Beni Archeologici del Molise) and previous analyses had already been presented in a publication from a collaboration between Marine Cotte and Jean Susini (ESRF), Nicole Metrich (Laboratoire Pierre Süe, CEA-CNRS), Alessandra Moscato, Corrado Gratziu (Universita di Pisa), Antonella Bertagnini (Istituto Nazionale di Geofisica e Vulcanologia) and Mario Pagano *[M. Cotte, 2006]*. These previous results showed that chlorine and sulfur were presumed to be involved in red mercury sulfide degradation. Additional analyses of these samples are presented below.

First, XRD and X-ray photoelectron spectroscopy (XPS) were performed directly on the large samples. Then, micro-samples from each sample were taken, embedded and cut in order to access the multi-layered structure of the degradation. The cross-section coming from the grey sample (Po-G) shows a thin dark layer on its top, whereas the one coming from the black sample (Po-B) presents a thicker degradation layer on top of the degraded area (on the left), and furthermore, a thin dark layer is also visible at the bottom of the cross-section (see Figure 2.14). μ-XRF/μ-XANES analyses at ESRF beamline ID21 (Grenoble, France) were performed on both cross-sections.

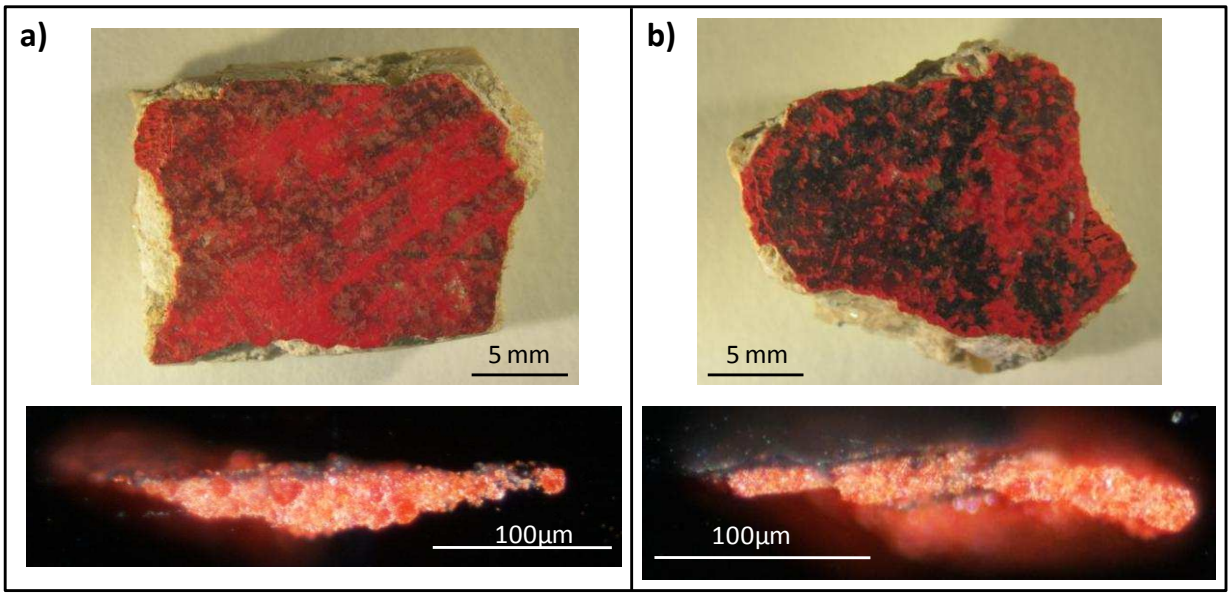

Figure 2.14.: *Visible images of* ***a)*** *sample Po-G and* ***b)*** *sample Po-B taken from a Pompeian fresco (surface and corresponding cross-section).*

Surface analyses on large Pompeii samples: XRD, µ-XRD and XPS

First, non-destructive analyses were performed directly on the large samples. XRD experiments were carried out with a laboratory instrument (at C2RMF, Paris, France) based on a Cu source (8 keV) delivering a 200 µm beam, in reflection mode, at the surface of both samples. In sample Po-G, only cinnabar (α-HgS) and calcite ($CaCO_3$) in the ground layer were identified, whereas in sample Po-B, sulfates (gypsum $CaSO_4.2H_2O$ and anhydrite $CaSO_4$) were also detected.

µ-XRD analyses were performed at ESRF beamline ID18F (Grenoble, France) in transmission mode on the surface of both large samples. For sample Po-B, only cinnabar and calcite were detected, whereas in the sample Po-G, additionally β-$Hg_3S_2Cl_2$ was identified in the degraded areas. In Figure 2.15, next to cinnabar and calcite which combination gives the red diffractogram, the additional peaks (green) correspond to the positions of the peaks of β-$Hg_3S_2Cl_2$ *[Y.V. Voroshilov, 1996]*.

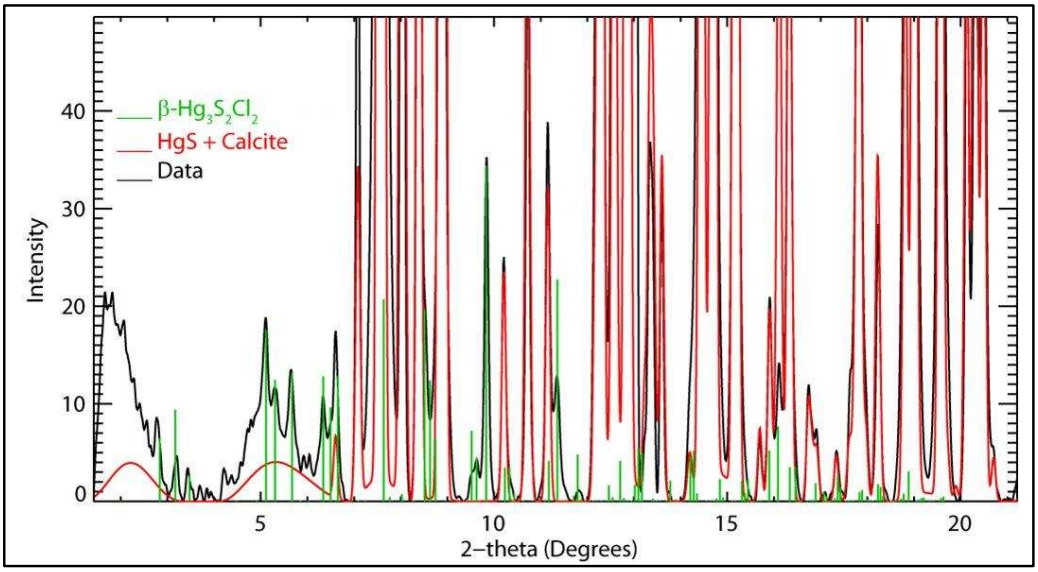

Figure 2.15.: *Diffractogram obtained by μ-XRD on the Pompeian sample Po-G at 28 keV, with in red the diffractogram obtained by combination of cinnabar (HgS) and calcite, and in green the position of the peaks for β-$Hg_3S_2Cl_2$ [Y.V. Voroshilov, 1996].*

The analysis results obtained on the surface of the samples did not help to fully explain their color. The hypothesis of nano-crystallized phases contributing to the visual aspect of the samples was considered. In order to have a better idea of the species present at the very surface of the degradation layer of these samples without disturbance of the mercury sulfide matrix, X-ray photoelectron spectroscopy (XPS) appeared to be a valuable technique. XPS analyses were performed at the Laboratoire de Réactivité de Surface (LRS, Ivry-sur-Seine, France), showing the elements of the first 5 nm of the surface and their oxidation state. These analyses were possible on the Pompeii fragments because of their large size and the presence of homogeneous areas several mm² in size. Next to the two degraded samples, for comparison purposes, also a non-altered sample from the same fresco was analyzed. The main drawback of this method is its sensitivity to any possible superficial pollution of the sample. If contamination compounds are present in the first 5 nm, it is no longer possible to obtain information from the material underneath this superficial layer. In the study of the Pompeii samples, even after cleaning with ethanol in an ultrasonic bath, carbon coming from aliphatic compounds (i.e. contamination by human handling) was still visible in all the spectra obtained. Especially on sample Po-G, this pollution represented 66 % of the elements identified; thus, for this sample, the results were not considered as relevant. In the non-altered samples, this aliphatic carbon represented 26 % of

the elements identified while in the black sample it was 37; these commonly encountered values for this type of analysis.

On sample Po-B, when comparing results with the non-altered part of the fresco, the relevant change is the relative amount of sulfates. Indeed, the doublet for the S 2p level in mercury sulfide, situated at 163 eV *[D. Lichtman, 1981]*, represents 5.5 % of the total intensities for the non-altered sample and 1.6 % for sample Po-B; for the non-altered sample, the peak for sulfur in its SO_4^{2-} form (as in gypsum), situated at 170 eV, represents 1.3 % of the total intensity and 4.0 % for the sample Po-B (see comparison in Figure 2.16). A very small amount of chlorine (Cl) was detected on both altered and non-altered samples (respectively 0.8 and 1.0 %), possibly due to pollution. These results therefore confirm the presence of sulfates on this degraded fragment of fresco; no other new element (next to Hg^{2+}, CO_3^{2-}, and Ca^{2+}) was detected at the very surface of the alteration layer.

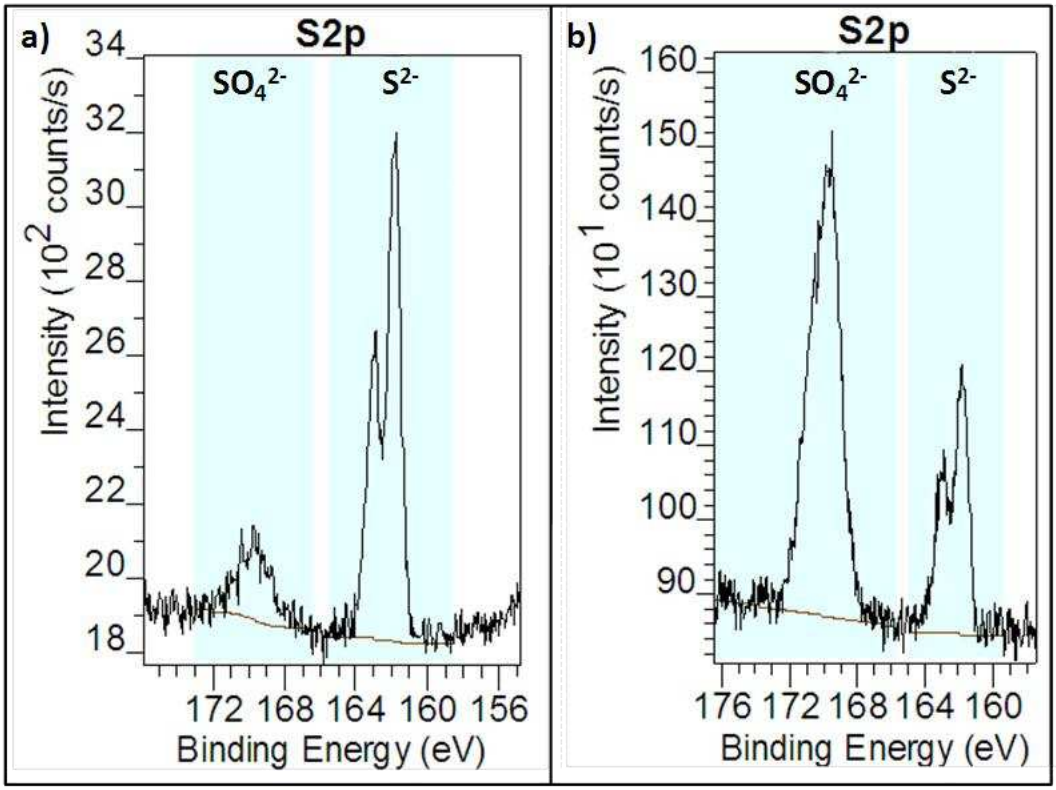

Figure 2.16.: *XPS results of sulfur peak intensity vs. electron binding energy for:* ***a)*** *the non-altered sample compared to* ***b)*** *sample Po-B.*

Cross-section of sample Po-G: µ-XRF/µ-XANES

Sample Po-G shows a thick preparation layer of calcite; on top of this is the original layer of red pigment, composed of large grains of cinnabar and calcite. The latter is the binder material used in the fresco technique. On sample surface, the degradation of cinnabar presents grey streaks (Figure 2.17b).

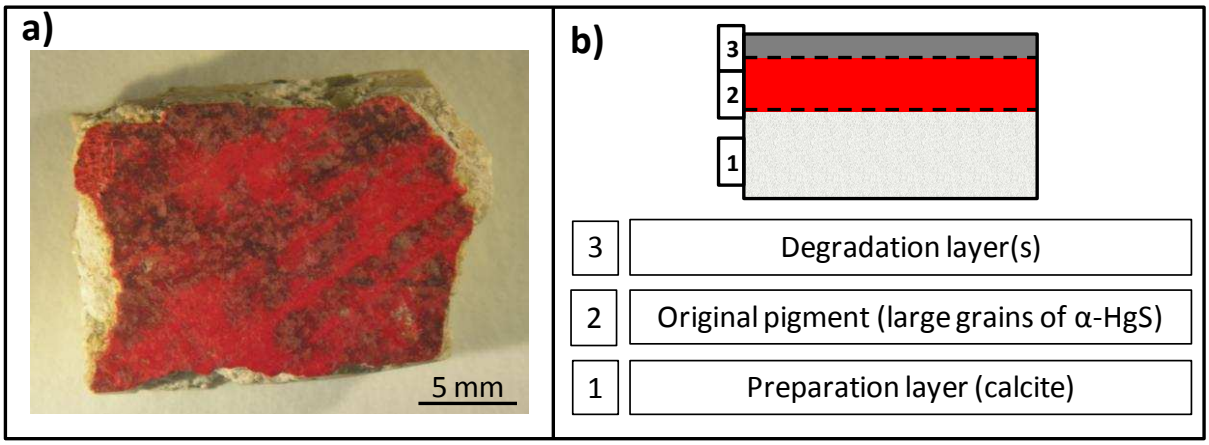

Figure 2.17.: a) *Visible picture of sample Po-G taken from a Pompeian fresco;* ***b)*** *Representation of the multi-layered structure of the sample.*

The composition of the different layers that make up sample Po-G was studied by µ-XRF/µ-XANES. First, elemental maps were acquired by µ-XRF at high energy (7.9 keV) in order to obtain the total signals of all elements of interest. Two relevant RGB composites are shown in Figure 2.18. In the first one (Figure 2.18b), next to large grains of mercury, corresponding to the pigment grains, large calcium-rich grains (assumed to be calcite) are also visible. Indeed, when a fresco is produced, pigments are applied on fresh lime ($Ca(OH)_2$), and the carbonation of this last product leads to the formation of calcite ($CaCO_3$), which acts as a binder in this type of artwork. The distribution of chlorine corresponds in the visible image to the thin grey layer at the top of the cross-section; this is even clearer in the RGB composite of Figure 2.18c. In this image, the presence of sulfur without any mercury nor chlorine (in green) suggests the presence of sulfates.

µ-XANES analyses at the chlorine K-edge were performed at different locations on the cross-section. The spectra of these points were compared to those of relevant reference compounds; the results confirm the presence of mercury and chlorine containing compounds at the surface of the sample. Figure 2.18d shows that the white line of these

compounds (at 2.8232 keV) matches the first peak of the spectrum from point 1 (see Figure 2.18b); all other points acquired in these areas show the same profile. The spectrum of the point 1 shows important similarities with the one of corderoite. These analyses therefore suggest the presence of mercury sulfo-chloride compounds in the grey altered areas of the fresco. Additionally, sulfur K-edge µ-XANES spectra show the presence of sulfates in the sulfur rich area (green in Figure 2.18c).

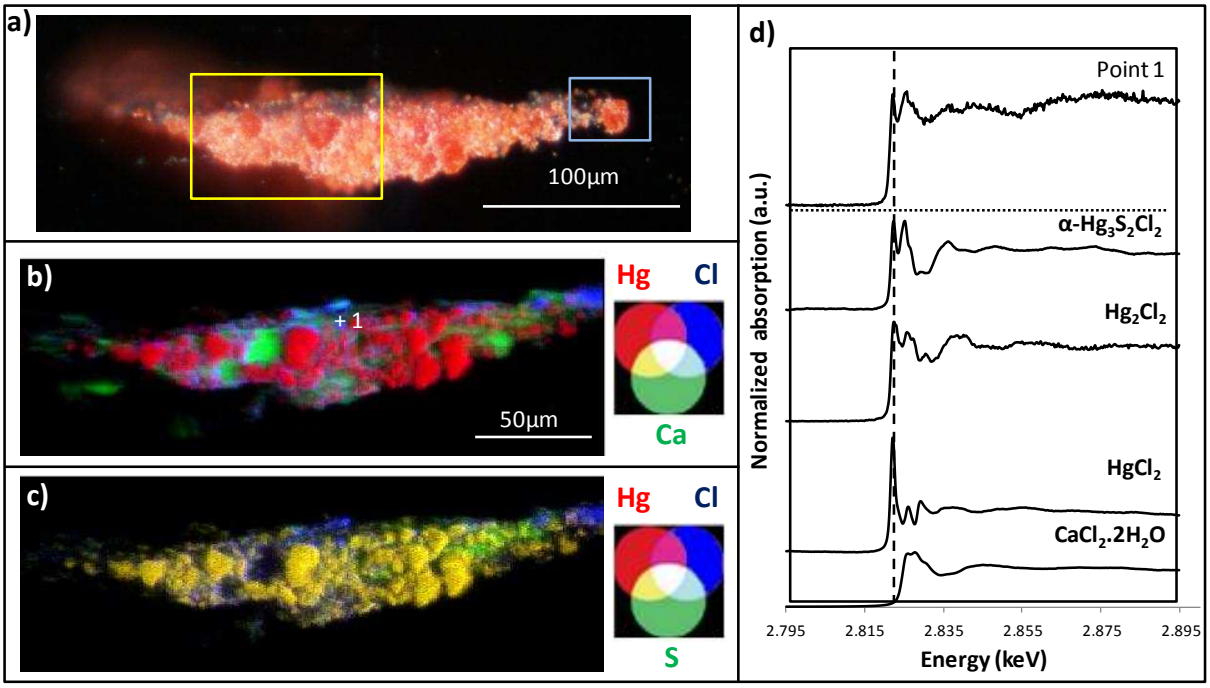

Figure 2.18.: a) *Visible image of the cross-section obtained from sample Po-G; µ-XRF maps of the entire sample acquired at high energy (7.9 keV) shown as two RGB composites:* ***b)*** *mercury (red), calcium (green) and chlorine (blue) and* ***c)*** *mercury (red), sulfur (green) and chlorine (blue);* ***d)*** *µ-XANES spectrum of point 1 (see (b)) acquired at the chlorine K-edge, compared to spectra of chlorine containing reference compounds. The dashed line indicated the white line for mercury,chlorine containing compounds (at 2.8232 keV).*

The acquisition of maps at different energies corresponding to the maximum absorption of compounds that are assumed to be present after XANES analyses allows for a better visualization of the composition of this cross-section. Indeed, the combination of maps acquired at 2.4716 keV (sulfur from cinnabar, red), at 2.4825 keV (sulfur from sulfates, green) and 2.8232 keV (chlorine from mercury,chlorine containing compounds, blue), shows the localization of possible mercury chlorides among the original pigment, and also some

sulfates at the top right part of this area (Figure 2.19a). In another area (represented by the blue rectangle in the Figure 2.18a), the combination of maps acquired at 2.4716 keV (sulfur from cinnabar, red), at 2.4825 keV (sulfur from sulfates, green) and 2.4726 keV (sulfur from $Hg_3S_2Cl_2$ compounds, blue), shows the localization of possible mercury sulfo-chloride compounds with on top of the latter layer, another very thin layer of sulfates (Figure 2.19b).

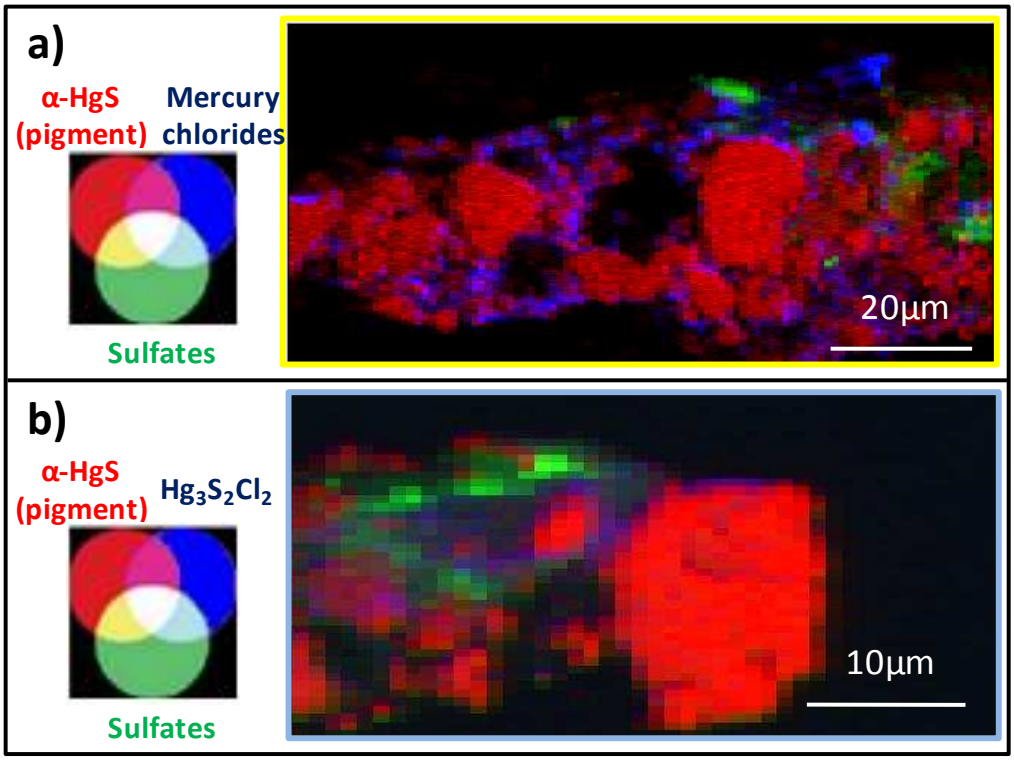

Figure 2.19.: a) *Results of mapping of the yellow rectangle in Figure 2.18a. An RGB composite of three intensity maps, sulfur at 2.4716 keV (cinnabar, red), sulfur at 2.4825 keV (sulfates, green) and chlorine at 2.8232 keV (mercury chlorine containing compounds, blue) is shown;* ***b)*** *Results of mapping of the blue rectangle in Figure 2.18a. An RGB composite of intensity maps of sulfur at 2.4716 keV (cinnabar, red), sulfur at 2.4825 keV (sulfates, green) and sulfur at 2.4726 keV ($Hg_3S_2Cl_2$, blue) is shown.*

Cross-section of sample Po-B: µ-XRF/µ-XANES

Sample Po-B shows the same multi-layered structure as Po-G, except for the black superficial layer that appears to be more homogeneous (Figure 2.20b).

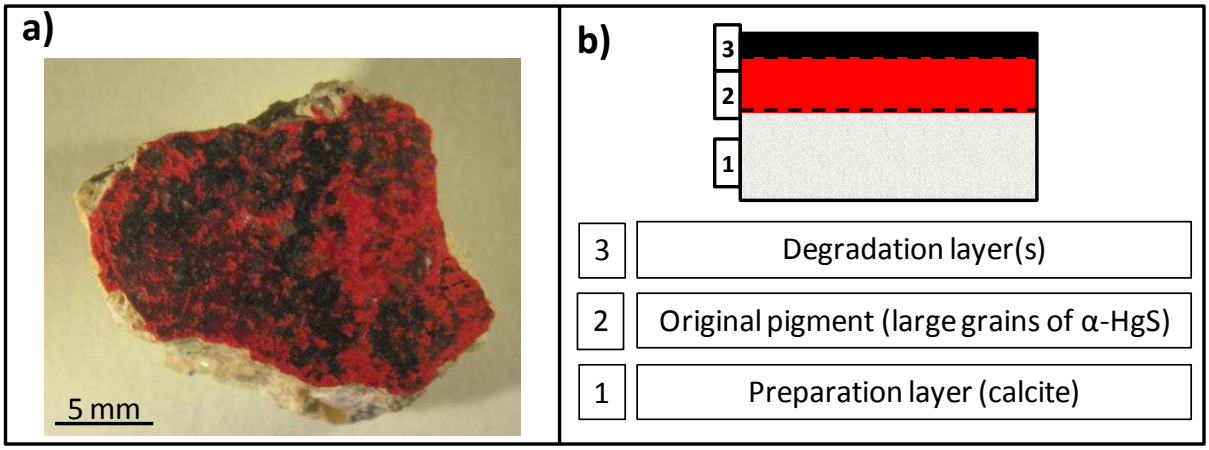

Figure 2.20.: a) *Visible picture of sample Po-B taken from a Pompeian fresco;* ***b)*** *Representation of the multi-layered structure of the sample.*

The composition of the different layers that make up fragment Po-B was studied by μ-XRF/μ-XANES. First, elemental maps were acquired by μ-XRF at high energy (7.9 keV) in order to obtain the total signals of all elements of interest. In Figure 2.21. two relevant RGB composites of the resulting elemental maps are shown. In Figure 2.21b, calcium is still present among the HgS grains, but also in high concentration at the top layer of the sample, where the visible image shows a thick black layer, perhaps corresponding to sulfates detected by XRD. Chlorine is also present in this sample both at the top and the bottom of the cross-section. In Figure 2.21c, the presence of sulfur without any mercury nor chlorine (in green) seems to be correlated to the presence of calcium, suggestive of the presence of calcium sulfates.

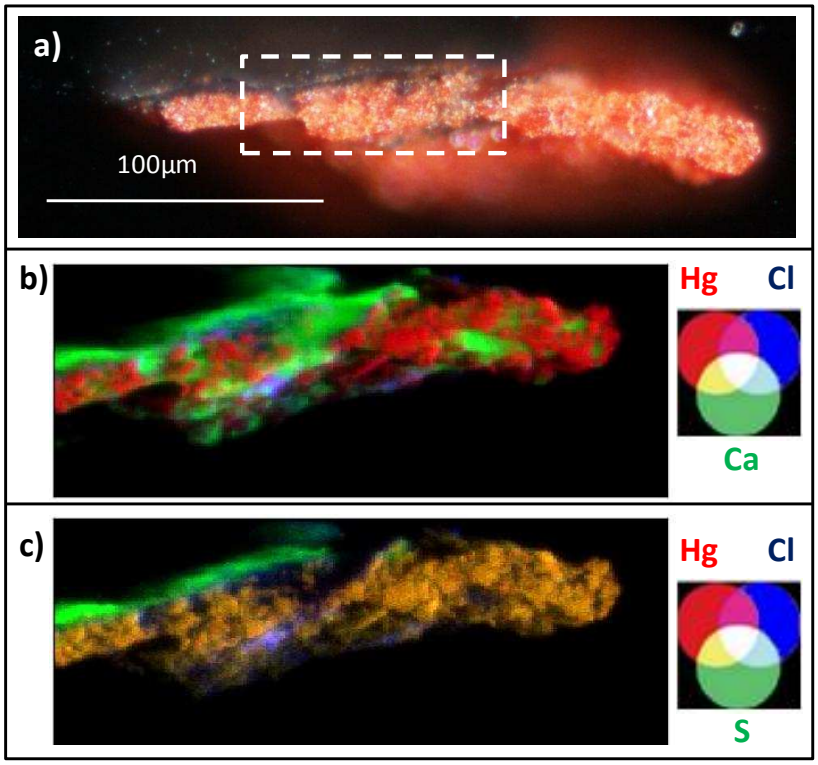

Figure 2.21.: a) *Visible image of the cross-section obtained from sample Po-B; µ-XRF maps of the entire sample acquired at high energy (7.9 keV) shown as two RGB composites:* ***b)*** *mercury (red), calcium (green) and chlorine (blue) and* ***c)*** *mercury (red), sulfur (green) and chlorine (blue).*

µ-XANES analyses at the sulfur and chlorine K-edges were performed at different locations on the cross-section. The Cl K-edge spectra did not have a sufficient quality to allow drawing conclusions from them. Among the S K-edge spectra, those from points 1-3 were particularly significant (see Figure 2.22c). Their similarity to that of gypsum suggests that sulfates are present in this sample (see third line at 2.4825 keV in Figure 2.22c). At lower energy, it is also possible to distinguish a small peak at 2.4785 keV, corresponding to the energy of sulfur in sulfites (see white line of Na_2SO_3 represented by the second line in Figure 2.22c). At point 2, the first peak of the spectrum is situated at 2.4726 keV, which is the white line for corderoite (see first line in Figure 2.22c) whereas in the spectrum of point 3, this peak is present at slightly lower energy, i.e. closer to the cinnabar reference.

In the area represented by a dashed white rectangle in Figure 2.21a, maps were acquired at 2.4716 keV (sulfur from cinnabar), at 2.4825 keV (sulfur from sulfates) and 2.8232 keV (chlorine from mercury chlorine containing compounds), and combined

respectively in red, green and blue (Figure 2.22a). In this image, mercury chloride compounds are present above and below the cinnabar layer, corresponding to grey regions in the visible image, and perhaps formed during a local reaction at the surface of the HgS grains; sulfates, on the other hand, form a thick layer at the top of the cross-section, which is more related to a superficial precipitation.

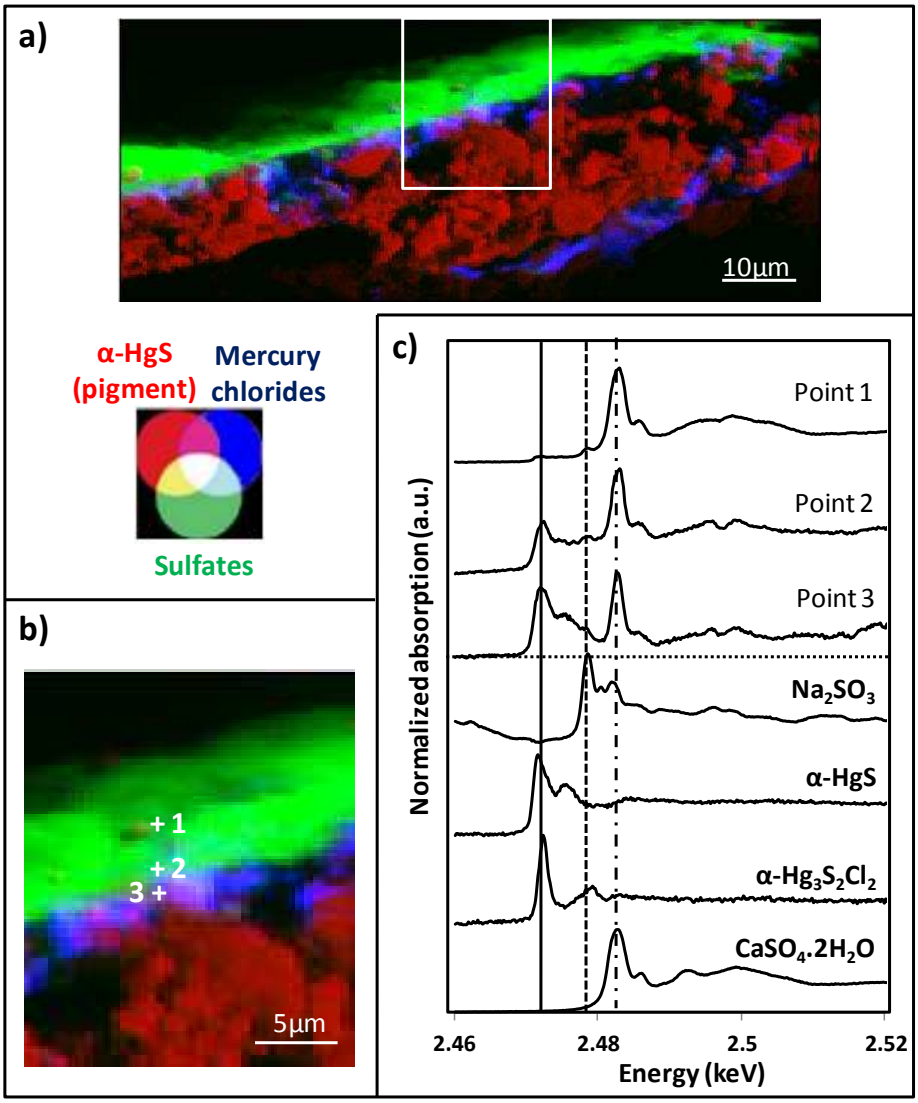

Figure 2.22.: a) *Results of mapping of the dashed white rectangle in Figure 2.21a: an RGB composite of three intensity maps, sulfur at 2.4716 keV (cinnabar, red), sulfur at 2.4825 keV (sulfates, green) and chlorine at 2.8232 keV (mercury chlorine containing compounds, blue) is shown;* ***b)*** *Enlargement of the white rectangle in (a) with localization of the 3 points where µ-XANES at the sulfur K-edge was performed;* ***c)*** *Spectra obtained from points 1-3 compared to sulfur reference spectra of sulfite (Na_2SO_3), cinnabar (α-HgS), corderoite (α-$Hg_3S_2Cl_2$) and gypsum ($CaSO_4.2H_2O$). The leftmost vertical line indicates the position of the white line for sulfides (2.4716 keV), the middle one that of sulfites (2.4785 keV) and the rightmost line that of sulfates (2.4825 keV).*

One interesting point concerning the two Pompeian samples is that they show a different aspect due to degradation. Indeed, mapping of the cross-section prepared from the sample Po-G (grey with Cl containing compounds) by SEM showed that the degradation layer is very thin, almost not visible, and seems to be distributed heterogeneously at the surface of each grain (Figure 2.23a). The second cross-section from Po-B (black sample with sulfates) presents a thicker, smoother and more homogeneous degradation layer at the surface of the entire cross-section (Figure 2.23b). These differences will be discussed in the Section 4.2.5.

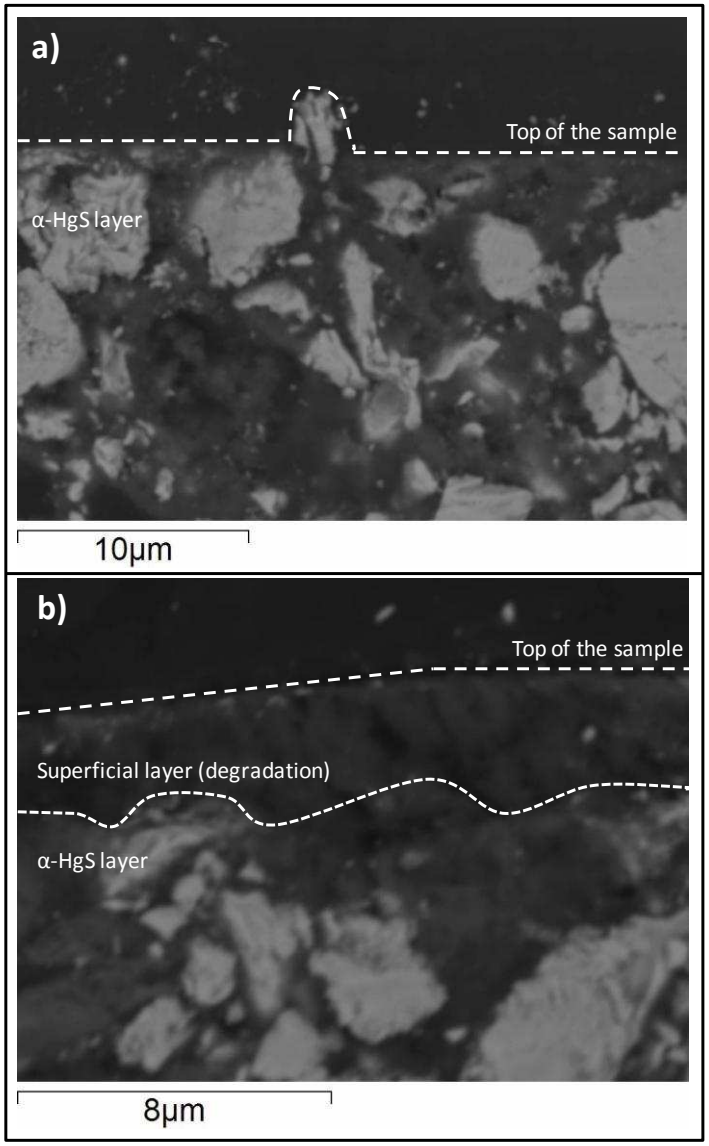

Figure 2.23.: *Back scattered electron images (SEM) of samples* ***a)*** *Po-G and* ***b)*** *Po-B.*

2.2.4. Panels from Brueghel

Pieter Brueghel the Younger (ca. 1564-1636) (first son of Pieter Brueghel the Elder) is a Flemish painter, well known for his numerous copies of original works of his father. In the corpus of panel paintings of Brueghel the Younger, some of the red vermilion areas are altered while the same areas in twin copy panels remained unaltered. The aim of this study was to make a direct comparison of paint samples obtained from the following panels: "Preaching of John the Baptist" (Stedelijk Museum Wuyts-Van Campen en Baron Caroly, Lier, Belgium), "The Village Lawyer" (inventory number 1952-G, Museum voor schone kunsten, Ghent, Belgium) and "The Wedding Dance" (inventory number 1914-CJ, Museum voor schone kunsten, Ghent, Belgium) (see paintings respectively in Figure 2.24a, b and c). Samples were kindly provided and previously studied by Dr. Jana Sanyova, conservation scientist at KIK-IRPA and Dr. Christina Currie, who published first analyses and observations *[C. Currie, 2012]*. Among these analyses, Raman spectroscopy revealed the presence of Hg_2Cl_2 above the pictorial layer in one sample; this motivated the additional investigations presented below.

Figure 2.24.: *Photographs of paintings from Brueghel's workshop:* ***a)*** *"Preaching of John the Baptist", Lier;* ***b)*** *"The Village Lawyer", Ghent;* ***c)*** *"The Wedding Dance", Ghent. White rectangles represent areas where samples were taken.*

"Preaching of John the Baptist"

Two samples were taken from this panel, one in the shadow **(Br-C006)** and another one in a degraded area **(Br-C007)** of the red coat of the figure visible in the enlargement in Figure 2.25a. Both samples present a thick preparation layer with calcite and lead white. Above this, two superimposed layers of red mercury sulfide are visible, separated by a varnish layer. On top of them, some black crusts are present below the superficial varnish. The second cross-section (Br-C007) shows in the middle an opening in the top layer of vermilion (Figure 2.25b and c).

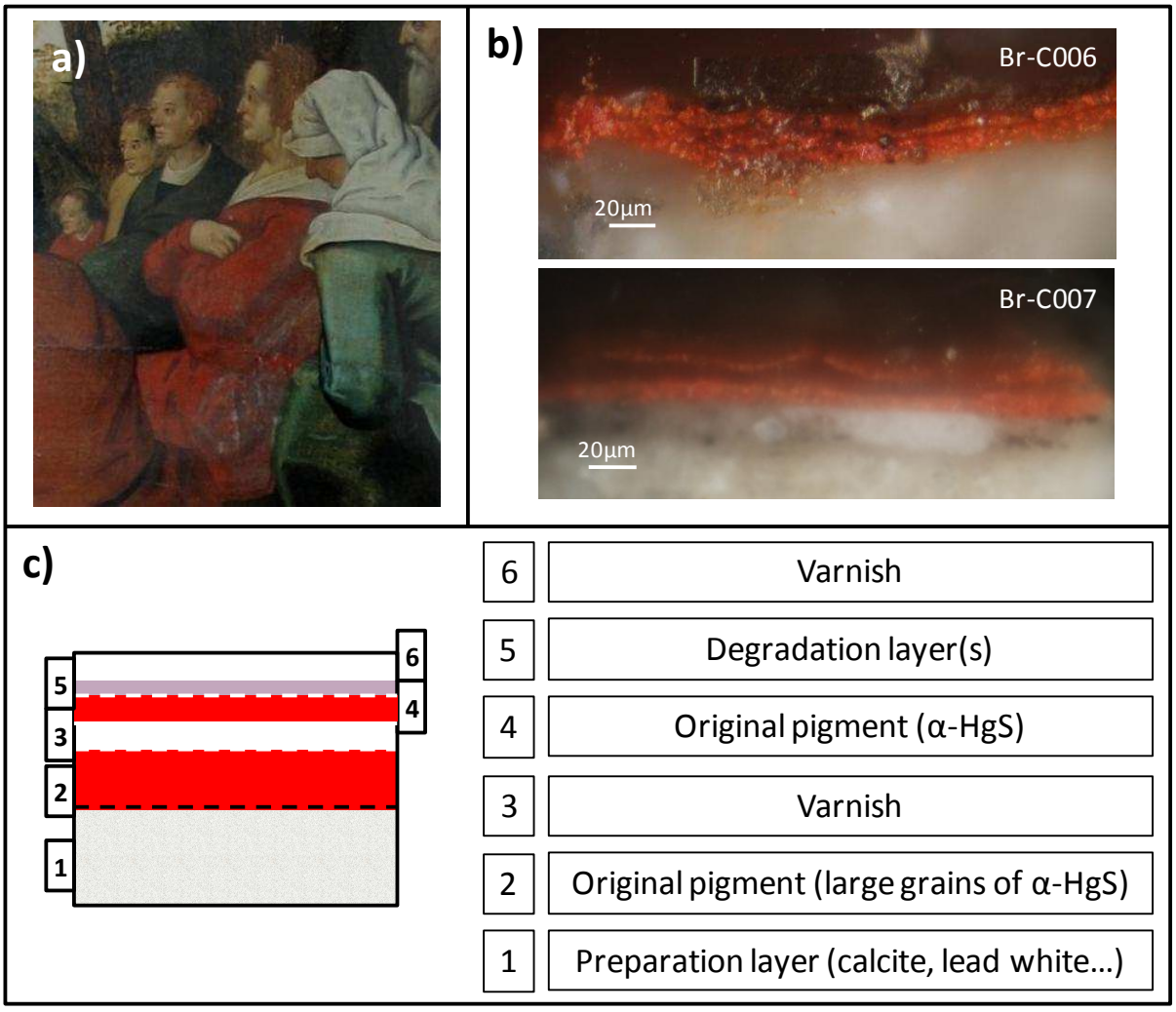

Figure 2.25.: a) *Detail of the painting "Preaching of John the Baptist" represented in Figure 2.24a;* ***b)*** *Visible pictures of the cross-sections from the Br-C006 and Br-C007 samples taken from the area (a);* ***c)*** *Representation of the multi-layered structure of the samples.*

Elemental maps were first acquired from sample Br-C006 at 2.9 keV (see Figure 2.26b). Different RGB composites of the resulting elemental maps show that chlorine is present all along the pictorial layer and even above in a thick layer, maybe in the binder. On top of the sample, a very thin layer of sulfur without any mercury nor chlorine is present that is co-localized with lead. Similar to chlorine, lead is present in the mercury sulfide layer and in the layer above it. A large grain of mercury is visible at the top of the cross-section, not co-localized with sulfur or chlorine, but with phosphorus (see purple area in the lower image of Figure 2.26b). When mapping at a higher energy (7.9 keV), iron was also seen throughout the entire pictorial layer and above it. μ-XANES spectra were acquired at the chlorine K-edge in different locations of the sample. In areas where chlorine is present, the spectra showed a first peak at 2.8242 keV, a slightly higher energy than 2.8232 keV (the white line of $HgCl_2$ and Hg_2Cl_2 containing references - see the spectrum of point 1 and the dashed line in Figure 2.26c). This peak is not well defined and do not show similarities with any of the references. μ-XANES spectra at the sulfur K-edge just show the presence of cinnabar and a peak at the energy of the white line for sulfates (2.4825 keV). To have a better idea of the distribution of these compounds, in the area represented by a dashed white rectangle in Figure 2.26a, maps were acquired at 2.4716 keV (sulfur from cinnabar), at 2.4825 keV (sulfur from sulfates), 2.9 keV (total chlorine); the RGB composite maps is shown in Figure 2.26d. It follows from the maps that the mercury sulfide was not finely ground as its layer presents large pigment grains. Chlorine is observed in and above the pigment layer, but the Cl-species are not yet clearly identified. On top of this chlorine-rich layer, a thin layer of sulfates is visible.

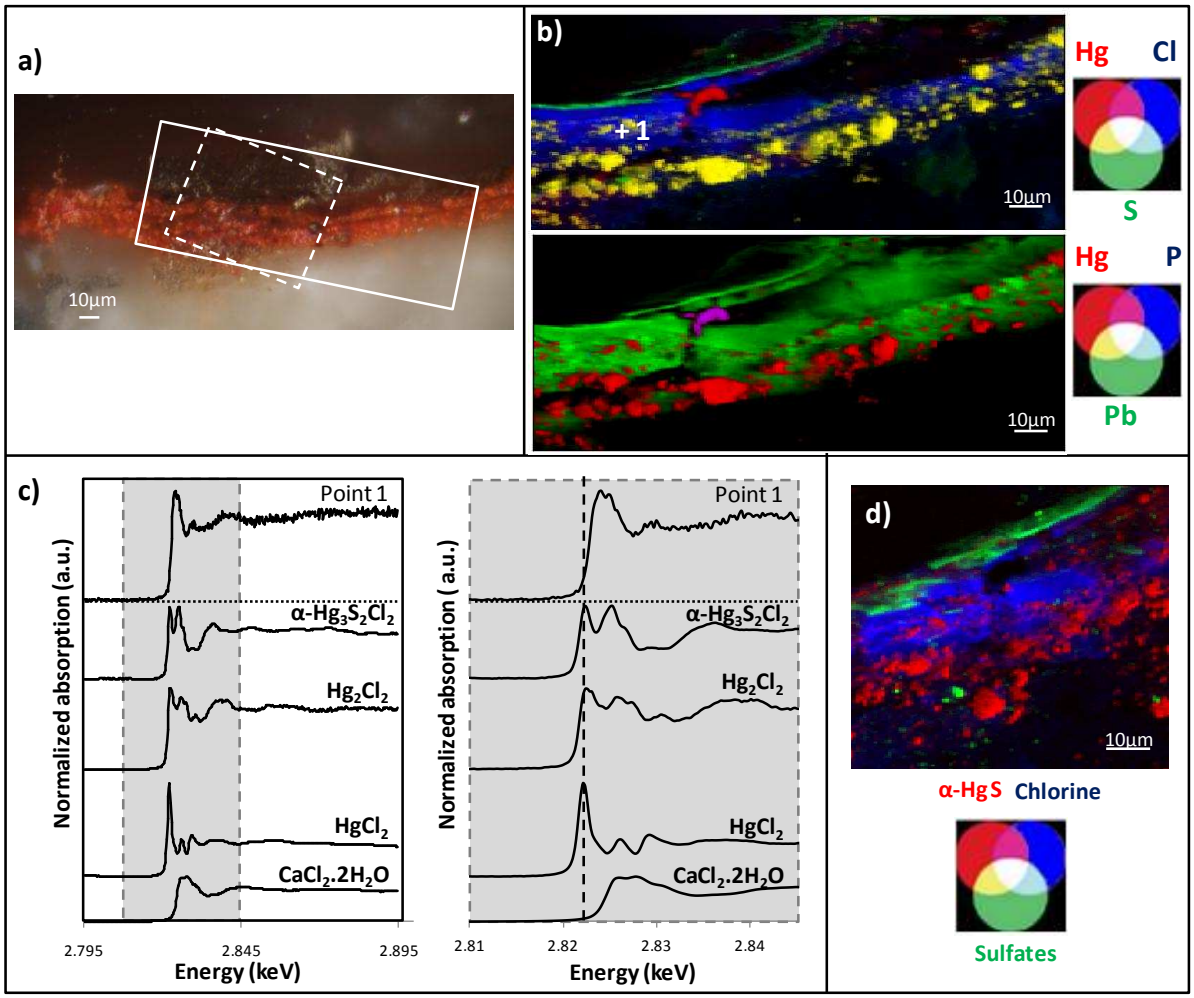

Figure 2.26.: a) *Visible picture of the cross-section prepared from sample Br-C006;* ***b)*** *µ-XRF maps of the area represented by the solid line rectangle on (a), acquired at 2.9 keV, showing two RGB composites: (upper image) mercury (red), sulfur (green) and chlorine (blue) and (lower image) mercury (red), lead (green) and phosphorus (blue);* ***c)*** *µ-XANES spectrum acquired at the chlorine K-edge at point 1 (see (b)) compared to spectra of chlorine containing reference compounds. On the right, a magnified area (2.810-2.845 keV) of the spectra is presented. The dotted black vertical line corresponds to 2.8232 keV (absorption maximum of Hg,Cl compounds);* ***d)*** *Results of mapping the dashed white rectangle in (a): RGB composite of three intensity maps, sulfur at 2.4716 keV (cinnabar, red), sulfur at 2.4825 keV (sulfates, green) and chlorine at 2.9 keV (total chlorine, blue).*

Elemental maps were acquired from the second sample (Br-C007) at 7.9 keV in order to see all elements including iron (see Figure 2.27b). The upper RGB composite image of mercury (red), sulfur (green) and chlorine (blue) shows that chlorine is present essentially at the top of the cross section, above the opened vermilion layer and surrounding the opening;

it is also present in almost all the pictorial layers at lower levels. Thus, as hypothesized for the previous sample, chlorine could be present in the binder. In the lower RGB composite image of Figure 2.27b (showing mercury (red), iron (green) and chlorine (blue)), it is noteworthy that iron is only present in the top part of the cross-section, in the upper pictorial layer and above it. µ-XANES spectra at the chlorine K-edge acquired in areas above the opening of the α-HgS layer show a maximum absorption at 2.8232 keV but without any features corresponding to known reference compounds. In other areas, the chlorine XRF signal was not intense enough to show any feature in the XANES spectra. In the sulfur K-edge spectra, and despite their low quality, the observed peaks were similar to the ones of sulfates. In order to investigate the distribution of these compounds, in the area represented by the dashed white rectangle in Figure 2.27a, maps were acquired at 2.4716 keV (sulfur from cinnabar), at 2.4825 keV (sulfur from sulfates) and 2.8232 keV (for the unidentified chlorine containing compounds), and combined in Figure 2.27c. The two layers of mercury sulfide are clearly visible, and as it was assumed from the chlorine map, unidentified chlorine-containing compounds are present above the opening of the upper vermilion layer (see Figure 2.27c). This map also shows that a thin sulfate layer is present between the two vermilion layers.

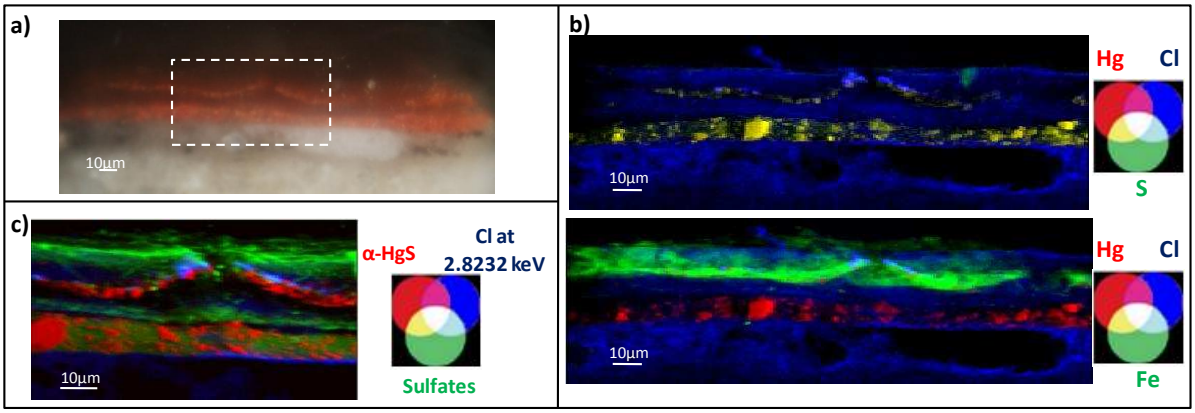

Figure 2.27.: a) *Visible picture of the cross-section prepared from sample Br-C007;* ***b)*** *µ-XRF maps of the entire sample, acquired at high energy (7.9 keV), showing two RGB composite images: (upper) mercury (red), sulfur (green) and chlorine (blue) and (lower) mercury (red), iron (green) and chlorine (blue);* ***c)*** *Results of mapping the dashed white rectangular area in (a): RGB composite of three intensity maps: sulfur at 2.4716 keV (cinnabar, red), sulfur at 2.4825 keV (sulfates, green) and chlorine at 2.8232 keV (unidentified species, blue).*

"The Village Lawyer"

One sample was taken from the red dress of the woman that is bending over in the center of the painting **(Br-C012)** (Figure 2.28a). The cross-section obtained from this sample shows a thick preparation layer with calcite and lead white, covered by a red layer of mercury sulfide with some black spots among and on top of the red layer. At the sample surface, a layer of varnish is present (Figure 2.28b and c).

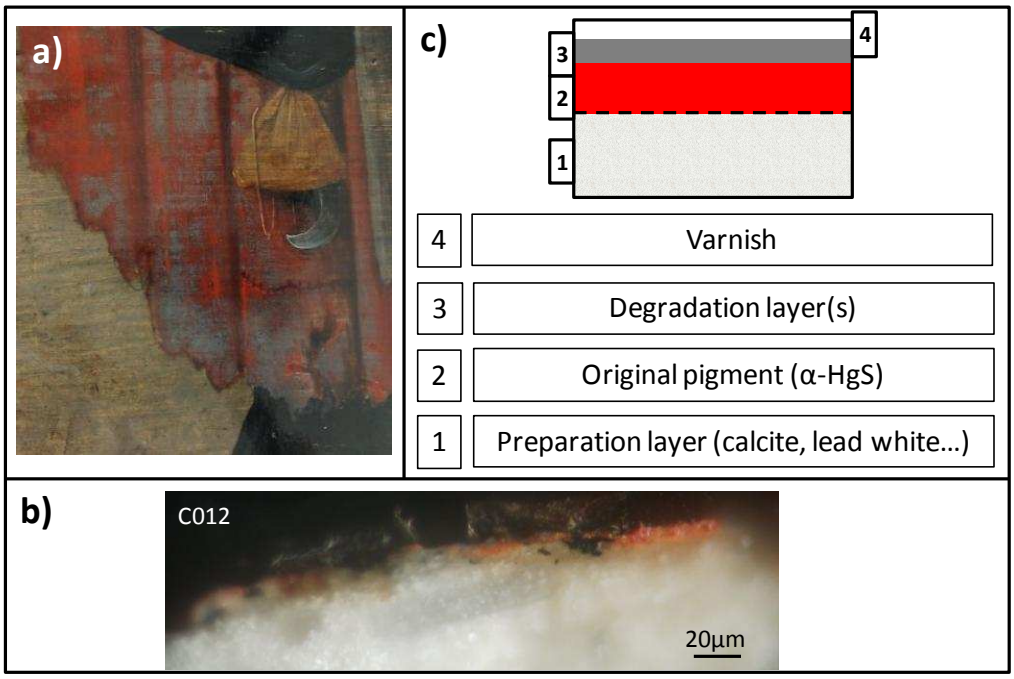

Figure 2.28.: a) *Detail of the painting "The Village Lawyer" represented in Figure 2.24b;* ***b)*** *Visible picture of the cross-section from sample Br-C012 taken from the area shown in (a);* ***c)*** *Representation of the multi-layered structure of the sample.*

Elemental maps were acquired from this sample at 2.9 keV in order to record the distribution of different elements. The RGB composite image of mercury (red), sulfur (green) and chlorine (see Figure 2.29b) shows that chlorine is present co-localized with mercury in a thin layer (purple) above the mercury sulfide layer, and on top of it and also just below one part of the pictorial layer, a layer of sulfur without any mercury nor chlorine is visible. µ-XANES spectra acquired at the sulfur K-edge in the position indicated, show the presence of sulfates. Despite the low quality of the spectra recorded at the Cl K-edge, peaks with similar features to the ones of mercury,chlorine containing compounds can be discerned with a maximum absorption at 2.8232 keV (especially $Hg_3S_2Cl_2$ compounds) but not intense enough

to allow a clear identification. In the chlorine-rich area below the pictorial layer, the µ-XANES spectra show a peak at 2.8241 keV, unrelated to a known reference. In order to investigate the distribution of these compounds, in the area represented by the dashed white rectangle in Figure 2.29a, maps were acquired at 2.4716 keV (sulfur from cinnabar), at 2.9 keV (total chlorine) and 2.4825 keV (sulfur from sulfates), resulting in the RGB composite of Figure 2.29c. As was the case for the previous samples (Br-C006 and Br-C007), chlorine is present above and below the pigment layer, maybe in the binder, and a layer of sulfates is present at the top of the cross-section.

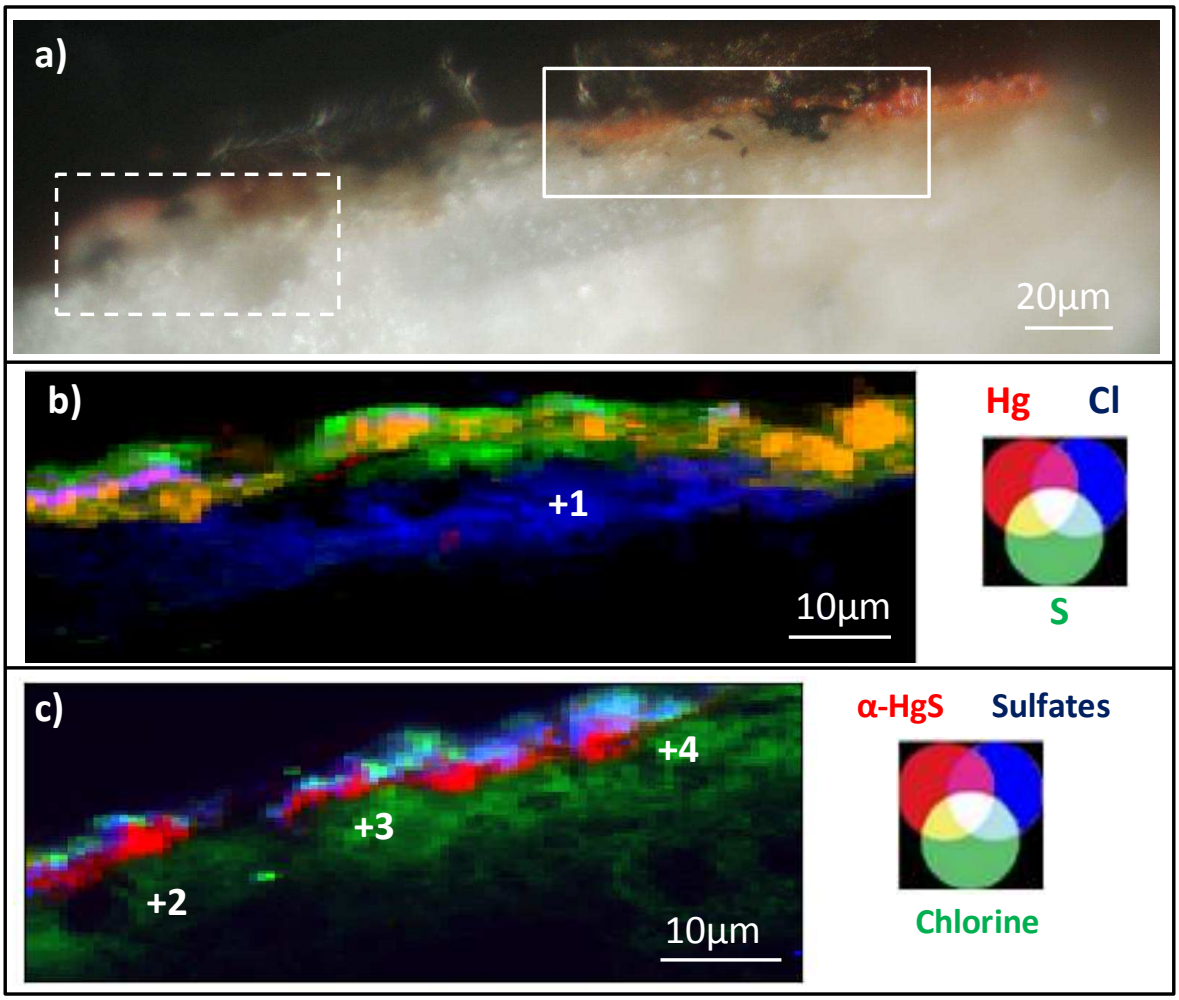

Figure 2.29.: a) *Visible picture of the cross-section prepared from sample Br-C012;* ***b)*** *µ-XRF maps of the area represented in (a) by the solid rectangle, acquired at 2.9 keV, shown as a RGB composite image of mercury (red), sulfur (green) and chlorine (blue);* ***c)*** *Results of mapping the dashed white rectangle in (a): RGB composite image with sulfur at 2.4716 keV (cinnabar, red), chlorine at 2.9 keV (total chlorine, green) and sulfur at 2.4825 keV (sulfates, blue).*

Cl K-edge μ-XANES analyses performed on the four points represented in Figure 2.29 show spectra similar the one of point 1 in Figure 2.26, showing an energy of maximum absorption at 2.8242 keV, not corresponding to any of the known references.

"The Wedding Dance"

One last sample was taken from the red shirt of the man in the center of this panel **(Br-C052)** (Figure 2.30a). The cross-section obtained from this sample shows a thick preparation layer with calcite and lead white; above this, a red layer of mercury sulfide is present that is degraded at the surface. Additionally, a layer of superficial varnish is present (Figure 2.30b and c).

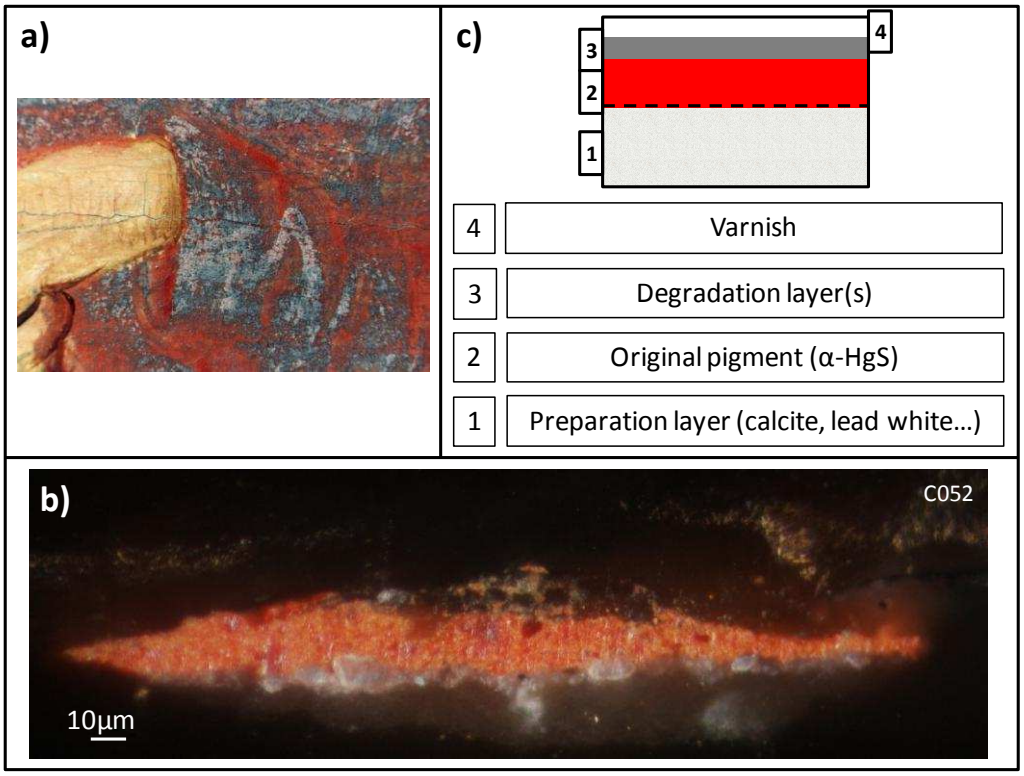

Figure 2.30.: a) *Detail of the painting "The Wedding Dance" represented in Figure 2.24c;* ***b)*** *Visible picture of the cross-section prepared from the sample Br-C052 taken from the area (a);* ***c)*** *Representation of the multi-layered structure of the sample.*

Elemental maps were acquired on this sample at 2.9 keV. The combination of mercury (red), sulfur (green) and chlorine (blue) (see Figure 2.31b) shows that chlorine is

present in high amounts in this sample, and also that a sulfur containing layer covers the pictorial layer. µ-XANES spectra were acquired at the chlorine and sulfur K-edges. The chlorine spectra were generally fairly noisy; in areas with the highest chlorine content, the same spectrum profile as for the sample Br-C012 (with a peak at 2.8241 keV) was obtained. In the pictorial layer a peak at 2.8232 keV was observed. The sulfur K-edge spectra show the presence of sulfates in the top part of the cross-section. In the area represented by a dashed white rectangle in Figure 2.31a, maps were acquired at 2.4716 keV (sulfur from cinnabar), at 2.9 keV (total chlorine) and 2.4825 keV (sulfur from sulfates) (see RGB composite image in Figure 2.31c). Chlorine is present below as well as above the pigment layer; the latter is essentially a thin layer with on top of it a thicker layer of sulfates superimposed on the mercury sulfide layer.

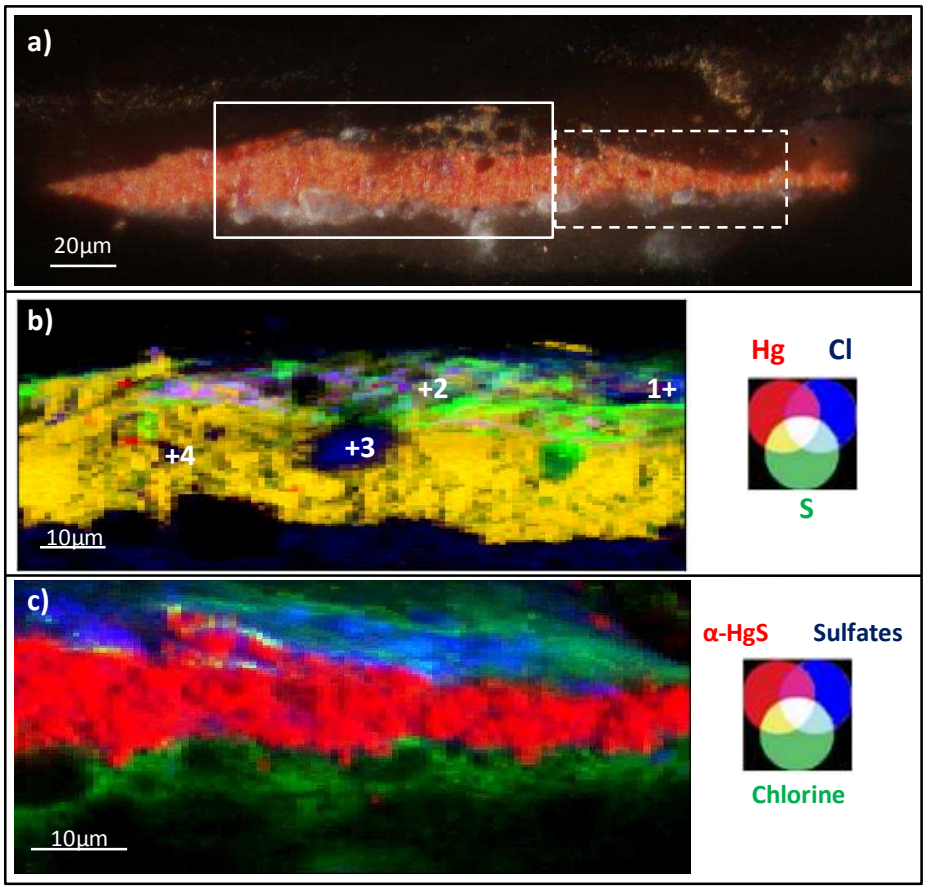

Figure 2.31.: a) *Visible picture of the cross-section prepared from sample Br-C052;* ***b)*** *µ-XRF maps of the area represented in (a) by the solid rectangle, acquired at 2.9 keV, shown as RGB composite of mercury (red), sulfur (green) and chlorine (blue);* ***c)*** *Results of mapping of area indicated by the dashed white rectangle in (a) shown as a RGB composite of the distributions of sulfur at 2.4716 keV (cinnabar, red), chlorine at 2.9 keV (total chlorine, green) and sulfur at 2.4825 keV (sulfates, blue).*

μ-XANES analyses performed at Cl K-edge on the four points represented in Figure 2.31b showed spectra similar that of the point 1 in Figure 2.26c, having an energy of maximum absorption at 2.8246 keV, not corresponding to any of the known references.

Unfortunately, XANES spectra of different areas in all these samples taken from Brueghel the Younger's panels did not allow a clear identification of the different chlorine containing compounds present in the cross-sections.

Especially for the chlorine present in all pictorial layers, the chlorine K-edge XANES spectrum is not similar to the Cl-reference compounds to which it was compared to (Figure 2.26c-point 1). When taking the white line values from the multiple references presented in the literature *[F.E. Huggins, 1995]*, it appears that this unknown compounds could not be an alkaline chloride (such as KCl and $CaCl_2$) as their energy of maximum absorption is higher in energy than the one of NaCl (at 2.8263 keV) whereas for the unknown compound it is at a lower energy (at 2.8242 keV). This energy would be more consistent with the presence of an inorganic metallic chloride (such as Hg,Cl-compound and Cu,Cl-compound), an oxychloride (such as CuOCl and $Ca(OCl)_2$) or an organic chloride (such as 1,4-bis(chloromethyl)benzene), all having their white line at a lower energy than the one of NaCl. However the identification of this compound is not possible yet with these references from the literature and with the ones analyzed during the present study.

In these samples, chlorine is present in all layers, which suggests that the binder used by the painter originally contained this element. It is therefore a potential chlorine source that could directly degrade red mercury sulfide under the influence of light. In samples Br-C007, Br-C012 and Br-C052, a chlorine-rich layer is present just on top of the original pigment layer; these three samples were taken from degraded areas of each panel. In sample Br-C006, however, taken in the shadowed area of a red coat, no such thin chlorine-rich layer is observed. In these cases, it is difficult to assert which chlorinated area of the sample is due to the red mercury sulfide instability and which area is not. Next to chlorine, sulfates compounds were detected but not identified in the four samples, and it is also difficult to establish if these phases come from α-HgS degradation or not.

2.2.5. A Crucifix painted by Giotto

In 2011, in the context of the restoration by the painting department of C2RMF of a Crucifix painted by Giotto di Bondone (1266/76-1337) and his workshop, exhibited in the Louvre (Figure 2.32a), an assessment was asked by curators to clarify the need of "cleaning" away the grey material that had developed at the surface of the red paint areas. Myriam Eveno, physical-chemistry engineer at C2RMF, was in charge of analyses and kindly provided two samples taken from the Crucifix with the aim of better understanding the degradation.

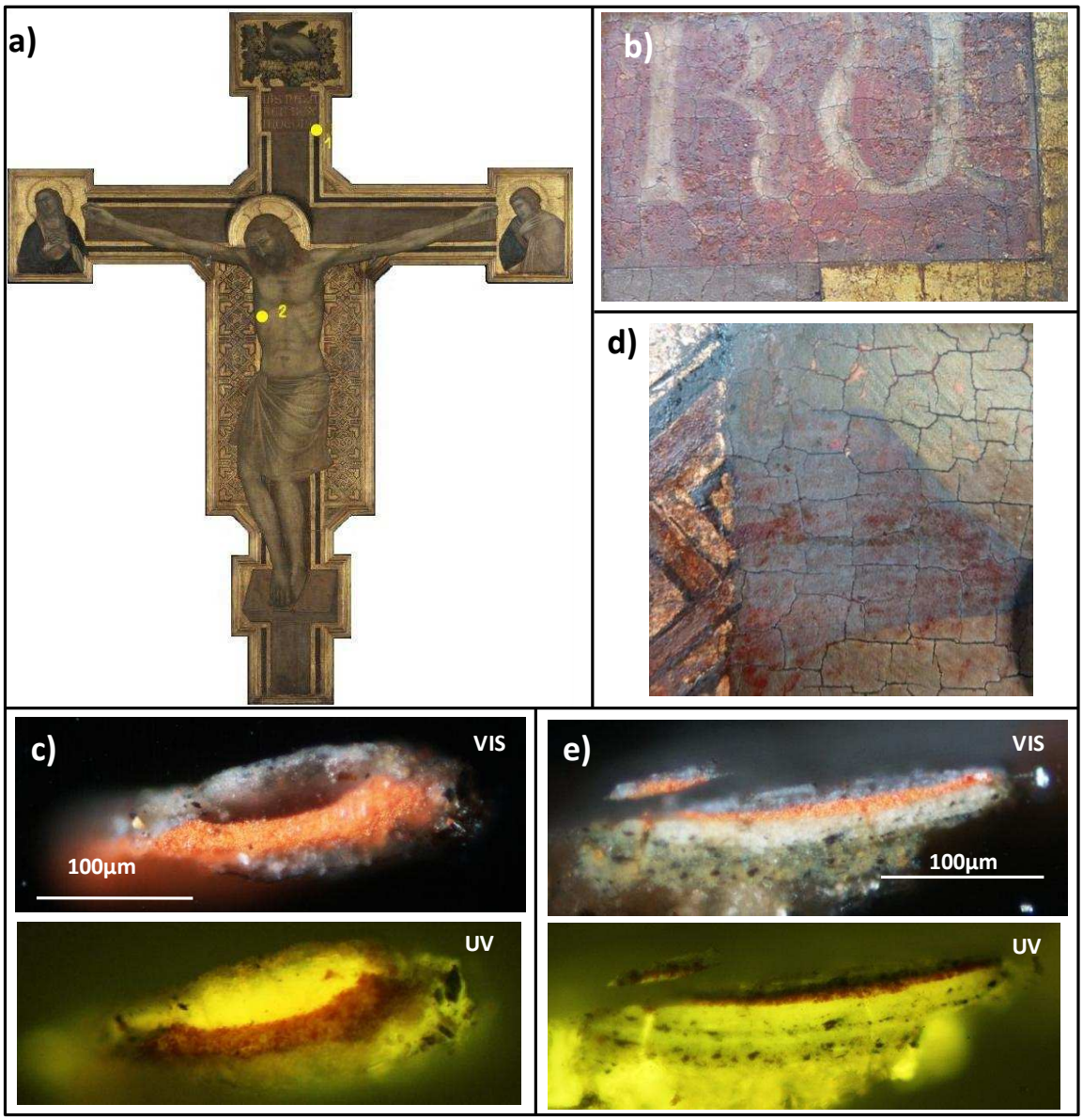

***Figure 2.32.: a**) Photograph of the Crucifix painted by Giotto; numbers indicate sampling locations. Detail photograph and pictures under VIS/UV lights of **b-c)** sample Gi-T (location #1) "Titulus" area; **d-e)** sample Gi-B (location #2) "Blood" area.*

Sample **(Gi-T)** was taken from the corner of the "titulus" area of the Crucifix where the title of the Christ ("*Iesvs Nazaraenvs Rex Ivdaeorum*", Jesus the Nazarene King of the Jews) is visible (Figure 2.32b). The cross-section shows a preparation layer of calcite, covered by a thick red layer of mercury sulfide, then a transparent-grey layer containing an UV-fluorescent material, in its turn covered by a light grey non-fluorescent layer (Figures 2.32c and 2.33).

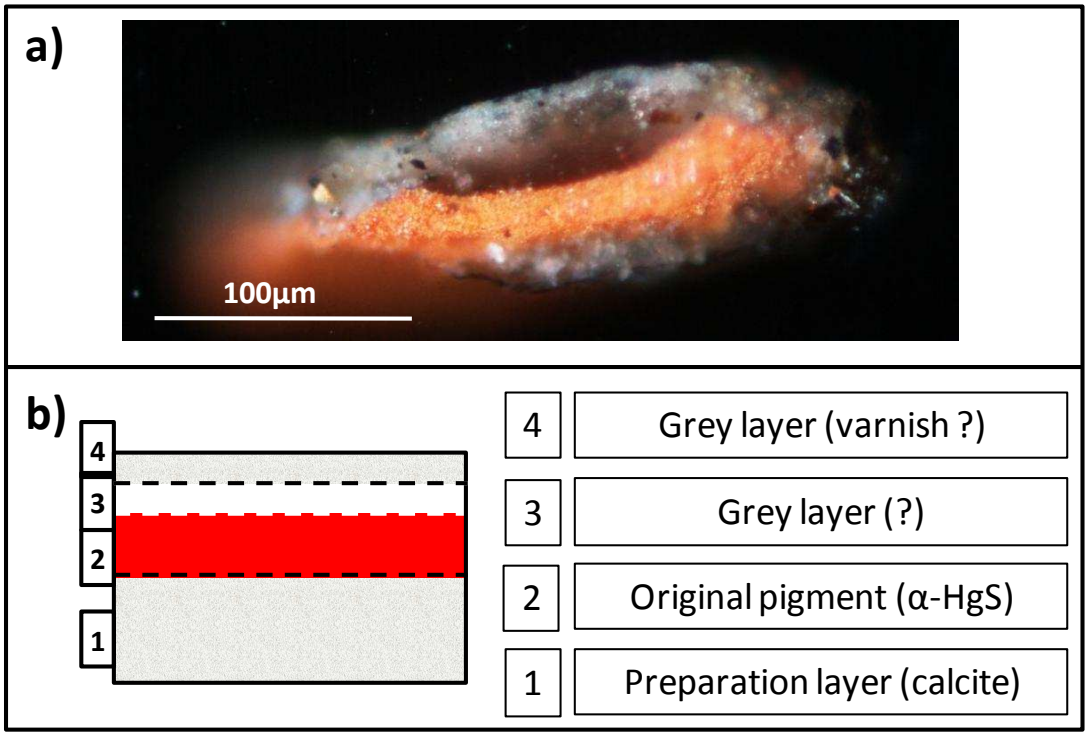

Figure 2.33.: a) *Visible picture of the cross-section from sample Gi-T, taken from the Crucifix painted by Giotto;* ***b)*** *Representation of the multi-layered structure of the sample.*

Sample **(Gi-B)** originates from one of the blackened blood areas on the chest wound of Christ (Figure 2.32d). The cross-section shows, above a preparation layer of calcite, a thin red layer of mercury sulfide, then a very thin layer of degradation products and on top of this, a dark grey layer that appears black under UV light (Figure 2.32e and 2.34).

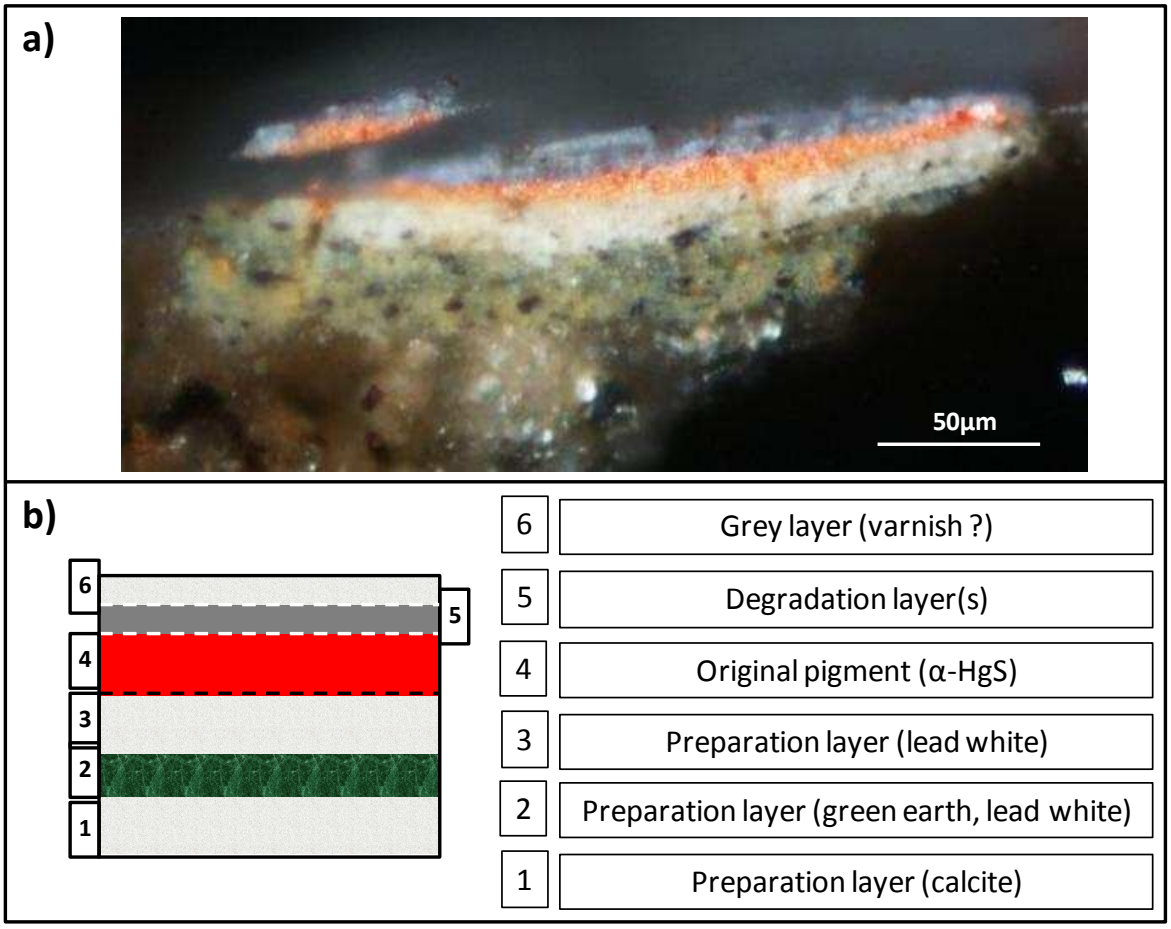

Figure 2.34.: a) *Visible picture of the cross-section from sample Gi-B, taken from the "blood" area, chest of Christ;* ***b)*** *Representation of the multi-layered structure of the sample.*

"Titulus" (sample Gi-T)

First, SEM analyses were performed to have a general idea of the composition of the two layers covering the mercury sulfide. The four layers composing the sample are visible and distinguishable by back scattered electron imaging (Figure 2.35b). Layer 1 is composed by calcite; layer 2 is the pictorial layer (mercury sulfide). In the third and the fourth layers, multiple elements were identified by SEM, including chlorine, present in what appears to be the varnish and not in the binder (Figure 2.35c). Since in layers 3 and 4, no mercury was detected it was concluded that in this case, no alteration of α-HgS was present and no additional investigation of this sample took place.

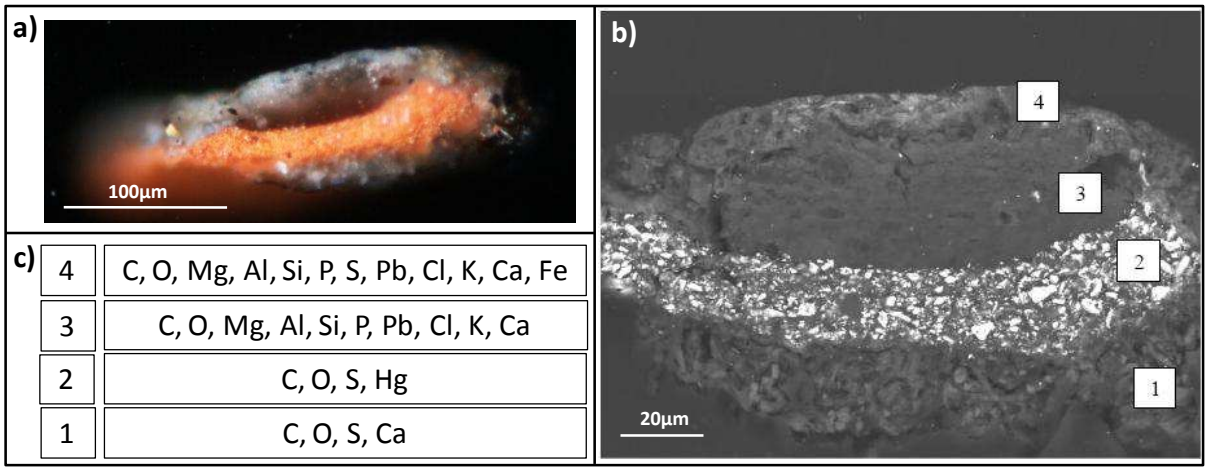

c)

4	C, O, Mg, Al, Si, P, S, Pb, Cl, K, Ca, Fe
3	C, O, Mg, Al, Si, P, Pb, Cl, K, Ca
2	C, O, S, Hg
1	C, O, S, Ca

Figure 2.35.: a) *Visible picture of sample Gi-T;* ***b)*** *Back scattered electron image showing four distinct layers;* ***c)*** *Elements detected by SEM in each layer.*

"Blood" area (sample Gi-B)

Similar to sample Gi-T, SEM analyses were performed on the cross-section. Six layers were distinguished by back scattered electron imaging (Figure 2.36b). Below the mercury sulfide layer (#4), multiple elements were identified in three distinct layers (Figure 2.36c). The grey color of the fifth layer suggested an alteration of the original pigment, and the identification of mercury and sulfur in this layer confirmed this. Next to these elements, chlorine was also identified. In the uppermost layer (#6), mercury was not detected, but the same multiple elements as present in the superficial layers of sample Gi-T were observed, including chlorine. To see if different compounds could be differentiated in the fifth layer, an enlargement from this area, represented in Figure 2.36b (dashed rectangle), was analyzed. The back scattered electron image shows that between the grains of the pigment layer and the superficial one, another layer with two distinct grain types is present: one adjacent to the HgS layer and showing a higher intensity in which the particles form small clusters, and another one covering the clusters (separated by a dashed line in Figure 2.36d). One point from each type was analyzed and both showed the presence of Hg, S and Cl, except that in the second sublayer, lead, potassium and calcium were also identified (Figure 2.36e). µ-XRF/µ-XANES analyses were performed on this sample in order to obtain information on the distribution of the degradation compounds.

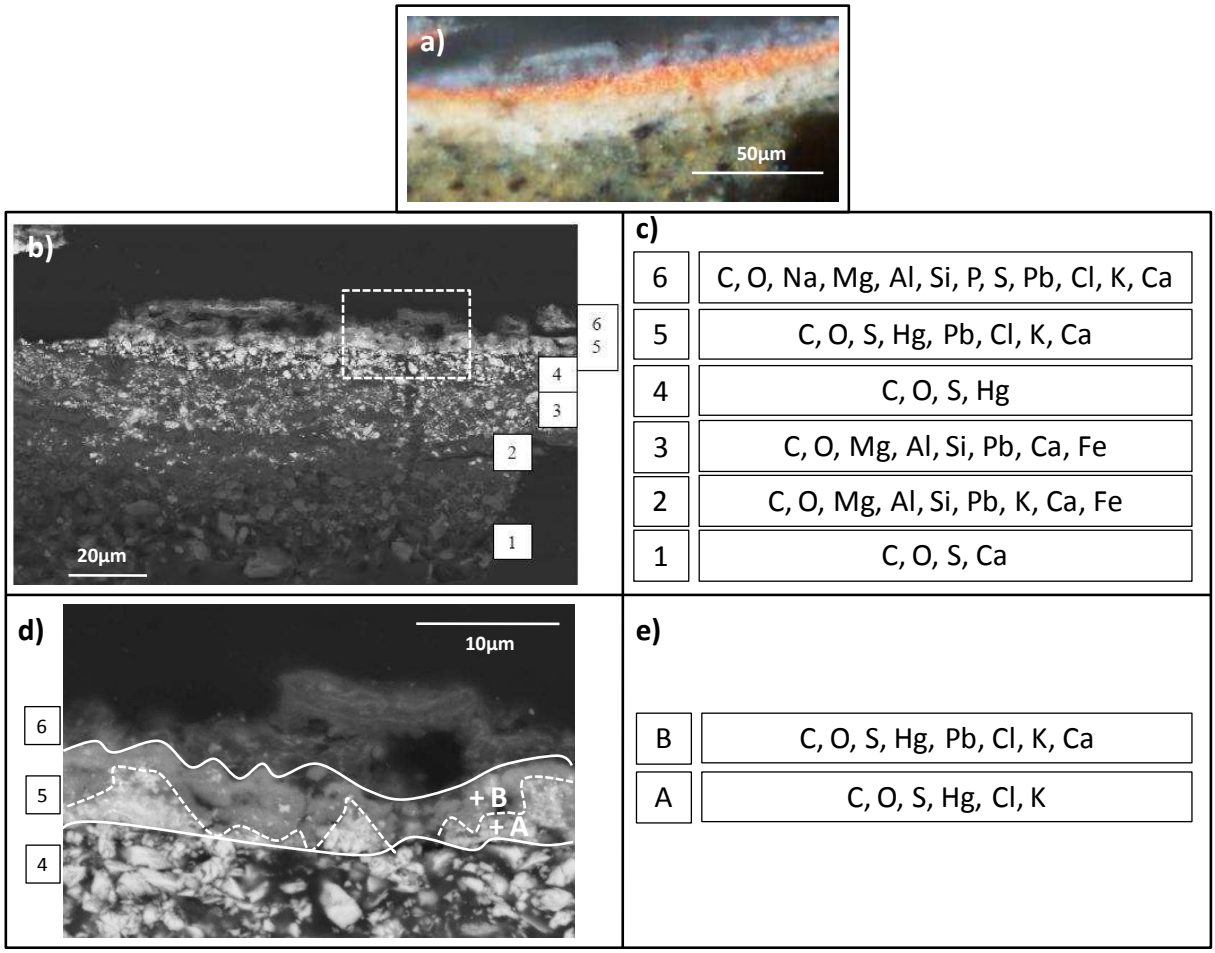

Figure 2.36.: a) *Visible picture of detail of sample Gi-B;* ***b)*** *Back scattered electron image showing six distinct layers;* ***c)*** *Elements detected by SEM in each layer of the cross-section;* ***d)*** *Enlargement corresponding to the dashed rectangle in (b) showing locations A and B at which the results in* ***e)*** *were obtained.*

The entire cross-section was analyzed by reflection mode XRD using an incident beam of 200 µm diameter; next to cinnabar (α-HgS), hydrocerussite ($(PbCO_3)_2.Pb(OH)_2$), gypsum ($CaSO_4.2H_2O$) and calomel (Hg_2Cl_2) were identified.

µ-XRF and µ-XANES measurements were performed at ESRF beamline ID21. First, elemental maps were acquired at 2.9 keV on an enlarged area containing original pigment and degradation layers (see dashed rectangle in Figure 2.37a). The RGB composite image of mercury (red), sulfur (green) and chlorine (blue) (see Figure 2.37b) shows that chlorine is present in high concentration in the layer that covers the mercury sulfide; this layer can be

divided in two parts: one where chlorine is co-localized with mercury and another one where chlorine is present together with low amounts of mercury and sulfur. In this image, sulfur is also present by itself in the material at the top of the cross-section. µ-XANES spectra were acquired at the chlorine and sulfur K-edges. The (noisy) chlorine spectra showed a peak at 2.8232 keV suggesting the presence of mercury chlorine containing compounds. Some of the sulfur spectra resemble those of $Hg_3S_2Cl_2$ compounds (pink area of Figure 2.37b), whereas sulfates seem to be present in all locations in the layer covering the mercury sulfide. In the area represented by the solid rectangle in Figure 2.37a, maps were acquired at 2.4716 keV (sulfur from cinnabar), at 2.8232 keV (chlorine in mercury chloride compounds), and at 2.4825 keV (sulfur from sulfates) (see RGB composite in Figure 2.37c). In the image obtained, a very thin layer of mercury chlorides is visible (in green) between the mercury sulfide and sulfate layers near the top of the cross-section. In the same area where elemental maps were recorded, analyses were made at 2.4716 keV (sulfur from cinnabar), 2.4726 keV (sulfur from $Hg_3S_2Cl_2$ compounds), 2.8232 keV (chlorine in mercury chloride compounds) and 2.4825 keV (sulfur from sulfates) (see two RGB composites in Figure 2.37d). These images clearly show that $Hg_3S_2Cl_2$ compounds are present between the original pigment and a sulfate layer, and also that in some areas, the mercury chlorides are not co-localized with $Hg_3S_2Cl_2$ ones. In view of the patterns observed in other works of art and considering the phases identified by XRD on this sample, it is plausible that the mercury chloride compounds involved here include calomel (Hg_2Cl_2).

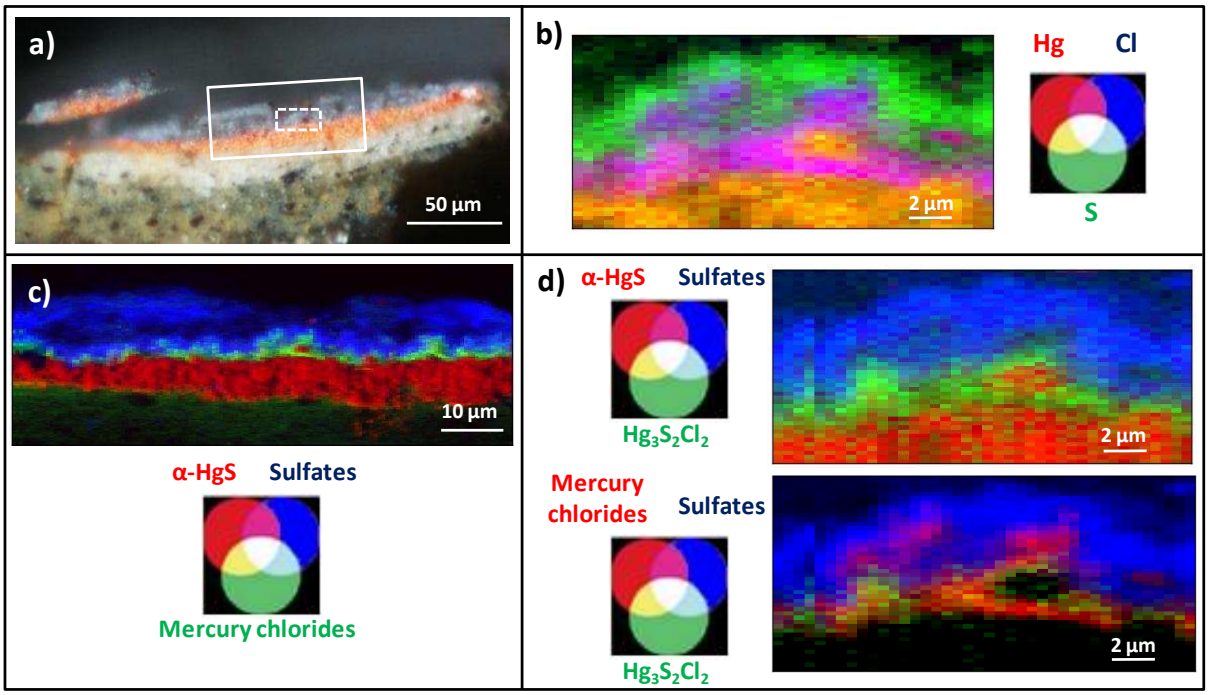

Figure 2.37.: a) *Visible picture of sample Gi-B;* ***b)*** *RGB composite of µ-XRF elemental maps from the area in (a) indicated by the dashed rectangle, acquired at 2.9 keV: mercury (red), sulfur (green) and chlorine (blue);* ***c)*** *Maps of the area indicated by the solid rectangle in (a): an RGB composite of sulfur at 2.4716 keV (cinnabar, red), chlorine at 2.8232 keV (mercury chloride compounds, green) and sulfur at 2.4825 keV (sulfates, blue) is shown;* ***d)*** *RGB composite of (upper image) sulfur at 2.4716 keV (cinnabar, red), sulfur at 2.4726 keV ($Hg_3S_2Cl_2$ compounds, green) and sulfur at 2.4825 keV (sulfates, blue) and (lower image) chlorine at 2.8232 keV (mercury chloride compounds, red), sulfur at 2.4726 keV ($Hg_3S_2Cl_2$ compounds, green) and sulfur at 2.4825 keV (sulfates, blue).*

All these results were summarized in a restoration committee report *[C2RMF report n°22484]*; this example showed that the restoration of a work of art is not only concerned with the identification of alterations. For some conservators, even the degraded material is part of the original pictorial layer, i.e. the material chosen by the artist, so that it must be left untouched. For others, having black-appearing blood in Christ's wounds is not consistent with the original intent of the artist. From a more pragmatic point of view, the degradation could be considered to be a protection layer, of which the removal may cause the start of a new alteration period for mercury sulfide. At the time of writing of this thesis, the discussion concerning the restoration procedure of the Giotto Crucifix was still ongoing. This case is a good example to show the importance of investigations concerning degradation of materials

as it involves the past, the present and also the possible future of works of art and how to improve their fate.

2.3. Conclusions from the analyses of original works of art

After studying different works of art affected by the degradation of red mercury sulfide, it is possible to conclude that the same (type of) degradation compounds were identified in most cases: Hg-Cl containing compounds (such as calomel), Hg-S-Cl containing compounds (corderoite, kenhsuite, β-$Hg_3S_2Cl_2$) and sulfates (gypsum, anhydrite and unidentified ones). Some of the observed compounds could not be clearly identified and also for some it also was not absolutely clear that they were formed as a consequences or the instability of α-HgS.

While the above-mentioned phases could not be identified in all samples analyzed, a very similar multi-layered stratigraphy was encountered in most cases (see Figure 2.38): partially intergrown with the original pigment layer and partially covering it, an intermediate layer of $Hg_3S_2Cl_2$ compounds is formed. When β-$Hg_3S_2Cl_2$ is present, it overlaps to a larger extent with the α-HgS layer than this is the case for corderoite and kenhsuite. The $Hg_3S_2Cl_2$ layer gradually turns into a layer of mercury chlorine containing compounds (such as calomel). On top of that, an additional sulfate-rich layer is usually present.

Images and schemes of samples	Layers	Elementary composition	Species	Phases
Rubens' painting, sample B 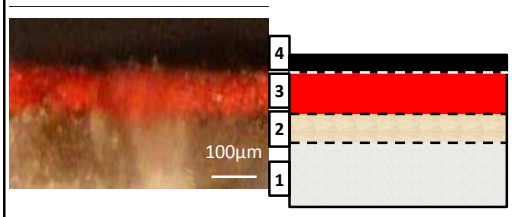	4	Hg, S, Cl	Mercury chlorides	Hg_2Cl_2 *(calomel)* γ-$Hg_3S_2Cl_2$ *(kenhsuite)*
	3	Hg, S	Mercury sulfides	α-HgS
	2	Pb, C, O, H	Preparation layer	$(PbCO_3)_2.Pb(OH)_2$
	1	Ca, C, O	Preparation layer	$CaCO_3$ *(calcite)*
Pedralbes' painting 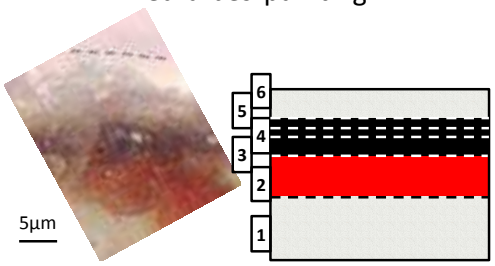	6	Ca, S, O, H	Sulfates (plaster)	$CaSO_4$ *(anhydrite)* $CaSO_4.2H_2O$ *(gypsum)*
	5	Hg, Cl	Mercury chlorides	Hg_2Cl_2 *(calomel)*
	4	Hg, S, Cl	Mercury chlorides	α-$Hg_3S_2Cl_2$ *(corderoite)* γ-$Hg_3S_2Cl_2$ *(kenhsuite)*
	3	Hg, S, Cl	Mercury chlorides	β-$Hg_3S_2Cl_2$
	2	Hg, S	Mercury sulfides	α-HgS
	1	Ca, C, O	Preparation layer	$CaCO_3$ *(calcite)*
Pompeian fresco, grey sample 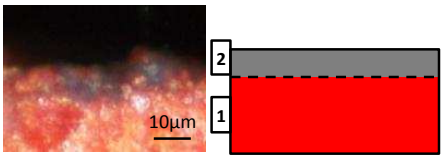	2	Hg, S, Cl, Ca, O, H, Al, Si, Mg, Na, Fe	Sulfates, mercury chlorides	Sulfates β-$Hg_3S_2Cl_2$
	1	Hg, S, Ca, C, O, Al, Si, Mg, Na, Fe	Mercury sulfides, mineral binder	α-HgS $CaCO_3$ *(calcite)*
Pompeian fresco, black sample 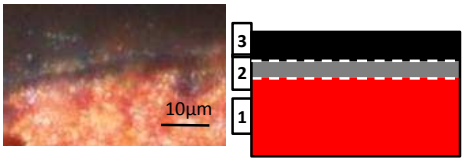	3	Ca, S, O, H, Al, Si, Mg, Na, Fe	Sulfates	$CaSO_4$ *(anhydrite)* $CaSO_4.2H_2O$ *(gypsum)*
	2	Hg, S, Cl, Al, Si, Mg, Na, Fe	Mercury chlorides	$Hg_3S_2Cl_2$
	1	Hg, S, Ca, C, O, Al, Si, Mg, Na, Fe	Mercury sulfides, mineral binder	α-HgS $CaCO_3$ *(calcite)*
Brueghel's panels 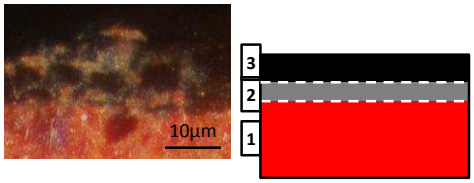	3	S, Pb, Al, Ca, K, Na	Sulfates	
	2	Hg, S, Cl, Fe, Pb, Al, Ca, K	Cl-containing compounds	
	1	Hg, S, Pb, Al	Mercury sulfides	α-HgS
The cross by Giotto 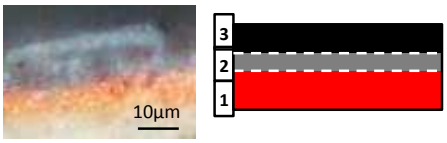	3	S, Cl, C, O, Pb, K, Ca, Na, Mg, Al, Si, P	Sulfates	
	2	Hg, S, Cl, C, O, Pb, K, Ca	Mercury chlorides	Hg_2Cl_2 *(calomel)* $Hg_3S_2Cl_2$
	1	Hg, S, C, O	Mercury sulfides	α-HgS

Figure 2.38.: *Summary of the compounds identified on the different works of art studied and the stratigraphy observed for each cross-section.*

Chapter 3: Experimental study of instability of α-HgS

Content

Abstract

Artificial ageing is commonly used to reproduce and understand the degradation of different materials. Assessing the effects of several environmental parameters (such as light, humidity, exogenous chemicals such as chlorine, SO_2…) is required to identify the factors causing materials alteration and possibly to propose restoration and conservation treatments. In this chapter, a number of experiments are described that were performed to reproduce the degradation of red mercury sulfide (vermilion and cinnabar) in order to better understand the physico-chemical processes governing the color change and to assess the role of the factors influencing the degradation.

3.1. Behavior of α-HgS during heating and laser irradiation

3.1.1. Hypotheses from previous studies

As mentioned in Chapter 1, the first hypothesis concerning the degradation of cinnabar, as it was taught in History of Art schools in previous centuries, was based on its transformation to metacinnabar. This compound is also mercury sulfide but in its black form, so that it might explain the dark color of the degraded works of art. The thought of metacinnabar as being responsible for the black color of degradation was also strong as it is difficult to distinguish α-HgS from β-HgS by chemical analyses (see reference spectra in Section 1.6). However, this hypothesis is disputable since the transformation of the hexagonal form into the cubic one is assumed to happen only from 344°C onwards *[F.W. Dickson, 1959]* (Figure 3.1).

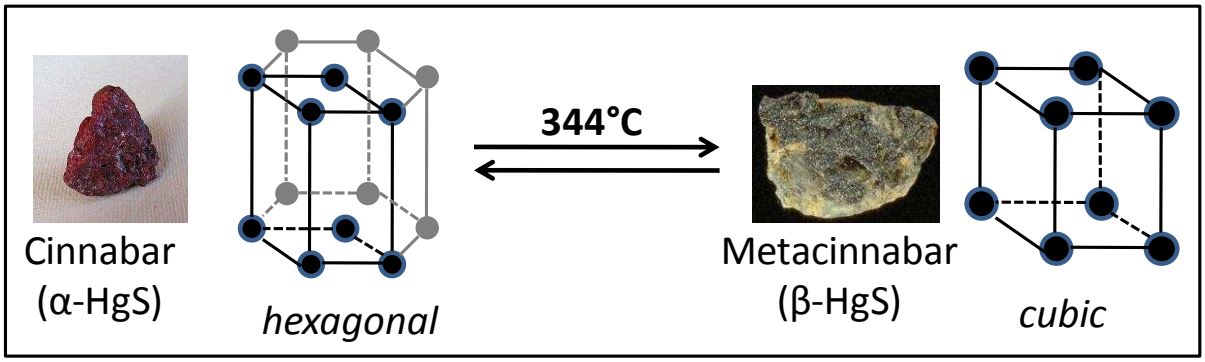

Figure 3.1.: *Summary of the transformation of cinnabar into metacinnabar from [F.W. Dickson, 1959].*

The study of the relations between these two phases by Dickson et al. showed that the presence of iron and zinc decreased the transformation temperature respectively to 305 and 204°C. In their experiments, the conversion of α-HgS to β-HgS was initiated at 355°C and completed at 381°C with a step of 10°C per minute by differential thermal analysis (DTA). Approximately the same transformation temperature was given by Ferro et al. (347°C) corresponding to an enthalpy of formation ($\Delta_{trans}H^0_T$) of 8 ± 2 kJ.mol^{-1} *[D. Ferro, 1989]*. In another study, relations between cinnabar, metacinnabar and hypercinnabar (γ-HgS) were compared and yielded the following transition temperatures *[R.W. Potter, 1978]*:

$$\text{Metacinnabar in equilibrium with Hg(l)} \xrightarrow{345\pm2^\circ C} \text{cinnabar}$$

$$\text{Metacinnabar in equilibrium with S(l)} \xrightarrow{315\pm3^{\circ}C} \text{cinnabar}$$

$$\text{Hypercinnabar in equilibrium with Hg(l)} \xrightarrow{481\pm3^{\circ}C} \text{metacinnabar}$$

$$\text{Hypercinnabar in equilibrium with S(l)} \xrightarrow{470\pm3^{\circ}C} \text{metacinnabar}$$

This same group gave a diagram showing the presence of these compounds according to the temperature and the atomic percentage of Hg (Figure 3.2).

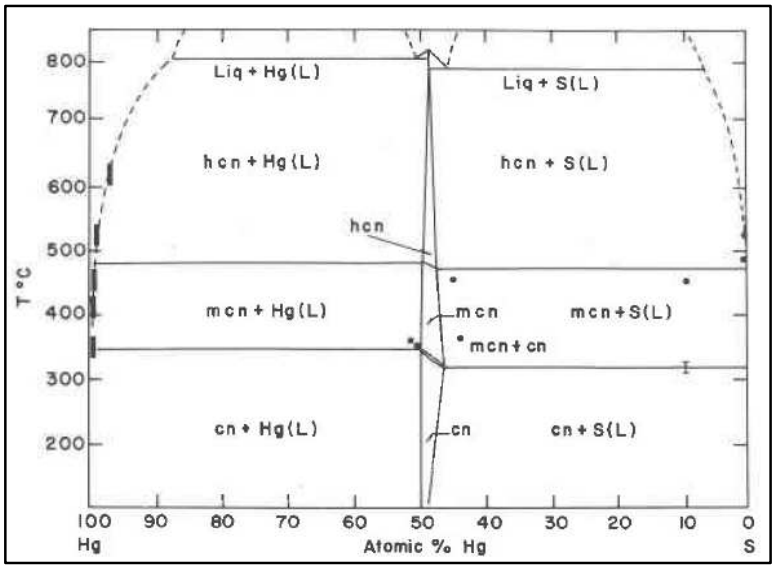

Figure 3.2.: *Diagram of the presence of cinnabar (cn), metacinnabar (mcn) and hypercinnabar (hcn) according to the temperature and the atomic percentage of Hg [R.W. Potter, 1978].*

Regarding the synthesis of HgS, a reverse stability is observed. Zeng et al. dissolved 0.6 g of mercury nitrate with 1.4 g of sodium thiosulfide in different solvents, and then heated it in an autoclave placed in a furnace for 12 hours. Below 80°C, nothing happened; at temperature above than 80°C, only metacinnabar is formed; then at higher temperature a mixture of α-HgS/β-HgS is formed up to 180°C where pure cinnabar was obtained *[J.H. Zeng, 2001]*. Controlling the parameters for the synthesis of α/β-HgS is then essential. Indeed, in another study, it was shown that when bisulfide was added to a goethite suspension at pH 7.5 to which Hg(II) was adsorbed, it induced the formation of metacinnabar *[A.J. Slowey, 2006]*.

According to the literature, it seems difficult to consider that on works of art, red mercury sulfide could transform into metacinnabar, except maybe during a building fire.

Concerning color changes, Grout et al. showed that, next to the phase transformation, visual changes could already be observed at lower temperature: vermilion blackens at 200°C and becomes red again when it is left to rest at room temperature; vermilion mixed with egg white remains red at 60°C in darkness whereas it darkened slightly at the same temperature when mixed with oil; vermilion prepared with egg white darkened at 60°C when exposed to light *[R. Grout, 2000]*.

During this study, α-HgS was heat-treated in an oven and by laser irradiation, first to form metacinnabar in order to obtain reference compounds, and then to try and observe an intermediate state of the material where cinnabar presents a black color but no metacinnabar is formed. This step in the transformation of cinnabar was not well described in the literature.

3.1.2. Experiments

Heating of red mercury sulfide

To understand the behavior of red mercury sulfide above room temperature, different samples of natural cinnabar and synthetic vermilion were heated respectively in a closed vessel or in a sealed tube placed in an oven.

When natural α-HgS ore was heated from 25°C to 400°C while waiting 10 minutes at each 50°C interval, visual changes were seen from 360°C (blackening and appearance of white spots) but no metacinnabar was identified. From 390°C, metacinnabar was identified by XRD. These two steps became 340 and 350°C when the waiting interval at each 10°C temperature increment was 1 hour; at 380°C the sample was completely evaporated. After heating 17 hours at 350°C, nothing was left from the ore.

When heating synthetic powders of vermilion, sealed tubes were used to keep gases inside and to allow observation of the reversibility of reactions (Figure 3.3a). After 20 hours of heating at 365°C, the powder inside the tube appeared brownish and XRD analyses showed the presence of metacinnabar in the capsule. After 7 hours at room temperature, the amount of metacinnabar among the vermilion was less important but it was still

detectable by XRD. The capsule was put again in the oven at 365°C and after 105 hours, a mixture of the two compounds was well identified by XRD (Figure 3.3c). After 267 hours of heating, no red grains were visible in the tube anymore (Figure 3.3b), but XRD analyses still showed the presence of vermilion in very low proportion.

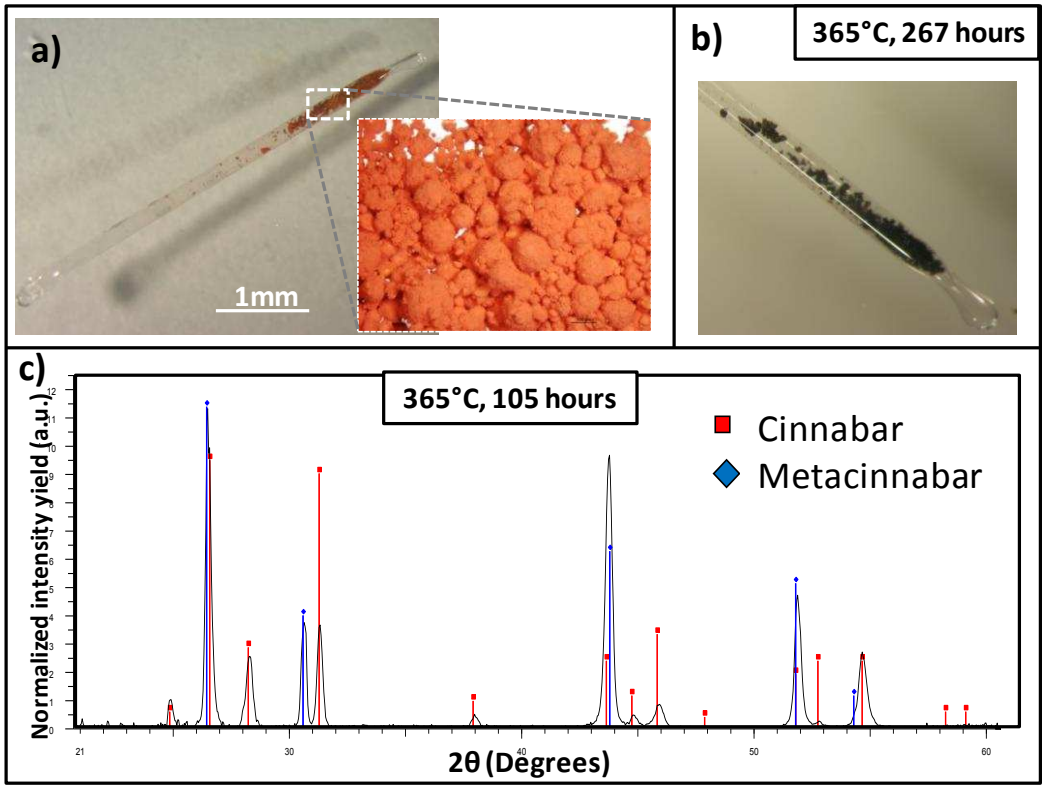

Figure 3.3.: a) *Visible pictures of vermilion before ageing;* ***b)*** *Visible pictures of vermilion heated at 365°C during 267 hours;* ***c)*** *Diffractogram obtained after heating α-HgS at 365°C during 105 hours.*

An intermediate state of red mercury sulfide during heating (dark brown color but no metacinnabar) was observed when cinnabar crystals were heated, but not when a similar procedure was applied to vermilion (i.e. synthetic α-HgS) crystals.

Laser irradiation and analyses by Raman spectroscopy

Next to heating, laser irradiation can also induce transformations to materials. These transformations were observed and studied during previous investigations, as laser irradiation is used in the Cultural Heritage field to clean stone statues and buildings from dust. Thus pigments present on these surfaces could suffer from this irradiation and be

altered. Cooper et al. already showed the influence of laser irradiation on lead white *[M.I. Cooper, 2002]*, but α-HgS is also very sensitive in this respect. Indeed, a study made with a typical laser used for restoration of works of art (1064 cm^{-1}), showed that its use on an α-HgS surface changed the Hg:S ratio and induced a very important and permanent discoloration *[P. Pouli, 2003]*. Other experiments on pure cinnabar and other pigments with different laser wavelengths (1064, 532, 355 and 266 nm) allowed to identify the formation of metacinnabar by XRD *[M. Chappé, 2003]*. Thus, it is recommended to not perform laser cleaning on polychrome statues or wall paintings containing red mercury sulfide.

It was seen that cinnabar transforms into metacinnabar at high temperatures. A laser is thus an interesting light source to study the behavior of red mercury sulfide as a high laser power can induce heating of materials; coupled to a spectrometer, it is possible to follow structural changes of the sample. Analyses to test the effect of laser irradiation on red α-HgS samples with Raman spectroscopy were performed on both instruments used for this research (see Appendix B.e). These tests also allowed determining a safe power to work without burning the samples. Results obtained on the Infinity Raman instrument at C2RMF are presented below.

A cinnabar crystal originating from China (Tongren deposit, Guizhou province) was irradiated during 30 seconds with a green laser (532 nm) of a Raman microspectrometer at different power values. When a power from 50 µW to 520 µW was applied on the sample, the resulting Raman spectrum did not change, showing typical peaks for cinnabar, and no visual change was seen on the crystal. At 1.7 µW, a broad band appeared in the Raman spectrum at 1442 cm^{-1} and continued to increase with higher values of power; at this (or higher) power, the sample turned black. The peak at 1442 cm^{-1} corresponds probably to a bending mode but the nature of the molecular bond causing this peak is still unknown. At 3.5 mW to 7 mW (where the experiment was stopped), two other peaks appeared in the Raman spectra at 493 cm^{-1} and 1253 cm^{-1}. Also these peaks were not identified yet. All these spectra are presented in Figure 3.4.

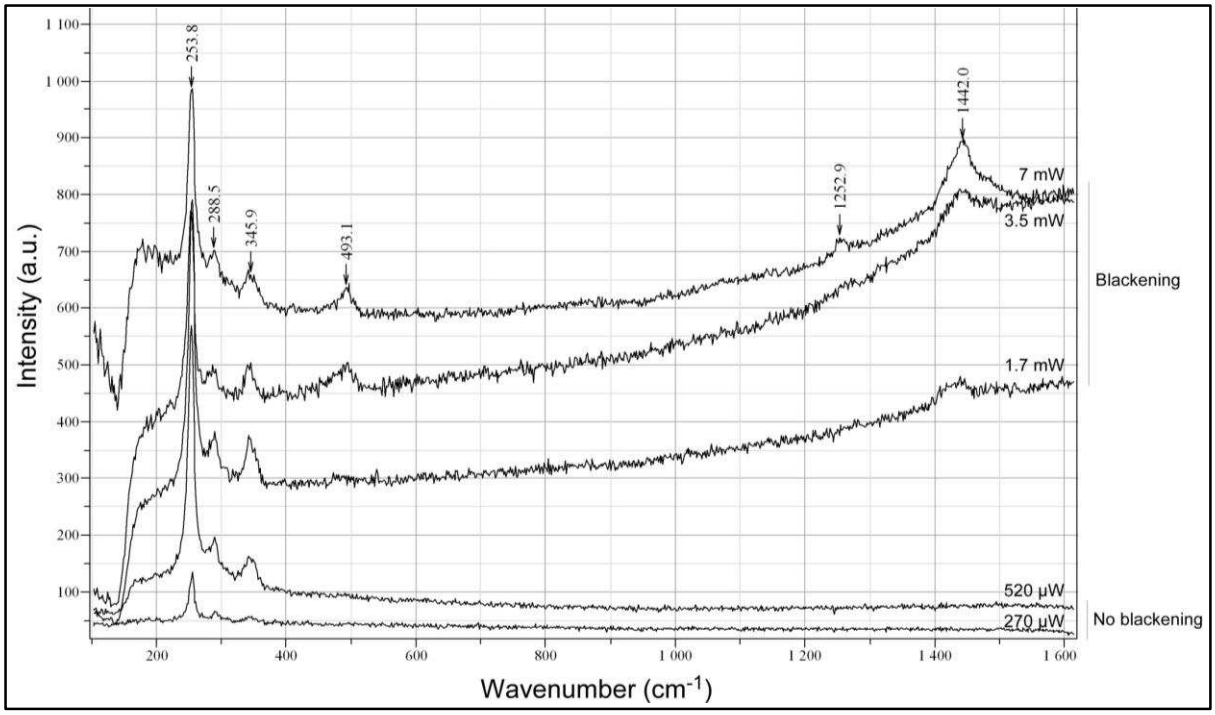

Figure 3.4.: *Raman spectra acquired from a red mercury sulfide crystal at C2RMF under different powers of irradiation (270 µW, 520 µW, 1.7 mW, 3.5 mW and 7 mW). The last three powers induced a blackening of the sample.*

The appearance of previously unseen peaks with increasing laser power suggests a structural modification, but contrary to what was expected, the peaks corresponding to cinnabar did not show any change. It was possible by means of laser irradiation to blacken the red mercury sulfide crystal on a thin surface (less than 1 µm) without forming metacinnabar nor secondary phases identifiable by any structural or elemental analysis. Since laser irradiation is effective on a small surface and thickness only, the presence of metacinnabar could not be totally excluded. Further analyses with superficial methods on blackened α-HgS surfaces could be useful to study this intermediate state of α-HgS in greater detail.

Following these experiments, all Raman analyses on red mercury sulfide were performed at a “safe” power value which was chosen to be below 100 µW.

3.2. Effects of light and different chemical treatments on α-HgS ageing

3.2.1. Bibliography

Artificial ageing is commonly used to study the influence of the environment on materials. Different factors can be considered such as temperature (variations), thermal shocks, atmospheric agents (polluting agents, moisture), aggressive chemical agents, cleaning products, closed or ventilated atmospheres, contact with other materials, mechanical constraints and the orientation of the exposed surfaces *[J. Verdu, 1984]*. To assess all these factors in the Cultural Heritage field, various protocols, usually involving ageing chambers, were previously employed by different research groups. As an example, with lead chromate pigments as the ones used by V. Van Gogh, it was possible to reproduce their degradation by artificial ageing and use it as a valuable tool to understand the natural processes that are taking place in the paintings of this artist *[L. Monico, 2011]*. Natural and artificial ageing were compared by Cohen et al. by preparing three types of sample (pigment, medium and pigment + medium), exposing them in museums, churches and galleries or to artificial ageing condutions (light, pollutants), and finally observing the resulting changes in the FTIR spectra of the samples *[N.S. Cohen, 2000]*. The presence of a binding medium was shown to increase the degradation of some pigments *[M.I. Cooper, 2002]* and the presence of specific pigments was found to catalyze the oxidative polymerization of resins *[M.T. Domenech-Carbo, 2006]*. Arbizzani et al. employed multiple ageing protocols including irradiation by UV light, presence of pollutants (SO_x and NO_x), relative humidity (between 55 and 80 %) and cycles at different temperature with the succession of all these different parameters *[R. Arbizzani, 2004]*. The same kind of protocols were performed by different research groups focusing on different factors *[M. Bacci, 2000; P. Ropret, 2007]*; for example, Casadio et al. showed that for the zinc yellow pigment the most influential parameters are the high relative humidity (90 %) and the presence of SO_2 *[F. Casadio, 2008]*. Cyclic conditioning were also used by Aze to study the alteration of lead pigments in order to represent the temperature and relative humidity changes (respectively from -10 to 40°C and from 0 to 80%) painting materials can suffer from *[S. Aze, 2005]*.

In order to perform artificial ageing on red mercury sulfide samples, factors playing a role in their degradation were studied in the literature in order to adjust the protocols used.

In most cases, the aim of artificial ageing is to accelerate processes that may take place spontaneously in nature but on time scales of months or years. One of the ways to perform artificial ageing is to increase the temperature *[Seves et al., 2000]*. Red mercury sulfide is very sensitive to temperatures higher than 50°C; therefore the study was focused on other factors potentially responsible for alteration and was carried out at room temperature.

Exposure to light

Since Pliny the Elder, all observations have identified light as one of the main factors inducing color alteration in α-HgS samples. For various pigments, Felder-Casagrande et al. applied a flux of 200.000 lux at room temperature on pigments mixed with egg yolk tempera and demonstrated changes in FTIR spectra of the samples *[S. Felder-Casagrande, 1997]*. Marengo et al. observed an oxidation of organic pigments after irradiating them 272 hours with UV-light at a power of 15 W *[E. Marengo, 2006]*. Gettens et al. showed that α-HgS darkens under 400 – 570 nm light, its absorbance region; however this phenomenon is reversible in darkness and can be reduced by covering the vermilion layer with red glazes *[R.J. Gettens, 1972].* Experiments also showed that the kinetics of alteration induced by light depends on the type of red mercury sulfide studied. Vermilion produced by the “wet process” appeared to darken faster than the one produced using the “dry process” (see Section 1.2.); both types of vermilion aged faster than natural cinnabar *[R. Grout, 2000]*. Another study identified that the granulometry of the pigment powder also plays a role: rough samples darkened faster than smooth and polished ones *[V. Terrapon, 2010]*. This last study also details the action of different wavelengths on the reaction kinetics and shows that after seven days under solar irradiation, α-HgS loses mass and forms an amorphous layer of mercury sulfide. Another relevant observation made during previous studies is that a long exposure to light intensifies the darkening but does not increase the thickness of the degradation layer *[R.M. Dreyer, 1939]*.

McCormack explains that the photosensitivity of cinnabar is due to the absorption of light energy which promotes electrons from low energy orbitals to higher ones. These electrons may return to the ground state, and this shifting can cause changes in color *[J.K. McCormack, 2000]*. Very recent works from Da Pieve et al. (not published yet) are going further in this consideration. Thanks to theoretical calculations, they estimated band edges positions at the surface of α-HgS: -6.39 eV for the valence band maximum (E_{VBM}) and -3.95 eV for the conduction band minimum (E_{CBM}). When an α-HgS surface is exposed to light, a photoexcited electron may be promoted from the valence band (maximum) to the conduction band (minimum). With this consideration, Da Pieve et al. compared redox potential of couples containing possible degrading species to these values. Since the redox potential of the Cl^-/Cl_2 couple is -5.80 eV and therefore higher than E_{VBM}, this may indicate that an electron transfer is possible from the Cl-/Cl_2 couple to the valence band of α-HgS. Taking the same path, Da Pieve et al. showed that for the Hg(II)/Hg(0) and Hg(I)/Hg(0) couples, the formation of metallic mercury after photoirradiation of corderoite do not appear to be possible whereas it could be favored by photoirradiation of calomel and $HgCl_2$ *[F. Da Pieve, 2012]*. This theoretical study, unfortunately only performed recently, could explain why some transformations in the degradation pathways of red mercury sulfide effectively take place and others do not.

Influence of chlorine

Next to light, the presence of halides also appears to be responsible for part of the instability of α-HgS. Davidson et al. made the following observation: red mercury sulfide suspended in aqueous potassium salt solutions and exposed to light, gave rise, after washing and drying at 80°C, to a black powder *[R.S. Davidson, 1981]*. Soon, chlorine-containing compounds were suspected to be related to the color change of degraded works of art; the compounds were identified by multiple analytical techniques such as SIMS *[K. Keune, 2005]*, Raman spectroscopy *[M. Spring, 2002]*, XRF and XANES *[M. Cotte, 2006; M. Cotte, 2008]*. Additionally, Spring et al. showed that the presence of sodium chlorine can accelerate vermilion blackening whereas red lake glazes appear to protect it by filtering out light and chlorides *[M. Spring, 2002]*.

Keune et al. proposed that the blackening induced by light and the formation of Hg,Cl compounds are two separate steps in the degradation process: they suggested that chlorine acts as a catalyst in the first step that consists of the light-induced transformation of HgS into Hg(0) and S(0); then mercury reacts with chlorine in multiple steps to form Hg,Cl compounds *[K. Keune, 2005]*. Among all the other experiments, McCormack tried different protocols with chlorinated solutions and observed the color obtained. He also qualified cinnabar as "photosensitive" (P) and "non-photosensitive" (NP) which correspond to red mercury sulfide that will respectively darken or not under light exposure. He also showed that the first type of red mercury sulfide contains noteworthy concentrations of chlorine whereas the second type does not. Some of these experiments are detailed in Figure 3.5. *[J.K. McCormack, 2000]*.

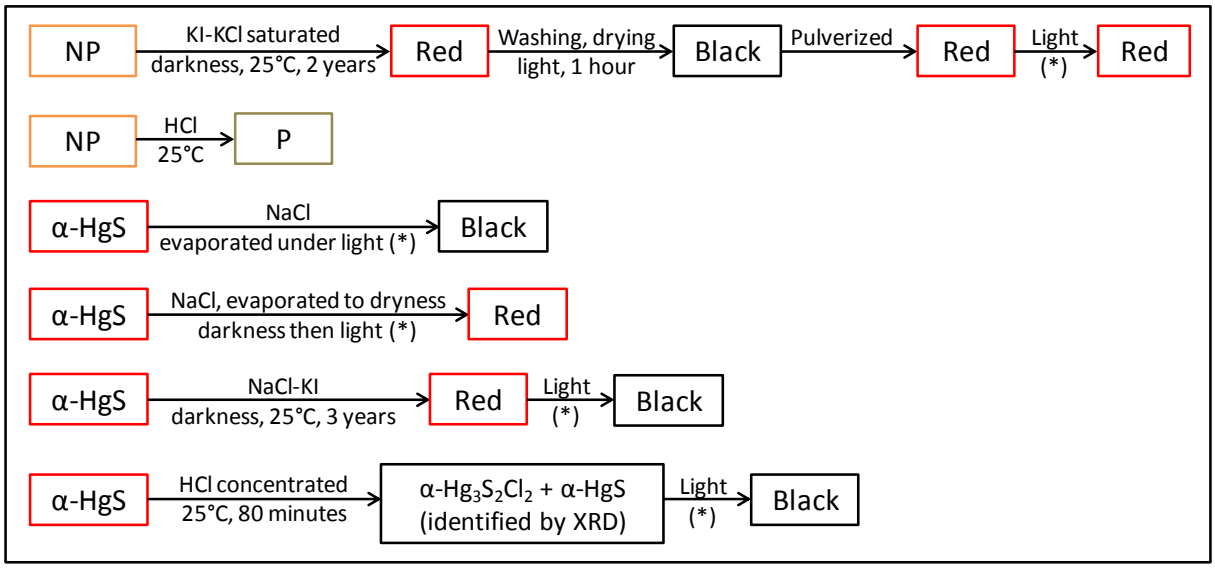

Figure 3.5.: *Summary of ageing experiments performed by McCormack giving the color of the products obtained at each step. "NP" and "P" correspond respectively to "non-photosensitive" and "photosensitive". (*) means that time of exposure was not indicated in the publication.*

As discussed in Chapter 2, samples analyzed from degraded works of art showed the presence of chlorinated compounds, i.e. Hg_2Cl_2 and different types of $Hg_3S_2Cl_2$. These results confirm what was found in the literature concerning the influence of chlorine on α-HgS degradation.

To chose an appropriate protocol for artificial ageing, favorable conditions for the formation of each phase identified as degradation products from red mercury sulfide have to be identified. A consideration of the pH of the solutions used to age red mercury sulfide showed that nothing happened in basic conditions whereas in acidic conditions a darkening was noticed *[E.E. Foord, 1974].* Among all Eh-pH diagrams constructed for the Hg-S-Cl-H_2O system, only one involves the presence of corderoite (α-$Hg_3S_2Cl_2$) (see Figure 3.6); it shows that corderoite requires extremely acid, and mildly reducing conditions to be formed *[G.A. Parks, 1979]*.

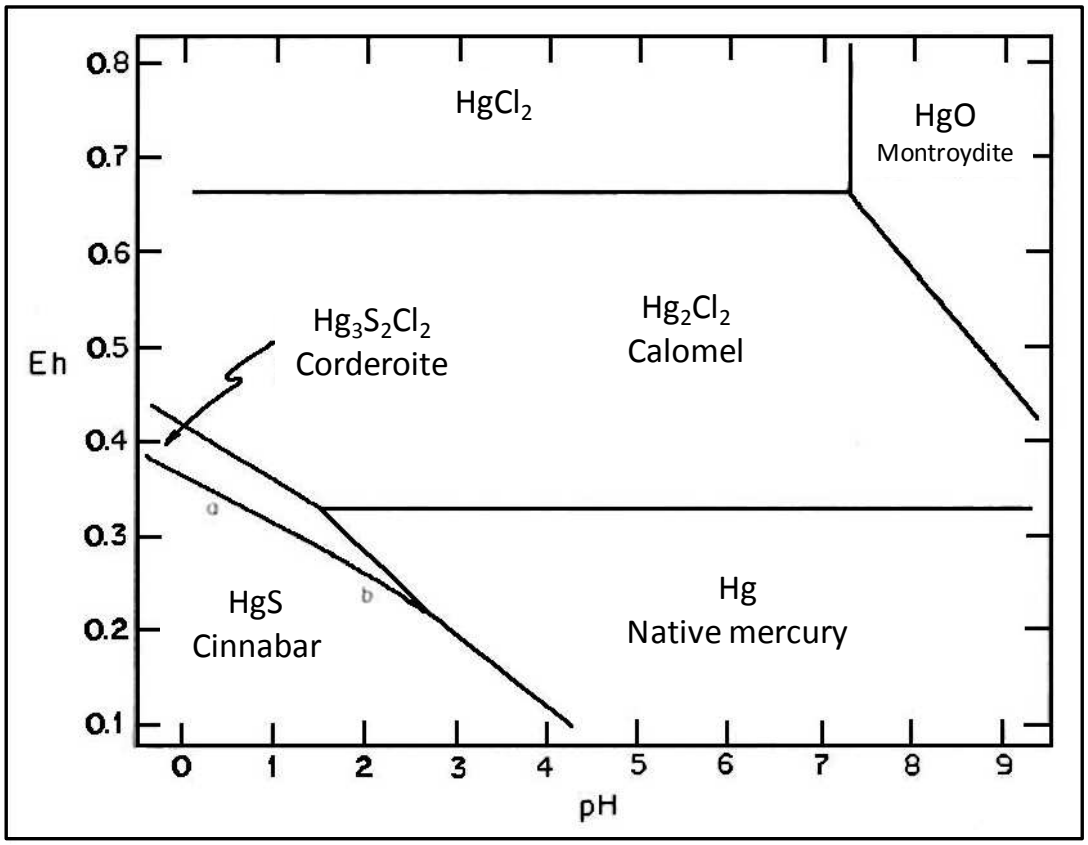

Figure 3.6.: *Eh-pH diagram for the system Hg-S-Cl-H_2O at 298 K presented by Parks et al. with activities of Cl^- and the dominant SO_4^{2-} species at 0.1 M [G.A. Parks, 1979].*

3.2.2. Sample preparation

Different types of samples were prepared for artificial ageing.

Vermilion pellets without any binder

Multiple methods were tried out to prepare pigments without any binder to strengthen the cohesion of the sample. Tests were prepared with powder mixed with resin, which resulted in heterogeneous and not reproducible samples. Mechanically stable pellets could be prepared by milling the powder and pressing it into a cylindrical pellet of 3 mm diameter and around 800 µm thickness (Figure 3.7a). The pellet was then partially embedded in resin in order to have at least one face not covered and to allow a direct exchange with the atmosphere.

The resin usually employed for embedding purposes is an epoxy resin (Araldite 2020); however, this material contains sulfur and chlorine, which are elements that play an important role in the degradation of red mercury sulfide. Thus, the resin employed here was a polyester resin (SODY 33) in which these disturbing elements are not present.

Vermilion powder (α-HgS, Prolabo) pellets were prepared. Binary mixtures of this pigment with other compounds (sodium chloride, NaCl (Prolabo); gypsum, $CaSO_4.2H_2O$ (Lafarge)) were also prepared in the same way and called “mixed pellets”.

The last type of pellet was composed of two layers, one layer containing various compounds (such as sodium chloride, NaCl (Prolabo); gypsum, $CaSO_4.2H_2O$ (Lafarge); calcite, $CaCO_3$ (Merck); potassium chloride, KCl (Prolabo); or sodium sulfate, Na_2SO_4 (Labosi)), covered by a second layer of vermilion; both layers were pressed together to form a pellet ready to be embedded. This is referred below as a “two-layered pellet”. The model samples were prepared in order to verify the influence of these phases on the reactions taking place and on the reactivity of α-HgS.

Vermilion mixed with binder

In order to be more realistic and close to paintings composition, samples were prepared with a binder, linseed oil (boiled oil from Talens, reference 026). A thin layer of vermilion powder ground and mixed with oil (1:3) was applied on Melinex® (polyester) slides (Figure 3.7b). As

for pellets, two other types of painted slides were prepared: the first type consisting of one layer of an additional compound [such as calcite ($CaCO_3$, Merck) or sodium chloride (NaCl, Prolabo)] mixed with linseed oil below the vermilion layer; the second type with a mixture of vermilion and lead white [$Pb(OH)_2.(PbCO_3)_2$, Prolabo] as this pigment was frequently found mixed with red mercury sulfide in paintings. As references, lead white mixed with linseed oil and the binder alone were also aged in similar conditions.

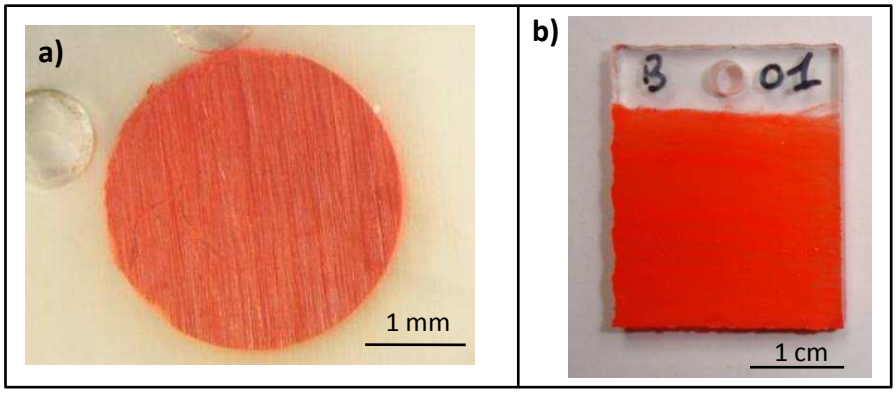

Figure 3.7.: *Pictures of samples prepared for artificial ageing:* ***a)*** *vermilion (α-HgS) pellet;* ***b)*** *painted slide with vermilion mixed with linseed oil.*

3.2.3. Protocols chosen

After considering all protocols described in previous studies, it become clear that different methods might be used to perform artificial ageing of α-HgS samples. In most cases, ageing chambers are used, especially for temperature studies, as environment and conditions of ageing can be controlled. In this study, the aim was to multiply experiments with different solutions and different systems (opened, closed, etc.), which seemed difficult to set up with the few chambers available. Thus, it was then decided to suspend the model samples in small tubes, made in a material transparent to visible and UV light; the tubes were placed in front of a neon emission tube (Figure 3.8a) that emits the solar spectrum; this ensures that a complete spectrum of visible and UV wavelengths impinges on the model samples.

Each tube contains a different aqueous solution (see Table 3.1. for a list). Among these solutions, the concentration of NaCl solution was chosen to be approximately equal to that of seawater (0.505 mol.L^{-1}). Some of the aqueous solutions were prepared at the same concentration in order to be able to compare their effect when only NaCl was present. Sodium hypochlorite was also chosen to be part of the protocol for its high oxidative power, which is useful to accelerate processes to the time scale of months. The other aqueous solutions were chosen for their pH.

Table 3.1.: *List of the aqueous solutions used in ageing protocols with their provenance, the concentration and pH of each one.*

Solution	Provenance	Concentration (mol.L^{-1})	pH
Ultra pure water (H_2O)	/	/	7
Sodium chloride (NaCl)	Prolabo	0.505	9
Sodium hypochloride (NaOCl)	La Croix	15.44	12
Hydrochloric acid (HCl)	VWR Prolabo	32.64	< 1
Potassium chloride (KCl)	Prolabo	0.505	4
Potassium iodide (KI)	Merck	0.505	5
Potassium hydroxide (KOH)	Aldrich	36.36	14
Sodium sulfate (Na_2SO_4)	Labosi	0.505	6
Calcium chloride dihydrate ($CaCl_2.2H_2O$)	J.T. Baker	0.505	4
Sodium hydroxide (NaOH)	Prolabo	16.80	11
Sulfuric acid (H_2SO_4)	Prolabo	18.66	<1

Next to these aqueous solutions, artificial ageing experiments were also performed with carbon tetrachloride (CCl_4), a solvent used in the past by curators on works of art against insects invasion; a concentration of 10.34 mol.L^{-1} was employed.

Due to the presence of these solutions, the relative humidity in the tubes was measured to be 90 %. Attemps to decrease this value were made. For the first test, $SiO_2.xH_2O$ grains were added to the system, but to obtain a relative humidity of 80 %, the volume of the solution could not exceed one droplet. However, with that volume, the solution evaporates quickly, thus not respecting the idea of acting as a container for elements susceptible to degrade the sample. The second test involved mixing a certain proportion of ethylene glycol ($C_2H_6O_2$) with the aqueous solution, but again the relative

humidity remained at a high value. Another answer to this problem would have been to increase the volume of the tube where artificial ageing was performed, but then we faced a laboratory equipment issue. As humidity was not one of the dominant factors in the study and it was preferred to be at saturated vapor pressure, we decided to stay at 90 % of relative humidity.

Each sample (pellet in resin or painted slide) was suspended in one of the tubes, exposed to light, with the solution in the bottom of the tube corresponding to the protocol chosen (Figure 3.8b). For each condition, two tubes were prepared in parallel: one was exposed to light while the second one was wrapped in Al foil to keep the sample in darkness.

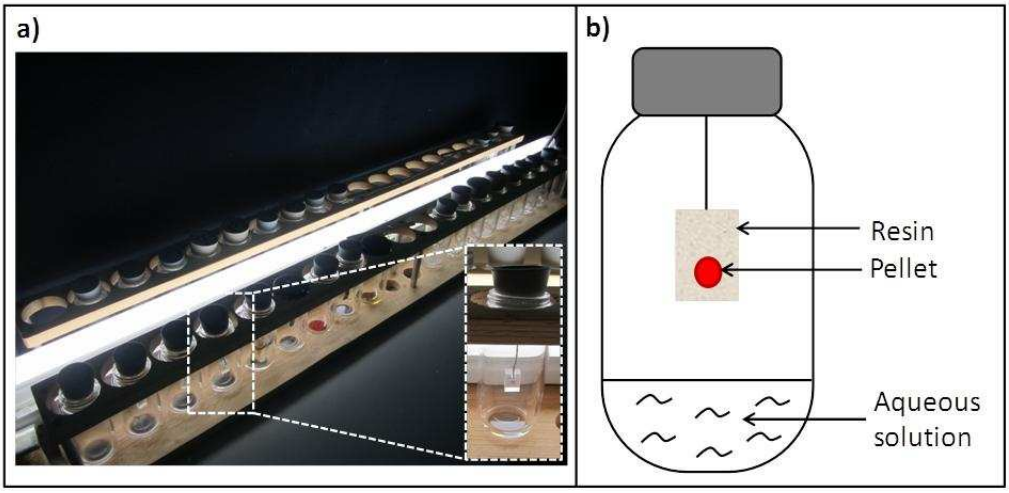

Figure 3.8.: a) *Photograph of the installation used for artificial ageing;* ***b)*** *Scheme of a test tube with a pellet exposed to its atmosphere.*

For all the ageing procedures, two different kinds of systems were used: a closed system and a cyclic one. The closed system consisted in a tube containing one of the solutions described above that was sealed in order to avoid exchange with the ambient air. The cyclic system was performed in a succession of periods of ca. 80 hours with the tube opened and ca. 80 hours with the tube sealed with one of the solutions inside. When tubes are closed, exchanges are limited and the system tends towards an equilibrium. When tubes are opened, this equilibrium is broken and the system is reactivated by the renewal of the atmosphere and the process of precipitation is speeded up. With the open tubes, the relative humidity was measured to be 80 %.

3.3. Results

All results obtained during these artificial ageing experiments are presented in this chapter, and the conclusions made from observations or analyses of the different samples will be given and discussed in the Chapter 4.

Artificially aged samples will be referred to via the following notation:

P *(pellet without any binder) or* **B** *(painted slide with linseed oil as a binder)*

-xxx *(single powder) or* **xxx+xxx** *(mixture of two powders) or* **xxx/xxx** *(two-layered sample, respectively lower/upper layers)*

-light *or* **dark** *(light exposure or not)*

-yyy *(solution to which the sample is exposed to)*

-closed *or* **cyclic** *(type of system)*

-zzzdays *(time of ageing)*.

The results obtained are presented below in three charts: one for results obtained in darkness (Figure 3.9), one for results of ageing due to exposure to light and aqueous solutions not containing chlorine – H_2O, KI, NaOH, Na_2SO_4, H_2SO_4, KOH – (Figure 3.10), and one for ageing due to exposure to light and chlorine containing solutions – KCl, HCl, $CaCl_2.2H_2O$, NaCl, NaOCl, CCl_4 – (Figure 3.11). In these charts, the number of days of exposure is indicated. The time at which visual changes (if any) were observed is not indicated since in general, the color and visual aspect of the model samples evolved gradually during ageing. This evolution is described below.

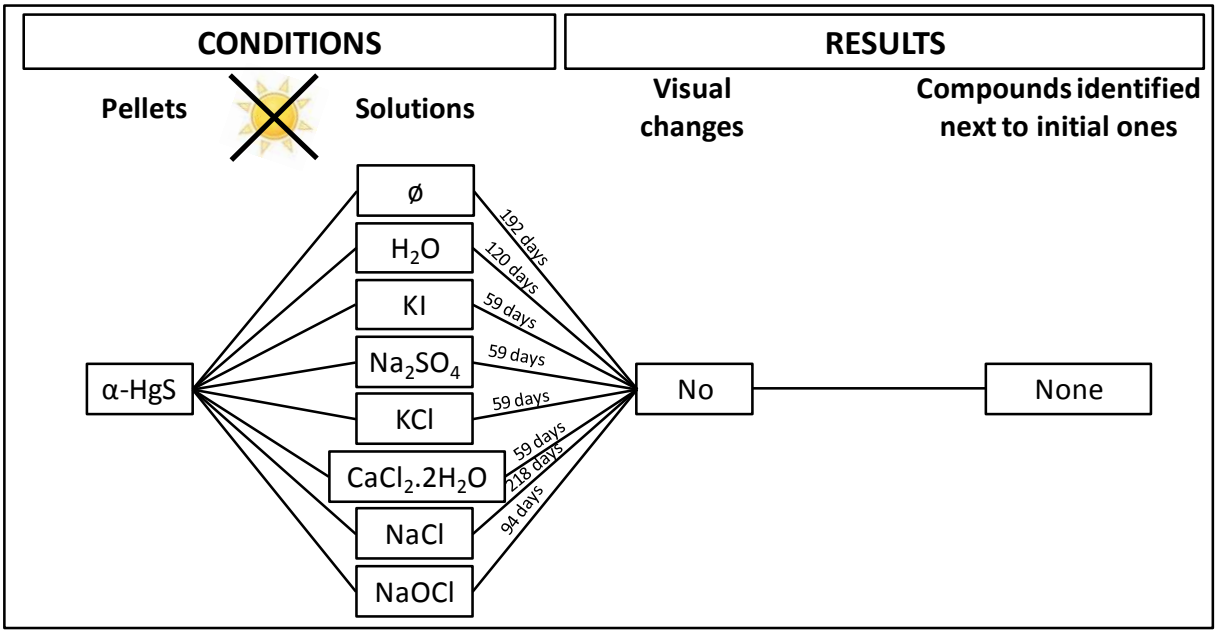

Figure 3.9.: *Summary of results obtained when ageing was performed in darkness, showing no modification to the visual aspect of the pellets and allowing no new compounds at the surface of the model samples to be identified by XRD or XANES. The number of days indicated reflects the total ageing time after which the experiment was stopped. Ø indicates ageing in ambient atmosphere, in the absence of any solution.*

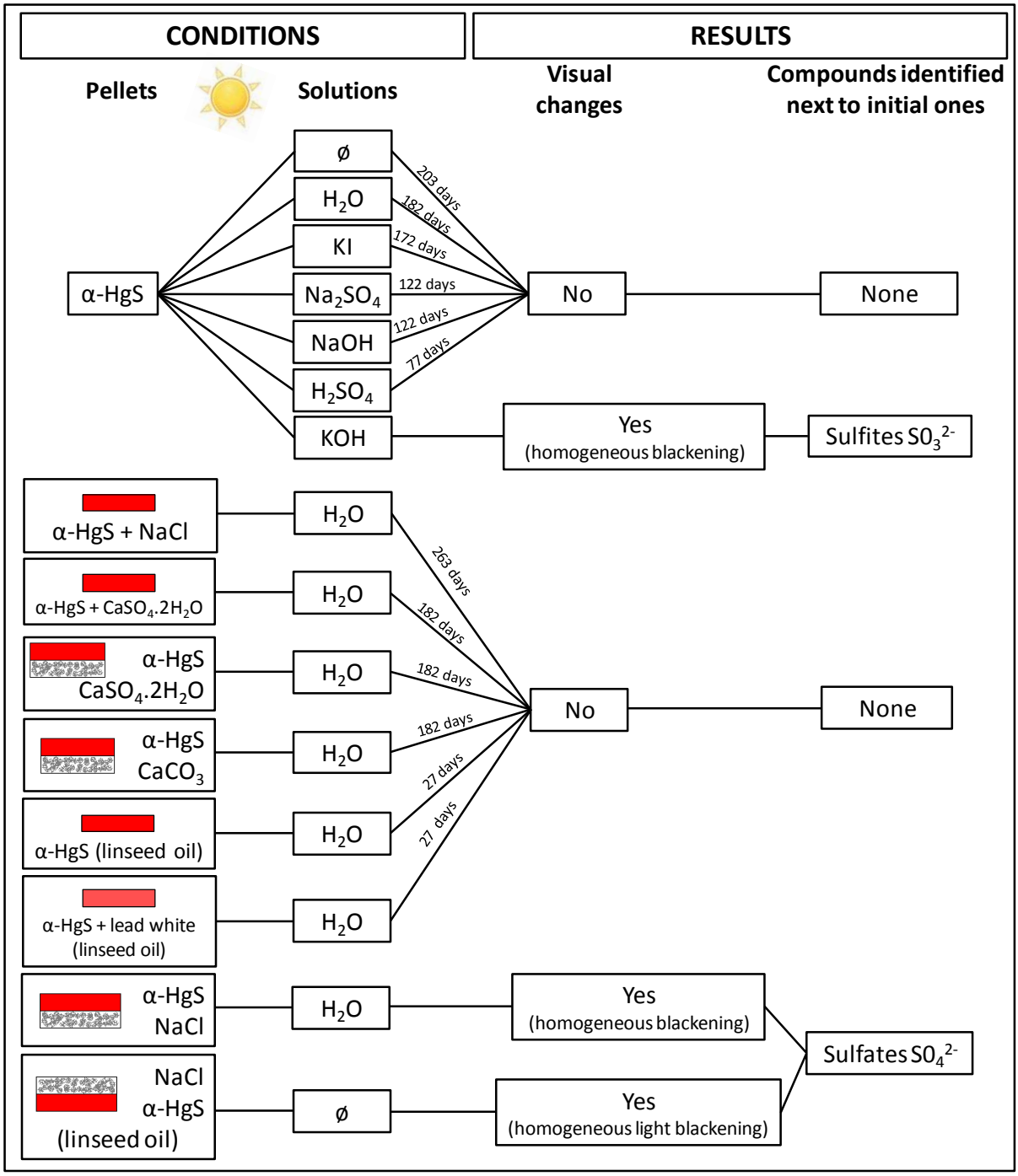

Figure 3.10.: *Summary of results obtained when ageing was performed by exposure to light with solutions not containing chlorine, showing modifications in the visual aspect of the pellets and allowing identification of new compounds at the surface of the model sample by XRD or XANES. The number of days indicated reflects the total time of ageing after which the experiment was stopped. Ø indicates ageing in ambient atmosphere, in the absence of any solution.*

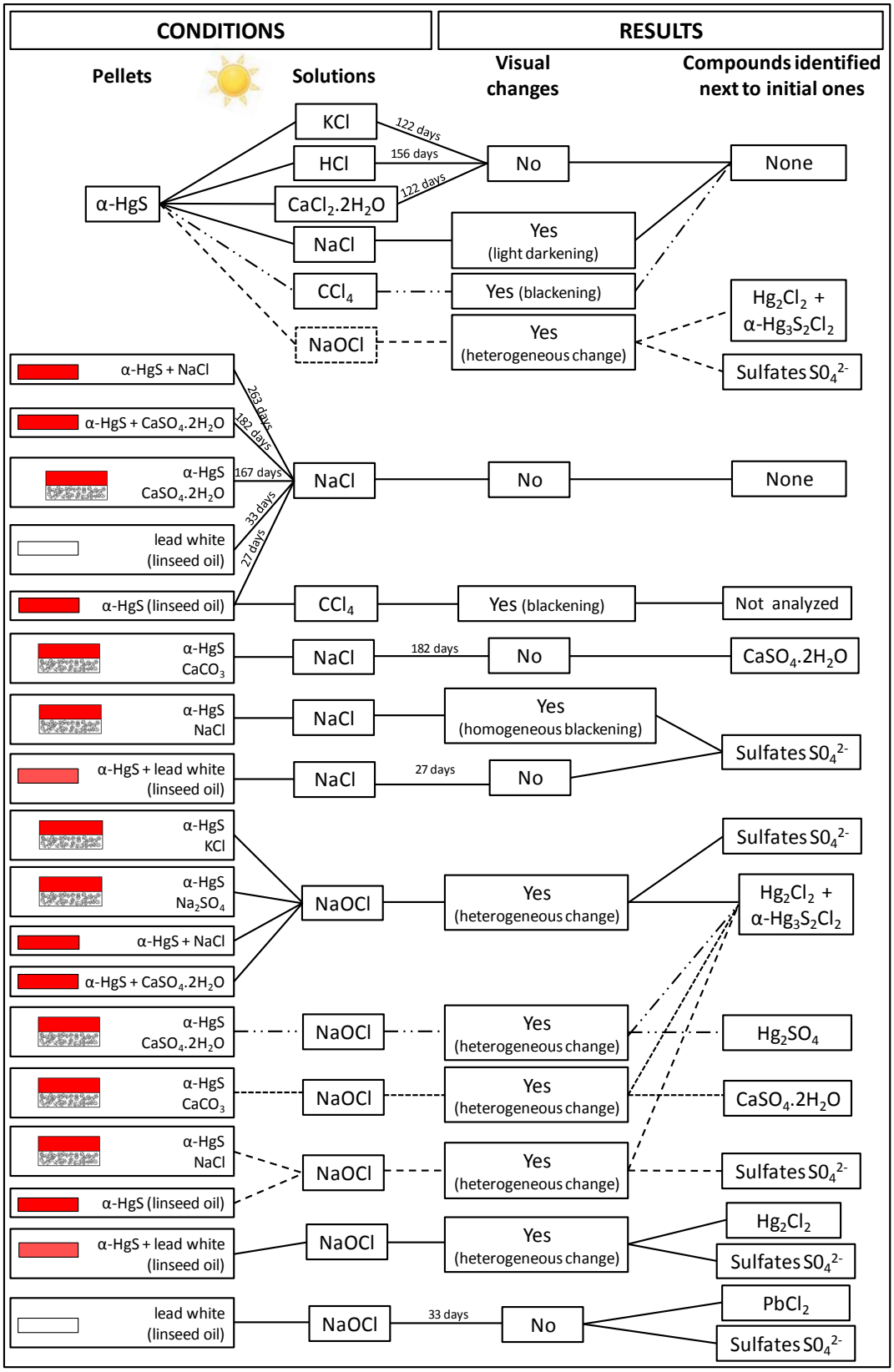

Figure 3.11.: *Summary of results obtained when ageing was performed by exposure to light with solutions containing chlorine, showing modifications in the visual aspect of the pellets and identification of new compounds at the surface of the model sample by XRD or XANES. The number of days indicated reflects the total time of ageing after which the experiment was stopped.*

Exposure to light

The first noteworthy result concerns the influence of activation by light exposure. Indeed, when samples were kept in darkness, whatever the type of sample or the environment present, no visual change was noticed; samples remained red, and nothing was detected by SEM, Raman spectroscopy, XRD or XANES. Light is therefore necessary for the degradation of α-HgS.

Non-chlorinated aqueous solutions

For the samples exposed to light and to non chlorinated aqueous solutions, a few cases gave rise to visual changes. The first one was an ageing performed in a tube containing a potassium hydroxide solution (KOH) where the α-HgS pellet turned grey (see Figure 3.12b). On the surface of this pellet, when XANES was performed at sulfur K-edge, next to the presence of vermilion (peaks at 2.4717 and 2.4760 keV), two other peaks were present which could be related to the presence of sulfite (SO_3^{2-}) or bisulfite ($S_2O_5^{2-}$) (see comparison with α-HgS, Na_2SO_3 and $Na_2S_2O_5$ references in Figure 3.12c). The analysis of this degradation phase by XRD showed new peaks in the diffractogram but belonging to a phase that could not be identified.

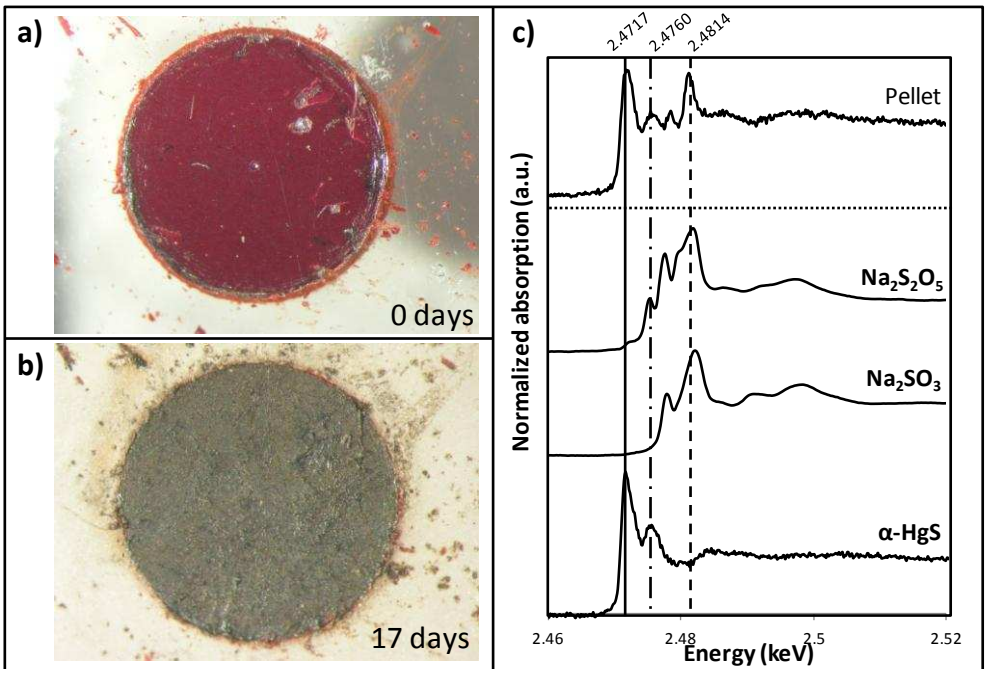

Figure 3.12.: *Ageing of α-HgS pellet by exposure to light and in the presence of potassium hydroxide (KOH) aqueous solution: visible images of* ***a)*** *the unaged pellet and* ***b)*** *the pellet after 17 days of ageing;* ***c)*** *S K-edge XANES spectrum of the surface of the sample compared to the ones of α-HgS, Na_2SO_3 and $Na_2S_2O_5$ references.*

The second case in which a visual change occurred in the presence of non chlorinated aqueous solutions was for the model samples prepared with a substrate layer consisting of NaCl powder. Observation and results of analyses performed on these samples will be detailed further in Section 3.3.2.

Chlorinated solutions

Concerning the chlorine containing solutions, experiments with KCl, HCl and $CaCl_2.2H_2O$ aqueous solutions did not yield any significant modification in the visual aspect nor the chemical composition of the model samples. Artificial ageing experiments were therefore focused on the tubes in which NaOCl (Section 3.3.1), NaCl (Section 3.3.2) and CCl_4 (Section 3.3.3) solutions were present. The results discussed in Section 3.3.4. correspond to the observation of the formation of sulfates on the surface of some model samples.

After several contact periods with the ambient environment, the pH of the NaOCl solutions always changed from 12.2 to 9.4 with production of a white deposit in the liquid, identified by XRD as halite (NaCl) and sodium chlorate ($NaClO_3$). This change in pH domain during the ageing protocol is important for the discussion and could explain the stability of some phases over others at certain periods.

3.3.1. Artificial ageing with NaOCl

As seen in Figure 3.11, in all cases of ageing in the presence of light and NaOCl aqueous solutions, whatever the composition of the sample (vermilion powder, mixed pellets, two-layered pellets, with or without any binder), this process produced color changes but not exactly with the same aspect in all circumstances.

Visual aspect

Color is an essential element in degradation studies, but even if during observations this parameter is frequently mentioned, color measurements made on artificially aged samples

are not frequently presented. The color differences between two samples (named ΔE*) are calculated by the following equation defined in 1976 by the CIE (Commission Internationale de l'Eclairage) *[J.J. Ezrati, 2002]*:

$$\Delta E^* = [(\Delta L^*)^2 + (\Delta a^*)^2 + (\Delta b^*)^2]^{1/2}$$

Here ΔE* denotes the total change in color, ΔL* the change in luminance while Δa* and Δb* respectively describe the change in the green/red and blue/yellow components. As an example, measurements were previously made to follow the ageing of canvas painting models by calculating the ΔE* between samples aged during different period *[Seves et al., 2000]*. Concerning red mercury sulfide, one research group showed color measurements results obtained by laser irradiation at different wavelengths and concluded from these observations that no laser cleaning is possible in a damage-free fashion at any wavelength on this pigment *[M. Chappé, 2003].* During these experiments, spectro-colorimetry measurements were also used to monitor color changes on aged samples.

The visual aspect of the degradation under the influence of NaOCl and light is, during a first step (after 5-10 days), a purple color due to the presence of a thin light grey layer of degraded material at the surface, sometimes accompanied by the formation of white crystals (square, translucent, hundreds of micrometers large, tens of micrometers thick). After a longer ageing time (ca. 30 days), a thick layer that appears white/light grey to the eye is formed on top of the vermilion. This white/grey color is not exactly the same for each pellet aged in these conditions, perhaps due to a variation in thickness of the degradation layer, or due to a change in the crystal morphology. In Figure 3.13, it is possible to see the different steps of this visual transformation for pellets aged with NaOCl exposed to light. But still differences remain between pellets. In Figure 3.13b, after 20 days the surface was covered by dark grey areas, a color that was seen only on few pellets. The pellet in Figure 3.13c had a very homogeneous surface before ageing, and with all the pellets of the same kind (very smooth surface), the formation of large crystals was observed after 7 days of ageing. Even after the formation of the thick white layer, traces of these crystals remained.

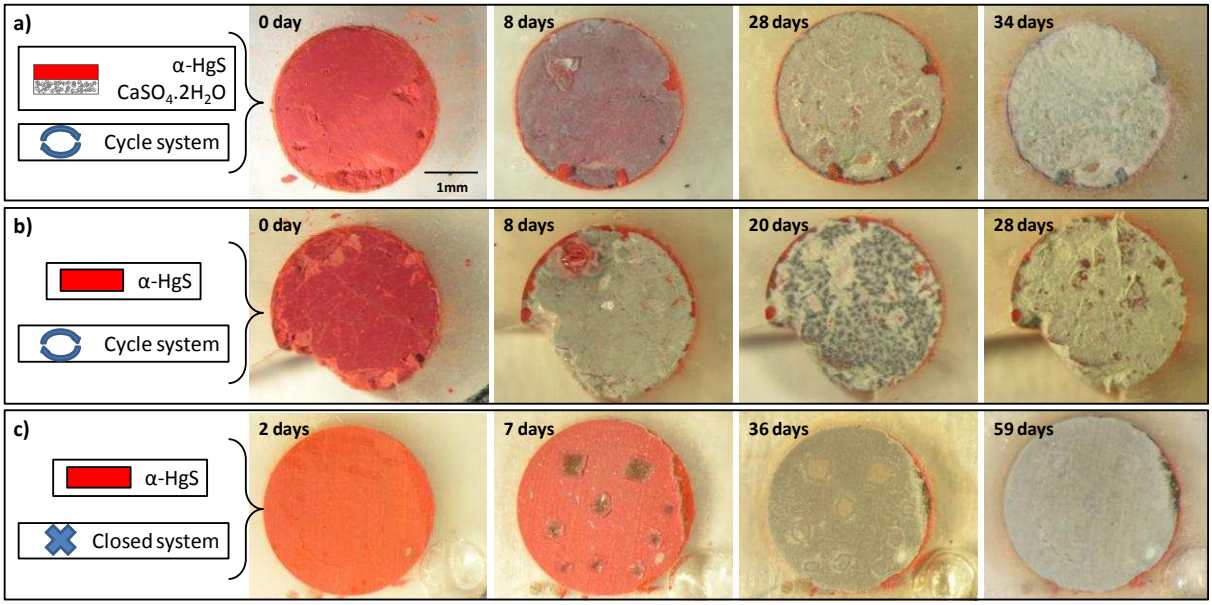

Figure 3.13.: *Pellets aged with NaOCl and light at different times of ageing:* ***a)*** *P-gypsum/vermilion-light-NaOCl-cyclic;* ***b)*** *P-vermilion-light-NaOCl-cyclic;* ***c)*** *P-vermilion-light-NaOCl-closed.*

Crystals observed during the first phase of vermilion degradation with NaOCl had different morphologies. Figure 3.14. presents pellets containing α-HgS and aged with NaOCl and light, showing three of the different aspects seen during this crystallization step. On the first pellet, white small crystals, a few micrometers in thickness, are distributed heterogeneously at the surface next to a homogeneous and powdery layer of fine white/light grey crystals that gives to the pellet its purple color. The second pellet presents grey heterogeneous crystals of different shapes localized above a homogeneous and thick white layer. The third pellet shows a few but large, thick, square and translucent crystals heterogeneously distributed at the surface of the pellet next to a fine, almost not visible, layer of white crystals. All other facies observed were similar to one of these three visual aspects.

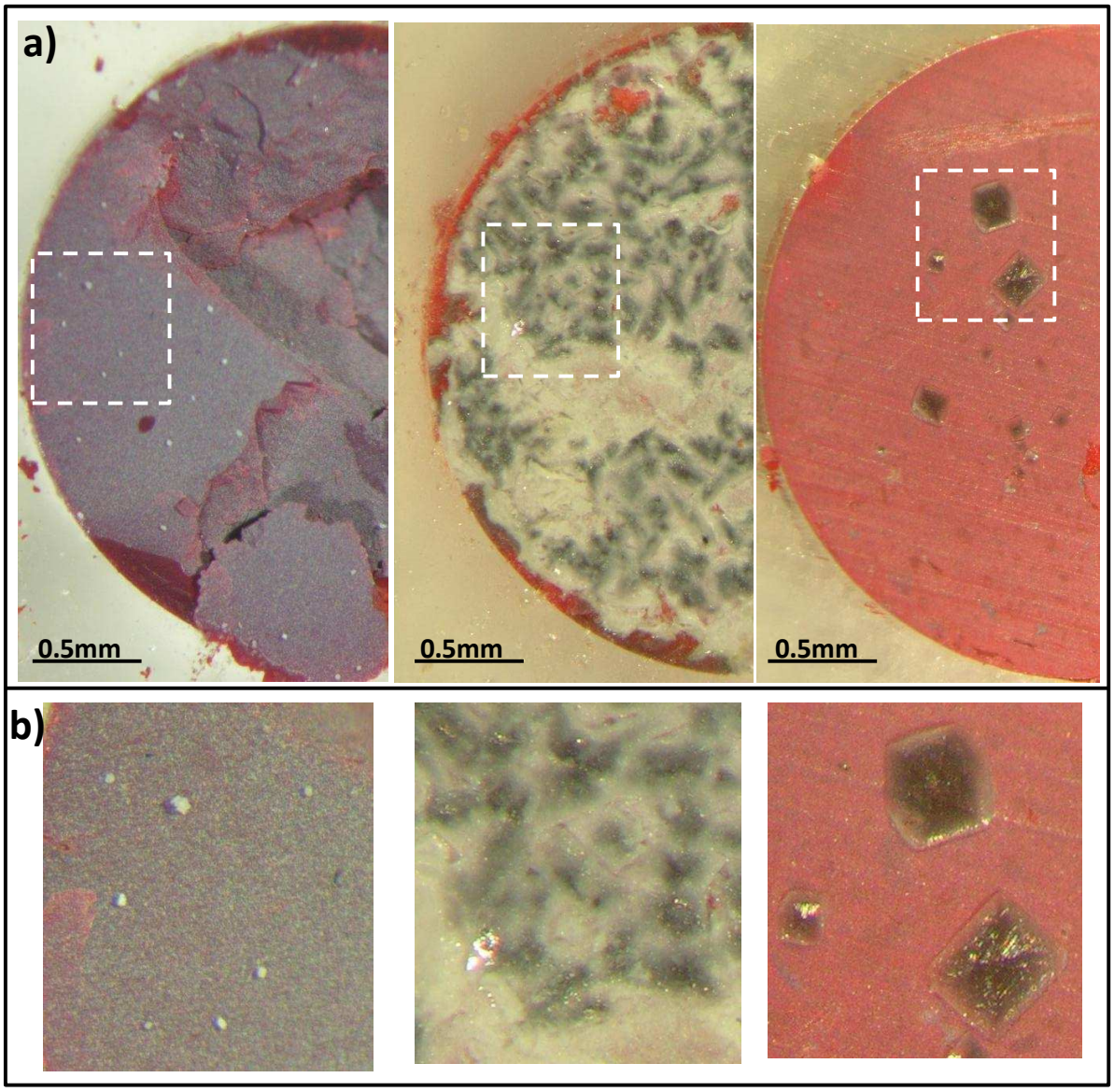

Figure 3.14.: a) *Different α-HgS pellets aged with NaOCl (P-vermilion-light-NaOCl-closed-17days, P-vermilion-light-NaOCl-cyclic-20days and P-vermilion-light-NaOCl-closed-7days, respectively from left to right) showing different crystals morphologies;* ***b)*** *Enlargements of dashed rectangles in (a).*

Table 3.2. lists the ΔE* values obtained (see formula in Appendix B.a) thanks to spectro-colorimetry measurements performed on different pellets. On α-HgS pellets aged in the same conditions (NaOCl, light) two different steps with important ΔE* values appeared during ageing: one at the appearance of crystals, and the second at the formation of the thick white layer.

Table 3.2.: *Evolution of color or differences between pellets (ΔE*) calculated by the CIE formula (see Appendix B.a). A change of color is perceptible to the eye starting from ΔE* values of 1-1.5.*

Ageing conditions	Time of ageing	L*	a*	b*	Color view	ΔE*
α-HgS NaOCl; light	0 day (red)	46	33	27		37
	10 days (crystals)	29	16	-1		
	10 days (crystals)	29	16	-1		23
	120 days (white)	47	1	0		
	0 days (red)	46	33	27		42
	120 days (white)	47	1	0		

The representation of these results in the CIE a* b* space (see Figure 3.15) shows that the largest color difference for the pellet surface is measured during the first days of exposure to NaOCl and is not as important thereafter, even if the aspect is still evolving.

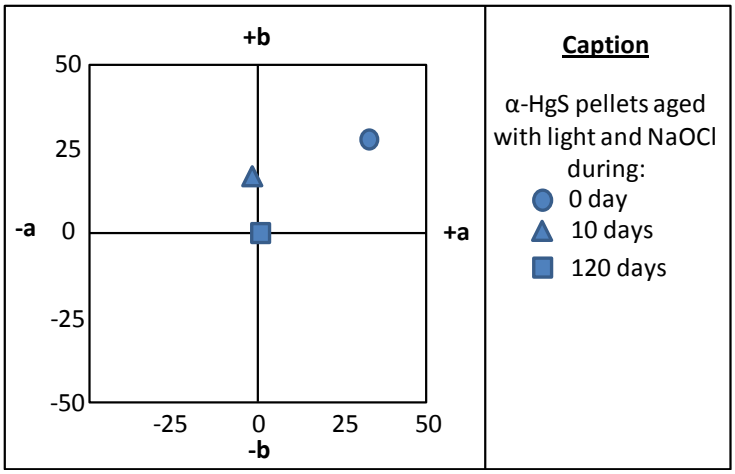

Figure 3.15.: *Color measurements cited in Table 3.2. represented in the CIE a* b* space for α-HgS pellets aged with light and NaOCl during different periods.*

Compounds identification

Before analyzing the aged pellets by XANES, the effects of the NaOCl exposure on the embedding resin were studied.

S K-edge

First, a piece of unaged SODY33 resin was analyzed by XANES. At the S K-edge, nothing was visible in the spectrum, thus no sulfur compounds were detected.

A piece of SODY33 resin aged in the presence of a NaOCl aqueous solution (P-resin-light-NaOCl-closed-21days) was analyzed by XANES. At the S K-edge, a peak with low intensity (0.16 counts after normalization) was present at 2.4824 keV (Figure 3.16a), consistent with the energy of maximum absorption of sulfates.

When analyzing a pellet of α-HgS embedded in SODY33 resin, aged in the same conditions (P-vermilion-light-NaOCl-closed-2days), next to a peak of mercury containing compounds (at 2.4725 keV, see identification further in this chapter), the same peak at 2.4824 keV with a higher intensity than above (7.35 counts after normalization, Figure 3.16b) was observed. Ageing of α-HgS with other solutions (NaCl, H_2O, etc.) did not appear to induce the presence of these compounds.

It can be concluded that light-induced ageing by NaOCl induces the formation of oxidized sulfur compound(s), probably sulfates. These products can be assumed as being formed by the action of NaOCl on the resin and not by environmental contamination as this observation was made in a closed system, i.e. without any exchange with the atmosphere. The presence of sulfates due to this aqueous solution and to sulfur from mercury sulfide will be discussed more in detail in Section 3.3.4.

Cl K-edge

When unaged SODY33 resin is analyzed by Cl K-edge XANES, a low intensity peak (0.04 counts after normalization) was present at 2.8253 keV. The spectrum of aged SODY33 resin (P-vermilion-light-NaOCl-closed-21days) shows a well-defined peak with high intensity (4.08 counts after normalization) at 2.8246 keV (Figure 3.16c), not corresponding to any of the references analyzed during the experiment.

In order to see the effect on the Cl K-edge XANES spectrum of a sample without red mercury sulfide, lead white mixed with linseed oil was aged in the presence of a NaOCl solution (B-lead white-light-NaOCl-closed-33days). Two peaks were present: one at 2.8246 keV as in the case of pure resin or pure linseed oil are aged in the same conditions; the second peak at 2.8317 keV appears to be the result of the interaction of NaOCl and light on lead white (Figure 3.16d).

It can be concluded that the exposure to NaOCl and light induces the presence of chlorine product(s) with a white line situated at 2.8246 keV. This energy of maximum absorption is also found back in Cl-compounds such as organic chloride, and especially for the 2-naphthoyl chloride which Cl K-edge XANES spectrum resembles the one of this unknown product(s) *[F.E. Huggins, 1995]*. The identification of this compound(s) is however not certain. These peaks are found in Cl K-edge XANES spectra of all samples aged under these conditions, and especially on the resin surrounding the pellets. These products can thus be assumed to be the result of the action of NaOCl on materials present as resin or linseed oil; that is consistent with the hypothetic identification of an organic chloride phase.

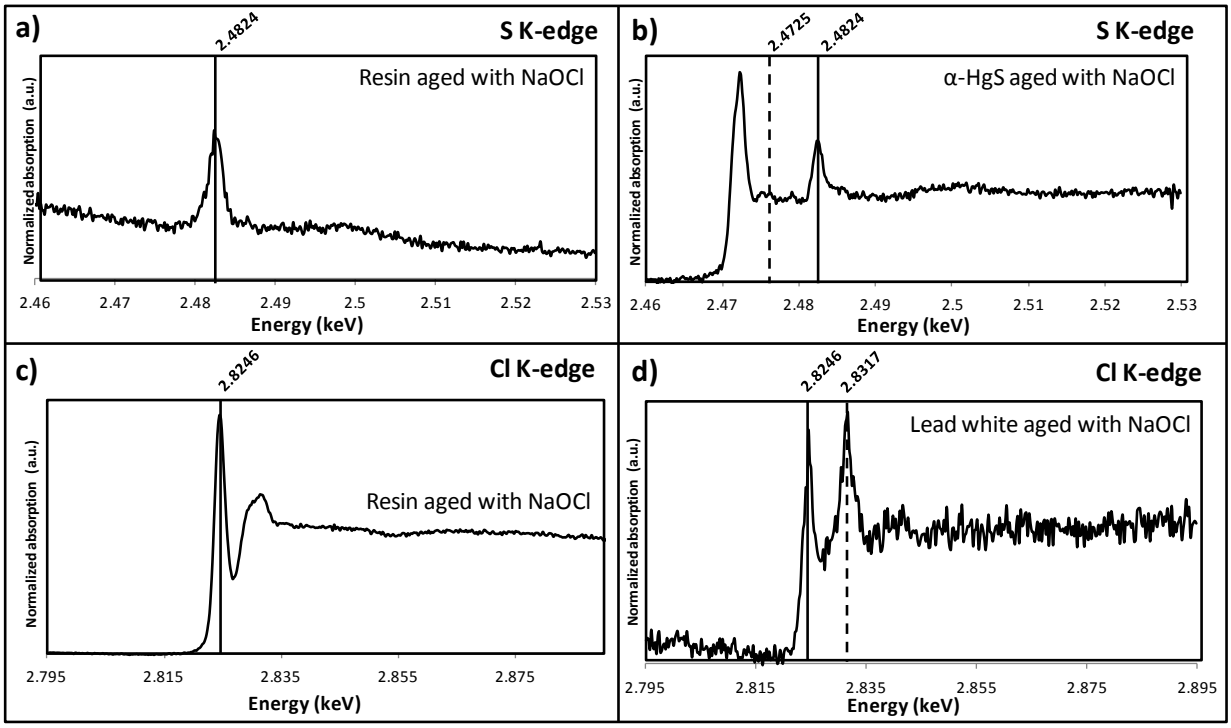

Figure 3.16.: *S K-edge XANES spectra acquired **a)** from aged SODY33 resin (P-resin-light-NaOCl-closed-21days) and **b)** from aged α-HgS pellet (P-vermilion-light-NaOCl-closed-2days); Cl K-edge XANES spectra acquired **c)** from aged SODY33 resin (P-resin-light-NaOCl-closed-21days) and **d)** from aged lead white mixed with linseed oil (B-lead white-light-NaOCl-closed-33days).*

The first noteworthy result when ageing vermilion with NaOCl is the identification by XRD, next to α-HgS, of calomel (Hg_2Cl_2) and corderoite (α-$Hg_3S_2Cl_2$) (Figure 3.17b), two degradation compounds also found to be present at the surface of degraded works of art (see Chapter 2).

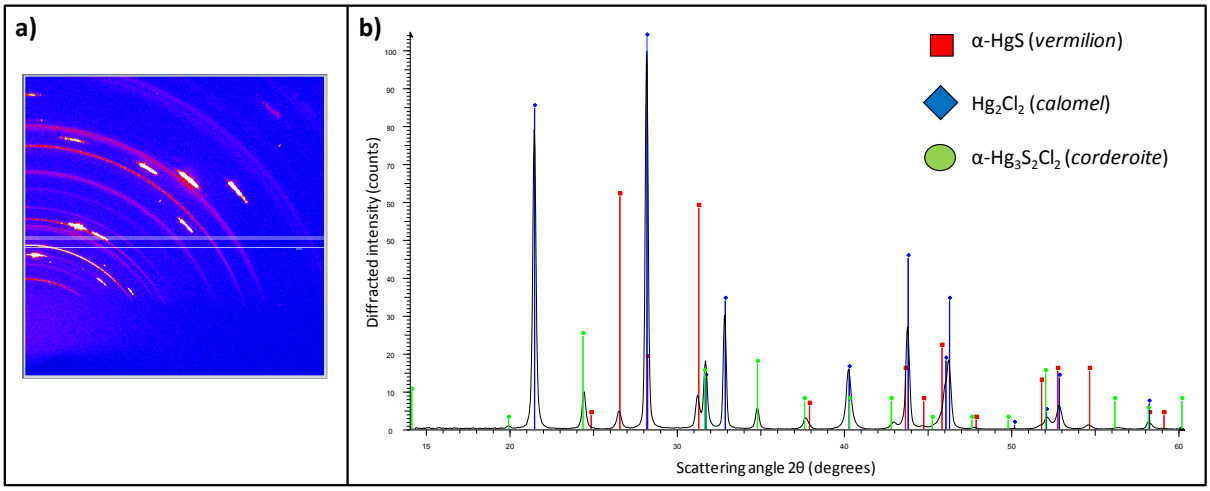

Figure 3.17.: a) *Example of a 2D image obtained when analyzing by reflection XRD the surface of pellet P-vermilion-light-NaOCl;* ***b)*** *1D diffractogram after integrating a), compared to files of reference phases: α-HgS (red), Hg_2Cl_2 (blue), α-$Hg_3S_2Cl_2$ (green).*

These two phases were found in all cases when α-HgS was aged in the presence of NaOCl and light. They always appeared at the same time and seemed to be present in the same ratio during all steps of ageing. In a few particular cases, one of these two compounds was not identified anymore after a given ageing time. These cases will be developed further in this chapter. In one case (P-gypsum/vermilion-light-NaOCl-cyclic-167days), the β-$Hg_3S_2Cl_2$ phase was detected next to corderoite and calomel. This compound, identified by μ-XRD, was also observed on degraded original works of art (see Section 2.2).

One interesting point from these experiments is the difference between the non-reproducible visual aspects of the surface (different crystals morphologies) and the reproducible formation of calomel and corderoite.

Differentiation of compounds

Analyses were performed at the surface of different pellets to differentiate the degradation compounds identified by XRD. Indeed, the localization of these alterations could provide information about the contribution of each product to the visual aspect of degraded samples.

Below are presented two examples of analyses performed with this aim.

Example 1: SEM and Raman spectroscopy of P-NaCl/vermilion-light-NaOCl-closed-90days

After 90 days of ageing in the presence of a NaOCl solution, this pellet showed a heterogeneous form of degradation and some light grey areas on its surface (Figure 3.18a). As for other pellets aged in these conditions, calomel and corderoite were identified by XRD after the first days of exposure. SEM analyses were performed on four locations in one of the light-grey areas: the resulting BSE images show the presence of small, squarish, translucent crystals at the surface, surrounded by fine crystallizations with a higher BSE intensity (Figure 3.18b). Elemental analyses at different points provide some hints regarding the identification of the compounds present. As first results did not show the presence of sulfates on the sample, carbon and oxygen were assumed not to be present in the analyzed areas. The aluminium present could originate from the Al-foil in which the samples were transported. Next to HgS (Figure 3.18c, point 1) that corresponds to the white areas of the BSE image, Na,Cl-rich areas became evident, still containing some atomic percents of Hg and S (Figure 3.18c and d, point 2). The squarish, translucent crystals, appearing in dark grey on the BSE images, were identified as halite in view of their Na,Cl composition (Figure 3.18c, point 3). These compounds originate from the sub-layer of the pellet. In the white and thick areas of the BSE images, Hg and Cl were present in approximately equal atomic abundance (Figure 3.18c and d, point 4), which is consistent with the presence of calomel (Hg_2Cl_2), identified via X-ray diffraction on this pellet just prior to the SEM analyses.

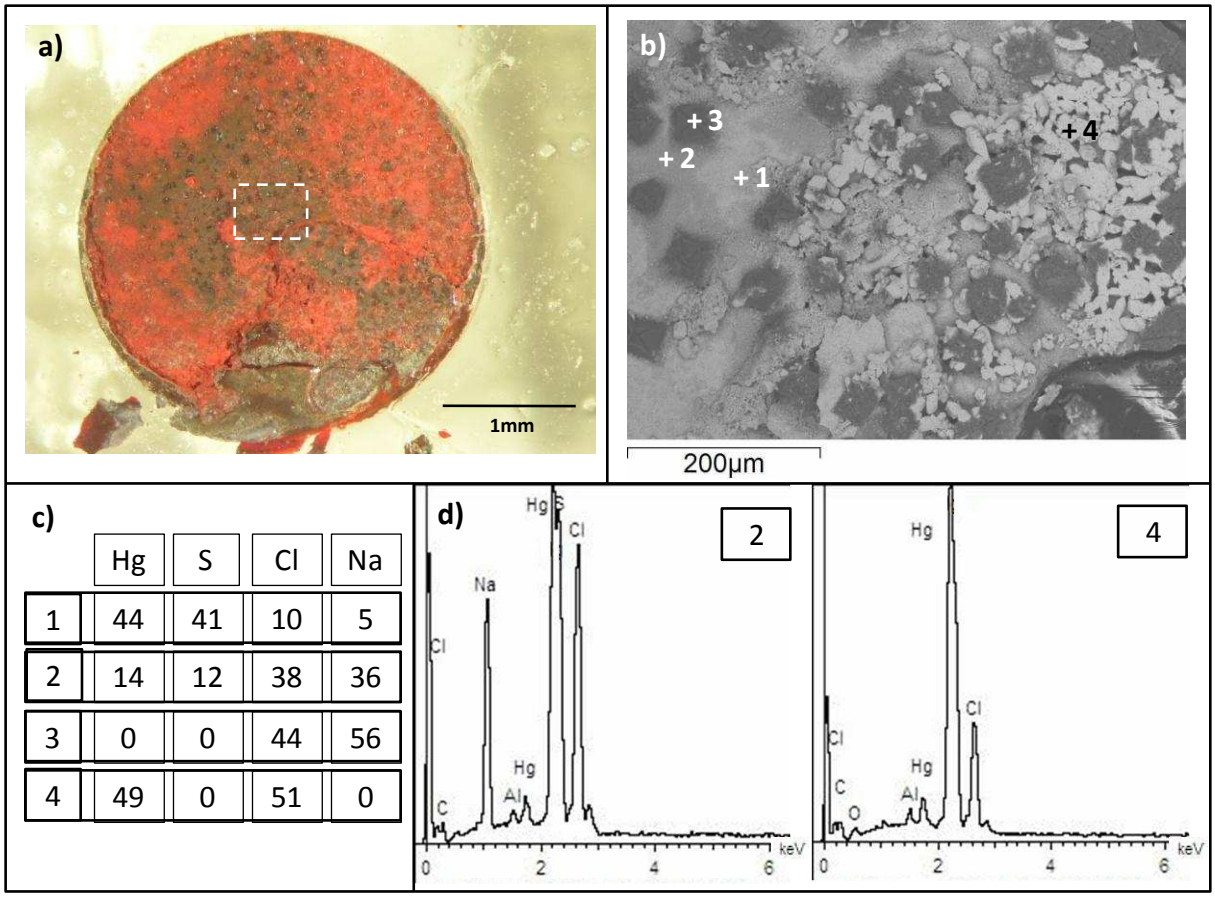

	Hg	S	Cl	Na
1	44	41	10	5
2	14	12	38	36
3	0	0	44	56
4	49	0	51	0

Figure 3.18.: *Analyses performed on sample P-NaCl/vermilion-light-NaOCl-closed-90days:* ***a)*** *Visible image of the pellet;* ***b)*** *BSE image of the area represented in (a);* ***c)*** *Normalized results of SEM analyses performed on the four points represented in b) in atomic percentage (with C, O and Al results not shown here);* ***d)*** *SEM spectra obtained at locations 2 and 4.*

The same pellet was also analyzed by high resolution Raman microscopy. In a first point situated in a darker area (see Figure 3.19a), the Raman spectrum obtained was similar to that of vermilion (α-HgS) (Figure 3.19b point 1). In a second point situated in a less dark area (see Figure 3.19a), the spectrum showed peaks corresponding to corderoite (α-$Hg_3S_2Cl_2$), associated with peaks from vermilion as the ones at 249 cm^{-1} and 37.7 cm^{-1}; the latter has a higher intensity than when pure corderoite is present (Figure 3.19b point 2). The differences at low Raman wave numbers between these spectra allowed scanning an area of the sample in order to obtain the distribution of corderoite. The intensity of a specific Raman peak at 63 cm^{-1} was used here. The map obtained shows that the corderoite areas (in blue in Figure 3.19c) correspond to the white/lighter grey areas of the visible image of the pellet (Figure 3.19a). Unfortunately, calomel disappeared from this pellet before the Raman

analyses were performed and was not identified during these experiments (see below for more details on pellets evolutions).

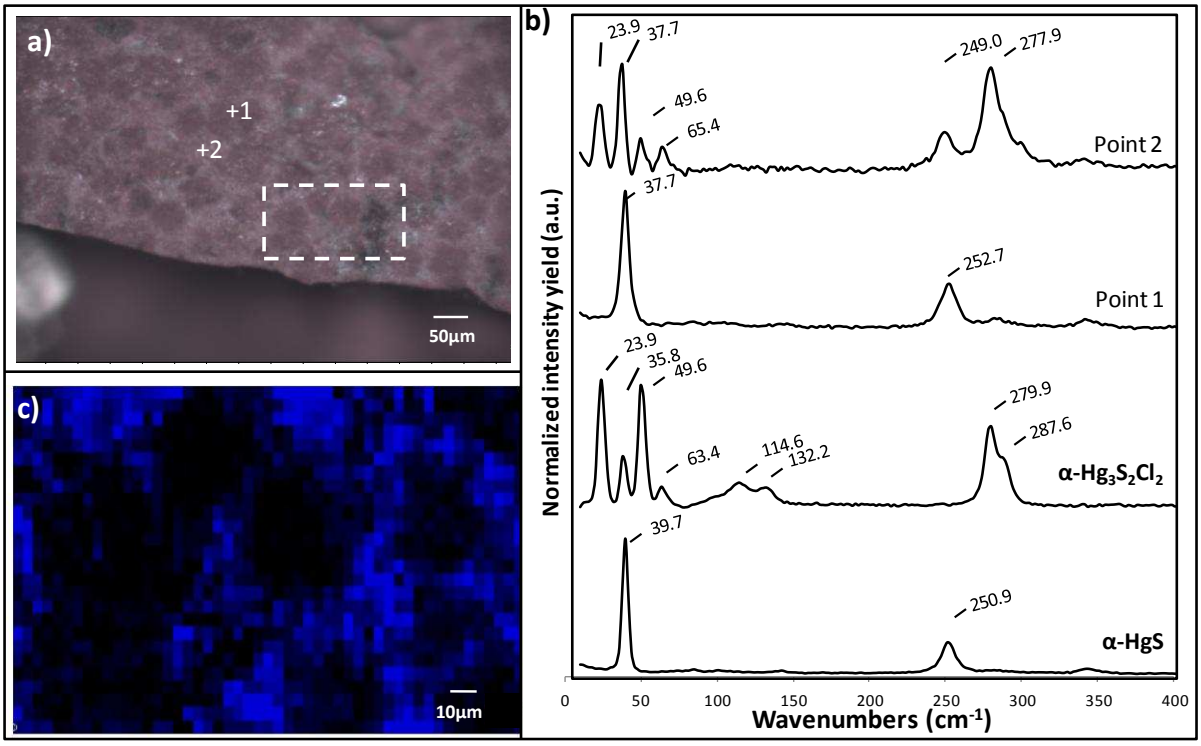

Figure 3.19.: a) *Visible image of a detail of pellet P-NaCl/vermilion-light-NaOCl-closed-90days;* ***b)*** *Raman spectra of points 1 and 2 localized in (a) compared to vermilion (α-HgS) and corderoite (α-$Hg_3S_2Cl_2$) references;* ***c)*** *Map of the corderoite Raman intensity (peak at 63 cm^{-1}) obtained from the dashed rectangle represented in (a).*

Example 2: µ-XRF/µ-XANES experiments on the surface of different pellets

The four pellets presented in this example looked similar to all the other α-HgS samples aged with NaOCl and light after several hundred days of exposure: a white/light grey layer of degradation covers the surface. These pellets were chosen because they present different alteration aspects. On the first two pellets (Figure 3.20a and b), the degradation layer appeared thicker that on the two others (Figure 3.20c and d). Different degradation compounds were identified by µ-XANES by comparing the spectra obtained on points on the samples' surface with spectra of references acquired in the same conditions. Pellets a) and

b) in this figure represent most of the cases observed: on the surface of the pellet (points 1 and 3) XANES spectra similar to that of calomel (Hg_2Cl_2) are encountered; on the resin surrounding the pellet (points 2 and 4), spectra similar to that of the (NaOCl, light) aged resin are obtained (see Figure 3.16b). Chlorine is clearly seen to be present in the resin (in blue) in the XRF map of Figure 3.20b. In the XRF map of the Figure 3.20a, an interesting halo of mercury (in red) appears around the pellet, but the phases it corresponds to were not identified. On some pellets, as is the case of pellet c), in this figure, Cl K-edge XANES spectra similar to the one of corderoite were obtained (point 5). As was the case of pellets a) and b), pellet d) showed spectra similar to that of calomel on its surface (point 6). In three special cases (samples P-gypsum/vermilion-light-NaOCl-cyclic-167days, P-calcite/vermilion-light-NaOCl-closed-28days and P-vermilion-light/dark-NaOCl-cyclic-120days), next to calomel (Hg_2Cl_2), spectra to some extent similar to that of $HgCl_2$ were also observed (point 7).

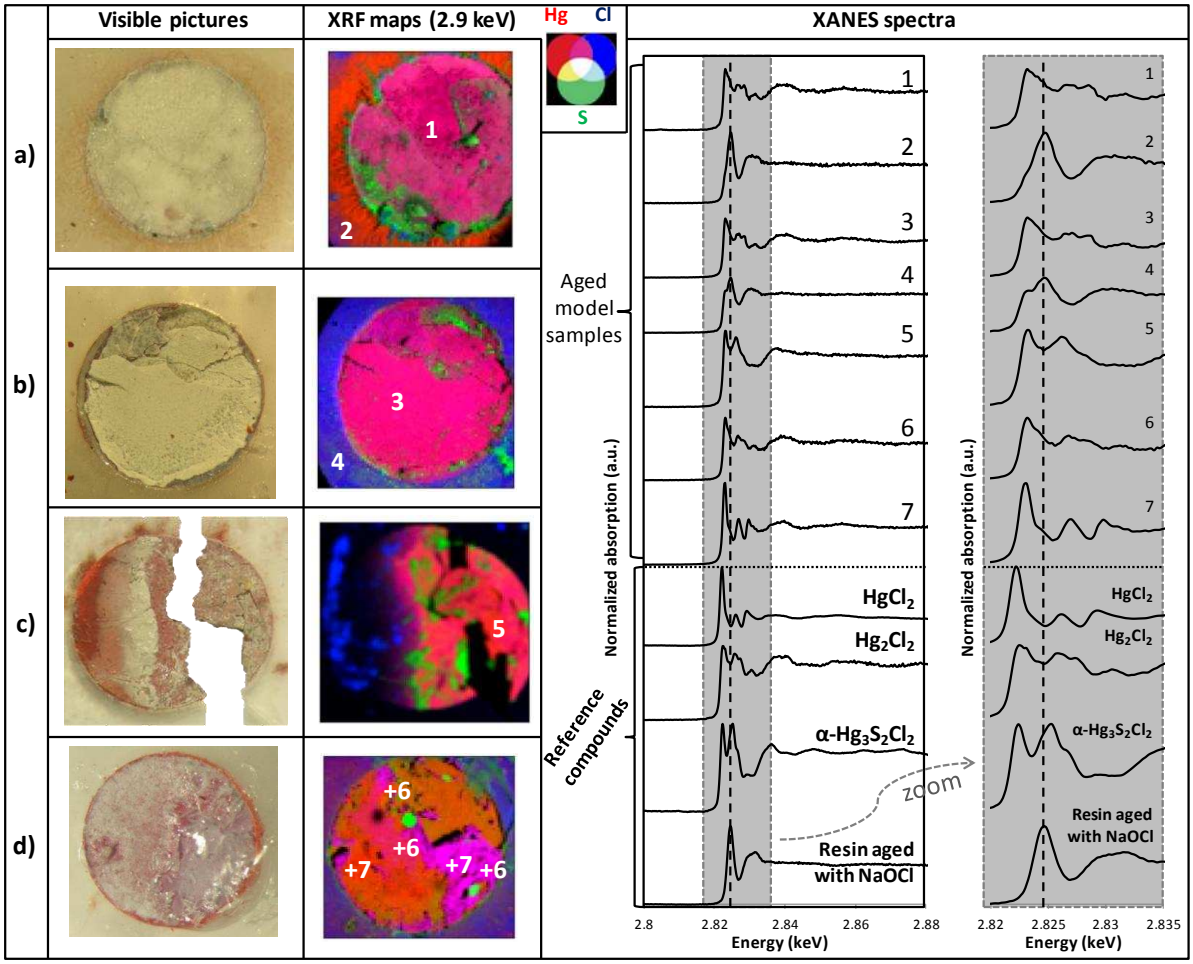

Figure 3.20.: *Visible images (first column) and XRF composite maps acquired at 2.9 keV primary energy (second column) from four pellets:* ***a)*** *P-gypsum/vermilion-light-NaOCl-cyclic-167days,* ***b)*** *P-calcite/vermilion-light-NaOCl-cyclic-142days,* ***c)*** *P-gypsum/vermilion-light-NaOCl-closed-167days,* ***d)*** *P-vermilion-light/dark-NaOCl-cyclic-120days; Cl K-edge XANES spectra from positions indicated in the XRF maps, compared to reference spectra (third column). On the right, a magnified area (2.820-2.835 keV) of the spectra is presented. The dotted black line in the fourth column corresponds to 2.8246 keV (absorption maximum of NaOCl-aged resin).*

Observation of multi-layered structures

The existence of multiple layers of degradation products in samples originating from works of art was already noticed (see Chapter 2). With the aim of observing similar structures in the model samples (if any), some of the artificially aged samples were prepared as cross-sections, via embedding in SODY 33 resin. All the cross-sections present a degradation layer 10-50 µm in thickness on top of the α-HgS layer. This layer appears white or light grey under visible light.

These cross-sections were analyzed by µ-XRF, µ-XANES and µ-XRD. The following examples summarize the results obtained.

Example 1: Visualization of degradation compounds on α-HgS pellet by µ-XRF/µ-XANES

The pellet presented here contains α-HgS and was aged with NaOCl (P-vermilion-light-NaOCl-cyclic). After 28 days of ageing, a white thick homogeneous layer was visible, composed of a powdery material (Figure 3.21a). µ-XRF/S K-edge µ-XANES analyses showed the material to contain corderoite (Figure 3.21d and e, point 3) and sulfates (Figure 3.21d and e, point 2). See also the RGB composite image in Figure 3.21b. Cl K-edge XANES spectra showed features similar to that of calomel (Figure 3.21e point1); a Cl XRF intensity map acquired at 2.8232 keV, i.e. the energy of maximum absorption for Hg,Cl containing compounds showed these compounds to be present between the corderoite and the sulfate layers. Thus, this may correspond to calomel. On the XRF maps of the surface it is also possible to see that sulfates are present on the surface of the resin surrounding the pellet (Figure 3.21b); this aspect will be discussed later (Section 3.3.4).

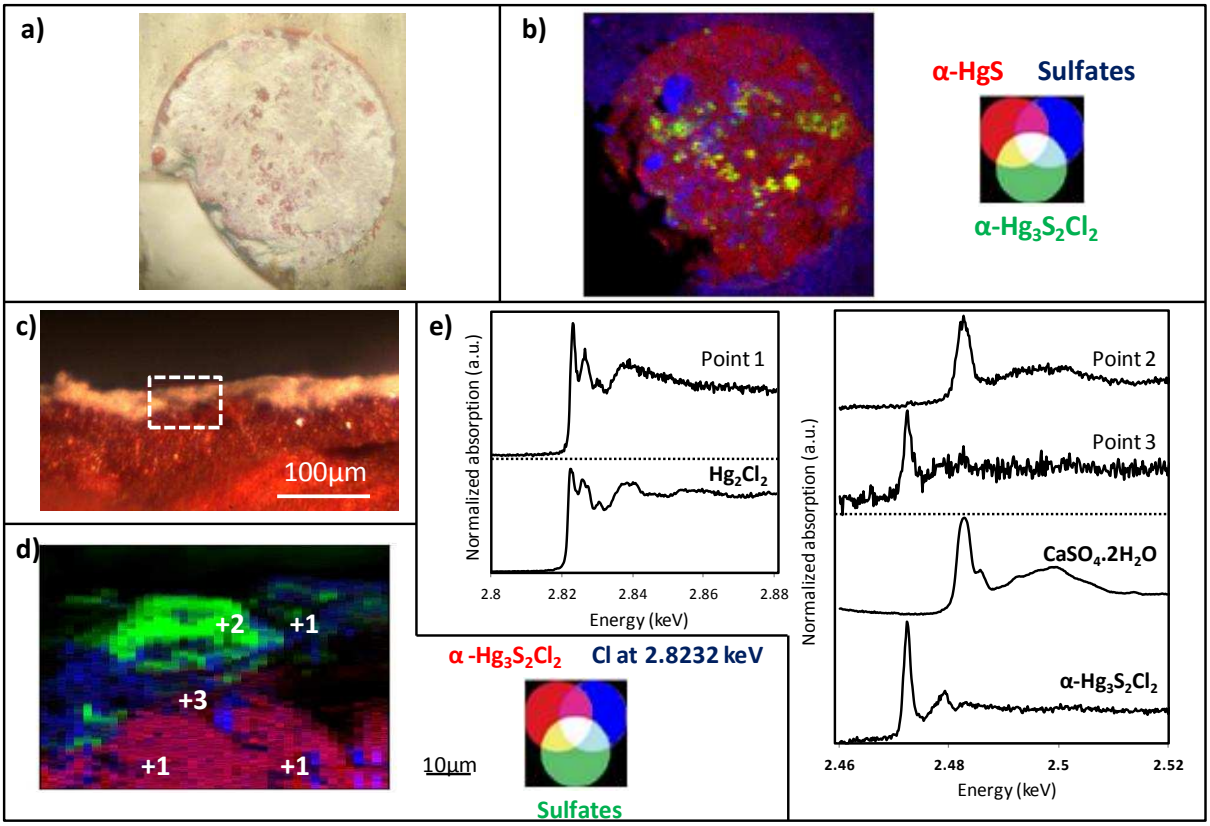

Figure 3.21.: *Results obtained from the sample P-vermilion-light-NaOCl-cyclic-28days:* ***a)*** *Visible image of the pellet;* ***b)*** *RGB composite map of different S-species, acquired at 2.4716 keV for vermilion (red), 2.4726 keV for corderoite (green) and 2.4828 keV for sulfates (blue);* ***c)*** *Visible image of the corresponding cross-section;* ***d)*** *RGB composite map of different Cl and S-species from the area represented by the dashed rectangle in (c) at 2.4726 keV for corderoite (red), 2.4828 keV for sulfates (green) and 2.8232 keV (Hg,Cl-compounds) (blue);* ***e)*** *XANES spectra at Cl and S K-edges recorded from points represented in (d), compared to reference spectra.*

Example 2: Visualization of a thin intermediate layer of degradation products on a two-layered pellet by µ-XRF/µ-XANES

This pellet consists of two layers of NaCl/α-HgS and was aged with NaOCl (P-NaCl/vermilion-light-NaOCl-closed). After 28 days of ageing, large light grey crystals were visible, localized heterogeneously on the surface of the sample. Next to these crystals, a fine layer of crystallized compounds gave the sample a purple aspect (Figure 3.22a). µ-XRF/µ-XANES analyses suggested the presence of corderoite, sulfates and possibly Hg,Cl compounds (Figure 3.22b).

Between the vermilion layer (XANES spectra in Figure 3.22d point 3) and the covering sulfate-rich layer (Figure 3.22d point 2), a thin layer of material with XANES spectra showing a peak at the characteristic energy for Hg,Cl-compounds (2.8232 keV) was observed (in blue in Figure 3.22c). These spectra, however, do not share any other features with the known references (Figure 3.22c and d-point 1).

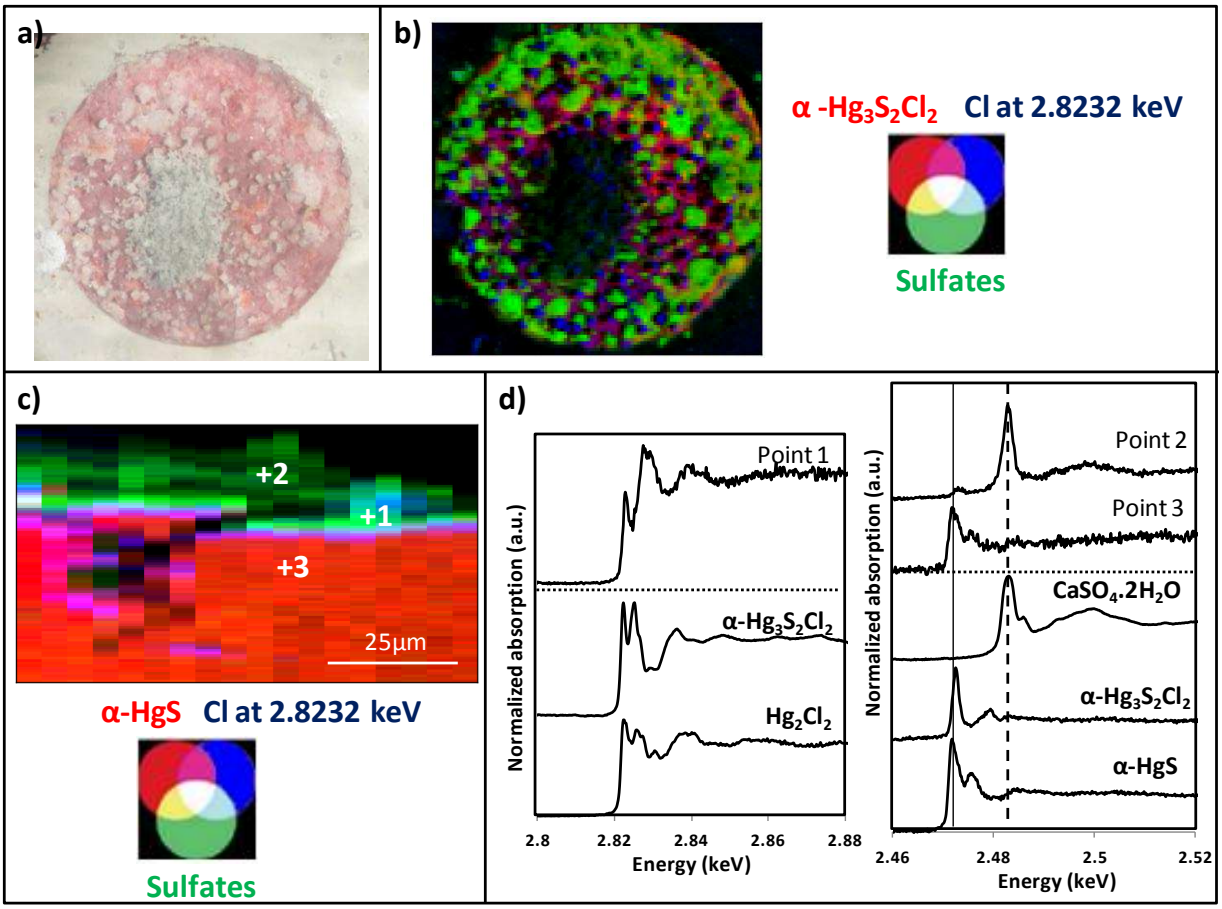

Figure 3.22.: *Results obtained from sample P-NaCl/vermilion-light-NaOCl-closed-28days:* ***a)*** *Visible image of the pellet;* ***b)*** *RGB composite of S,Cl species acquired at 2.4726 keV for corderoite (red), 2.4828 keV for sulfates (green) and 2.8232 keV for Hg,Cl compounds (blue);* ***c)*** *RGB composite of S,Cl compounds recorded from the side of the pellet (in cross-section) at 2.4716 keV for vermilion (red), 2.4828 keV for sulfates (green) and 2.8232 keV (Hg,Cl compounds, blue);* ***d)*** *Cl and S K-edges XANES spectra recorded at locations shown in (c), compared to references.*

Example 3: Visualization of a degradation layer assumed to contain $HgCl_2$ on a two-layered pellet by µ-XRF/µ-XANES

This pellet contains two layers of calcite/α-HgS and was aged with NaOCl (P-calcite/vermilion-light-NaOCl-closed). After 28 days of ageing, a thin and homogeneous layer of degradation products gave the sample a light grey aspect (Figure 3.23a). µ-XRF/µ-XANES spectra collected from the surface suggest the presence of Hg,Cl-compounds and sulfates, especially on the resin surrounding the pellet (Figure 3.23b).

As is the case for the other examples presented, sulfates were present at the surface of the sample; they present a XANES spectrum similar to that of gypsum ($CaSO_4.2H_2O$) (Figure 3.23c and d-point 1). Contrary to the other cross-sections analyzed, in the intermediate degradation layer (purple in Figure 3.23c), the Cl K-edge XANES spectra were more similar to that of $HgCl_2$ than to that of calomel (Hg_2Cl_2) or corderoite (α-$Hg_3S_2Cl_2$) (Figure 3.23c and d-point 2).

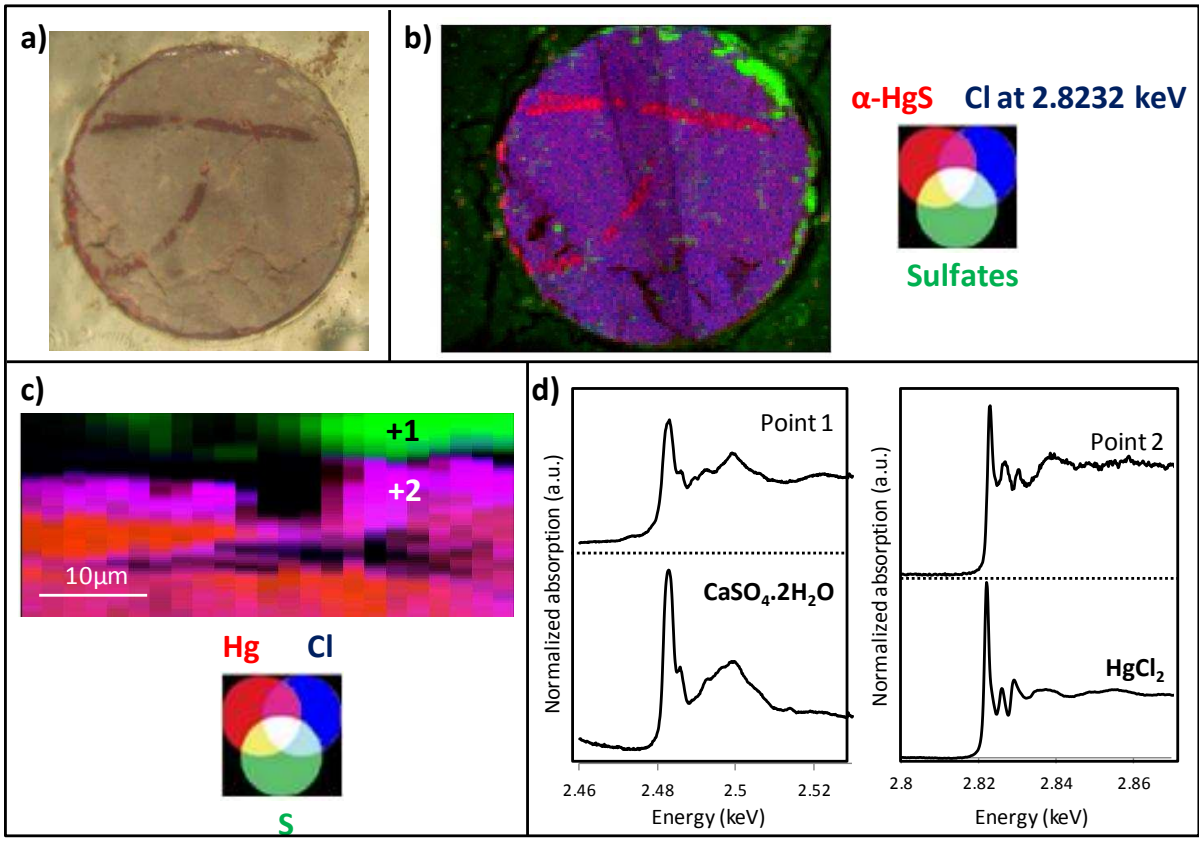

Figure 3.23.: *Results obtained from sample P-calcite/vermilion-light-NaOCl-closed-28days:* ***a)*** *Visible image of the pellet;* ***b)*** *RGB composite of S,Cl species acquired at 2.4716 keV for vermilion (red), 2.4828 keV for sulfates (green) and 2.8232 keV (Hg,Cl compounds, blue);* ***c)*** *RGB composite acquired at 2.9 keV from the cross-section showing the repartition of mercury (red), sulfur (green) and chlorine (blue);* ***d)*** *S and Cl K-edges XANES spectra recorded at locations shown in (c), compared to references.*

Example 4: Visualization of degradation compounds on α-HgS pellets by µ-XRD

This pellet contains α-HgS and was aged with NaOCl (P-vermilion-light-NaOCl-closed). After 7 days of ageing, only a few large, squarish, translucent crystals were visible at its surface next to an homogeneous and thin crystallized layer, giving the sample a matt purple color (Figure 3.24a). This pellet was analyzed by µ-XRD in order to identify degradation compounds and to be able to localize them via mapping.

XRD performed in transmission on the cross-section prepared from this sample allowed identifying two degradation compounds: calomel and corderoite (see d-spacing values of reference files in Appendix B.h). XRD maps were obtained by fitting data from diffractograms using reference files, and resulted in an intensity distribution of the identified

phases. These maps show that, within the achievable resolution (ca. 2 µm in this case), the two Hg,Cl-containing phases are co-localized in the same layer (Figure 3.24b). No sulfates were detected by XRD on this pellet.

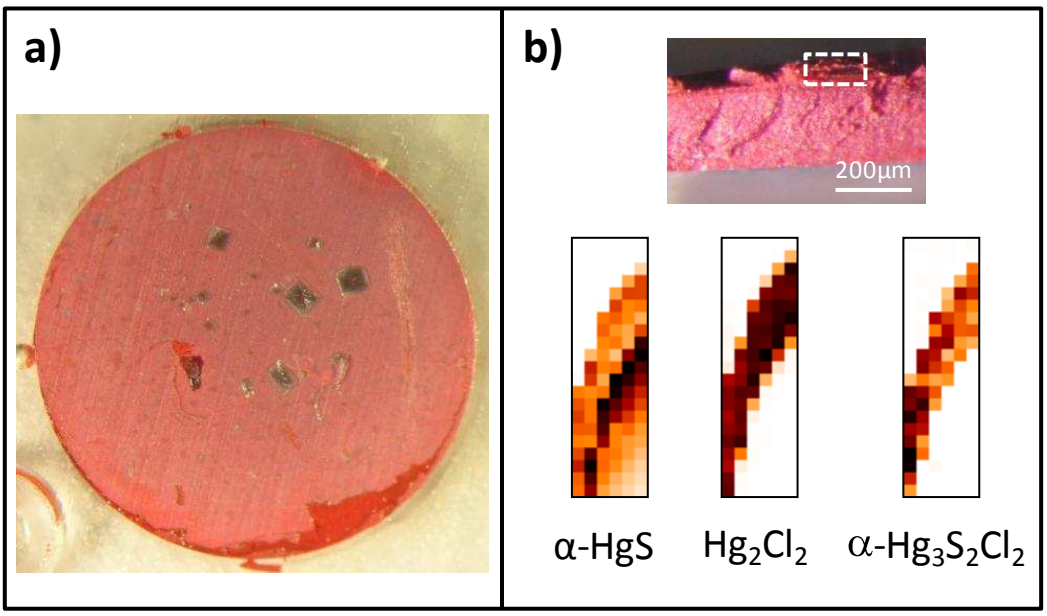

Figure 3.24.: *Results obtained from sample P-vermilion-light-NaOCl-closed-7days:* ***a)*** *Visible image of the surface of the pellet;* ***b)*** *µ-XRD maps acquired on the area indicated in the visible picture (side of the pellet); next to vermilion (α-HgS) two degradation compounds (calomel Hg_2Cl_2 and corderoite α-$Hg_3S_2Cl_2$) are present. (The distortion of the maps is due to technical problems during the experiment)*

Evolution of the degradation products found on model samples

In the majority of the cases (9 out of 13), and after a minimum of 40 hours exposed to light and NaOCl, the degradation products calomel and corderoite were found to be present simultaneously. However, in some cases, after a specific ageing time, only one of them, either calomel or corderoite, remained (see Table 3.3**.** for a summary). It is noteworthy among these cases that the pellets aged in a closed system (2 cases) retained corderoite, while those aged in the cyclic system (3 cases) retained calomel. The latter three cases developed a thick white/light grey superficial layer while the former two acquired a purplish hue.

Table 3.3.: *List of the pellets aged by suspension in tubes containing NaOCl and by exposure to light on which calomel (Hg_2Cl_2) and corderoite (α-$Hg_3S_2Cl_2$) were first formed and where, after some time of ageing, one of these two compounds was not detectable by XRD anymore.*

Composition of the pellet	Type of system	Time of ageing when only one product remained	Compound remaining (identified by XRD)
Two-layered {NaCl/vermilion}	Closed	130 days	Corderoite
Two-layered {KCl/vermilion}	Closed	95 days	Corderoite
Vermilion	Cyclic	85 days	Calomel
Two-layered {NaCl/vermilion}	Cyclic	104 days + 13 days out	Calomel
Two-layered {gypsum/vermilion}	Cyclic	58 days	Calomel

In addition, four peculiar cases were observed:

- For one pellet (P-NaCl+vermilion-light-NaOCl-closed) at first only corderoite was detected by XRD while, after 52 days, calomel and corderoite were detected together.

- With a two-layered pellet (P-NaCl/vermilion-light-NaOCl-closed), only corderoite was detected all along the ageing process. Thus, no significant amount of calomel was formed.

- With a similar two-layered pellet (P-NaCl/vermilion-light-NaOCl-closed), first only corderoite was detected by XRD, then after 84 days, calomel and corderoite were co-detected, and finally from 181 days of ageing onwards only corderoite remained again. One phase could be identified in this pellet while in the diffractograms one peak that might correspond to metacinnabar (β-HgS) was observed (Figure 3.25a). In Figure 3.25b, XANES spectra from four points of the surface are shown that prove to be more similar to β-HgS than to α-HgS (Figure 3.25c). Based on these results, the presence of metacinnabar may be suspected in this case.

- The last case concerns the ageing of a painted slide (B-lead white-light-NaOCl-closed) showing only calomel all along the ageing process.

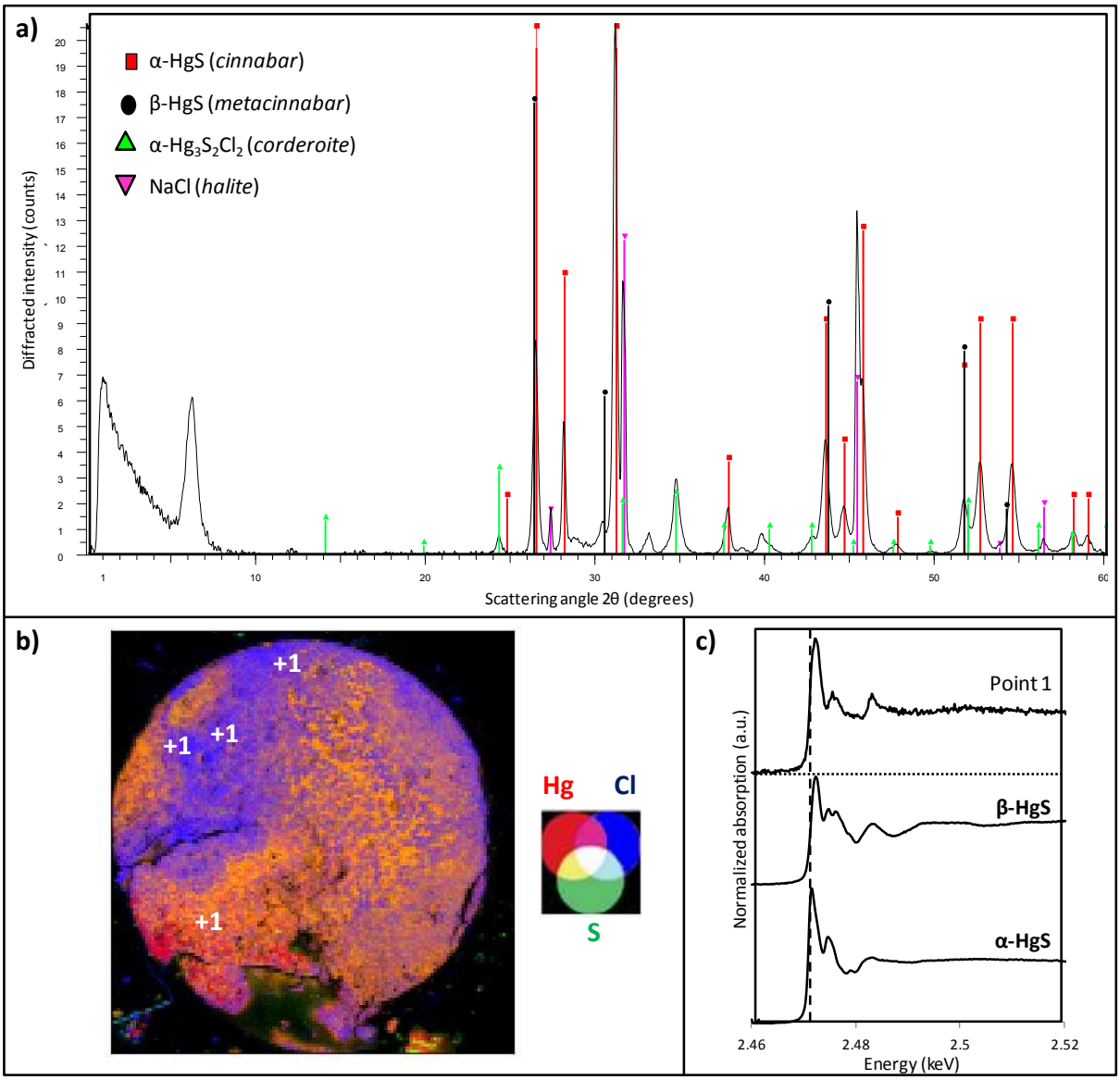

Figure 3.25.: *Results of analyses obtained from sample P-NaCl/vermilion-light-NaOCl-closed:* ***a)*** *Diffractogram obtained in reflection mode compared to reference files (α-HgS in red, β-HgS in black, α-$Hg_3S_2Cl_2$ in green and NaCl in pink);* ***b)*** *RGB composite of three μ-XRF maps acquired at 2.9 keV showing the distribution of mercury (red), sulfur (green) and chlorine (blue);* ***c)*** *S K-edge XANES spectrum from position 1 shown in (b), compared to reference spectra of α-HgS and β-HgS.*

Artificial ageing of natural α-HgS ores with NaOCl

In order to evaluate whether chlorine has the same influence on natural cinnabar as on synthetic vermilion, six α-HgS crystals (#420 and #43041 from USA, #7790 and #20591 from Mexico, #7799 from Brazil and #cin_esp from Spain; see Appendix C.a) were selected from cinnabar ores of different provenances and aged by exposure to NaOCl and light in a closed system. After 24 hours, all surfaces of these samples were covered by small white crystals, identified as calomel (Hg_2Cl_2) by XRD analysis. This visual and chemical change is faster than for synthetic vermilion samples (40 hours). After eight days of ageing, next to calomel, XRD analyses also showed the presence of corderoite (α-$Hg_3S_2Cl_2$). This difference in speed of formation of calomel and corderoite was not observed for synthetic vermilion ageing. All aged ores showed the same visual aspect and chemical composition at each ageing interval. The time allocated to this part of the present study did not allow finding suitable conditions to observe differences in degradation behavior depending on the origin of the ores.

3.3.2. Influence of NaCl on ageing results

Next to the ageing phenomena realized by means of NaOCl, also some others were observed. Ageing with a NaCl solution appeared to take much longer and gave rise to a less important change in color in a few cases. Indeed, as presented in Table 3.4, for α-HgS pellets aged with a NaCl solution during 230 days, the ΔE* value calculated was ca. 9 which is not important compared to the results obtained for the pellets aged in NaOCl solution (where ΔE* values between 20 and 40 were obtained, see Table 3.2) and in view of the fact that a change of color is perceptible to the eye from ΔE* values of 1-1.5.

Table 3.4.: *Evolution of color differences between pellets (ΔE*) calculated by the CIE formula (see Appendix B.a). A change of color is perceptible to the eye from a ΔE* value of 1-1.5.*

Ageing conditions	Time of ageing	L*	a*	b*	Color view	ΔE*
α-HgS NaCl; light	0 day	33	39	11		9
	230 days	38	34	16		

The representation of these results in the CIE a* b* space compared to those corresponding to NaOCl ageing (see Figure 3.26) shows that for NaCl ageing, even after 230 days, the difference from the unaged pellet is far smaller than for NaOCl ageing after 120 days. The L*a*b* differences between the two unaged pellets are attributed to sample preparation variations; even with the same α-HgS quantity introduced in the press, it is difficult to apply reproducible pressures on the powders. Thus, pellets did not all show the same red shade prior to ageing.

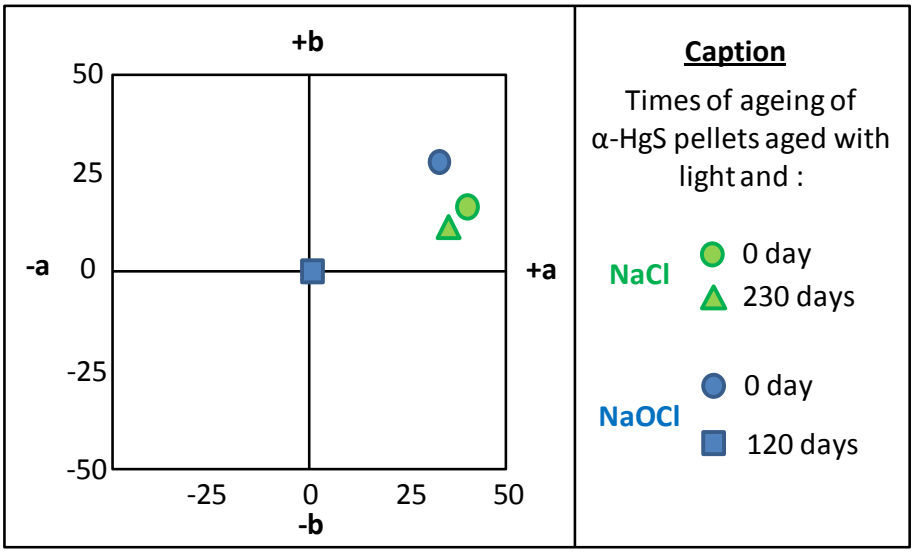

Figure 3.26.: *Color measurements cited in Table 3.2. and 3.4. represented in the CIE a* b* space for α-HgS pellets aged with NaCl and NaOCl.*

In the cases where ageing was performed in the presence of NaCl solutions, no chlorine compound could be detected at the surface of aged pellets by any elemental or structural analysis method. Therefore, in order to investigate the direct influence of sodium choride solutions on vermilion, droplets of NaCl solution were directly applied on the surface of a pellet exposed to light. Except from halite (NaCl) crystals, nothing could be detected at the surface of this sample.

In a next step, NaCl crystals were mixed with linseed oil and applied as a varnish layer on top of a paint layer of vermilion, itself painted on a glass slide. After a 129 day exposure to light, dark brown stains were visible on the paint slide (Figure 3.27a). When looking at the side of the sample, the vermilion layer still appeared red, so that the dark aspect of the sample was attributed to the dissolution of some of the halite crystals in oil, hereby changing the refraction index of the binder and causing it to look darker. Next to vermilion and halite (NaCl), in S K-edge XANES spectra, peaks corresponding to corderoite (α-$Hg_3S_2Cl_2$) and to sulfates were identified by µ-XANES (Figure 3.27b). The peak assumed to correspond to the sulfates features a shoulder at a lower energy than the mean peak, somewhat similar to the S K-edge spectrum of $HgSO_4$.

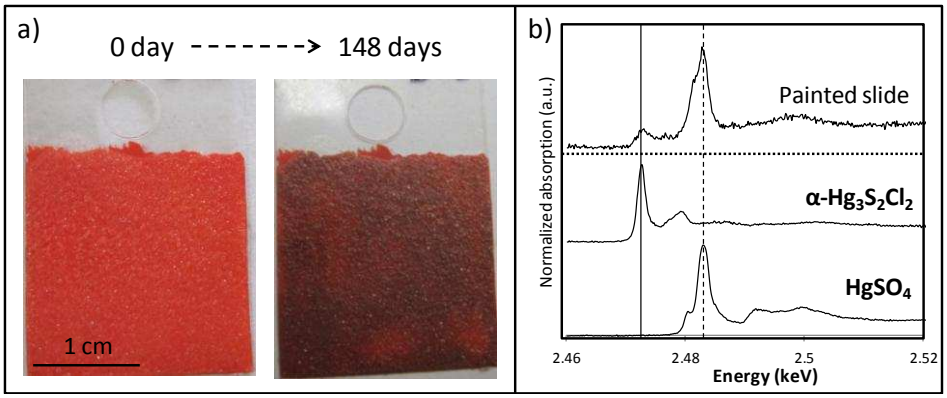

Figure 3.27.: a) *Visible images of sample B-vermilion/NaCl-light, before and after 148 days of light-induced ageing;* ***b)*** *S K-edge µ-XANES spectrum of the same sample after 150 days of ageing showing a sulfate peak at 2.4826 keV and one at 2.4728 keV characteristic for Hg,S,Cl compounds such as corderoite.*

The NaCl-based ageing experiments that yielded important visual differences involved preparing vermilion pellets on top of a substrate layer of NaCl (two-layered pellets). Irrespective of the ageing solution (without any, with H_2O, NaCl or NaOCl), all two-layered NaCl/α-HgS pellets exposed to light developed dark superficial areas. The pellets aged in a

closed system only showed some grey spots (Figure 3.28d) whereas the ones aged in an cyclic system became dark grey (Figure 3.28a-b-c). For two two-layered pellets with a NaCl layer, one aged in the cyclic system and the other in a closed one, a ΔE* value of 22 was obtained, which corresponds to an important color change. In those areas of the samples that were covered by the embedding resin, the blackening was still observed and the color appear darker there (Figure 3.28a). Even in the case of ageing with a NaOCl solution, when other compounds such as calomel and corderoite were formed, the surface sample still looked dark grey (Figure 3.28b), i.e. much darker than in the cases no NaCl substrate layer was present. However, for all these cases, no other compounds than α-HgS (and the usual calomel and corderoite for pellets aged by NaOCl) could be identified by XRD; in S K-edge XANES spectra, a peak corresponding to sulfates (at 2.4825 keV) was present. It is also noteworthy that after the ageing was stopped, after some time in darkness, these dark grey pellets became red again, except for the parts situated below the resin (see Figure 3.28a).

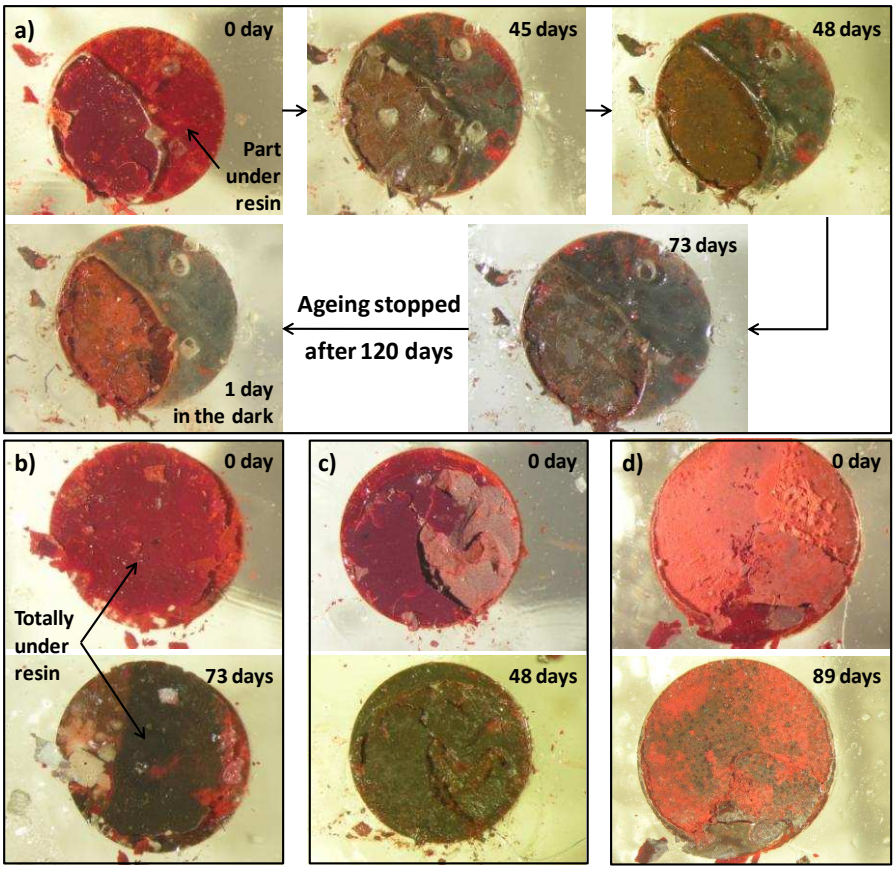

Figure 3.28.: *Two-layered pellets of NaCl/vermilion powders aged by exposure to light:* ***a)*** *P-NaCl/vermilion-light-NaCl-cyclic;* ***b)*** *P-NaCl/vermilion-light-NaOCl-cyclic;* ***c)*** *P-NaCl/vermilion-light-H_2O-cyclic;* ***d)*** *P-NaCl/vermilion-light-NaOCl-closed.*

On one of the two-layered (NaCl/α-HgS) pellets that were exposed to NaOCl, P-NaCl/vermilion-light-NaOCl-cyclic-73days (see visible images in Figure 3.28b), μ-XANES analyses of the surface revealed the presence of another sulfur compound; its peak maximum absorption at 2.4799 keV (see spectrum in Figure 3.29) corresponds to that of sulfone compounds (R-S(=O)$_2$) *[J. Prietzel, 2007]*.

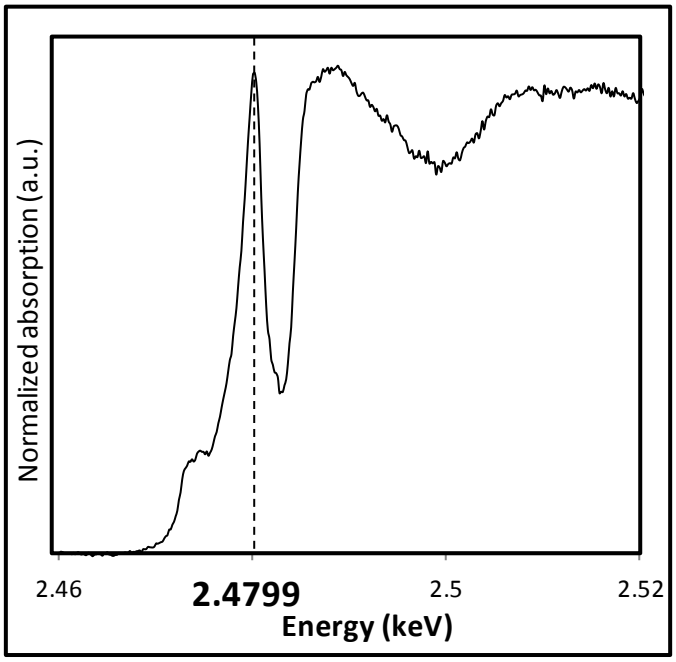

Figure 3.29.: *μ-XANES spectrum at S K-edge of sample P-NaCl/vermilion-light-NaOCl-cyclic-73days, showing a peak at the energy corresponding to sulfone compounds R-S(=O)$_2$ (2.4799 keV).*

3.3.3. Ageing in CCl_4 conditions

As chlorine is known to have an influence on red mercury sulfide alteration while the solvent carbon tetrachloride (CCl_4) was used by curators as part of a procedure to treat wooden supports against insect infestations, additional ageing experiments were performed involving this product. Initially, vermilion pellets were suspended in tubes containing 3 mL of this solution; however, since the CCl_4 dissolves the resin, it was not possible to expose the pellets during a long time period. Nevertheless, a darkening appeared to have taken place, even though no other compounds than α-HgS could be detected.

To be closer to the real conditions of use of this product, CCl_4 was regularly applied on different types of samples. On a suspended vermilion pellet that received several coatings of CCl_4 during a period of 8 months, no color change was seen upon exposure to light. No chlorine could be detected by SEM at the surface of this sample, but when analyzing its surface by Cl K-edge µ-XANES, a spectrum resembling that of the NaOCl-aged embedding resin was obtained (see Figure 3.16b). So chlorine deposited by use of CCl_4 yielded the same type of superficial product as the one formed during NaOCl induced ageing. Another sample was a painted slide of vermillon mixed with linseed oil that received 5 applications of CCl_4 during a period of one month and that was then left untouched during the rest of the ageing procedure. After 186 days of light exposure, this sample presented a brown superficial discoloration (see Figure 3.30). Unfortunately at the time of this writing, this sample has not been analyzed yet. Thus it is not yet clear whether or not the same type of degradation compounds are formed when α-HgS is degraded by CCl_4 as when this takes place under the influence of NaOCl.

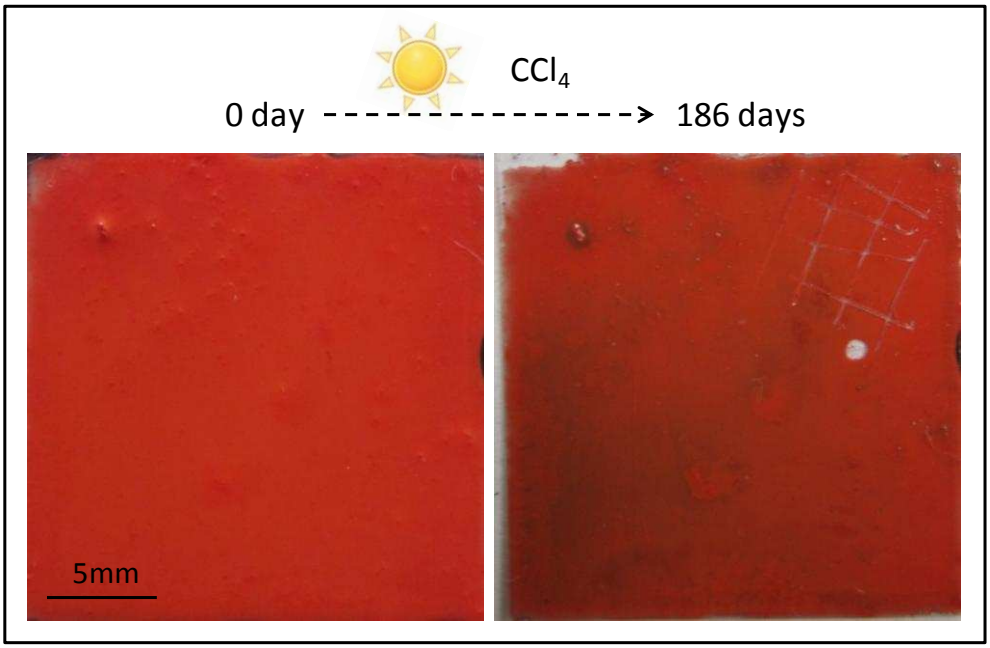

Figure 3.30.: *Visible images of a painted slide of vermilion mixed with linseed oil before ageing (left) and after 186 days of ageing by light exposure with 5 applications of CCl_4 during the first month of ageing (right). The second image presents a hole on the right of the slide due to sampling for analyses, and stripes on its top right due to intentional notches made in the pictorial layer.*

3.3.4. Formation of sulfates

In order to work with pellets of which the composition is closer to that of frescoes, two-layered vermilion pellets were prepared having a calcite $CaCO_3$ substrate layer. After exposure to light and air or water, these samples remained unaltered (no visual changes, no difference detected by structural analyses). After exposure to light in a closed tube containing a NaCl solution, only one pellet showed a very slight visual change (some areas presented a purple aspect). After 182 days of ageing, gypsum ($CaSO_4.2H_2O$) was detected on its surface. However, this result could not be reproduced. After 28 days of exposure to light in a closed tube containing NaOCl, the powder without any binder (two-layered pellet) presented a light grey color (Figure 3.23a). In case the powder was mixed with linseed oil (two-layered painted slide), gypsum was detected after 170 days of ageing and the red color of the surface completely turned brown-dark grey. For these experiments with NaOCl aqueous solution, the results were reproducible and the presence of gypsum was identified by XRD and XANES (see the S K-edge spectrum on point 1 Figure 3.23d compared to the one of gypsum).

As already encountered in Figure 3.11, during some of the μ-XANES analyses, a characteristic peak for sulfates at 2.4825 keV appeared in the S K-edge spectra; however, these peak does not have the specific shape that is typical of e.g. gypsum (see Figure 3.31d). As mentioned in Section 3.3.1, these sulfates were observed in all pellets aged with NaOCl solutions and also in all two-layered pellets composed of NaCl/α-HgS that were aged with H_2O and NaCl aqueous solutions. By recording S-K_α XRF maps of the surface of these pellets at E_0 = 2.4825 keV, it was possible to see that these sulfates are also present at the surface of the resin embedding the pellets. In Figure 3.31, three examples of pellets are shown. In the XRF maps, it can be seen that sulfur is present on the resin surrounding the pellets, and on a simple vermilion pellet (Figure 3.31a), all areas with high concentration in sulfur present a XANES spectrum similar to the one in Figure 3.31d-points 1, with only a single peak at 2.4825 keV and no features typical for gypsum. Thus, another type of sulfate is likely to be present here. On two layered {gypsum/vermilion} pellets (Figure 3.31b), next to these areas of unidentified sulfates, some gypsum is also visible that originate from the substrate layer (see Figure 3.31b-points 2 and the XANES spectrum in d). As cited above, on two-layered {calcite/vermilion} pellets (Figure 3.31c), gypsum is visible on the surface of the pellet but

also areas in which the other type of sulfate is present are observed. In this case, gypsum was also found on the resin surrounding the pellet.

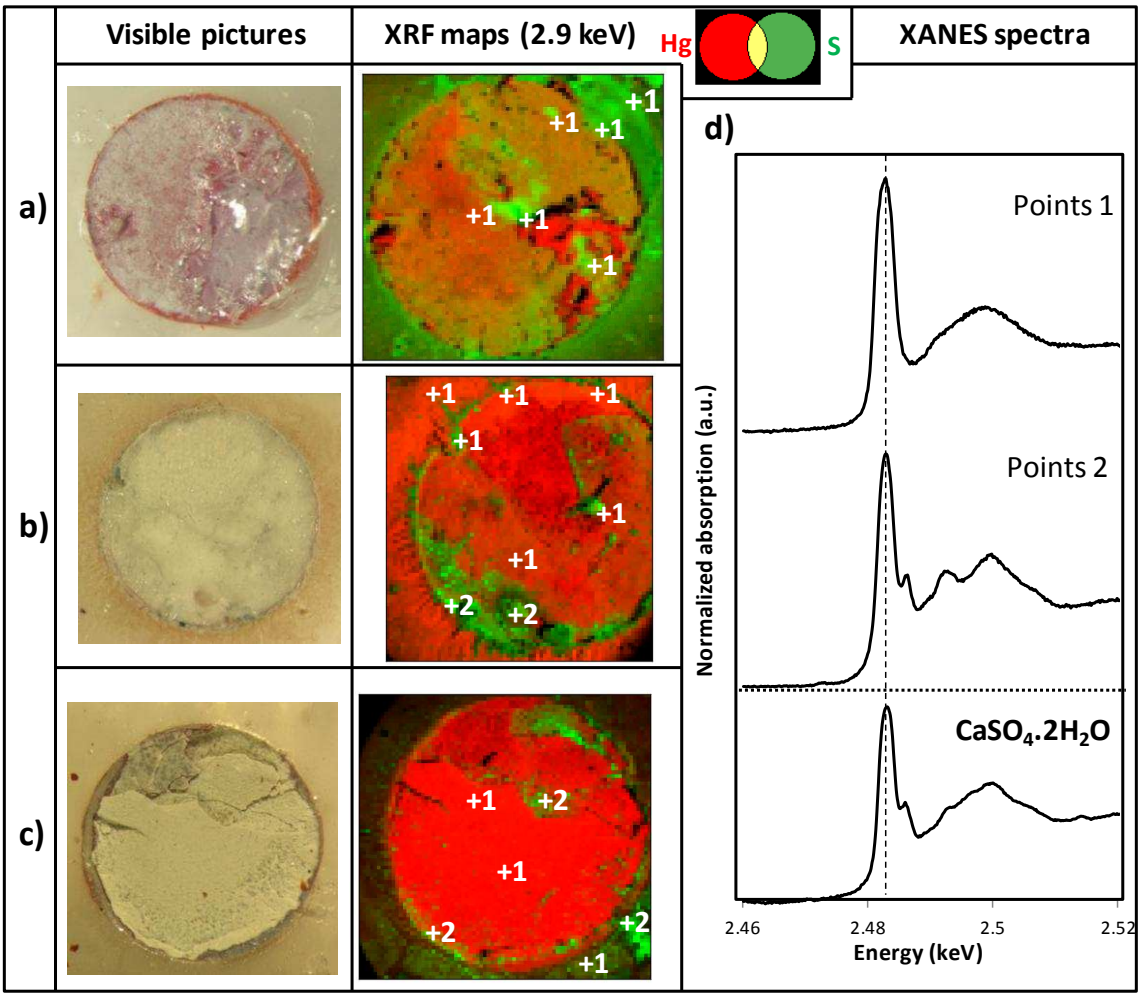

Figure 3.31.: *Visible images and RG composites of XRF maps acquired at E_0 = 2.5 keV (showing mercury in red and sulfur in green) for three pellets:* ***a)*** *P-vermilion-light/dark-NaOCl-cyclic-120days,* ***b)*** *P-gypsum/vermilion-light -NaOCl-cyclic-167days,* ***c)*** *P-calcite/vermilion-light -NaOCl-cyclic-142days;* ***d)*** *S K-edge XANES spectra representative of all investigated locations: those in locations labeled "1" are different from those labeled "2", compared to the S K-edge XANES spectrum of gypsum.*

It is noteworthy that by analyzing the surface layer of a two-layered pellet composed of $CaSO_4.2H_2O$/α-HgS aged with NaOCl by μ-XRD at the SLS facility, another sulfate compound was identified: Hg_2SO_4. This phase was only identified once within the range of model samples and was not detected on original degraded artworks.

Chapter 4: Discussion

Content

Abstract

Starting from the literature, from analyses of original works of art and from artificial ageing experiments, conditions of formation, stability and evolution of degradation compounds identified or hypothesized are discussed. The contribution of these phases to the color of degradation is also discussed in this chapter. Simulation of the α-HgS degradation by exposure to a NaOCl solution and the consideration of the Pourbaix diagrams for the Hg-S-Cl-H_2O system bring new arguments to the present study of the reaction mechanisms governing red mercury sulfide alteration.

4.1. Conditions to observe red mercury sulfide degradation

An important question raised in the conservation field is which factors influence the degradation of different types of materials. This information is useful to determine the optimal manner in which to preserve works of art for future generations. It is therefore relevant to discuss the conditions that induce the instability of cinnabar/vermilion.

4.1.1. Summary of bibliography

The instability of mercury sulfide has been studied for many centuries and different conditions were considered to be responsible for its degradation. Some of these are presented below.

Geological context of formation of cinnabar ores

The photosensitivity of natural cinnabar is well known and the darkening of α-HgS ores has been observed. Previous studies showed that ores originating from different deposits do not turn black after comparable exposure times *[R.M. Dreyer, 1939]*.

Differences in the trace element contents of these ores can be due to variations in the ore formation of the cinnabar, the nature of the surrounding rocks and of the mineralizing fluids. This variation can lead to different degradation properties according to the geographical situation of the deposit. The differences in trace elements content may play a role in the kinetics of the reactions induced by the photosensitivity of each ore, as is the case for chlorine *[J.K. McCormack, 2000; B. Pal, 2003]*. However, the specific influence of the trace element pattern on the photosensitivity of cinnabar ores is not clear and differences in elements present are not uniquely linked to the localization of the deposits (see Section 1.4).

Light

The absorption of light energy can promote electrons from low energy orbitals to higher energy orbitals; this can induce direct or indirect changes in the color of materials *[J.K. McCormack, 2000; F. Da Pieve, 2012]* (see Section 3.2.1).

A longer exposure of α-HgS to sunlight does not appear to increase the thickness of darkened layer *[R.M. Dreyer, 1939]*. Thus it can be hypothesized that the degraded layer acts as a protective cover for the HgS situated below. Accordingly, restorers and curators were advised to leave the darkened layer untouched that had developed on top of a degraded mercury sulfide area of the Giotto Crucifix (see Section 2.2.5) until another protective intervention for this type of cultural heritage artifact is established.

Concerning European paintings, synthetic vermilion and natural cinnabar from Almadén (Spain) are known to be relatively stable considering photosensitivity. However, next to light, also other factors appear to play a role in the degradation of α-HgS in the Cultural Heritage field.

Chlorine presence near altered red mercury sulfide

Recently, the presence of stable mercury chloride compounds next to cinnabar in deposits raised questions about the influence of chlorine on natural red mercury sulfide *[J.K. McCormack, 2000]*. Chlorine was shown to be possibly involved in the degradation of red mercury sulfide and in the formation of grey or black compounds at the surface of works of art that comprise α-HgS *[M. Spring, 2002; K. Keune, 2005; M. Cotte 2006; M. Cotte, 2008; M. Cotte, 2009; M. Maguregui, 2009]* (see Section 2.1)

These results corroborate the idea that next to light exposure, the presence of chlorine is an important factor in the degradation process of red mercury sulfide.

Other conditions favoring α-HgS degradation

In order to better understand what reactions may take place during alteration processes involving red mercury sulfide, it is relevant to consider the oxidizing and reducing powers of a number of species. Their redox potential depends on the activity of the considered species and on the environment. If other reactions, such as acid-base ones, can take place in the system, they can change the activity of some of these compounds and hence indirectly influence their effective redox potential. Thus, the pH is an important factor determining possible reactions and compound stabilities. These considerations are also important when

studying alteration of works of art, as the contact with the atmosphere and the possible condensation of products on their surface can induce reactions between materials and fluids. From previous studies, it was noted that a darkening of red mercury sulfide can only be obtained in acidic conditions *[E.E. Foord, 1974]* and that one of the degradation compounds found on works of art, corderoite, can only be formed in extremely acid and mildly reducing conditions *[G.A. Parks, 1979]*. These specific conditions will be discussed in more detail in Section 4.3.

The support materials (wood, panel, stone, etc.), the binders (egg yolk, oil, etc.) and the varnishes can also have some influence on the degradation phenomena, in view of the interfering chemical elements they contain. In the present work, supports and binders were chosen to be as neutral as possible with respect to artificial ageing. Some factors appear to inhibit the alteration, such as the presence of red lake mixed with or on top of the vermilion layer *[M. Spring, 2002]*. Among all works of art in which cinnabar or vermilion have been used, only in few cases, a (significant) degradation is observed, which may be explained by the presence of inhibiting factors or the absence of stimulating agents.

4.1.2. Summary of analyses of original painting samples

Conditions in which natural cinnabar ores and original works of art are exposed are discussed below on the basis of information obtained from the original samples analyzed in the present study.

Light

Concerning natural cinnabar, it is noteworthy that in mineralogical galleries, the most photosensitive ores are exposed in display cabinets protected from light.

For example in Pedralbes, Spain, it was observed that the same vermilion red features, painted on walls partially exposed to light and partially in the shade, became totally black in the light while keeping their vivid red color in the shade.

Chlorine presence on original painting samples

Chlorine was not identified on natural cinnabar, even on the samples that darkened. This element was nevertheless detected on cinnabar samples originating from altered works of art. On panels from Brueghel, it was difficult to assert whether or not chlorine was originating from the areas showing vermilion degradation.

4.1.3. Summary of artificial ageing experiments

Based on the observations made during the artificial ageing experiments, the influence of the conditions inducing degradation are discussed and compared to the ones described in the literature.

Photosensitivity of natural cinnabar ores depending on their origin

Unfortunately, not enough time was available to study the influence of trace elements on the degradation behavior of natural cinnabar. A difference between crystals originating from different deposits might have been observed via trace analyses, and might have allowed us to understand the differences in photosensitivity observed among cinnabar ores described in the literature.

Observation of the photosensitivity of synthetic HgS

During artificial ageing experiments, light was demonstrated to have a primordial role in the degradation of red mercury sulfide. Indeed, none of the ageing experiments conducted in the dark gave rise to any visual or chemical change (see p.119, Section 3.3).

Contrary to what was observed with natural cinnabar, in the time scale of this study (three years), exposure to light needed to be combined with another factor to induce any change in the synthetic vermilion contained in the model samples. In the present study, this other factor was the presence of chlorine, except in one case where blackening occurred in the presence of a KOH aqueous solution (see p.119, Section 3.3).

Conditions during artificial ageing with NaCl

Artificial ageing experiments with aqueous NaCl solutions were performed, with a concentration approximately equal to that of sea water (0.505 $mol.L^{-1}$) and a pH of 9. In a few cases, this gave rise to a slight color change after a minimum of 200 days of light exposure.

Ageing experiments were also performed with $NaCl_{(s)}$ present in the model sample as a powder mixed with α-HgS in pellets, or mixed with a binder (linseed oil) and applied as a varnish layer on top of a α-HgS layer, itself painted on microscope slides. These ageing experiments gave rise to more important visual changes than those where aqueous NaCl solutions were used.

Conditions during artificial ageing with NaOCl

Artificial ageing experiments with aqueous NaOCl solutions were performed with a highly concentrated solution (15.44 $mol.L^{-1}$) and in alkaline conditions (pH 12). The aim of these experiments was to assess the evolution of α-HgS under extreme chlorinated conditions.

All ageing experiments with a aqueous NaOCl solution gave rise to visual and chemical changes on the model sample surfaces. This solution produced more reactive species and induced more degradation of α-HgS than aqueous NaCl solutions. The species formed and their influence on the α-HgS degradation process will be discussed more in detail below (see Section 4.3.2).

4.1.4. Possible sources of chlorine

To understand the degradation of original works of art, possible sources of chlorine are discussed according to their origin: these can be natural or anthropogenic.

Natural sources of chlorine

In the atmosphere, chlorine can be found as various gaseous species originating from the sea for one large part and from volcanoes for a smaller part. Most of these compounds are

naturally decomposed in the troposphere (i.e. the lowest portion of atmosphere) and form either HCl (as a result of the protonation of chloride ions) or $ClONO_2$, chlorine nitrate. These phases will then generate a small amount of chlorine-containing radicals by reacting with ozone. In this manner, Cl, ClO, ClO_2, and related species are formed *[D.A. Johnston, 1980; http://zebu.uoregon.edu/text/ozone]*.

The total concentration of chlorine in the atmosphere in coastal areas was evaluated to be between 6 and 20 $\mu g.m^{-3}$ in 1974 in Japan *[T. Okita, 1974]*, and more recently up to 5 $\mu g.m^{-3}$ anywhere in Japan, even far inland *[G. Thomson, 1986]*.

Concerning wall paintings degradation, both material sets studied originate from cities adjacent to the sea (Pompeii, South-Western Italy and Pedralbes, near Barcelona, North-Eastern Spain), where the concentration of chlorine in the atmosphere is higher than elsewhere.

Sources of chlorine related to human activities

The sources of chlorine-containing gaseous species in the atmosphere due to human activities are mainly industrial activities that emit HCl, chlorofluorocarbons (CFC), hydrofluorocarbons, CCl_4, CH_3CCl_3 and CH_3Cl in the air. The CFC and CCl_4 species exhibit a particularly long lifetime in the troposphere (from 50 to more than 200 years); consequently, chlorine is more present in this part of the atmosphere as CFCs than as HCl, even if the latter is produced in much larger quantities *[http://zebu.uoregon.edu/text/ozone]*.

Chlorine can be present not only in the atmosphere, but also directly in the materials of works of art themselves. Varnishes or binders may contain chlorine, as suggested by the unidentified chlorine compounds seen by µ-XANES in all pictorial layers in the Brueghel panel samples (see p.88, Section 2.2.4), or on the superficial organic layers (varnish) of the Gi-T and Gi-B samples (Giotto Crucifix, see p.91-92, Section 2.2.5). The chlorine pollution of the cross-sections by immersion oil used during optical microscopy can be excluded as chlorine wan only present in the varnish and not in the pictorial layers of these samples.

Specific actions of curators may also be responsible for the presence of chlorine in the environment of some works of art. Indeed, carbon tetrachloride (CCl_4) has been used in the past by curators to treat wood supports against insect invasion *[S. Bergeon, 1990; C.*

Paolini, 2000]. Even the wood support of the famous Mona Lisa portrait by Leonardo da Vinci is recorded to have been treated with this solution in 1977 because worms' holes were observed; the treatment was repeated in 1985 "as a preventive measure" *[J.P. Mohen, 2006]*. More interestingly, several paintings containing mercury sulfide showing grey or black crusts at the surface of the red areas are reported to have been treated with CCl_4 in the 1960's *[Reports from C2RMF n°9684 ("Annonciation" by Caporali), P3 ("Couronnement de la Vierge" by Fra Angelico), P158 ("Retable de Thouzon", artist unknown) and P248 ("Réunion dans un cabaret" by Le Valentin)]*. The limited access to paint micro-samples of these works of art only allows to report the results of the previous analyses made on them, which mostly consisted of visual observations of cross-sections and does not include any information on the presence of chlorine compounds.

During artificial ageing experiments, when α-HgS model samples were exposed to CCl_4, a blackening of the surface was observed (see p.146, Section 3.3.3); when chlorine (in the form of NaCl) was added to a superficial layer of varnish applied on top of mercury sulfide, the sample acquired a brown aspect (see p.143, Section 3.3.2). It can be concluded that chlorine-containing solutions applied directly on the surface of works of art are able to induce a darkening of red mercury sulfide.

Next to CCl_4, it is known that marbles and marbly limestone were cleaned with diluted sodium hypochlorite in order to obtain a surface with a better luster. Thus, in the museum environment, chlorine could also have originated from cleaning products that induced the presence of this element in the atmosphere of the room.

4.2. Degradation products identified or hypothesized

The degradation compounds that may be formed during the alteration of mercury sulfide will be summarized below; some of these have been identified without any doubt during previous or the present studies while the presence of others remains hypothetical.

4.2.1. Summary of bibliography

Calomel – Hg_2Cl_2

Calomel was recently identified on works of art by different analytical techniques such as Raman spectroscopy *[M. Spring, 2002; M. Maguregui, 2009]* and μ-XANES *[M. Cotte, 2006; 2008; 2009]*. However, by means of XANES analyses, a clear identification of the exact compounds concerned is difficult in the case of complex mixtures. In this respect, XRD provides more specific information. On the basis of SIMS analysis results, Keune et al. assumed the presence of calomel in degraded paint layers *[K. Keune, 2005]* (see Section 2.1).

Corderoite – α-$Hg_3S_2Cl_2$

As for calomel and mercuric chloride, SIMS analyses only allowed presuming the presence of corderoite on degraded paintings *[K. Keune, 2005]*. By μ-XANES, combination of analyses at the S and Cl K-edges supported the presence of corderoite on different altered works of art *[M. Cotte, 2006; 2008; 2009]* (see Section 2.1).

Gypsum – $CaSO_4.2H_2O$

Gypsum was identified on wall paintings and frescoes, and on the surface of some degraded layers of red mercury sulfide, either by Raman spectroscopy *[M. Perez-Alonso, 2004]* or by μ-XANES *[M. Cotte, 2006]* (see Section 2.1).

Metacinnabar – β-HgS

The black color observed as a result of the degradation of red mercury sulfide was often interpreted as being caused by the transformation of cinnabar into metacinnabar (β-HgS). Nevertheless, most of the time only elemental analyses were made and none of them could prove the presence of metacinnabar on altered works of art. To our knowledge, only one paper presenting an identification of β-HgS via a structural analysis method (XRD) on a degraded wall painting *[I. Istudor, 2007]* was ever published (see Section 2.1).

4.2.2. Summary of analyses of original painting samples

Some of the degradation compounds encountered in the artificially aged model samples were also identified on degraded works of art. In the present study for the first time, μ-XRD was used for this purpose. It is noteworthy that metacinnabar was never identified in these samples. Details on the analyses of the original painting samples can be found in Section 2.2.

Calomel – Hg_2Cl_2

Calomel was identified on three of the original paint samples: in sample B from the Rubens painting (Ru-B), in the wall painting from Pedralbes (Pe-W) and in the sample of the blood of Christ on the Giotto Crucifix (Gi-B).

Polymorphous phases of $Hg_3S_2Cl_2$

Different forms of $Hg_3S_2Cl_2$ were found on altered works of art. In sample Gi-B, μ-XANES analyses showed the presence of $Hg_3S_2Cl_2$ co-localized with Hg_2Cl_2; however, identification of the exact form of this compound was not possible with this technique. The same problem was encountered with the black sample from the Pompeian fresco (Po-B), where this compound was found to be present on the surface of the α-HgS layer, and on sample A from the Rubens painting (Ru-A).

In the Pe-W sample, corderoite (α-$Hg_3S_2Cl_2$) was found to be present as an intermediate layer between intact α-HgS and a layer of Hg_2Cl_2.

On the grey sample from the Pompeian fresco (Po-G), β-$Hg_3S_2Cl_2$ was identified on the surface of α-HgS; this compound was also encountered in the Pedralbes material.
The third form, kenhsuite (γ-$Hg_3S_2Cl_2$) was identified in two samples: in the Pe-W sample, co-localized with corderoite, and in the Ru-B sample, co-localized with calomel.

Sulfates found on degraded works of art

Sulfates were found on almost all samples analyzed in this study. In four of these, the compounds could not be completely identified: this was the case for the Gi-B sample, for samples from the three Brueghel panels, the Po-G and the Ru-A samples. In these cases, sulfates were present on top of the paint stratigraphy, except for the Po-G sample where they were co-localized with β-$Hg_3S_2Cl_2$.
Gypsum ($CaSO_4.2H_2O$) and anhydrite ($CaSO_4$) were identified in the top layer of cross-sections prepared from the Po-B and Pe-W samples. In this last case, the sulfates could be the remains of plaster, intentionally applied to cover the wall paintings.

4.2.3. Summary of artificial ageing experiments

Next to assumptions found in the literature, multiple degradation compounds were formed during the artificial ageing experiments on model samples in the present study. Details on the results obtained during the artificial ageing experiments can be found in Section 3.3.

Calomel – Hg_2Cl_2

Calomel was identified on all model samples aged with aqueous NaOCl and exposed to light, with the exception of one case (see p.139, Section 3.3.1). In only two cases where ageing experiments were performed in a closed system, calomel was not identified anymore after some time of ageing; in these cases, only corderoite remained.

Corderoite – α-$Hg_3S_2Cl_2$

As for calomel, corderoite was identified in all samples aged with NaOCl except in one case (see p.139, Section 3.3.1). In only three cases where ageing experiments were performed using the cyclic system, corderoite was not identified anymore after some time of ageing (with calomel remaining). For all model samples studied, within the achievable resolution of analytical techniques, calomel and corderoite were co-localized in the same layer covering the vermilion. In one case (a two-layered pellet {gypsum/α-HgS} exposed to NaOCl and light for 167 days), the polymorphous β-$Hg_3S_2Cl_2$ phase was also detected next to corderoite and calomel.

During the artificial ageing experiments, no visual change was visible on the pellets before Hg,Cl-compounds could be identified. As seen in Section 3.3, during the experiments on synthetic vermilion, both calomel and corderoite were detected simultaneously, whereas with natural cinnabar, first corderoite was identified by itself, followed after a few days by calomel.

Sulfates

In the case of the ageing of model samples containing α-HgS and calcite ($CaCO_3$), aged with either NaOCl or with NaCl solutions in combination with light, gypsum ($CaSO_4.2H_2O$) was identified (see p.147, Section 3.3.4).

Sulfates (of which the precise composition was not identified) were detected on α-HgS model samples in all ageing experiments with NaOCl. Some sulfates were also observed during the ageing experiments with solid NaCl (either a NaCl layer present below the vermilion layer or NaCl mixed with oil applied on top of the vermilion layer).

Mercury sulfate Hg_2SO_4 was identified only once in a two layered gypsum/vermilion pellet when aged with NaOCl (see p.148, Section 3.3.4).

Sulfites

Sulfites (SO_3^{2-}) were only identified once during the artificial ageing experiments when a α-HgS pellet was aged with a KOH solution (see p.119, Section 3.3.).

Metacinnabar – β-HgS

Metacinnabar was only identified once among all artificial ageing experiments, when a two layered NaCl/α-HgS pellet was aged with NaOCl, and its presence could not be established with certainty (see p.139, Section 3.3.1).

4.2.4. Non detected compounds

Among the species detailed above, in the literature two other specific compounds were hypothesized to be formed during degradation of red mercury sulfide: Hg(0) and $HgCl_2$. Nevertheless, as shown below, these could not be identified.

Metallic mercury - Hg(0)

The formation of metallic mercury is one of the hypotheses that could explain the black color of some degraded works of art and model samples after ageing (see Section 4.2.5), especially when no (other) degradation compounds were found. Indeed when studying red mercury sulfide alteration, sometimes only α-HgS is identified. Among this matrix, the presence of Hg(0) could be difficult to detect. This proposition comes from multiple previous studies made on this subject.

Previous hypotheses on Hg(0) presence

To explain the alteration compounds found on degraded works of art, Keune et al. proposed the idea of a light-induced conversion of Hg(II) from α-HgS into Hg(0) with the excess of sulfur converted into $SO_{2(g)}$; the Hg(0) may then react with the other phases that are present to form $HgCl_2$ and Hg_2Cl_2 *[K. Keune, 2005].* The same explanation was used by Terrapon et al.

to explain the black color of mercury sulphide after light exposure, attributing the loss of sulfur of the original HgS lattice to oxidation and volatilization, which induces an excess of Hg(0). In this case mercury was assumed to volatilize, thus rebalancing the composition of the crystal *[V. Terrapon, 2010]*.

According to Pal et al., the photo-irradiation of α-HgS induces the production of H_2S and Hg^{2+}, which leads to the deposition at the surface of Hg(0) *[B. Pal, 2003]*. Gustin et al. demonstrated that light energy is a more dominant process controlling mercury emissions from naturally enriched substrates than soil temperature *[M.S. Gustin, 2002]*. This last study also showed that substrates containing corderoite, metacinnabar and metallic mercury exhibited a higher degree of light-enhanced emissions than the ones containing essentially only cinnabar. According to this study, rocks from New Idria, California, present one of the lowest light enhanced mercury emissions. Gustin et al. performed mercury speciation by thermodesorption analysis, a method limited by the high detection limit needed for species identification (ca. 100 µg Hg/g) and by EXAFS; however, by means of the latter method, the presence of Hg(0) could not be certified. Thus, metallic mercury was assumed to be formed from mercury sulfide under specific conditions, and this production appears to be more important in case chlorine-containing substrates are involved.

To verify the production of metallic mercury from mercury sulfide, Dreyer diluted HgS into an alkaline solution, forming colloidal mercury. When pouring this solution over a porcelain surface, a mercury mirror was deposited that in its turn formed a black deposit when wiped off *[R.M. Dreyer, 1939]*.

Nevertheless, in all these studies, Hg(0) was not identified by any reliable analytical means. In order to assess whether we would be able to detect the presence of metallic Hg droplets on sample surfaces, different analytical methods were tried out. Only analytical techniques that can make a distinction between different oxidation states of Hg were used.

XANES analyses of metallic mercury droplets

As shown by Gustin, Hg(0) is hardly detectable by EXAFS, especially if mercury is present as a mixture of various species *[M.S. Gustin, 2002]*. In our case, an identification was attempted by means of Hg M-edge XANES. Droplets of Hg(0) were analyzed confined between two Ultralene foils at ID21 (ESRF, Grenoble). The resulting Hg M_5-edge spectra did not show any characteristic feature (Figure 4.1a) while the Hg M_4-edge spectra showed one broad shoulder at 2.3892 keV (Figure 4.1b). Since all mercury references showed similar XANES spectra, this means that there is not be enough chemical contrast between Hg(0) and other mercury species to identify its presence by means of Hg M-edge XANES.

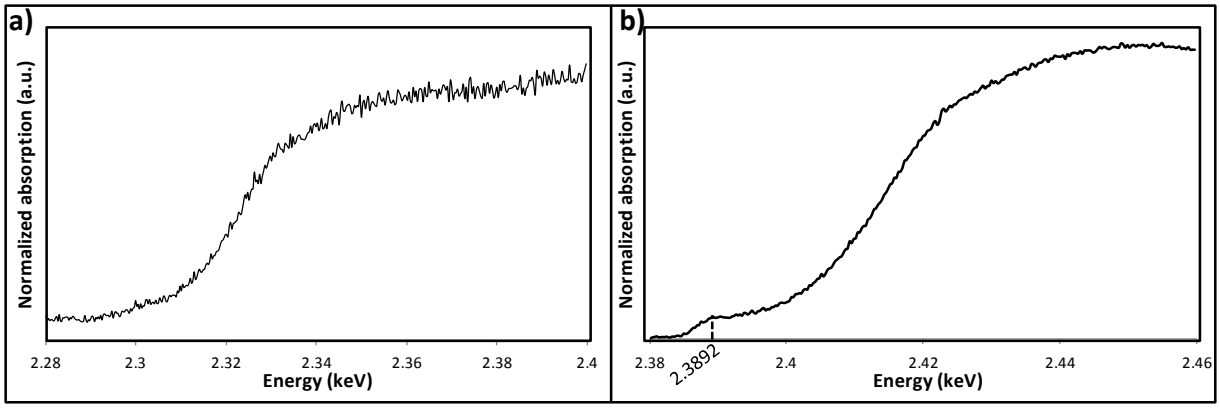

Figure 4.1.: *XANES spectrum of a Hg(0) droplet at:* ***a)*** *Hg M_5-edge;* ***b)*** *Hg M_4-edge.*

XPS analyses of original degraded samples

Another analytical technique is X-ray photoelectron spectroscopy. In principle, XPS can distinguish metallic mercury from more oxidized forms, even when the HgS matrix is present, as this technique only probes the topmost nanometers of the sample. This technique allowed Pouli et al. to detect a change in the HgS stoechiometry after laser irradiation at 1064 nm *[P. Pouli, 2003]*: the Hg/S ratio increased from 1 to 1.29. While the stoichiometric measurements suggested the presence of metallic Hg, Pouli et al. could only demonstrate the presence of Hg_2^{2+} using curve-fitting analysis.

The possibilities of this method encouraged us to carry out experiments performed at the LRS (Ivry-sur-Seine). XPS analyses were not possible directly on Hg(0) droplets due to the ultra-vacuum that could lead to Hg-pollution of the instrument. To avoid pollution of the XPS instrument by volatilized mercury, cryo-measurements could be envisaged in order to

solidify mercury(0) in the sample. Instead, measurements were performed on a cinnabar ore from China that darkened under exposure to light, showing a silvery aspect (see Figure 4.2a). However, the XPS results (Hg_{4f} peaks) only show the presence of mercury (II) (presenting a doublet at binding energies 105-100.6 eV) at the surface of this ore (Figure 4.2b); the peaks corresponding to Hg(0) would have been situated around 99.8 eV *[http://www.lasurface.com]* but were not visible. Thus, metallic mercury could not be identified at the surface of this sample. On the basis of the peak integrals, it was possible quantitative measure the Hg/S ratio: this was calculated to be 1.18, i.e. with a slight excess of mercury. Other elements found were oxygen, carbon and less than 1 atomic % of chlorine.

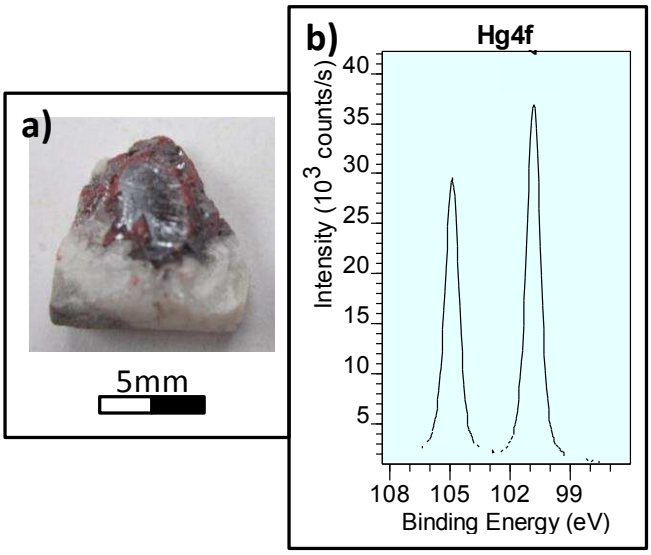

Figure 4.2.: a) *Photograph of a darkened cinnabar ore from China analyzed by XPS;* ***b)*** *XPS spectrum obtained at the Hg_{4f} binding energy.*

A similar experiment, performed on degraded Pompeian materials (Po-B and Po-G) also only revealed the presence of Hg(II) at the surface (see Section 2.2.3).

Chemical tests on Hg(0) droplets and natural cinnabar ores

By adding nitric acid (HNO_3) to Hg(0), a white precipitate of $Hg(NO_3)_2$ can be formed, following the equation:

$$Hg(0) + 4HNO_3 \rightarrow Hg(NO_3)_2 + 2NO_{2(g)} + 2H_2O$$

When the same solution was applied on natural HgS ores on which Hg(0) droplets were visible, the formation of the same precipitate was observed (see example of cinnabar ore samples from Almadén in Figure 4.3). This white precipitate was not observed on ores without metallic droplets before the HNO_3 treatment. Chemical analyses on ores after this test could help to better assess the presence of the precipitate; nevertheless the pollution induced by mercury droplets limits the use of many analytical techniques, in particular those carried out under vacuum. Since this approach is destructive, it will be difficult to use it on any sample originating from a work of art.

Figure 4.3.: *Photograph of a natural ore from Almadén, El Entredicho, showing Hg(0) droplets and the white $Hg(NO_{3)2}$ precipitate formed after the application of nitric acid on its surface.*

Another chemical test is based on the formation of amalgams between mercury and gold or silver. For this purpose, Hg(0) droplets were deposited on Au and Ag foils. No visual change was visible on the foils or droplets. Analyses would be necessary to identify the formation of amalgams and also here, the possible pollution of instruments did not allow elaborating on these chemical tests.

In summary, these experiments did not show the presence of Hg(0) on any sample. However, many of analytical protocols used in the present study concerning metallic mercury had to be stopped because of instrument pollution issues.

Mercuric chloride – $HgCl_2$

Mercuric chloride was only presumed to be present on degraded paintings by SIMS analyses *[K. Keune, 2005]*. This compound could not be unambiguously identified by any other analytical techniques on altered works of art.

Calomel (Hg_2Cl_2), is known for its possible dismutation into Hg(0) and $HgCl_2$ *[F. Souil, 1997]*. In order to verify the influence of light on this compound, ageing of calomel was performed by irradiating Hg_2Cl_2 powder with UV light. Before ageing, the Cl K-edge XANES spectrum of this sample was similar to the one of Hg_2Cl_2; however, after ageing, the spectrum showed the same features as that of the $HgCl_2$ reference spectrum (Figure 4.4). Moreover, the sample, originally white before ageing, turned dark after irradiation.

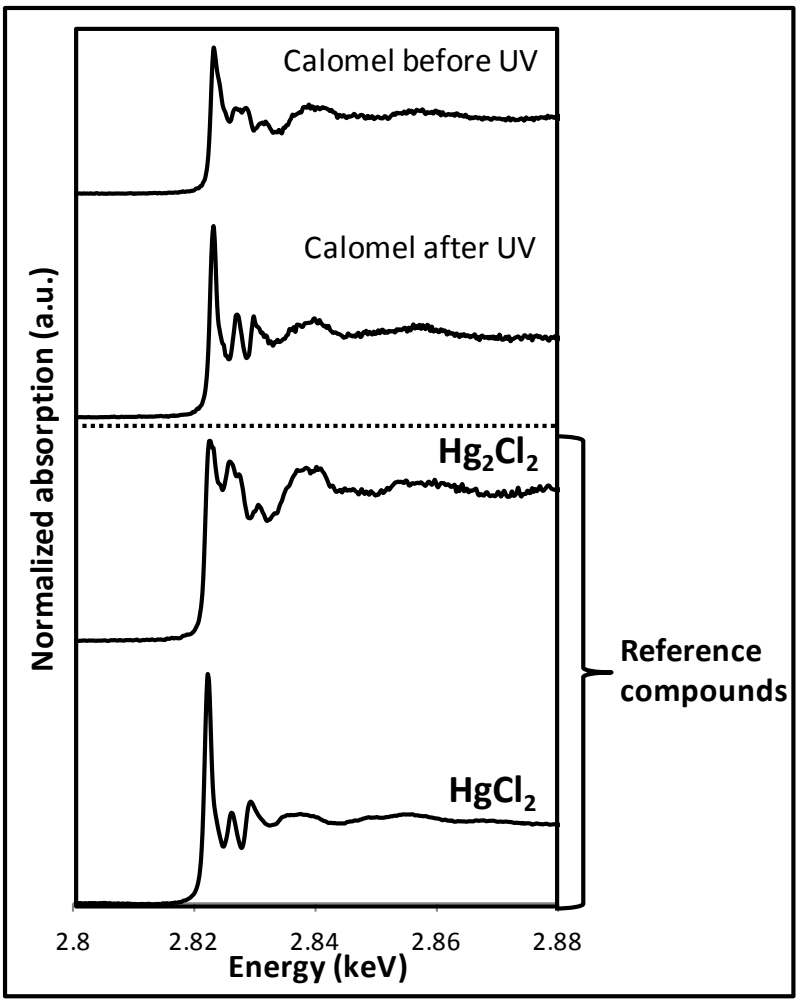

Figure 4.4.: *XANES spectra of calomel before and after UV irradiation compared to reference spectra of Hg_2Cl_2 and $HgCl_2$.*

This observation of the probable transformation of Hg_2Cl_2 into $HgCl_2$ under light irradiation and the dark color obtained supports the formation of metallic mercury on the surface of degraded works of art due to dismutation:

$$Hg_2Cl_2 \rightarrow HgCl_2 + Hg$$

However, in the present study, $HgCl_2$ was never identified on original samples and only in few non reproducible cases for artificially aged samples. Multiple reasons other than its absence may be cited for this lack of observations. $HgCl_2$ is not a salt but form linear triatomic molecules, that in the presence of chloride ions, forms soluble $HgCl_4^{2-}$ complexes. Its solubility is fairly high in water (7.4 g/100 mL at room temperature) and either (4 g/100 mL). When attempt was made to analyze pure $HgCl_2$ powder (Prolabo) by XRD, no clear diffractogram was obtained allowing its identification. The presence of this phase on degraded works of art therefore cannot be excluded, even if it is not observed by XRD.

4.2.5. Relationship between color and composition

Description of visual aspect of red mercury sulfide degradation

Degradation of red mercury sulfide on works of art having a grey or black color, gives rise to heterogeneous or homogeneous facies. In the cases of panel paintings, in most of the cases, the degradation follows the shadowed areas of the painted garments and/or brushmarks (see Figure 2.1., p.51, Section 2.2.1). This distribution of the degraded areas over a painted region may indicate that a mechanical action lies at the origin of the alteration; such may be the application of a product at the surface of the painting by a brush, or the heterogeneous application of the pictorial layer. These marks are not visible on altered wall paintings; here, degradation layers seem to be more homogeneous, an observation that could be consistent with a degradation agent originating from the atmosphere that spreads homogeneously across the surface of the wall.

During artificial ageing experiments, alteration on α-HgS model samples induced by the presence of light and chlorine does not give rise to the same black color as seen on, for

example, Pompeian frescoes (Section 2.2.3). The degraded model samples present different kind of crystals: these may be small, white and homogeneously distributed on the surface, giving to the surface a purple color; or they may be large, squarish, translucent and localized heterogeneously, so that the original red color of the vermilion remains visible. After some time, a thick and homogeneous layer may appear, giving the surface a white to light-grey color (see Figure 3.13., p.122, Section 3.3.1). The presence of the different degradation compounds appears to give rise to different surface aspects.

Despite all the phases identified on the surface of the degraded samples, their natural color cannot explain the color of the alteration found on works of art. Indeed, calomel (Hg_2Cl_2) is usually white in nature, corderoite (α-$Hg_3S_2Cl_2$) orange-pink to purple while kenhsuite (γ-$Hg_3S_2Cl_2$) is yellow. Thus, the influence of each compound on the residual color and aspect of the degraded areas is still not fully understood. It is not impossible, however, that a combination of the red vermilion (absorbing visual light up to 630 nm) with a yellow compound (absorbing light in the 600-660 nm region) may give rise to a dark brown to black mixture that absorbs light in almost the entire visual range.

The colors of the degraded layers appear to be related to its composition. The most clear case is encountered among the Pompeian samples (see Section 2.2.3). Sample Po-G (grey) predominantly contains chlorine-containing compounds at its surface, while sample Po-B (black) predominantly features sulfates. Next to the color, the visual aspect is also different. Maps recorded from a cross-section of Po-G show a thin and heterogeneous degradation layer whereas those of Po-B present a thicker, smoother and more homogeneous alteration layer. Following the previous hypotheses on the formation of sulfates, an explanation could be that the chlorine containing compounds originate from the direct transformation of mercury sulfide that is in contact with the pigment grains, whereas the superficial sulfate layers originate from the diffusion of SO_2 (produced during the alteration of HgS) that further oxidize and precipitate at the sample surface.

Hypotheses concerning the dark color of degraded α-HgS

During the artificial ageing experiments, the degradation of red mercury sulfide induced a blackening of some model samples. This dark color can also be found on degraded areas of works of art. As the natural color of the degradation compounds identified could not explain the residual color of the altered surfaces, some hypotheses are suggested here to clarify this situation. All these hypothese are based on two main ideas:

1- <u>All compounds were identified and some of them are responsible for the dark color</u>

In some cases, α-HgS could appear black. When vermilion is prepared according to a historical recipe by heating a mixture of Hg(0) and S(0), the product in the reaction vessel is black and needs to be ground to allow the red color to appear *[R.J. Gettens, 1993]*. Spring et al. suggested the formation of Hg_2Cl_2 and black HgS from the action of light on corderoite (α-$Hg_3S_2Cl_2$) *[M. Spring, 2002]*, which could be possible during degradation processes. During previous experiments, HgS particles were formed inside hair strands by making HgO react with the sulfur contained in the proteins. These particles were observed by TEM and had dimensions below 10 nm. After the "HgO-dying" process, the visible color of the original white hairs became black *[G. Patriarche, 2012]*. From this observation, it can be concluded that, when nanoparticles of α-HgS are formed inside or on the surface of a degraded sample, it is possible that they darken the visual aspect of the altered surface. The dark color could thus be attributed to (nanoparticles of) α-HgS.

Concerning the black color of α-HgS after photo-irradiation, McCormack suggested that the change of color from red mercury sulfide to black after light exposure may be explained by the absorption of red wavelengths (reflected by unaged α-HgS and giving its red color) which results in the black appearance of cinnabar *[J.K. McCormack, 2000]*. α-HgS model samples aged with NaOCl and light feature, similar to material from original works of art, calomel and corderoite on their surface. Their white-grey color is more easily explained by the natural colors of these two compounds than the dark color of the altered material observed on original works of art. Accordingly, the light color obtained during artificial ageing is not corroborating this hypothesis.

2- Dark color is due to a non-detected compound

The dark color of degradation could be caused by the formation of metacinnabar during the degradation process. As it was not detected on altered works of art, β-HgS can be assumed to be present as small particles, perhaps of nanometric dimensions, perhaps not well crystallized; such a compound would not be identified in the presence of the α-HgS matrix, even by XRD.

Metallic mercury (Hg^0) could be formed on the surface of the altered samples, however, it also would be difficult to identify in the presence of the α-HgS matrix. This specific hypothesis was discussed above (see Section 4.2.4).

When crystallized compounds such as gypsum are formed on the surface of works of art, their crystals could incorporate dust and give to the degraded area a darkened color. This hypothesis is only conceivable for original works of art, especially for those exposed outdoors, and not for model samples aged in sealed tubes. However, this hypothetic presence of dust was not detected during analyses performed on original altered samples.

In the present study no indications were encountered that might allow to prove or disprove either of the two hypotheses. However, the observations made from original and artificially aged samples permit to refine and discuss the propositions found in the literature.

Concerning the dark grey color of the two layered NaCl/α-HgS pellets (see p.141, Section 3.3.2), the presence of solid NaCl appears to be an important parameter to obtain this visual aspect; with aqueous NaCl solutions, the same color was not obtained, even with longer ageing times. This difference is still not understood.

4.3. Reaction mechanisms of the α-HgS alteration process

4.3.1. Summary of bibliography

In the past, research groups *[G.A. Parks, 1979; N.P. Brandon, 2001; M. Svensson, 2006]* have studied the Hg-S-Cl-H_2O system (or part of it), and have proposed reactions among mercury compounds; this was done in the context of the study of stability conditions of different compounds for environmental or theoretical concerns. These previous propositions helped the discussion concerning the mechanisms and conditions of formation of degradation compounds. Three examples of Pourbaix diagrams for the Hg-S-Cl-H_2O system reproducing these previous studies are shown in Figure 4.5.

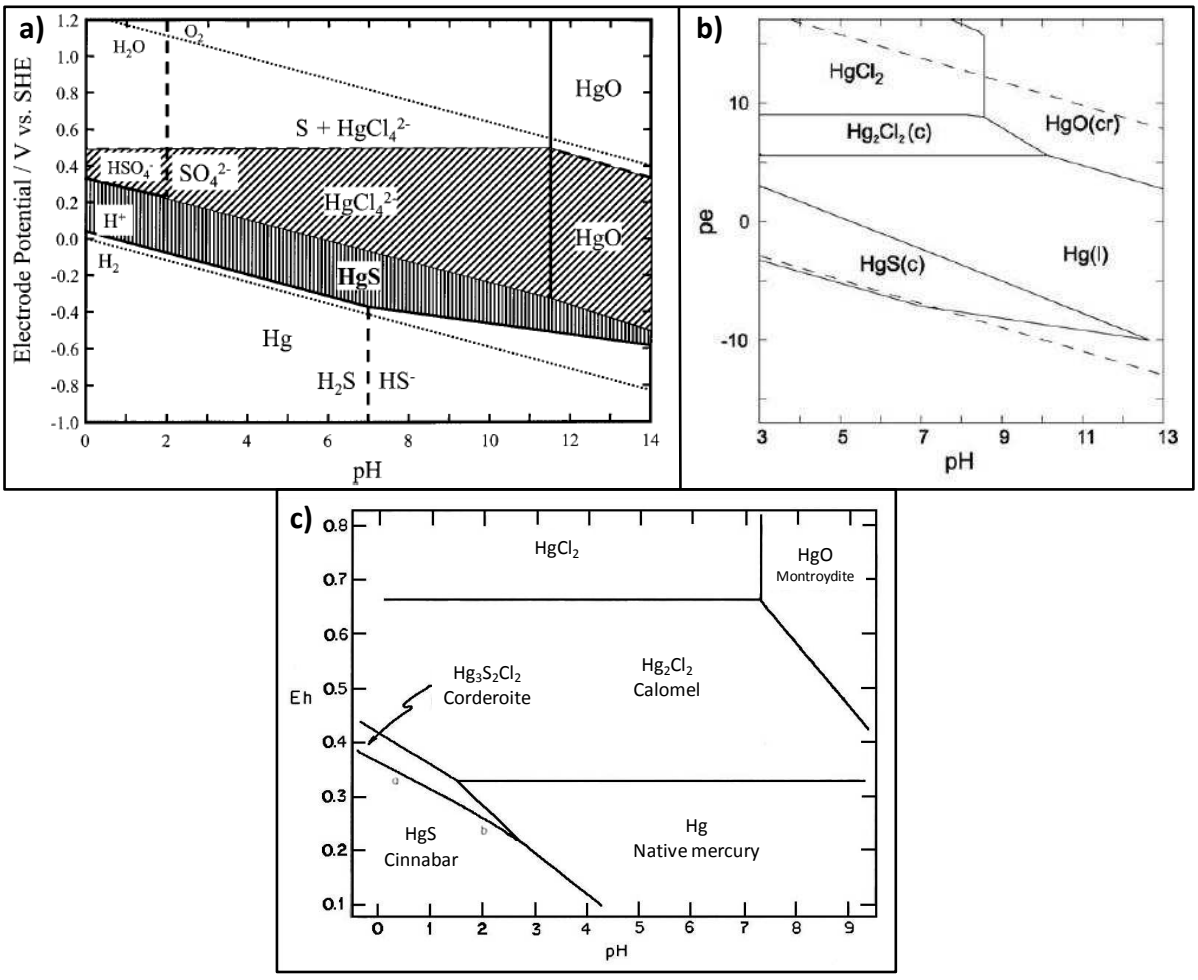

Figure 4.5.: *Pourbaix diagrams of the Hg-S-Cl-H_2O system at 25°C taken from the literature:* ***a)*** *with activities of dissolved mercury, sulfur and chlorine equal to 10^{-6}, 1 and 1 respectively [N.P. Brandon, 2001];* ***b)*** *with Hg:S:Cl = 1:3:100 [M. Svensson, 2006];* ***c)*** *with activities of Cl^- and the dominant SO_4^{2-} species equal to 0.1 M [G.A. Parks, 1979].*

Brandon et al. ***[N.P. Brandon, 2001]*** **–** cf. Figure 4.5a

In the first study, Brandon et al. showed that the presence of chlorine in Hg-Cl-H_2O system extends the stability areas of Hg_2^{2+} and Hg^{2+} ions, forming respectively Hg_2Cl_2 and $HgCl_4^{2-}$.

For the Hg-S-H_2O system, oxidation of HgS to S(VI) and Hg(0) is predicted via the reaction:

$$HgS + 4H_2O = Hg + SO_4^{2-} + 8H^+ + 6e^-$$

though this may not be expected to take place in kinetic experiments due to the strong interaction of sulfur with mercury. S(0) is not predicted to form in this system. The HgS reduction is predicted to either give rise to Hg(0) and H_2S at pH < 7 or to Hg(0) and HS^- at pH > 7. Sulfite ions (SO_3^{2-}) and Hg are also predicted to be formed from HgS at high pH (> 8) and at potential values < 0.2 V. When the Hg activity is decreased from 0.1 to 10^{-6}, the formation of Hg_2SO_4 and $HgSO_4$ is predicted at low pH.

When adding chlorine to the system, Brandon et al. draw the potential-pH diagram of the Hg-S-Cl-H_2O system at 25°C with activities of mercury, sulfur and chlorine respectively at 10^{-6}, 1, 1 while excluding sulfoxy species from the calculation. This diagram, presented in Figure 4.5a, appears to best predict the behavior of HgS in neutral chloride-containing media.

Svensson et al. ***[M. Svensson, 2006]*** **–** cf. Figure 4.5b

Svensson et al. constructed potential-pH diagrams of mercury species and studied the possible formation of α-HgS from Hg(0) and HgO in order to be able to build a repository for permanent storage of mercury. Adding chlorine to the Hg-S-H_2O system did not seem to have an impact on the stability region of α-HgS.

When considering the Hg-S-Cl-H_2O system at 25°C with relative proportions of mercury, sulfur and chlorine respectively equal to 1, 3 and 100, mercury chloride compounds (Hg_2Cl_2 and $HgCl_2$) are formed in aerobic conditions (at high potential) and at pH < 10.

Parks et al. ***[G.A. Parks, 1979]*** **–** cf. Figure 4.5c

Contrary to the two previous studies, Parks et al. studied the formation of corderoite. To estimate the free energy of formation (ΔG_f^0) of corderoite, they considered the experimental study by Carlson, which gave the following equations *[E.H. Carlson, 1967]*:

$$HgS_{(s)} + 2\ HCl = HgCl_{2(g)} + H_2S$$

$$3\ HgCl_{2(g)} + 2\ H_2S = Hg_3S_2Cl_{2(s)} + 4\ HCl$$

Parks et al. estimated from the last equation the free energy of formation of corderoite to be probably more negative than -332.2 $kJ.mol^{-1}$.

From this value, a potential-pH diagram was calculated for the Hg-S-Cl-H_2O system at 25°C with activities for chlorine and sulfoxy species (that are considered to be predominant in the system) both at 0.1 M, and presented in Figure 4.5c. This diagram shows that corderoite requires rather acidic and mildly reducing conditions to be formed.

Another study confirmed the estimation of ΔG_f^0 from Parks et al. for the formation of corderoite with a calculated value of -396 (+3,-11) $kJ.mol^{-1}$ and considered that in highly acidic conditions, cinnabar reacts directly with chlorine to form corderoite *[K. Paquette, 1995]*:

$$3\ \alpha\text{-}HgS + 2\ H^+ + 2\ Cl^- \leftrightarrows Hg_3S_2Cl_2 + H_2S$$

The same equation was used by another group to explain the dissolution of cinnabar at pH 6.5 (in the human small intestine) *[X. Zhou, 2010]*.

In the present study, chlorine is not considered as a neutral medium, and the sulfoxide species are considered to be the predominant phases. Moreover, the elemental ratio chosen to draw the potential-pH diagram of Svensson et al., with 3 times more sulfur than mercury, does not correspond to the conditions of the present study. Thus, potential-pH diagrams were calculated to fit the conditions encountered in paint layer systems.

4.3.2. Formation and evolution of degradation compounds

As discussed in previous chapters, samples obtained from degraded original works of art and from artificially ageing experiments show the presence of chlorinated compounds, i.e. Hg_2Cl_2 and three polymorphous phases of $Hg_3S_2Cl_2$. The understanding of the formation and the stability of these different products is an essential point of this study for a conservation and restoration point of view.

In order to achieve this goal, different diagrams were calculated by means of the HSC Chemistry 7.0 software package.

Pourbaix diagrams of Hg-S-Cl-H_2O systems

Pourbaix diagrams were calculated using thermodynamic data of Balej (1985), cited by Brandon et al. *[N.P. Brandon, 2001]*. The free energy of formation of corderoite is the lower estimation value from Paquette et al. *[K. Paquette, 1995]*. These data are available in Appendix B.i.

Cl-H_2O system

During artificial ageing of α-HgS with NaOCl, different phases are present in the ageing vessel (see Figure 4.7), of ionic, aqueous, solid and gaseous nature as detailed below.

In a NaOCl aqueous solution, chlorine is present in the form of $ClO^-_{(aq)}$, via dissolution of this ion in water. A Pourbaix diagram for the Cl-H_2O system was calculated (see Figure 4.6). This diagram shows that in basic conditions, $ClO^-_{(aq)}$ is stable.

$Cl^-_{(aq)}$ can be obtained by reduction of $ClO^-_{(aq)}$ (the standard potential of this redox couple is E^0 = 0.90 V *[www.hyperphysics.phy-astr.gsu.edu/hbase/tables/electpot.html]*), corresponding to the half-reaction:

$$ClO^- + H_2O + 2\ e^- = Cl^- + 2\ OH^-$$

$ClO^-_{(aq)}$/ $Cl^-_{(aq)}$ is therefore a highly oxidant couple and will be able to extract electrons from many species.

Among all species available in the Cl-H_2O system, chlorine phases coming from the oxidation of $ClO^-_{(aq)}$ (such as ClO_2^-, ClO_3^-, ClO_4^-) are not visible in the diagram of Figure 4.7. Only the stability domain of $ClO_{(g)}$ is indicated; this is associated with the oxidation of $ClO^-_{(aq)}$ via:

$$ClO^-_{(aq)} = ClO_{(g)} + e^-$$

$ClO_{(g)}$ can therefore be present in the vessel atmosphere.

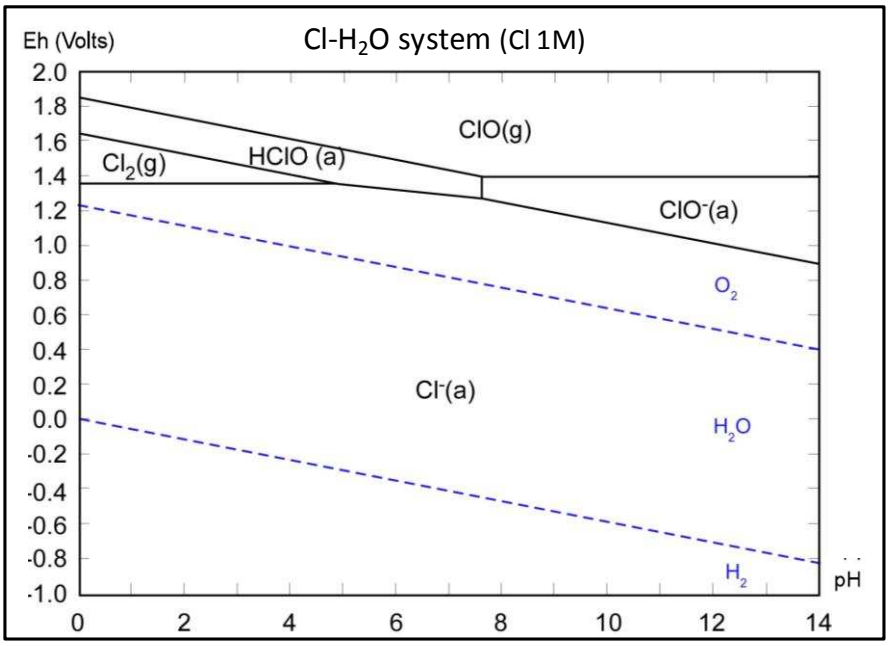

Figure 4.6.: *Potential-pH diagram at 25°C for Cl-H_2O system with in brackets activity of chlorine.*

Two solid phases were found in the NaOCl solution after few weeks in the tubes (see p.120, Section 3.3): $NaClO_{3(s)}$ and $NaCl_{(s)}$, which may be formed by decomposition of NaOCl:

$$3\ NaOCl \rightarrow NaClO_3 + 2\ NaCl$$

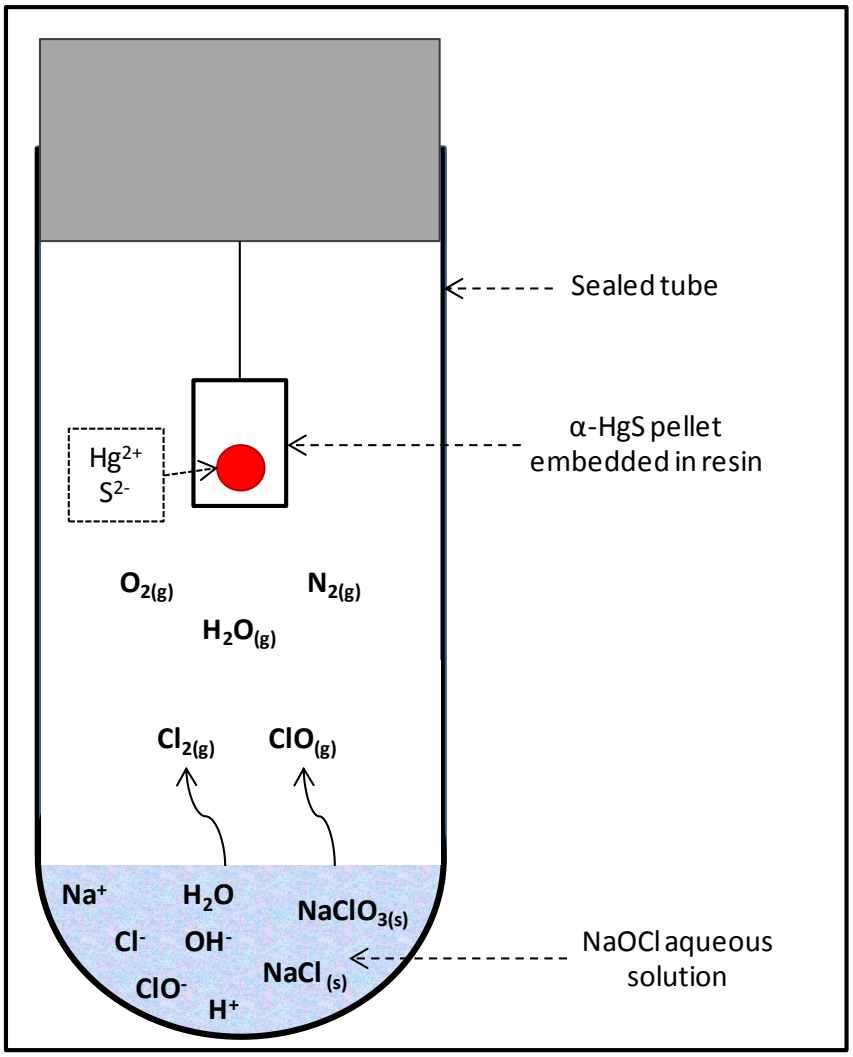

Figure 4.7.: *Representation of the different compounds present in the ageing vessel during ageing of α-HgS with an aqueous NaOCl solution.*

Considering the NaCl solution used during ageing, chlorine is present in the solution by dissolution of $NaCl_{(s)}$ into water as $Cl^-_{(aq)}$ and in the atmosphere of the tube possibly by oxidation of Cl^- to $Cl_{2(g)}$ ($E^0_{Cl2/Cl-}$ = 1.36 V *[J. Sarrazin, 1991]*):

$$2\ Cl^- = Cl_{2(g)} + 2\ e^-$$

<u>Hg-S-H_2O and Hg-Cl-H_2O systems</u>

First, the Hg-S-H_2O system was studied at 25°C. When considering S as the predominant species (Figure 4.8a), we see that at low pH (< 4) and high potential (0.6 < Eh < 0.8 V), mercury sulfate (Hg_2SO_4) is stable and could be formed. Sulfates can indeed come from the

oxidation of sulfur in α-HgS and even if the Hg_2SO_4 stability domain is at low pH, other sulfates (such as gypsum when calcite is present) could be formed in different conditions. The stability domain of α-HgS is surrounded by the one of Hg, which means that metallic mercury could be formed from reduction or oxidation of mercury sulfide. Above a potential of 0 Volts, HgO can be formed, which could happen when the tube is open; nevertheless it was never identified in the aged model samples. Sulfite ions (SO_3^{2-}) are not represented in the diagram; they do not appear to be stable in these conditions.

For the same system with Hg as the predominant species and an S activity of 10^{-3} M instead of 1 M (Figure 4.8b), the stability domain of Hg_2SO_4 is not present anymore, and Hg_2^{2+} is predicted as being stable at low pH (< 2) and high potential (0.7 V < Eh < 0.8 V).

For the Hg-Cl-H_2O system at 25°C, with the activities of mercury and chlorine respectively at 10^{-3} M and 1 M, the calculated diagram with Hg as predominant species (Figure 4.8c) shows that below pH 9, Hg_2Cl_2 is stable (with 0.3 < Eh < 0.6 V). During ageing experiments, a change of pH was observed for the NaOCl solution, going from 12 to 9, which could explain the formation of Hg_2Cl_2. Even when not identified during experiments, on this diagram $HgCl_2$ has a large stability domain at pH values below 6 when 0.6 < Eh < 1.4 V, due to oxidation of Hg_2Cl_2.

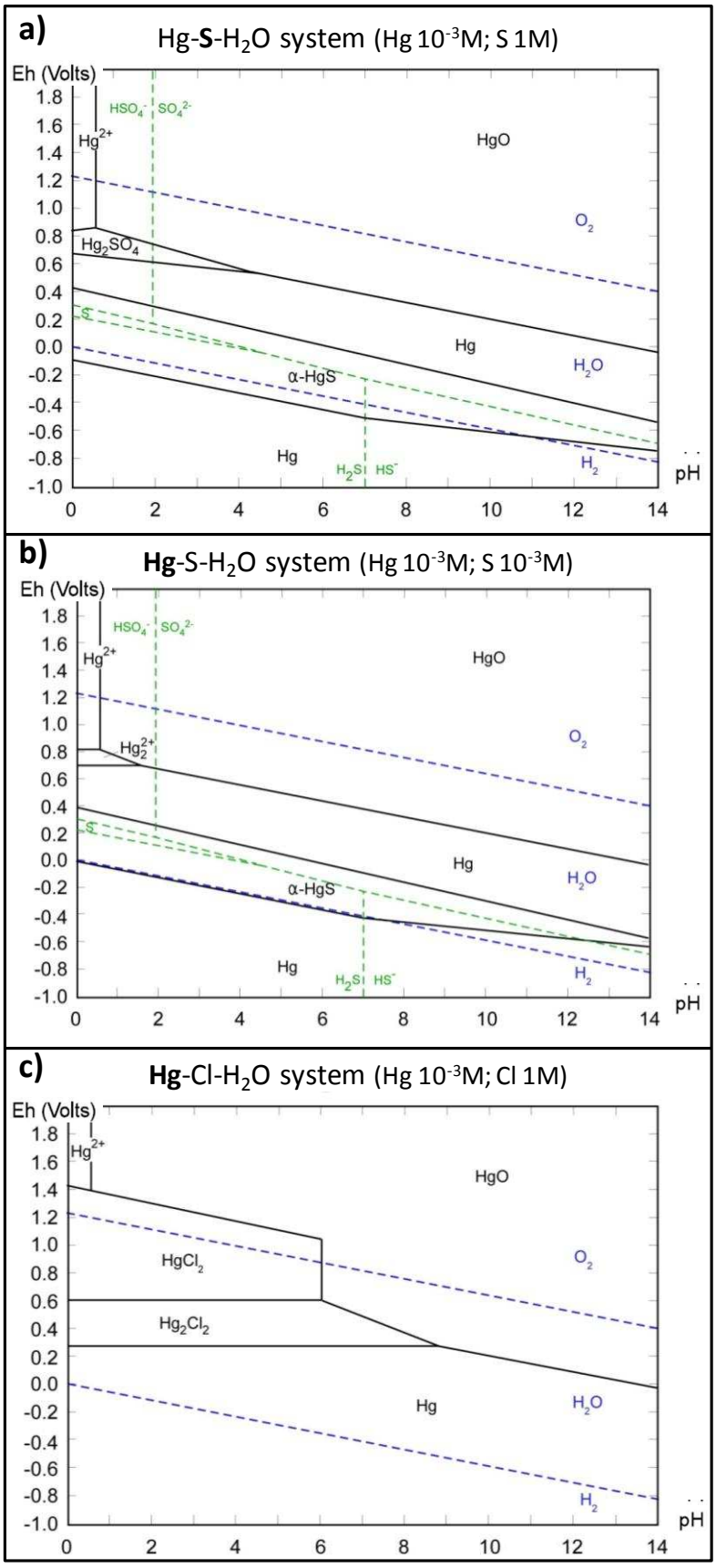

Figure 4.8.: *Potential-pH diagrams at 25°C for different systems with in bold the predominant species and in brackets the activities of the corresponding elements.*

Hg-S-Cl-H_2O system

When superimposing the previous figures, two diagrams of the Hg-S-Cl-H_2O system at 25°C were obtained. The first one shows the stability domains of different mercury containing compounds when Cl is the predominant element in the system, which means it will always be available for possible reactions (Figure 4.9a), whereas the second one corresponds to the situation in which Hg is the predominant element (Figure 4.9b).

The first diagram shows that calomel (Hg_2Cl_2) and corderoite (α-$Hg_3S_2Cl_2$) can be formed at relatively low potential (Eh < 0.5 V). Moreover, in the chosen conditions (with chlorine in excess), whatever the redox potential or the pH, α-HgS and Hg(0) are not stable in this system. With chlorine predominant, the stability domain of corderoite ranges from pH 0 to 14 and is relatively large in the potential scale. Thus, contrary to what was concluded in previous studies, where it was stated that the formation of corderoite is not favorable in nature due to the necessity of an extremely acid environment *[G.A. Parks, 1979]*, this diagram could explain the feasability of the formation of corderoite at high pH values. From this diagram, it is possible to observe that when corderoite is present, when the potential (Eh) increases, calomel can be formed. During ageing experiments, in a closed tube containing an NaOCl solution, effectively corderoite and calomel are formed on the surface of α-HgS model samples. When the vessel is opened, the activity of $O_{2(g)}$ will increase, which will also increases the Eh and could therefore induce the formation of calomel from corderoite. This could explain the predominance of calomel in the samples aged using the cyclic system.

In the second diagram (Hg predominant), the stability field of calomel (Hg_2Cl_2) is situated in the lower pH range (pH < 9), as mentioned above. With these conditions, α-HgS can be stable, and if the potential increases due to the presence of oxidyzing species, Hg_2Cl_2 can be formed from it. When chlorine is not considered as predominant, corderoite is not stable.

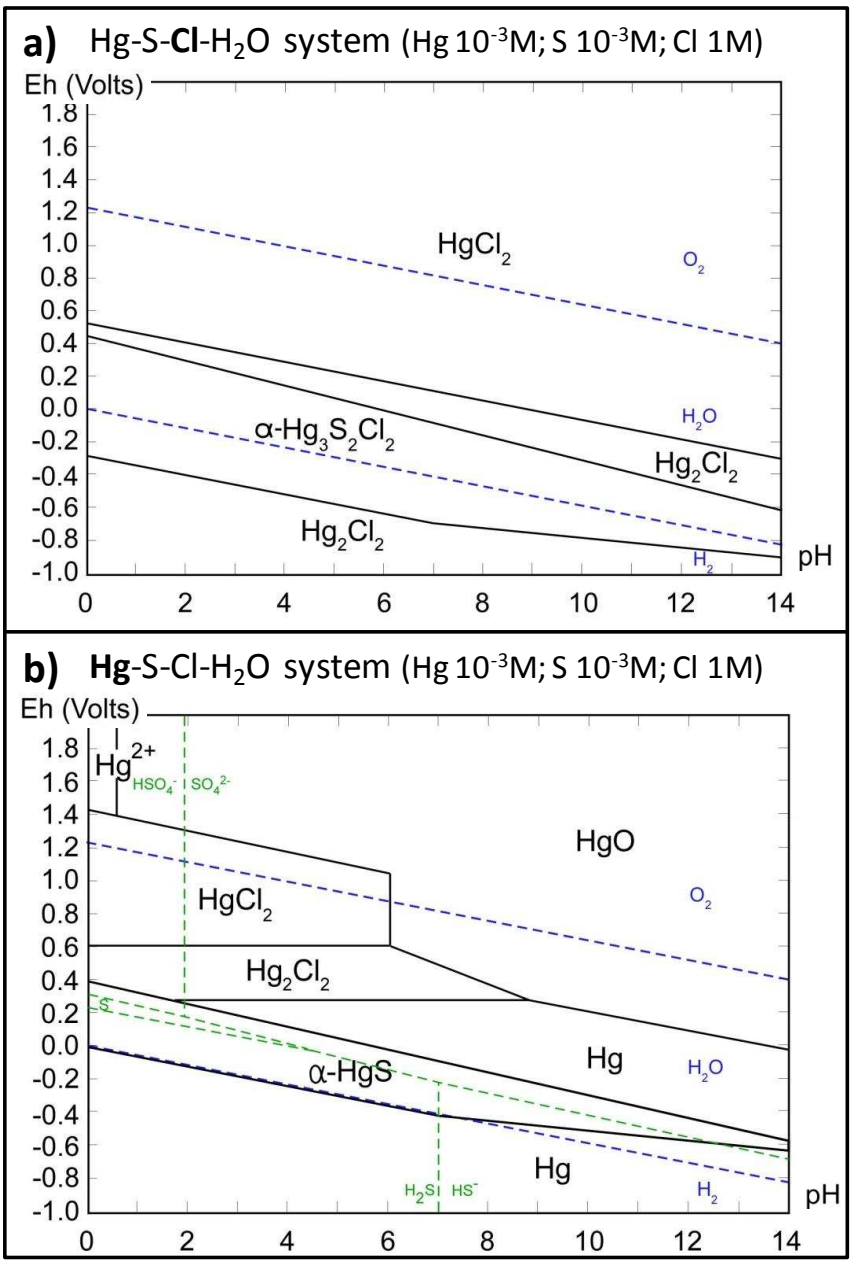

Figure 4.9.: *Potential-pH diagrams at 25°C for the Hg-S-Cl-H_2O system with in bold predominant species and in brackets activities of corresponding elements (free energy formation of corderoite α-$Hg_3S_2Cl_2$ taken from [Paquette et al., 1995]).*

These Eh-pH diagrams did not take into account the presence of kenhsuite (γ-$Hg_3S_2Cl_2$) and of β-$Hg_3S_2Cl_2$ because these phases were only identified once on artificially aged samples up to now while also the thermodynamic data are missing for these phases. We therefore implicitely assume that these phases react and are formed in a similar manner and under similar conditions as corderoite.

Considering the phases present in the ageing vessels during alteration of α-HgS with an aqueous NaOCl solution, the degradation compounds formed (Hg_2Cl_2 and $Hg_3S_2Cl_2$) and the hypothetic formation of sulfates, the following equilibria are proposed:

$$9\ HgS_{(s)} + 8\ ClO_{(g)} + 8\ OH^- \leftrightarrows 3\ Hg_3S_2Cl_{2(s)} + 2\ Cl^- + 3\ SO_4^{2-} + 4\ H_2O \quad (1)$$

$$6\ HgS_{(s)} + 14\ ClO_{(g)} + 20\ OH^- \leftrightarrows 3\ Hg_2Cl_{2(s)} + 8\ Cl^- + 6\ SO_4^{2-} + 10\ H_2O \quad (2)$$

As seen during artificial ageing experiments, NaOCl ageing combined with exposure to light always induces the formation of sulfates on the surface of the model samples. These compounds were not specifically identified, but are present in much higher concentration when the model sample was constituted by α-HgS even in case the closed system of ageing was used (see p.125, Section 3.3.1). This suggests that the sulfur that is forming the sulfates in these cases, instead of coming from the atmosphere, originates from the mercury sulfide. When the two-layered $CaCO_3$/α-HgS model samples were aged with NaOCl and light, gypsum ($CaSO_4.2H_2O$) was specifically identified by XRD (see p.147, Section 3.3.4). An ageing experiment using HgS with a modified S-isotopic composition, followed by isotopic analysis of the sulfate layer could definitively answer the questions of the origin of the sulfur in the formation of gypsum on cinnabar paintings but was not performed.

Evolution of the system during artificial ageing experiments

From our first experiments, the simultaneous presence of both calomel and corderoite in two superimposed layers on original altered works of art led us to two hypotheses concerned with their formation:

1- Either they are formed in parallel, or

2- a sequential, multi-step process of formation takes place: α-HgS $\leftrightarrows$ α-$Hg_3S_2Cl_2$ $\leftrightarrows$ Hg_2Cl_2

When artificial ageing was performed on natural cinnabar, calomel (Hg_2Cl_2) was the first degradation compound to be detected, and corderoite (α-$Hg_3S_2Cl_2$) was identified after a few days, whereas for synthetic vermilion both compounds were detected at the same

time. This difference between natural and synthetic samples is not understood yet. As seen in Table 3.3. (p.139, Section 3.3.1), in some cases during artificial ageing of synthetic vermilion, only one of the two compounds calomel and corderoite remained after some time of ageing: calomel was the most frequent when ageing in a cyclic system was performed. When the tube is opened, the atmosphere of the tube is equilibrated with the ambient atmosphere, decreasing the chlorine concentration in the tube. In such a system, it is possible that chlorine is not the predominant species. According to the diagram in Figure 4.9b, corderoite cannot be stable in these conditions, which would explain why it is no longer detected after some time of ageing.

Via the HSC Chemistry 7.0 software, the reaction between α-HgS and $ClO_{(g)}$ at 25°C and the equilibrium between these starting products and corderoite on the one hand and calomel on the other hand, could be studied (Figure 4.10a), involving the reactions:

$$9\ HgS_{(s)} + 8\ ClO_{(g)} + 8\ OH^- \leftrightarrows 3\ Hg_3S_2Cl_{2(s)} + 2\ Cl^- + 3\ SO_4^{2-} + 4\ H_2O\ (1)$$

$$6\ Hg_3S_2Cl_{2(s)} + 26\ ClO_{(g)} + 44\ OH^- \leftrightarrows 9\ Hg_2Cl_{2(s)} + 20\ Cl^- + 12\ SO_4^{2-} + 22\ H_2O\ (3)$$

with $\Delta_rG^0(1)$ = -838 kcal.mol^{-1} and $\Delta_rG^0(3)$ = -2593 kcal.mol^{-1} (free energies of reaction calculated via the HSC Chemistry 7.0 software). The negative values indicate that both reactions are thermodynamically possible.

In its initial state, the system only contains a limited quantity of α-HgS (arbitrarily chosen at 0.03 kmol). Small quantities (0.2 mol) of $ClO_{(g)}$ are added, and the composition of the system is followed as a function of increasing $ClO_{(g)}$ concentration or amount added. Corderoite (α-$Hg_3S_2Cl_2$) is then observed to be the first compound formed from the reaction of $ClO_{(g)}$ with α-HgS. After the amount of $ClO_{(g)}$ added to the α-HgS system exceeds a threshold value, the concentration of α-$Hg_3S_2Cl_2$ begins to decrease while that of calomel (Hg_2Cl_2) starts to rise. Thus, when $ClO_{(g)}$ is added in excess compared to the initial quantity of α-HgS, all of this last compound becomes transformed in α-$Hg_3S_2Cl_2$ and Hg_2Cl_2, the first one being in lower proportion. For even higher $ClO_{(g)}$ concentrations, the equilibrium completely shifts towards Hg_2Cl_2 (see Figure 4.10a).

A second diagram was calculated, showing the stability of each compound as a function of the fugacity of $S_{2(g)}$ and $ClO_{(g)}$ (Figure 4.10b). At the beginning of the degradation process of red mercury sulfide, the system is situated in the stability domain of α-HgS. Then when via the NaOCl solution, $ClO_{(g)}$ is added to the system, the transformation of α-HgS to α-$Hg_3S_2Cl_2$ is started. Consistent with what is shown in Figure 4.10a, when the activity of $ClO_{(g)}$ is sufficiently high, corderoite in its turn may be transformed into $HgCl_2$. However, this was not observed during our artificial ageing experiments. A noteworthy observation from this diagram is that by simply changing the activity of $S_{2(g)}$ or of $ClO_{(g)}$ it is not possible to form Hg_2Cl_2 directly from α-HgS, α-$Hg_3S_2Cl_2$ will always be the intermediate product.

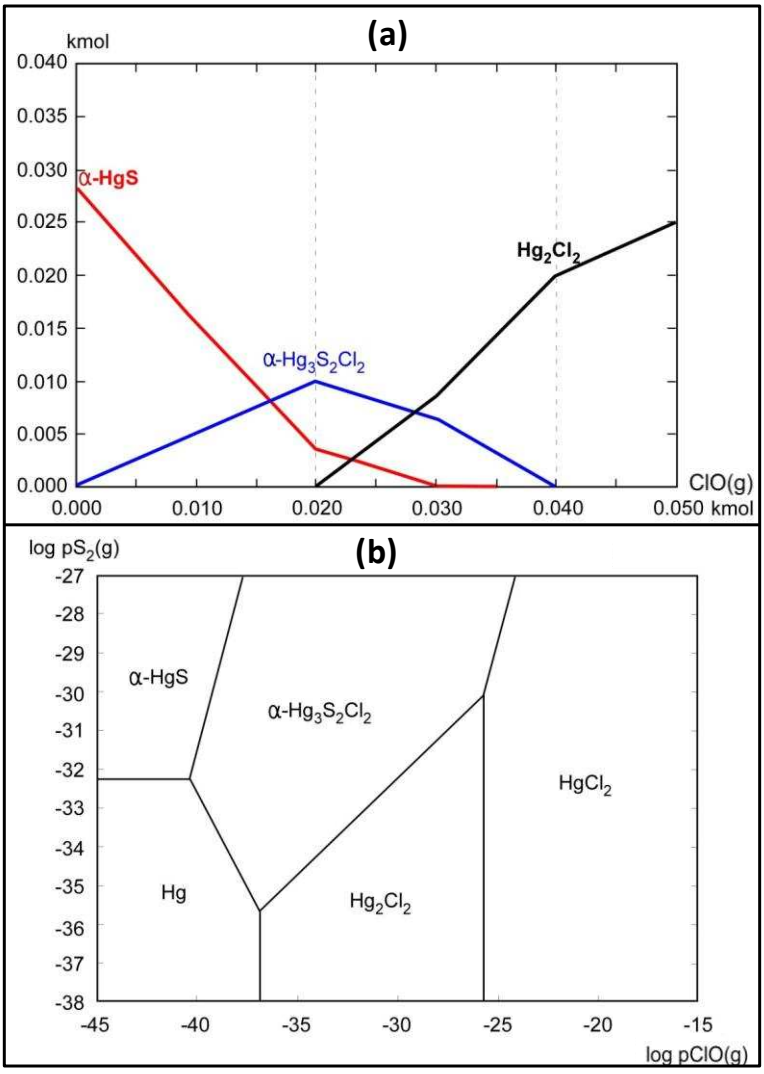

Figure 4.10.: a) *Thermodynamic simulation of reactions occurring during artificial ageing experiments when adding $ClO_{(g)}$ to α-$HgS_{(s)}$ at 25°C;* ***b)*** *Diagram of Hg-S-Cl phases stability vs. the fugacities of $S_{2(g)}$ and $ClO_{(g)}$ at 25°C.*

From the study of the Hg-S-Cl-H_2O system, it can be concluded that corderoite (α-$Hg_3S_2Cl_2$) and calomel (Hg_2Cl_2) can be formed from the reactions of α-HgS with $ClO_{(g)}$. Corderoite needs chlorine to be always available as a reagent to be stable. Both compounds can be formed at basic pH, which is consistent with their formation in the presence of NaOCl solution (pH 12) during artificial ageing experiments. In the cases of the cyclic system, the potential is higher than for the closed system and chlorine is not the predominant species, which could explain the disappeance of corderoite after some time of ageing in this system. Moreover, when α-HgS is in the presence of chlorine predominant, it cannot be stable and transforms into corderoite for low quantities of $ClO_{(g)}$ and calomel for higher quantities. It appears also that corderoite is an intermediate products in the reaction of formation of calomel from α-HgS.

These Pourbaix diagrams and simulations obtained from thermodynamics calculation appear to be consistent with the evolution of the composition of α-HgS pellets during ageing by exposure to light and NaOCl solution.

Conclusions and perspectives

The main objective of this investigation was to confirm preliminary hypotheses regarding the factors influencing the alteration of red mercury sulfide in order to understand better the conditions and gain more insights into the mechanism(s) involved in the degradation of this pigment. To achieve this goal, several samples from original works of art showing red mercury sulfide degradation were studied. After identifying the degradation compounds present in these altered paintings, artificial ageing experiments were performed in order to assess the effects of light and of different chemical treatments on α-HgS model samples. Thermodynamical calculations allowed discussing the formation and evolution of the different compounds in the considered system during ageing.

Among all the methods used, the laboratory instruments offered the opportunity to investigate different sample types, originating from works of art or model preparations. Elemental analytical techniques showed in particular the presence of chlorine in degraded samples, and structural methods allowed to identify some of the phases present. The high resolution and sensitivity of synchrotron radiation based methods of analysis allowed studying the micrometer-sized alteration layers in complex structures. In this context, it was possible to perform high resolution imaging of cross-sections prepared from original samples and observe the co-localized or multi-layered distribution of the different alteration products. Despite the high resolution offered by the synchrotron radiation source, some phases present in degraded samples could not be identified.

Polymorphous phases of $Hg_3S_2Cl_2$ were found in samples originating from degraded works of art. For the first time, the rare mineral kenhsuite (γ-$Hg_3S_2Cl_2$) was identified. It was found to be present by itself, or as a mixture with its more stable form corderoite (α-$Hg_3S_2Cl_2$). The third form, β-$Hg_3S_2Cl_2$, was also found, both in micro-samples of original works of art as well as in some of the artificially aged model samples. In all cases examined, the presence of calomel (Hg_2Cl_2) was identified. Contrary to the

classical hypothesis, no black metacinnabar (β-HgS) was found in any of the examined altered works of art. On the surface of the degraded paint samples, invariably sulfates were encountered in great abundance; on some of the works of art these were identified as being gypsum ($CaSO_4.2H_2O$) and anhydrite ($CaSO_4$).

Alteration of red mercury sulfide could be reproduced during artificial ageing experiments, where photo-activation proved itself to be a mandatoray parameter in order to obtain visual and chemical changes. During these experiments, chlorine was also needed to form the Hg- and Cl-containing compound calomel (Hg_2Cl_2) and the Hg-, S- and Cl-containing mineral corderoite (α-$Hg_3S_2Cl_2$) and related compounds. These compounds were formed and identified on model samples aged with aqueous sodium hypochlorite (NaOCl) solution while exposed to light and appeared to be formed simultaneously. However, ageing experiments with other chlorinated solutions (NaCl, CCl_4, etc.) did not induce the formation of calomel or corderoite. Thus, the type and activity of chlorine is playing a role in the process of degradation of red mercury sulfide. The visual aspect of the samples showed an evolution suggesting that different transformations took place: first, the formation of crystals (different among various model samples, small or large, white or translucent, homogeneously scattered or not) that gave the sample a purple color, then, the formation of a thick and homogeneous white-grey layer. As with original paint samples, the presence of sulfates on the surface of the degraded model samples was observed; these were identified as being gypsum when calcium ions were present in the model samples, e.g. due to the presence of calcite ($CaCO_3$).

The Pourbaix diagrams drawn for the Hg-S-Cl-H_2O system showed that, contrarily to what was found in previous studies, when chlorine is considered to be in excess in the system, corderoite (α-$Hg_3S_2Cl_2$) and calomel (Hg_2Cl_2) can be formed at basic pH. Moreover, in the same conditions α-HgS cannot be present; α-HgS can remain stable when mercury is considered to be always available as a reagent. Calomel can be formed in both conditions (chlorine or mercury predominant in the system). According to these diagrams, $HgCl_2$ can also be formed when the activity of Cl is higher than the one required to form Hg_2Cl_2, even if it was not identified during the present study. Nevertheless, the presence of this compound cannot be excluded.

Some questions are still unsolved. One of them concerns the understanding of the origin of the dark color of some degraded works of art (such as one of the Pompeian sample Po-B). Indeed all HgS-related degradation compounds obtained by artificial ageing and identified via one of the analytical methods employed, present a white, light grey or light purple colour. When degradation of red mercury sulfide in works of art caused it to darken, the contribution of none of these identified phases can explain this dark aspect in a satisfactory manner. In follow-up research, different hypotheses may be considered, following two main ideas. Either the dark color is caused by:

- one or more of the identified compounds (with the dark color e.g. caused by the combined absorption in the visual range of red HgS and one or more degradation compounds) or

- one or more non-detected compounds (such as metallic mercury).

Next to light exposure, the presence of chlorine was shown to be an important parameter in the degradation of red mercury sulfide present in works of art. However, the sources of this element are still unidentified: the ambient atmosphere, the painting materials (binder, varnish, etc.) or added products? One of the favored hypotheses in this respect is that chlorine was originally present within the material comprising the works of art. In particular, this can be the case for the oils and resins used as a binding medium or varnish. In order to validate this hypothesis, the analysis of organic materials used for works of art in order to determine the amount of chlorine they contain will therefore be relevant.

In order to critically assess previous studies in the literature in which different kinetics of photo-induced degradation of cinnabar were observed depending on its origin, natural α-HgS ores can be analyzed to determine the (trace) elements they contain. In this context, XRF analyses were already performed on some single crystals of α-HgS from different origins; significant differences were observed in their trace elements pattern. Such an investigation could contribute to a better understanding of the influence of some elements on the stability of α-HgS ores, and more in particular the fact that cinnabar, used in works of art originating from South-America or China for example, appear to show less alteration than the ones from Europe. Such a study could also be deepened by including S-isotopic analyses in the investigation. Next to investigations concerning the degradation of red mercury sulfide, this aspect of cinnabar related research could help establishing a link

between the trace constituents present and the geographical location of cinnabar deposits in order to better understand trade routes for this pigment.

Furthermore, analytical techniques are being improved to be used with precious samples coming from original works of art or directly *in-situ* on cultural heritage objects. In the XAS context, the implementation of the "full-field" method is already showing great promise: it consists of recording a radiography of an entire sample at each energy composing the XAS spectrum at the edge of interest at many sample locations in parallel *[V. De Andrade, 2011]*. This technique allows performing full 2D measurements in a reasonable total acquisition time. Since spectral information is recorded from the entire sample and not just from a few points, as it was the case for XANES analyses performed during this research, more representative information is obtained. "Full-field" measurements were recently performed at BM23 and ID21 (ESRF) on model and historic samples and showed the great possibilities offered by this method.

The contribution of this research to the cultural heritage field is important from two points of view. On the one hand, from a chemical point of view, it is relevant to better understand the different reactions governing the degradation of mercury sulfide; on the other hand, from a conservation point of view, these insights could help restorers and curators to deal with the preservation of works of art that comprise the α-HgS pigment.

On the basis of the results collected and the insights gained in this study, a general advice to musea is to protect cultural heritage artifacts by isolating them from chlorine sources (such as cleaning products, some organic binders or resins, the general atmosphere in marine areas, etc.). For some years, the growing awareness of musea makes them taking some measures concerning harmful compounds; however, measurements of chlorine in the atmosphere of musea are still rare and the presence of chlorine in oils or resins used in paintings is rarely indicated by suppliers. With respect to the wisdom of removing the thin altered part that may have formed on the surface of red mercury sulfide paint layers, the most cautious behavior would be to leave these alteration layer untouched, hoping that in the (near) future a process will be developed to succeed in keeping α-HgS from being degraded.

Bibliography

ARBIZZANI R., CASALLATO U., FIORIN E., NODARI L., RUSSO U. and VIGATO P.A., "Decay markers for the preventative conservation and maintenance of paintings", *Journal of Cultural Heritage*, **5**, p.167-182 (2004).

AURISICCHIO C., FERRO D., MARTINELLI G., CESARO S.N. and RAPINESI I.A., "A study of a distaff of the second century A.D. from a necropolis of Boccone D'Aste (Roma, Italy) – tomb 75", *Journal of Cultural Heritage*, **3**, p.107-116 (2002).

AZE S., "Chromatic alterations of lead-containing pigments in artworks – Experimental study of the alterations observed on mural paintings", *PhD thesis, Géosciences, Aix-Marseille, Université de Droit, d'Economie et des Sciences*, p.208 (2005).

BACCI M., PICOLLO M., PORCINAI S. and RADICATI B., "Evaluation of the museum envorinmental risk by means of tempera-painted dosimeters", *Thermochimica Acta*, **365**, p.25-34 (2000).

BARALDI P., BARALDI C., CURINA R., TASSI L. and ZANNINI P., "A micro-Raman archaeometric approach to Roman wall paintings", *Vibrational Spectroscopy*, **43**, p.420-426 (2007).

BARBET A., "L'emploi des couleurs dans la peinture murale romaine antique, « marqueurs » chronologiques et révélateurs du « standing » social?", *Pigments et Colorants, Editions du CNRS*, p.255-271 (1990).

BELLOT-GURLET L., POUPEAU G., SALOMON J., CALLIGARO T., MOIGNARD B., DRAN J.C., BARRAT J.A. and PICHON L., "Obsidian provenance studies in archaeology: a comparison between PIXE, ICP-AES and ICP-MS", *Nuclear Instruments and Methods in Physics Research B*, **240**, p.583-588 (2005).

BERGEON S., "Science et patience ou la restauration des peintures", *RMN*, p.17 (1990).

BERGEON S. and CURIE P., "Peinture & Dessin, Vocabulaire typologique et technique", **vol. 2**, *Editions du Patrimoine Centre des Monuments Nationaux*, p.942 (2009).

BLUM J.D. and BERGQUIST B.A., "Reporting variations in the natural isotopic composition of mercury", *Analytical and Bioanalytical Chemistry*, **388**, p.353-359 (2007).

BOCTOR N.Z., SHIEH Y.N. and KULLERUD G., “Mercury ores from the New Idria Mining District, California: Geochemical and stable isotope studies”, *Geochimica et Cosmochimica*, **51**, p.1705-1715 (1987).

BORISOV S.V., MAGARILL S.A and PERVUKHINA N.V., “Module principle in structure formation studies of mercury oxo and chalcogen halides”, *Journal of Structural Chemistry*, **42**, p.429-435 (2001).

BOYLE R.W. and JONASSON I.R., “The geochemistry of antimony and its use as an indicator element in geochemical prospecting”, *Journal of Geochemical Exploration*, **20**, p.223-302 (1984).

BRANDON N.P., FRANCIS P.A., JEFFREY J., KELSALL G.H. and YIN Q., “Thermodynamics and electrochemical behavior of Hg-S-Cl-H_2O systems”, *Journal of Electroanalytical Chemistry*, **497**, p.18-32 (2001).

BRECOULAKI H., “Sur la technè de la peinture grecque ancienne d’après les monuments funéraires de Macédoine”, *Bulletin de correspondance hellénique*, **124**, p.189-216 (2000).

CARLSON E.H., “The growth of HgS and Hg3S2Cl2 single crystals by a vapor phase method”, *Journal of Crystal Growth*, **1**, p.271-277 (1967).

CASADIO F., FIEDLER I., GRAY K.A. and WARTA R., “Deterioration of zinc potassium chromate pigments: elucidating the effects of paint composition and environmental conditions on chromatic alteration”, *ICOM Committee for Conservation*, **2**, p.572-580 (2008).

CERSOY S., RICHARDIN P., WALTER P. and BRUNELLE A., “Cluster TOF-SIMS imaging of human skin remains: analysis of a South-Andean mummy sample”, *Journal of Mass Spectrometry*, **47**, p.338-346 (2012).

CHAPPE M., HILDENHAGEN J., DICKMANN K. and BREDOL M., “Laser irradiation of medieval pigments at IR, VIS and UV wavelengths”, *Journal of Cultural Heritage*, **4**, p.264-270 (2003).

CLEMENTI C., CIOCAN V., VAGNINI M., DOHERTY B., TABASSO M.L., CONTI C., BRUNETTI B.G. and MILIANI C., “Non-invasive and micro-destructive investigation of the Domus Aurea wall painting decorations”, *Analytical and Bioanalytical Chemistry*, **401**, p.1815-1826 (2011).

COHEN N.S., ODLYHA M., CAMPANA R. and FOSTER G.M., “Dosimetry of paintings; determination of the degree of chemical change in museum exposed test paintings (lead

white tempera) by thermal analysis and infrared spectroscopy", *Thermochimica Acta*, **365**, p.45-52 (2000).

COOPER M.I., FOWLES P.S. and TANG C.C., "Analysis of the laser-induced discoloration of lead white pigment", *Applied Surface Science*, **201**, p.75-84 (2002).

COTTE M., SUSINI J., METRICH N., MOSCATO A., GRATZIU C., BERTAGNINI A. and PAGANO M., "Blackening of pompeian cinnabar paintings: X-ray microspectroscopy analysis", *Analytical Chemistry*, **78**, p.7484–7492 (2006).

COTTE M., SUSINI J., SOLE V.A., TANIGUCHI Y., CHILLIDA J., CHECROUN E. and WALTER P., "Applications of synchrotron-based micro-imaging techniques to the chemical analysis of ancient paintings", *Journal of Analytical Atomic Spectrometry*, **23**, p.820-828 (2008).

COTTE M. and SUSINI J., "Watching ancient paintings through synchrotron-based X-ray microscopes", *Interfaces MRS Bulletin*, **34**, p.403-405 (2009).

CURRIE C. and ALLART D., "The Brueg(H)el phenomenon. Paintings by Pieter Bruegel the Elder and Pieter Bruegel the Younger, with a special focus on techniques and copying practices", *Scientia Artis*, 8, p.685 (2012)

DA PIEVE F., HOGAN C., LAMOEN D., VERBEECK J., JANSSENS K., RADEPONT M., GONZE X. and VAN TENDELOO G., "Casting light on the darkening of colours in historical paintings", *Analyst* (Submitted 2012).

DAVIDSON R.S. and WILLSHER C.J., "The light-induced blackening of red mercury (II) sulphide", *Dalton*, p.833–835 (1981).

DE ANDRADE V., SUSINI J., SALOME M., BERALDIN O., RIGAULT C., HEYMES T., LEWIN E. and VIDAL O., "Submicrometer hyperspectral X-ray imaging of heterogeneous rocks and geomaterials: applications at the Fe K-edge", *Analytical Chemistry*, **83**, p.4220-4227 (2011).

DE NOLF W., DIK J., VAN DER SNICKT G., WALLERT A. and JANSSENS K., "High energy X-ray powder diffraction for the imaging of (hidden) paintings", *Journal of Analytical Atomic Spectrometry*, **26**, p.910-916 (2011).

DEVEZEAUX DE LAVERGNE E., DIARTE O. and VAN HUONG P., "Caractérisation de pigments picturaux d'une enluminure médiévale par microspectrométrie Raman", *Pigments et Colorants, Editions du CNRS*, p.143-152 (1990).

DICKSON F.W. and TUNELL G., "The stability relations of cinnabar and metacinnabar", *The American Mineralogist*, **44**, p.471-487 (1959).

DOMENECH-CARBO M.T., KUCKOVA S., DE LA CRUZ-CANIZARES J. and OSETE-CORTINA L., "Study of the influencing effect of pigments on the photoageing of terpenoid resins used as pictorial media", *Journal of Chromatography A*, **1121**, p.248-258 (2006).

DRAN J.C., SALOMON J., CALLIGARO T. and WALTER P., "Ion beam analysis of artworks: 14 years of use in the Louvre", *Nuclear Instruments and Methods in Physics Reasearch B*, **219-220**, p.7-15 (2004).

DREYER R.M., "Darkening of cinnabar in sunlight", *Notes and News* (1939).

DURAN A., CASTAING J. and WALTER P., "X-ray diffraction studies of Pompeian wall paintings using synchrotron radiation and dedicated laboratory made systems", *Applied Physics A*, **99**, p.333–340 (2010).

DUROVIC S, "The crystal structure of γ-$Hg_3S_2Cl_2$", *Acta Crystallographica Section B*, **24**, p.1661-1670 (1968).

ESBRI J.M., BERNAUS A., AVILA M., KOCMAN D., GARCIA-NOGUERO E.M., GUERRERO B., GAONA X., ALVAREZ R., PEREZ-GONZALEZ G., VALIENTE M., HIGUERAS P., HORVAT M. and LOREDO J., "XANES speciation of mercury in three mining districts – Almaden, Asturias (Spain), Idria (Slovenia)", *Journal of Synchrotron Radiation*, **17**, p.179-186 (2010).

EZRATI J.J., "Théorie, technique et technologie de l'éclairage muséographique", *Editions AS*, p.117 (2002).

FELDER-CASAGRANDE S. and ODLYHA M., "Development of standard paint films based on artists' materials", *Journal of Thermal Analysis*, **49**, p.1585-1591 (1997).

FERRO D., PIACENTE V. and SCARDALA P., "Vaporization enthalpies of black and red mercury sulphides and their heat of transition from vapour pressure measurements", *Journal of the Less-Common Metals*, **147**, p.1-8 (1989).

FOORD E.E. and BERENDSEN P., “Corderoite, first natural occurrence of α-$Hg_3S_2Cl_2$, from the Cordero mercury deposit, Humboldt County, Nevada”, *The American Mineralogist*, **59**, 652-655 (1974).

FUCHS R., “New non-destructive FTIR spectroscopic investigations on work of art”, *Art* (2002).

GETTENS R.J., FELLER R.L. and CHASE W.T., “Identification of the materials in paintings”, Chapter 7: “Vermilion and Cinnabar”, *Studies in Conservation*, **17**, p.45–69 (1972).

GETTENS R.J., FELLER R.L. and CHASE W.T., “Vermilion and Cinnabar”, *Artists’ Pigments*, **2**, p.159–182 (1993).

GROUT R. and BURNSTOCK A., “A study of the blackening of vermilion”, *Zeitschrift*, p.15-22 (2000).

GUSTIN M.S., BIESTER H. and KIM C.S., “Investigation of the light-enhanced emission of mercury from naturally enriched substrates”, *Atmospheric Environment*, **36**, p.3241-3254 (2002).

HUGGINS F.E. and HUFFMAN G.P., “Chlorine in coal: an XAFS spectroscopic investigation”, *Fuel*, **74**, p.556-569 (1995).

ISTUDOR I., DINA A., ROSU G., SECLAMAN D. and NICULESCU G., “An alteration phenomenon of cinnabar red pigment in mural paintings from Sucevita”, *e_conservation*, **2**, p.24-33 (2007).

JOHNSTON D.A., “Volcanis contribution of chlorine to the stratosphere: more significant to ozone than previously estimated?”, *Science,* **209**, p.491-493 (1980).

KENNEDY D., “X-ray diffraction studies of ancient hairs”, *Cosmetics & Toiletries*, **96**, p.121-122 (1981).

KEUNE K. and BOON J.J.,” Analytical imaging studies clarifying the process of the darkening of vermilion in paintings”, *Analytical Chemistry*, **77**, p.4742-4750 (2005).

KIM C.S., BROWN Jr G.E. and RYTUBA J.J., "Characterization and speciation of mercury-bearing mine wastes using X-ray absorption spectroscopy", *The Science of the Total Environment*, **261**, p.157-168 (2000).

KIM C.S., BLOOM N.S., RYTUBA J.J. and BROWN Jr G.E., "Mercury speciation by X-ray absorption fine structure spectroscopy and sequential chemical extractions: a comparison of speciation methods", *Environmental Science and Technology*, **37**, p. 5102-5108 (2003).

LAVRIC J.V. and SPANGENBERG J.E., "Stable isotope (C, O, S) systematic of the mercury mineralization at Idrija, Slovenia: constraints on fluid source and alteration processes", *Mineralium Deposita*, **38**, p.886-899 (2003).

LE FUR D., "Les pigments dans la peinture égyptienne", *Pigments et Colorants, Editions du CNRS*, p.181-188 (1990).

LICHTMAN D., CRAIG J.H., SAILER V. and DRINKWINE M., "AES and XPS spectra of sulfur in sulfur compounds", *Applications of Surface Science*, **7**, p.325-331 (1981).

LIU J., SHI J.Z., YU L.M., GOYER R.A. and WAALKES M.P., "Mercury in traditional medicines: Is cinnabar toxicologically similar to common mercurials?", *Experimental Biology Medicine*, **233**, p.810-817 (2008).

LU Y.F., WU Q., LIANG S.X., MIAO J.W., SHI J.S. and LIU J., "Evaluation of hepatotoxicity potential of cinnabar-containing *An-Gong-Niu-Huang Wan*, a patent traditional Chinese medicine", *Regulatory Toxicology and Pharmacology*, **60**, p.206-211 (2011).

MAGUREGUI M., KNUUTINEN U., CASTRO K. and MADARIAGA J.M., "Raman spectroscopy as a tool to diagnose the impacts and conservation state of Pompeian 2nd and 4th style wall paintings (House of Marcus Lucretius) exposed to divers environments", *Book of Abstracts: RAA2009*, 5th International Conference on the application of Raman spectroscopy in Art and Archaeology, Bilbao (14-18 September 2009).

MARENGO E., LIPAROTA M.C., ROBOTTI E. and BOBBA M., "Monitoring of paintings under exposure to UV light by ATR-FT-IR spectroscopy and multivariate control charts", *Vibrational Spectroscopy*, **40**, p.225-234 (2006).

MARTIN-GIL F., MARTIN-GIL F.J., DELIBES-DE-CASTRO G., ZAPATERO-MAGDALENO P. and SARABIA-HERRERO F.J., "The first known use of vermillion", *Experientia*, **51**, p.759-761 (1995).

McCORMACK J.K. and DICKSON F.W., “Kenhsuite, γ-$Hg_3S_2Cl_2$, a new mineral species from the McDermitt mercury deposit, Humboldt County, Nevada”, *The Canadian Mineralogist*, **36**, p.201-206 (1998).

McCORMACK J.K., “The darkening of cinnabar in sunlight”, *Mineralium Deposita*, **35**, p.796-798 (2000).

MINAMI T., IMAI A., BUNNO M., KAWAKAMI K. and IMAZU S., “Short contribution: using sulfur isotopes to determine the sources of vermilion in ancient burial mounds in Japan”, *Geoarchaeology*, **20**, p.79-84 (2005).

MOHEN J.P., MENU M. and MOTTIN B., “Au coeur de la Joconde : Léonard de Vinci décodé”, *Gallimard Musée du Louvre Editions*, p.25 (2006).

MONICO L.,VAN DER SNICKT G., JANSSENS K., DE NOLF W., MILIANI C., VERBEECK J., TIAN H., TAN H., DIK J., RADEPONT M. and COTTE M., "Degradation Process of Lead Chromate in Paintings by Vincent van Gogh Studied by Means of Synchrotron X-ray Spectromicroscopy and Related Methods. 1. Artificially Aged Model Samples", *Analytical Chemistry*, **83**, p.1214-1223 (2011).

MONICO L., VAN DER SNICKT G., JANSSENS K., DE NOLF W., MILIANI C., DIK J., RADEPONT M., HENDRIKS E., GELDOF M. and COTTE M., "Degradation Process of Lead Chromate in Paintings by Vincent van Gogh Studied by Means of Synchrotron X-ray Spectromicroscopy and Related Methods. 2. Original Paint Layer Samples", *Analytical Chemistry*, **83**, p.1224-1231 (2011).

OKITA T., KANEDA K., YANAKA T. and SUGAI R., “Determination of gaseous and particulate chloride and fluoride in the atmosphere”, *Atmospheric Environment*, **8**, p.927-936 (1974).

PAL B., IKEDA S. and OHTANI B., “Photoinduced chemical reactions on natural single crystals and synthesized crystallites of mercury(II) sulfide in aqueous solution containing naturally occurring amino acids”, *Inorganic Chemistry*, **42**, p.1518-1524 (2003).

PAOLINI C. and FALDI M., “Glossario delle techniche artistiche e del restauro”, *Edizioni Palazzo Spinelli*, p.307 (2000).

PAQUETTE K. and HELZ G., “Solubility of cinnabar (red HgS) and implications for mercury speciation in sulfidic waters”, *Water, Air, and Soil Pollution*, **80**, p.1053-1056 (1995).

PARKS G.A. and NORDSTROM D.K., “Estimated free energies of formation, water solubilities, and stability fields for schuetteite ($Hg_3O_2SO_4$) and corderoite ($Hg_3S_2Cl_2$) at 298 K”, *Chemical Modeling in Aqueous Systems*, **93**, p.339-352 (1979).

PATEL B.K., RATH S., SARANGI S.N. and SAHU S.N., “HgS nanoparticles: structure and optical properties”, *Applied Physics A*, **86**, p.447-450 (2007).

PATRIARCHE G., WALTER P., VAN ELSLANDE E., AYACHE J., CASTAING J., “Characteristics of HgS nanoparticles formed in hair by a chemical reaction”, *Philosophical Magazine*, DOI:10.1080/14786435.2012.674225 (2012).

PEREZ-ALONSO M., CASTRO K., ALVAREZ M. and MADARIAGA J.M., “Scientific analysis versus restorer’s expertise for diagnosis prior to a restoration process: the case of Santa Maria Church (Hermo, Asturias, North of Spain)”, *Analytica Chimica Acta*, **524**, p.379-389 (2004).

PEREZ-ALONSO M., CASTRO K. and MADARIAGA J.M., “Investigation of degradation mechanisms by portable Raman spectroscopy and thermodynamic speciation: The wall painting of Santa Maria de Lemoniz (Basque country, north of Spain)”, *Analytica Chimica Acta*, **571**, p.121-128 (2006).

PETERS M.J., McNEIL L.E. and DY K., “Resonant Raman scattering in trigonal HgS”, *Solid State Communications*, **97**, p.1095-1099 (1996).

PLINY THE ELDER, *Naturalis Historia*, **XXXIII** (ca. 77-79).

POTTER R.W. and BARNES H.L., “Phase relations in the binary Hg-S”, *American Mineralogist*, **63**, p.1143-1152 (1978).

POULI P., EMMONY D.C., MADDEN C.E. and SUTHERLAND I., “Studies towards a thorough understanding of the laser-induced discoloration mechanisms of medieval pigments”, *Journal of Cultural Heritage*, **4**, p.271-275 (2003).

PRIETZEL J., THIEME J., SALOME M. and KNICKER H., “Sulfur K-edge XANES spectroscopy reveals differences in sulfur speciation of bulk soils, humic acid, fulvic acid, and particle size seperates”, *Soil Biology and Biochemistry*, **39**, p.877-890 (2007).

RADEPONT M., DE NOLF W., JANSSENS K., VAN DER SNICKT G., KLAASSEN L. and COTTE M., “The use of microscopic X-ray diffraction for the study of HgS and its degradation products

corderoite (α-$Hg_3S_2Cl_2$), kenhsuite (γ-$Hg_3S_2Cl_2$) and calomel (Hg_2Cl_2) in historical paintings", *Journal of Analytical Atomic Spectrometry*, **26**, p.959-968 (2011).

ROPRET P., ZOUBEK R., SEVER SKAPIN A. and BUKOVEC P., "Effects of ageing on different binders for retouching and on some binder-pigment combinations used for restoration of wall paintings", *Materials Characterization*, **58**, p.1148-1159 (2007).

SALVADO N., BUTI S., NICHOLSON J., EMERICH H., LABRADOR A. and PRADELL T., "Identification of reaction compounds in micrometric layers from gothic paintings using combined SR-XRD and SR-FTIR", *Talanta*, **79**, p.419-428 (2009).

SALVADO N., BUTI S., LABRADOR A., CINQUE G., EMERICH H. and PRADELL T., "SR-XRD and SR-FTIR study of the alteration of silver foils in medieval paintings", *Analytical and Bioanalytical Chemistry*, **399**, p.3041-3052 (2010).

SAN MIGUEL A., POLIAN A. and ITIE J.P., "A variable coordination structure in II-VI semiconductors: the cinnabar phase", *Journal of Physics and Chemistry of Solids*, **56**, p.555-558 (1995).

SANTORO A., TERZANO R., BLO G., FIORE S., MANGOLD S. and RUGGIERO P., "Mercury speciation in the colloidal fraction of a soil polluted by chlor-alkali plant: a case study in the South of Italy", *Journal of Synchrotron Radiation*, **17**, p.187-192 (2010).

SARRAZIN J. and VERDAGUER M., "L'oxydoréduction, Concepts et expériences", Editions Ellipses, p.95-97, p.250 (1991).

SAUPE F. and ARNOLD M., "Sulphur isotope geochemistry of the ores and country rocks at the Almaden mercury deposit, Ciudad Real, Spain", *Geochimica et Cosmochimica*, **56**, p.3765-3780 (1992).

SEVES A.M., SORA S., SCICOLONE G., TESTA G., BONFATTI A.M., ROSSI E. and SEVES A., "Effect of thermal accelerated ageing on the properties of model canvas paintings", *Journal of Cultural Heritage*, **1**, p.315-322 (2000).

SLOWEY A.J. and BROWN JR G.E., "Transformations of mercury, iron and sulfur during the reductive dissolution of iron oxyhydroxide by sulfide", *Goldschmidt conference abstracts*, **A596** (2006).

SOLE V.A., PAPILLON E., COTTE M., WALTER P. and SUSINI J., "A multiplatform code for the analysis of energy-dispersive X-ray fluorescence spectra", *Spectrochimica Acta Part B-Atomic Spectroscopy*, **62**, p.63-68 (2007).

SOMOGYI A., DRAKOPOULOS M., VINCZE L., VEKEMANS B., CAMERANI C., JANSSENS, K., SNIGIREV A. and ADAMS F., "ID18F: a new micro-X-ray fluorescence end-station at the European Synchrotron Radiation Facility (ESRF): preliminary results", *X-Ray Spectrometry*, **30**, p.242-252 (2001).

SOUIL F., "Expériences de Chimie, Agrégation de Sciences Physiques – Compléments de Chimie Inorganique, 20 montages décrits et commentés", *Bréal*, p.85-94 (1997).

SPANGENBERG J.E., LAVRIC J.V., MEISSER N. and SERNEELS V., "Sulfur isotope analysis of cinnabar from Raman wall paintings by elemental analysis/isotope ratio mass spectrometry – tracking the origin of archaeological red pigments and their authenticity", *Rapid Communications in Mass Spectrometry*, **24**, p.2812-2816 (2010).

SPRING M. and GROUT R., "The blackening of vermilion: an analytical study of the process in paintings", *National Gallery Technical Bulletin*, **23**, p.50-61 (2002).

SUSINI J., SALOME M., FAYARD B., ORTEGA R. and KAULICH B., "The scanning X-ray microprobe at the ESRF "X-ray microscopy" beamline", *Surface Review and Letters*, **9**, p.203-211 (2002).

SVENSSON M., DUKER A. and ALLARD B., "Formation of cinnabar – estimation of favourable conditions in a proposed Swedish repository", *Journal of Hazardous Materials*, **136**, p.830-836 (2006).

TAYLOR R.E., CARVEN C.T., LARSEN R.E., DMITRENKO O., BAI S. and DYBOWSKI C., "Revisiting $HgCl_2$: A solution- and solid-state ^{199}Hg NMR and ZORA-DFT computational study", *Journal of Molecular Structure*, **930**, p.99-109 (2009).

TERRAPON V. and BEARAT H., "A study of cinnabar blackening: new approach and treatment perspective" (2010).

TERZANO R., SANTORO A., SPAGNUOLO M., VEKEMANS B., MEDICI L., JANSSENS K., GOTTLICHER J., DENECKE M.A., MANGOLD S. and RUGGIERO P., "Solving mercury (Hg) speciation in soil samples by synchrotron X-ray microspectroscopic techniques", *Environmental Pollution*, **158**, p.2702-2709 (2010).

THOMSON G. “The museum environment”, *Butterworth-Heinemann Edition*, **2**, p.153 (1986).

VERDU J., “Vieillissement des plastiques”, Afnor Technique (1984).

VOROSHILOV Y.V., KHUDOLII V.A. and Pan’ko V.V., “Phase equilibria in the HgS-HgTe-$HgCl_2$ system and the crystal structure of β-$Hg_3S_2Cl_2$ and Hg_3TeCl_4”, *Russian Journal of Inorganic Chemistry*, **41**, p. 274-280 (1996).

WANG H. and ZHU J.J., “A sonochemical method for the selective synthesis of α-HgS and β-HgS nanoparticles”, *Ultrasonics Sonochemistry*, **11**, p.293-300 (2004).

YAMADA M., MINAMI T., YAMADA G., TOHNO Y., TOHNO S., IKEDA Y., TASHIRO T., KOHNO Y. and KAWAKAMI K., “Different element ratios of red cosmetic excavated from ancient burials of Japan”, *The Science of the Total Environment*, **199**, p.293-298 (1997).

ZENG J.H., YANG J. and QIAN Y.T., “A novel morphology controllable preparation method to HgS”, Materials Research Bulletin, **36**, p.343-348 (2001).

ZHOU X., ZENG K., QI W., YANG X. and WANG K., “In vitro studies on dissolves substance of cinnabar: chemical species and biological properties”, *Journal of Ethnopharmacology*, **131**, p.196-202 (2010).

Reports

C2RMF report n°3143, "*Prophète au phylactère*", ca. 1300, Anonymous (2003).

C2RMF report n°9684, "*Annonciation*", 15th century, Caporali (1968).

C2RMF report P3, "*Couronnement de la Vierge*", 15th century, Fra Angelico (1964).

C2RMF report P158, "*Retable de Thouzon*", 15th century, artist unknown (1963, 1971).

C2RMF report P248, "*Réunion dans un cabaret*", 17th century, Le Valentin (1968).

C2RMF report n°22484, "*Crucifix*", ca. 1315, Giotto di Bondone, (2011).

Web sites

http://cst-www.nrl.navy.mil

http://en.wikipedia.org/wiki/

http://fr.wikipedia.org/wiki/

http://hyperphysics.phy-astr.gsu.edu/hbase/tables/electpot.html

http://pymca.sourceforge.net

http://rruff.info/

http://webmineral.com

http://www.esrf.eu/computing/scientific/FIT2D

http://www.esrf.eu/UsersAndScience/Experiments/Imaging/ID21/php

http://www.hudong.com/wiki/

http://www.lasurface.com

http://www.mindat.org

http://xrdua.ua.ac.be

http://zebu.uoregon.edu/text/ozone

APPENDICES

Appendix A: Abbreviations list

AGLAE: Accélérateur Grand Louvre d'analyses élémentaires

BSE: Backscattered electrons

C2RMF: Centre de Recherche et de Restauration des Musées de France

CCD: Charged coupled device

CFC: Chlorofluorocarbons

CIE: Commission Internationale de l'Eclairage

EDX: Energy dispersive X-ray spectroscopy

ESRF: European Synchrotron Radiation Facility

EXAFS: Extended X-ray absorption fine structure

FTIR: Fourier transform infra-red spectroscopy

ICP-AES: Inductively coupled plasma atomic emission spectroscopy

ICP-MS: Inductively coupled plasma mass spectrometry

KIK-IRPA: Koninklijk Instituut voor het Kunstpatrimonium – Institut royal du Patrimoine artistique

KMSKA: Koninklijk museum voor schone kunsten Antwerpen (royal museum of fine arts Antwerp)

LADIR: Laboratoire de dynamique, interactions et réactivité

LA-ICP-MS: Laser ablation inductively coupled plasma mass spectrometry

LRS: Laboratoire de réactivité de surface

PIGE: Proton induced gamma-ray emission

PIXE: Proton induced X-ray emission

PSI: Paul Scherrer institute

SE: Secondary electrons

SEM: Scanning electron microscopy

SHE: Standard hydrogen electrode

SLS: Swiss lightsource

XANES: X-ray absorption near edge structure

XAS: X-ray absorption spectroscopy

XPS: X-ray photoelectron spectroscopy

XRD: X-ray diffraction

XRF: X-ray fluorescence

Appendix B: Information on analytical techniques used

Content

B.a. Spectro-colorimetry

Spectro-colorimetry is the quantitative measurement of the reflection properties of a material as a function of wavelength in order to correlate the results to color perception. This technique allows comparing visual aspects of different samples or visual changes with time of the same sample.

Spectrocolorimetry measurements were performed at C2RMF (Paris, France) using a NCS-RUBY spectrometer (STIL) with a tungsten halogen light source, using a spot of 3 mm diameter and a detection angle of 22°. The software used to visualize spectra and export data was RUBY Manager (STIL). Spectra were measured with a wavelength λ situated between 380 and 760 nm. The coordinates used were L*a*b* (CIE 1931) (representing respectively: the lightness of the color – L* = 0 yields black and L* = 100 indicates diffuse white, its position between red/magenta – positive values of a* – and green – negative values of a*, and its position between yellow – positive values of b* – and blue – negative values of b*), with the standard illuminant D65, the colour indice Eab and the RMS index for spectra. Colour differences ΔE were calculated by the following equation defined in 1976 by the CIE (Commission Internationale de l'Eclairage) *[J.-J. Ezrati, 2002]*:

$$\Delta E^* = [(\Delta L^*)^2 + (\Delta a^*)^2 + (\Delta b^*)^2]^{1/2}$$

B.b. Scanning electron microscopy - Energy dispersive X-ray spectroscopy (SEM-EDX)

Scanning electron microscopy investigations are based on the electron-material interactions. The surface of the sample is bombarded by electrons which interactions with atoms composing the surface of the sample produce different electrons (secondary, backscattered, Auger) and X-rays. Information is then extracted using specific detectors.

When the electrons from the incident beam (primary electrons) hits the atoms at the surface of the sample, they can give up a part of their energy to electrons from these atoms, the latter being ionized by the ejection of these electrons (called secondary electrons – SE).

These secondary electrons are sensitive to surface variations; thus, when they reach the detector, they give information on the topography of the sample analyzed.

Backscattered electrons (BSE) originate from the interaction of primary electrons (from the incident beam) with the atoms of the sample analyzed. These electrons are re-emitted with a low energy loss. Heavy elements with high atomic number deflect more electrons than light elements, so that areas containing such atoms appear whiter in BSE images. Backscattered electrons can therefore be used to visualize the chemical contrast between areas with a different composition.

When incident electrons induce the ejection of a strongly bound electron, characteristic X-rays are emitted and will allow determining the elemental composition of the sample by performing energy dispersive X-ray spectroscopy (EDX). Quantitative measurements are possible by calibrating the instrument e.g. with a reference sample before the analysis.

SEM analyses were performed at C2RMF (Paris, France) with a PHILIPS XL30CP (Controlled Pressure) instrument, using a tungsten filament electron source (see pictures in Figure B.1). Observations were made under vacuum at 20 keV, with a SDD detector OXFORD Inca for EDX analyses (50 mm² of active area) coupled to a Peltier cooler, and INCA software to acquire data. Before introducing the emdedded cross-sections prepared from original works of art, the conductivity of samples is increased by applying a thin layer (ca. 10 nm) of carbon.

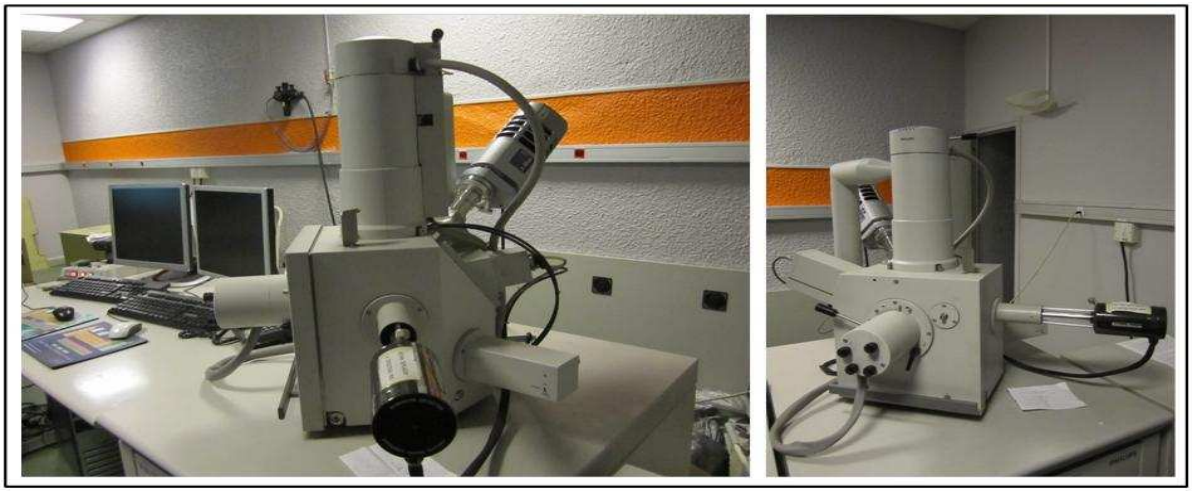

Figure B.1.: *Pictures of the SEM instrument at the C2RMF.*

B.c. Proton induced X-ray emission - Proton induced gamma-ray emission (PIXE-PIGE)

Particle induced X-ray emission (PIXE) is a three step process, with an ionization of an inner shell of the target atom by the incident accelerated proton, filling of the vacancy by an electron from an outer shell and relaxation by the emission of a characteristic X-ray. The spectrum obtained by detection of these X-rays provides information on the elemental composition of the sample. For particle induced gamma-ray emission (PIGE), accelerated ions interact with the atomic nucleus; the resulting nucleus can be formed in an excited state which will emit gamma-rays when de-exciting. PIXE and PIGE are complementary methods as PIGE features a higher sensitivity to certain light elements which are hard to detect by PIXE.

In the cultural heritage field, the qualities of PIXE-PIGE had been assessed: their non-destructive character (when used properly) is of great value. An important improvement was realized via external beam PIXE: by allowing in-air analysis for the study of large or fragile artworks where sampling is not possible became possible *[J.C. Dran, 2004]*.

PIXE-PIGE analyses were performed at C2RMF (Paris, France) by using the Accélérateur Grand Louvre d'Analyses Elémentaires (AGLAE) with an extracted proton beam of 3 MeV, two Si(Li) detectors (low/high energies) for X-rays and one HPGe detector for gamma-rays, cooled with liquid nitrogen and set at 45° with respect to the beam *[J.C. Dran, 2004]*. An aluminum filter of 50 µm thickness was used when analyzing the surrounding rocks of cinnabar.

Figure B.2.: *Photographs of AGLAE at C2RMF.*

B.d. X-ray photoelectron spectroscopy (XPS)

X-ray photoelectron spectroscopy (XPS) consists in irradiating a sample with X-rays and measuring the binding energy and number of electrons emitted. It probes the composition and electronic state of atoms and is selective to the first ten nanometers of the surface of a sample. Furthermore, the intensity of the peaks obtained on spectra is related to the concentration of the element within the analyzed area.

Cooper et al. used XPS and its superficial sensitivity to show that laser irradiation on lead white induced the formation of elemental lead at its surface *[M.I. Cooper, 2002]*. This application is a good example of the use of XPS in the context of alteration studies.

X-ray photoelectron spectroscopy (XPS) analyses were performed at the Laboratoire de Réactivité de Surface (LRS, Ivry-sur Seine, France) with a beam of 2 x 1 mm^2 (hor. X ver.), showing the elements of the first 5 nm of the surface and their chemical environment. Before analyses, in order to prevent detection of pollution, samples were cleaned in ethanol using ultrasounds.

B.e. Raman spectroscopy

Raman spectroscopy is based on the interaction between light and the components of the material analyzed. Raman scattering is induced by a monochromatic light (usually a laser) which photons will interact with the electron cloud and the bonds of the molecules present in the sample analyzed. When light hits the surface of a material, it can be reflected by the first layer of atoms, it can be transmitted, absorbed, or it can be scattered. In this last case, three phenomena can be observed:

- the excited electron goes back to its initial energy level, emitting the same wavelength as the one received, it is a Rayleigh scattering
- the excited electron goes back to a higher energy level, emitting a shorter wavelength, it is Raman Stokes scattering
- the excited electron goes back to a lower energy level, emitting a longer wavelength, it is Raman anti-Stokes scattering.

When the molecule relaxes, it emits a photon with a frequency which depends from the type of scattering, resulting in the energy of the laser photons being shifted up or down. Wavelengths due to Rayleigh scattering are filtered out while the rest of the light is collected and analyzed with a wavelength dispersive detection system (grating + CCD detector). This shift in frequency allows studying vibrational, rotational, and other modes which are related to bounds between atoms in molecular groups and will allow identifying phases present in the analyzed material.

Most of the Raman measurements were performed at the LADIR (Laboratoire de Dynamique, Intéractions et Réactivité – UMR 7075, Paris, France) with a dispersive spectrometer HR800 Jobin-Yvon Horiba characterized by a focal distance of 800 mm (see Figure B.3). Ionized argon laser was used to produce a 514 nm excitation and the detection was operated by a CCD detector with a Peltier cooler. Low frequency spectra recording (<10 cm^{-1}) was achieved thanks to a Rayleigh filtering using three ultra narrow band Notch BragGrate filters and a signal analysis by a 600 lines/mm grating. Micrometric analyses were possible thanks to the Olympus microscope coupled to the instrument (diameter of analyses of ca. 3 µm with the x50 objective). Power modulation was possible using different filters in order not to go higher than 100 µW and limit the risk to alter the sample (value determined by tests of laser irradiation on mercury sulfide, see Section 3.1.2). Acquisitions were performed thanks to LabSpec software. Each spectrum represents the average of 3 iterations of 180 s each.

Laser damages were tested at the C2RMF with an instrument shared between this laboratory and the LADIR. The spectrometer used is a “LabRam Infinity” Dilor (Jobin Yvon-Horiba S.A.) equipped with a 532 nm Nd-YAG laser, a 1800 t/mm grating, a Notch filter and a CCD detector with a Peltier cooler to record spectra between 150 and 4000 cm^{-1}. Backscattering illumination and collection of the scattered light were through an Olympus confocal microscope (x50, x100 or long working distance Olympus objectives). Acquisitions were performed thanks to LabSpec software. Each spectrum represents the average of 8 iterations of 30s each.

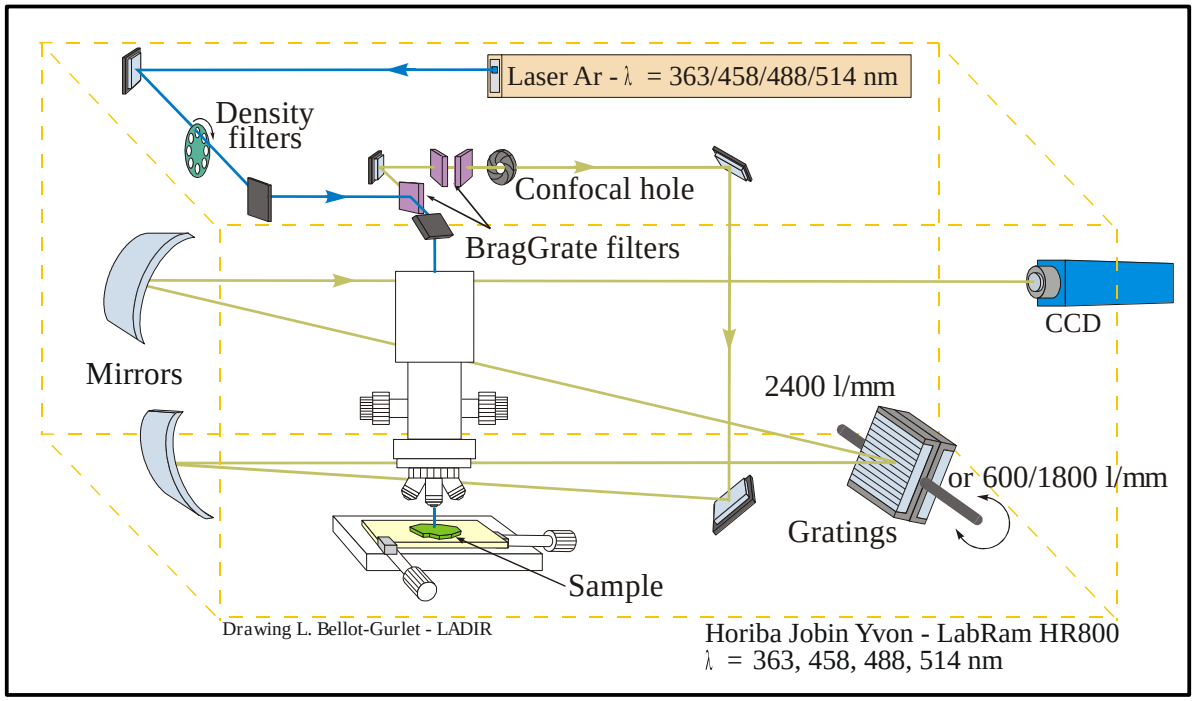

***Figure B.3.**: Diagram of the LabRam HR800 used for Raman spectroscopy at LADIR (Paris) [courtesy of L. Bellot-Gurlet].*

B.f. Micro-X-ray fluorescence (µ-XRF)

X-ray fluorescence (XRF) corresponds to the emission of secondary X-rays from a material that has been excited by an incident X-ray beam. The exposition of a material to X-rays can induce the excitation of electrons, and the formation of a hole; this hole is then filled by another electron from a higher orbital which will release the surplus of energy in the form of a photon. Thus the material emits radiation which has the energy characteristic of the atoms excited. Therefore, XRF gives access to the elemental composition of the samples analyzed. With a synchrotron source, this technique can be carried out with improved lateral resolution (going down to a few tens of nm), good detection limit (down to ppm) and reduced acquisition times, when compared with laboratory instruments.

Synchrotron based µ-XRF analyses were performed at ESRF beamline ID21 (see Figure B.4), described by Susini et al. *[Susini et al., 2002]*. A monochromatic primary beam is obtained thanks to a fixed-exit Si(111) double crystal monochromator. The energy range goes from 2 to 9 keV with a resolution of $\Delta E/E = 10^{-4}$. At the S and Cl K-edge energies, the beam size was reduced down to 0.60 x 0.25 µm² (hor. X ver.) by means of a Fresnel zone plate. The µ-XRF signals were collected in the horizontal plane, perpendicular to the incident beam direction, using an energy-dispersive Silicon Drift Diode detector. The resulting spectra were fitted using the PyMCA software (*[http://pymca.sourceforge.net]*; *[Sole et al., 2007]*) which is essential to differentiate overlapping emissions lines, such as the M-emission lines of mercury from the K-lines of sulfur and chlorine. Batch fitting of the XRF spectra corresponding to each pixel of the 2D maps yielded elemental maps.

Additionally, a few µ-XRF maps were acquired at specific energies chosen following results obtained by µ-XANES analyses (see description and calculations in Section B.g).

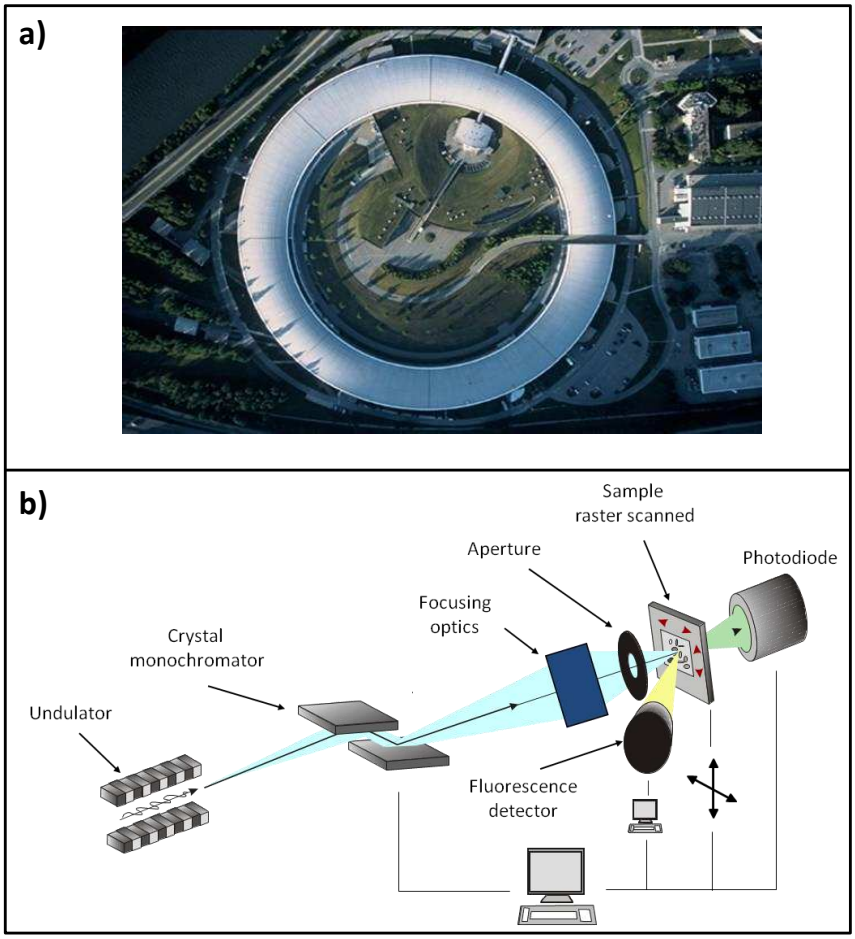

***Figure B.4.**: **a)** Aerial photograph of ESRF (Grenoble); **b)** Diagram of the X-ray microscope of the ID21 beamline at ESRF [courtesy of M. Cotte].*

B.g. Micro-X-ray absorption near edge structure (µ-XANES)

X-ray absorption near edge structure (XANES) is one of the X-ray absorption spectroscopy (XAS) techniques, measuring the variation of the absorption of X-rays by a target element in a matrix as a function of the energy of the incident X-ray beam. In the spectrum obtained, the XANES region represents the first ~ 100 eV, around the edge, which corresponds to the binding energy of the electron ejected by the incident beam. The features observed at higher energies (~ 1000 eV above the edge) are called “extended X-ray absorption fine structure” (EXAFS). XANES spectra give information about electronic configuration, atoms symmetry and oxidation state of the considered atom. When comparing spectra to the ones of references, XANES gives access to the speciation of the elements and helps for identification of compounds present in the sample. For these analyses, synchrotron radiation sources offer an essential spectral continuity.

Synchrotron based µ-XANES analyses were performed at ESRF beamline ID21 (see description of the set-up in Section B.f). µ-XANES spectra were recorded in XRF mode at locations determined from elemental maps and in the following energy ranges: from 2.46 to 2.53 kev and from 2.795 to 2.895 keV for S and Cl K-edges, respectively. XANES spectra were then decomposed as a linear combination of a set of chlorine- and sulfur-reference compound spectra (see references in Table B.1).

Table B.1.: *References used for XANES experiments and their source.*

Compounds	**Origins**
α-HgS	Prolabo
β-HgS	Mineralogical gallery of Jussieu
Hg(0)	University of Antwerp
α-$Hg_3S_2Cl_2$	Mineralogical gallery of the Ecole des Mines
Hg_2Cl_2	Aldrich
$HgCl_2$	Prolabo
Hg_2OCl	Museum National d’Histoire Naturelle
$Hg_3O_2(SO_4)$	Mineralogical gallery of the Ecole des Mines
$Hg_6Cl_3O(OH)$	Museum National d’Histoire Naturelle
$HgSO_4$	Touzart et Matignon
NaCl	Prolabo
$CaSO_4.2H_2O$	Lafarge
Na_2SO_3	ESRF ID21 reference *[www.esrf.eu/UsersAndScience/Experiments/Imaging/ID21/php]*
$Na_2S_2O_5$	ESRF ID21 reference *[www.esrf.eu/UsersAndScience/Experiments/Imaging/ID21/php]*
$CaCl_2.2H_2O$	Prolabo

From these results, it is assumed that each spectrum can be fitted as the combination of "n" reference spectra (n ≤ 3 in our cases). In order to obtain chemical maps showing the distribution of these different "n" compounds, "m" XRF maps (with m ≥ n) are acquired at specific energies E_i. Usually, these energies are chosen to correspond to the maximum absorption of the reference compounds and consequently the best sensitivity. At each energy E_i, the intensity I_i is a linear combination of the absorption of each of the "n" components.

At chlorine K-edge, all mercury chlorine containing compounds show the same characteristic peak at 2.8232 keV. The other Cl references studied here (alkaline and alkaline-earth chlorides, organic chlorine) do not absorn at this energy. Consequently, XRF maps acquired at this energy give, in first approximation, the map of "mercur-chlorine" species. For normalization, a second map is usually acquired at 2.9 keV.

At the sulfur K-edge, a simple ternary system (cinnabar, corderoite, calcium sulfate) was considered and three XRF maps were collected at E_0 = 2.4716, E_1 = 2.4725 and E_2 = 2.4825 keV. After normalization of the spectra of these reference compounds, XRF intensities can be expressed as:

$$I_0=2.14[cin]+1.84[cor]+0.01793[sul]$$

$$I_1=1.74[cin]+3.97[cor]+0.020393[sul]$$

$$I_2=0.97[cin]+1.03[cor]+2.817414[sul]$$

where [cin], [cor] and [sul] are the relative concentrations of cinnabar, corderoite and sulfates, respectively. Coefficients where obtained by analyzing the normalized spectra of reference compounds of cinnabar, corderoite and calcium sulfate and measuring the intensities for each spectrum at the three energies E_0, E_1 and E_2 named above. This calculation relies on the assumption that only these three phases are present and can contribute to the XANES spectra at S K-edge.

The matrix inversion thus gives access to these contributions:

$$[cin]=0.753I_0-0.35I_1-0.002I_2$$

$$[cor]=-0.329I_0+0.414I_1-0.001I_2$$

$$[sul]=-0.139I_0 -0.028I_1 +0.345I_2$$

B.h. X-ray diffraction, micro-X-ray diffraction (XRD, µ-XRD)

As for XRF, X-ray diffraction (XRD) is a technique based on interactions between X-rays and analyzed material; however, for this technique it is not the elemental composition but the structure of the sample which is studied. When X-rays hit an atom, they will be diffused by this one in all directions. If atoms are ordered, as in crystallized material, interferences between X-rays will be constructive in some directions whereas they will be destructive in others. These interferences form the diffraction phenomenon and can be observed using different detectors. The angles of diffracted beams are related to the atoms arrangements. Accordingly, a diffractogram is a fingerprint of the phase composition. Moreover, average spacing between rows of atoms and the size, shape and internal stress of small crystalline regions can be measured and the orientation of a single crystal can be determined.

Synchrotron facilities offer several advantages, in particular the access to high energy beams which are primordial in some studies in the cultural heritage field, as when scanning an entire painting in transmission mode in order to penetrate through all the layers and the support of the artworks *[W. De Nolf, 2011]*. In other situations, the beam can be focused to less than one micrometer diameter, allowing the acquisition of high resolution maps. This second aspect was very important in the present work.

X-ray diffraction experiments were performed with two types of instrumentation: one using a laboratory source of X-rays and another based on synchrotron radiation.

For the laboratory source, samples were analyzed in reflexion mode with an instrument developed at C2RMF *[A. Duran, 2010]* (see pictures in Figure B.5), based on a Rigaku MSC MicroMax 002 X-ray tube with a copper anode (providing a wavelength of 1.5418 Å). After collimation to 200 µm, a monochromatic beam with a flux of 2 x 10^8 photons.s^{-1} is obtained. 2D XRD patterns are collected by means of Rigaku R-axis imaging plates. FIT2D *[www.esrf.eu/computing/scientific/FIT2D]* is used to transform the 2D images into standard diffractograms and the software package EVA is employed to identify the crystalline phases *via* comparison to a database of XRD diagrams.

Synchrotron based µ-XRF/µ-XRD analyses were performed at ESRF beamline ID18F (France), at SLS beamline Micro-XAS (Switzerland) and at PETRA III beamline P06 (Germany). For the first instrument, a wide energy range (6-70 keV) was accessible[1] thanks to a Si (111) and Si (311) double crystal monochromator. The excitation energy was fixed at 28 keV and the primary beam was focused to 5.3 x 1.8 µm² (hor. X ver.) by means of a compound refractive lens. µ-XRD patterns were collected in transmission mode by means of a MarCCD camera simultaneous to the recording of XRF spectra using an energy-dispersive Si(Li) detector. Details about the set-up can be found in different publications *[Cotte et al., 2008; Somogyi et al., 2001]*. At SLS, the excitation energy was fixed at 17 keV and the primary beam was focused to 1x1 µm² (hor. X ver.). µ-XRD patterns were collected in transmission mode by means of a Pilatus Detector. At Petra III, the energy (18 keV) was selected by means of a Si(111) double crystal monochromator. The beam was focused to 1.6 x 0.6 µm² (hor. X ver.) employing a Kirkpatrick-Baez mirror optic. µ-XRD signals were recorded in transmission geometry with a 2k x 2k MarCCD area detector and XRF signals were collected with a Si-drift detector. In the three cases, XRD data were analyzed by using the XRDUA *[http://xrdua.ua.ac.be]* software. To localize the different phases identified, maps are obtained by fitting data from diffractograms using reference files (see Table B.2), yielding the intensity of the phases identified for each pixel.

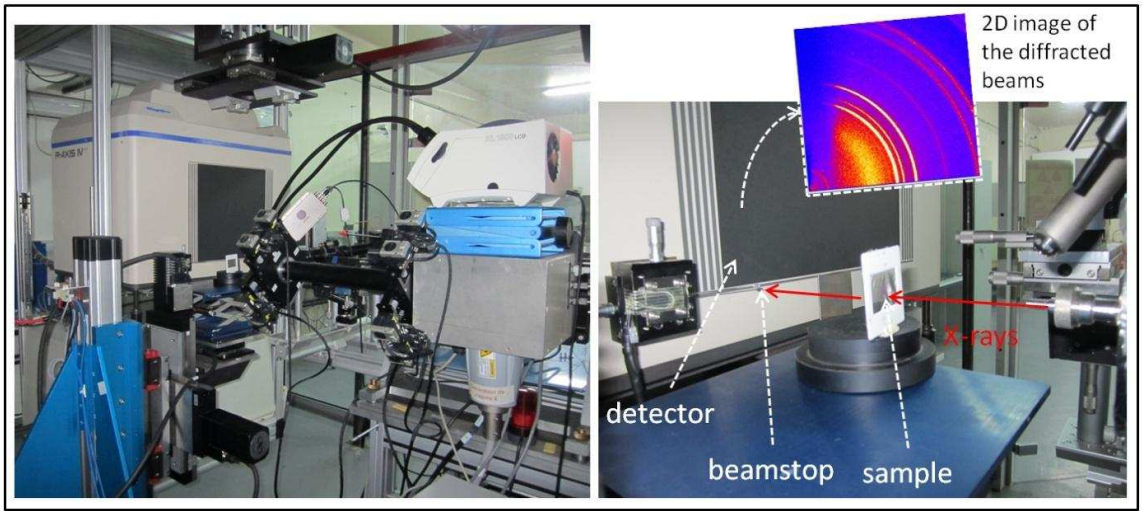

Figure B.5.: *Pictures of the XRD instrument at C2RMF.*

[1] The ID18F end-station was closed in 2011.

Table B.2.: *D-spacing values corresponding to the five most intense peaks (sorted out from 1 to 5) in diffractograms of reference compounds used as reference files in XRD experiments.*

Phases names	D-spacing values (Å) (Intensities)
Cinnabar/Vermilion (α-HgS)	3.363(1) 3.169(4) 2.860(2) 2.073(5) 1.978(3)
Metacinnabar (β-HgS)	3.363(1) 2.929(4) 2.066(2) 1.763(3) 1.342(5)
Calomel (Hg_2Cl_2)	4.147(2) 3.170(1) 2.724(4) 2.061(3) 1.961(5)
Corderoite (α-$Hg_3S_2Cl_2$)	6.279(5) 3.661(1) 2.833(3-4) 2.583(2) 1.759(3-4)
β- $Hg_3S_2Cl_2$	4.972(5) 3.329(3) 2.988(4) 2.587(1) 2.241(2)
Kenhsuite (γ- $Hg_3S_2Cl_2$)	3.673(3) 3.109(5) 2.929(4) 2.573(1) 2.566(2)
Hydrocerussite ($(PbCO_3)_2.Pb(OH)_2$)	4.475(4-5) 4.252(4-5) 3.607(2-3) 3.290(2-3) 2.621(1)
Calcite ($CaCO_3$)	3.029(1) 2.285(2-3) 2.092(2-3) 1.914(4-5) 1.872(4-5)
Gypsum ($CaSO_4.2H_2O$)	7.610(1-2) 4.269(1-2) 3.064(3) 2.872(4) 2.686(5)
Anhydrite ($CaSO_4$)	3.497(1) 2.843(2) 2.327(3-4) 2.205(3-4) 1.869(5)
Goethite (FeO(OH))	4.183(1) 2.694(3) 2.449(2) 2.191(5) 1.719(4)
Weddellite ($Ca(C_2O_4).2H_2O$)	6.172(1) 4.401(3) 2.776(2) 2.408(5) 2.242(4)

B.i. Thermochemical calculations/simulations

Thermodynamical calculations/simulations are an essential tool to visualize theoretical concepts, to anticipate processes and reactions and to validate and understand phenomena observed during experiments. In chemistry it offers the possibility to verify if hypothetical reactions are possible in specific conditions of pressure and temperature.

To obtain potential-pH diagrams of Hg-Cl-S-H_2O systems, the chemical reaction and equilibrium software package HSC Chemistry® 7.0 was used in combination with an extensive thermochemical database and flowsheet simulation by Outotec Research Oy. Some thermodynamic data were taken from Balej (1985), as cited by Brandon et al. *[N.P. Brandon, 2001]*. For corderoite (α-$Hg_3S_2Cl_2$) data, the free energy of formation was taken from Paquette et al. *[K. Paquette, 1995]*. Other data were taken from the HSC Chemistry database.

Table B.3.: *Free energies of formation used to calculate Pourbaix diagrams in Chapter 4.*

Species	ΔG^0_f (kcal.mol^{-1})	*References*
$Hg_{2(g)}$	16.317	*[HSC Chemistry database]*
Hg_2^{2+}	36.713	*[N.P. Brandon, 2001]*
Hg^{2+}	39.365	*[N.P. Brandon, 2001]*
$Hg^{+}_{(g)}$	244.732	*[HSC Chemistry database]*
$Hg_{(g)}$	7.620	*[HSC Chemistry database]*
Hg	0.000	*[HSC Chemistry database]*
$HgO_{(s)}$ (red, orthorhombic)	-13.995	*[N.P. Brandon, 2001]*
$HgO_{(s)}$ (yellow, orthorhombic)	-13.970	*[N.P. Brandon, 2001]*
$HgO_{(s)}$ (red, hexagonal)	-13.940	*[N.P. Brandon, 2001]*
$HgO_{(a)}$	-8.918	*[HSC Chemistry database]*
$HgO_{(g)}$	5.693	*[HSC Chemistry database]*
$Hg(OH)^+$	-12.431	*[N.P. Brandon, 2001]*
$HHgO_2^-$	-45.411	*[N.P. Brandon, 2001]*
Hg_2O	-13.017	*[HSC Chemistry database]*
$Hg(OH)_2$	-65.607	*[N.P. Brandon, 2001]*
$HgH_{(g)}$	51.625	*[N.P. Brandon, 2001]*
$HgCl^+$	-1.195	*[N.P. Brandon, 2001]*
$HgCl_{2(s)}$	-43.093	*[N.P. Brandon, 2001]*
$HgCl_2$ (undissociated)	-41.300	*[N.P. Brandon, 2001]*
$HgCl_3^-$	-73.805	*[N.P. Brandon, 2001]*
$HgCl_4^{2-}$	-106.692	*[N.P. Brandon, 2001]*
$Hg_2Cl_{2(s)}$	-50.281	*[N.P. Brandon, 2001]*
α-$HgS_{(s)}$	-11.090	*[N.P. Brandon, 2001]*
β-$HgS_{(s)}$	-10.612	*[N.P. Brandon, 2001]*
$HgS_{(g)}$	19.980	*[HSC Chemistry database]*
Hg_2S	-2.817	*[HSC Chemistry database]*
$HgSO_{4(s)}$	-141.969	*[N.P. Brandon, 2001]*
$HgSO_4$ (dissociated)	-140.511	*[N.P. Brandon, 2001]*
$HgSO_4.HgO$	-149.599	*[HSC Chemistry database]*
$HgSO_4.2HgO$	-180.058	*[HSC Chemistry database]*
$Hg_2SO_{4(s)}$	-149.699	*[N.P. Brandon, 2001]*
$HgSO_{3(a)}$	-76.948	*[HSC Chemistry database]*
HgS_2^{2-}	ca. 4.947-5.425	*[N.P. Brandon, 2001]*
$Hg(S_2O_3)_2^{2-}$	-248.504	*[N.P. Brandon, 2001]*
$Hg(S_2O_3)_2^{4-}$	-374.369	*[N.P. Brandon, 2001]*
$Hg(SO_3)_2^{2-}$	-226.073	*[N.P. Brandon, 2001]*
$Hg(SO_3)_2^{4-}$	-344.951	*[N.P. Brandon, 2001]*
H_2O	-56.687	*[N.P. Brandon, 2001]*
OH^-	-37.594	*[N.P. Brandon, 2001]*
S	0.000	*[HSC Chemistry database]*
$HS_{(g)}$	27.201	*[HSC Chemistry database]*
$HS^-_{(a)}$	2.973	*[HSC Chemistry database]*
$H_2S_{(g)}$	-7.964	*[HSC Chemistry database]*
$H_2S_{(a)}$	-6.607	*[HSC Chemistry database]*
$SO_4^{2-}{}_{(g)}$	-154.949	*[HSC Chemistry database]*
$HSO_4^-{}_{(a)}$	-180.524	*[HSC Chemistry database]*
H_2SO_4	-164.894	*[HSC Chemistry database]*

Species	ΔG^0_f (kcal.mol^{-1})	*References*
$H_2SO_{4(g)}$	-156.158	*[HSC Chemistry database]*
$HSOH_{(g)}$	-30.111	*[HSC Chemistry database]*
α-$Hg_3S_2Cl_2$	-97.275	*[K. Paquette, 1995]*
$Cl_{(g)}$	25.169	*[HSC Chemistry database]*
$Cl_{2(g)}$	0.000	*[HSC Chemistry database]*
$ClO_{(g)}$	23.507	*[HSC Chemistry database]*
$Cl_{2(a)}$	1.660	*[HSC Chemistry database]*
$Cl^-_{(a)}$	-31.372	*[HSC Chemistry database]*
$ClO^-_{(a)}$	-8.668	*[HSC Chemistry database]*
$HClO_{(a)}$	-19.094	*[HSC Chemistry database]*

For the thermochemical simulation (Figure 4.4a), initial compounds introduced in the system were the following, given in weight percentage:

- gaseous phases: ClO (0.016%) + CO_2 (0.137%) + O_2 (99.289%) + H_2O (0.559%)

- aqueous phases: H_2O (92.355%) + NaOCl (3.822%) + Na^+ (1.180%) + ClO^- (2.642%)

- solid phase: HgS.

Then $ClO_{(g)}$ is added with a step amount of 0.2 mol.

Appendix C: Study of cinnabar ores

Content

C.a.Description of ores studied

Most of the natural ores studied and presented in this appendix were lent by the Mineralogical Gallery of the Ecole des Mines of Paris. The ores are coming from Europe, all America and Asia, and present different colors and aspects. The following Tables show the visual aspect of each ore with a picture and give comments made from optical observation of crystals and gangues.

Europe

Table C.1.: *List of the cinnabar ores studied coming from Europe with a picture and some visual observations made from them.*

Provenance	Picture	Observation	Reference number
Spain, Almaden (El Entredicho)	 2cm	Metallic mercury droplets	Cin_alm_1
Spain, Almaden (El Entredicho)	 2cm		Cin_alm_2
Italy, Tuscany (Monte Amiata, Montalcino, Siena)	 2cm		Cin_monteamiata_1
Italy, Tuscany (Monte Amiata, Montalcino, Siena)	 2cm	Presence of a yellow non-identified phase	27960

Germany, Rhineland-Palatinate (Wolfstein, Zweibrücken)	 2cm	Black cinnabar, ankerite	27935
Germany, Rhineland-Palatinate (Wolfstein, Zweibrücken)	 2cm	Small vein of quarts, yellow phase, brown cinnabar	428
Germany, Saxe-Anhalt (Mansfeld, Halle)	 2cm	Metallic mercury droplets	7825
Slovenia, Idrija	 2cm		Cin_Idrija_1
Slovenia, Podljubelj	 2cm		Cin_podljubelj_1
Slovenia, Podljubelj	 2cm	Grey and purple gangue with white crystals	Cin_podljubelj_2

Slovenia, Podljubelj	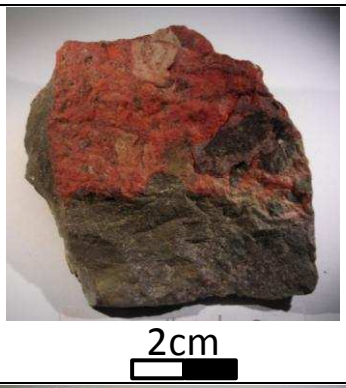		Cin_podljubelj_3
Slovenia, Podljubelj	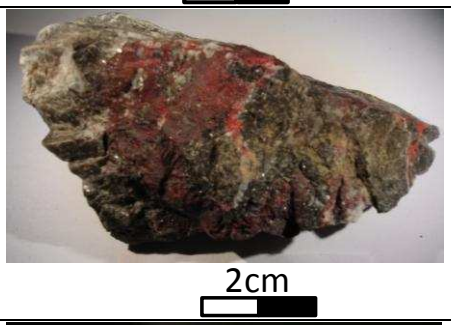		Cin_podljubelj_4
Slovenia, Podljubelj	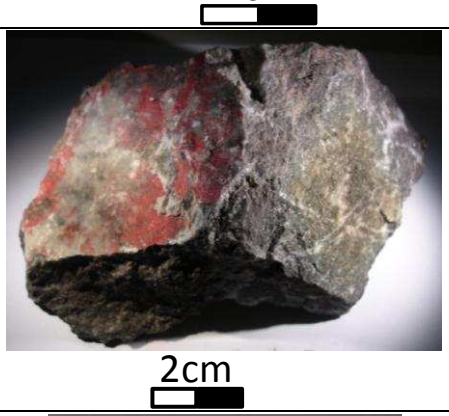		Cin_podljubelj_5
Austria, Carinthia (Loibl pass)		Shiny black phase	7807

America

Table C.2.: *List of the cinnabar ores studied coming from America with a picture and some visual observations made from them.*

Provenance	Picture	Observation	Reference number
USA, California (Altoona, Trinity City, Trinity Co)	 2cm	Smooth aspect	27951
USA, California (Redington, Knoxville, Napa Co)	 2cm	Cinnabar in needles shape	7834
USA, California (Napa Co)	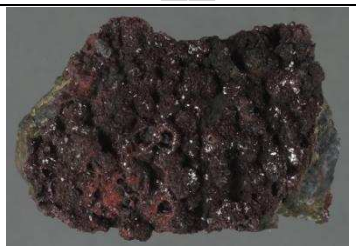 2cm	Yellow phase (native sulfur ?)	420
USA, California (Napa Co)	 2cm	Not well crystallized silica	7801
USA, California (New Almaden, Santa Clara (Co))	 2cm	Black phase, yellow phase	7794

USA, Nevada (Lovelock, Churchill (Co))	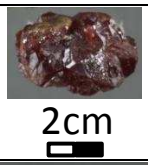 2cm	Sediment	39641
USA, Arkansas (Pike Co)	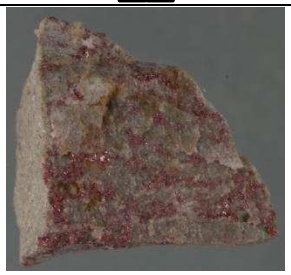 2cm	Quartzite	27948
USA, Alaska (Red Devil mine, Kuskokwim (Co))	 2cm		43041
Mexico, San Louis Potosi (Charcas)	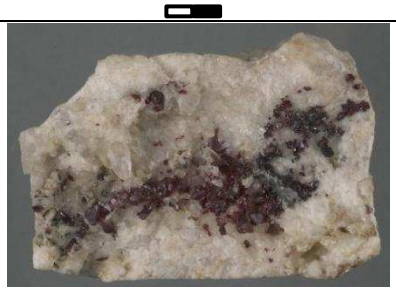 2cm		20591
Mexico, San Louis Potosi (Guadalcazar)	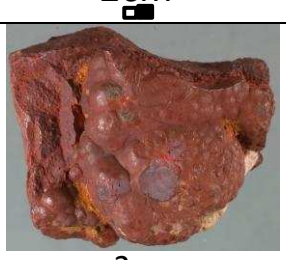 2cm	Presence of kaolinite from the soil	7790
Mexico, Guerrero (Huitzuco)	 2cm		7791

Mexico, Guerrero (Huitzuco)	 2cm	No red color, no crystals	8066
Mexico, Jalisco (Puerto de Ledesma)	 2cm		27950
Mexico, Guanajuato (Victoria, Atarjea)	 2cm	Presence of a white pulverulente hydrated phase, prey phase (blackened cinnabar?)	7793
Chile, Coquimbo (Ovalle)	 2cm	Black phase	27940
Peru, Huancavelica (Santa Barbara, Huancavelica)	 2cm		29042
Colombia, Caldas (La Esperanza, Aranzazu)	 2cm		40432

Brasil, Minas Gerais (Tripuhy, Ouro Preto)		Black and yellow phases, secondary quartz	7799

Asia

Table C.3.: *List of the cinnabar ores studied coming from Asia with a picture and some visual observations made from them.*

Provenance	Picture	Observation	Reference number
China	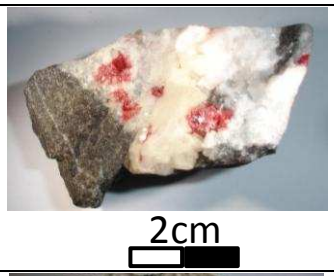		Cin_chin_1
China		Red crystal which blackened after few months	Cin_chin_2

Origin not known

Table C.4.: *List of the cinnabar ores studied coming from an unknown origin with a picture and some visual observations made from them.*

Provenance	Picture	Observation	Reference number
Not known			10196

All the ores studied show different aspects and different type of gangues. Chemical analyses of these samples aim at creating a database to be able to identify the origin of a natural cinnabar from its composition.

C.b. Results of analyses

Isotopic analyses were considered by laser ablation inductively coupled plasma mass spectrometry (LA-ICP-MS) but the pollution induced by the analysis of mercury sulfide make the finding of a laboratory accepting to work with our samples difficult. Analyses were then focused on the composition of each ore (phases composing the gangue and elements present in the sample).

PIXE-PIGE (proton induced X-ray/γ-ray emission) analyses were performed with AGLAE (Accelérateur Grand Louvre d'Analyses Élémentaires) with three detectors, two for X-rays (low and high energy) and one for γ-rays, and data were treated by GupixWin. Tests were first performed on a non-precious ore, and we realized that the beam caused the sublimation of mercury and polluted the detectors. In order to preserve the ores and keep the instrument clean, it was decided to analyze only the gangue surrounding the cinnabar by PIXE-PIGE to determine elements present (see example of spectrum in Figure C.1a) and then to identify by XRD all phases composing each sample (see example of diffractogram in Figure C.1b) in order to verify if they are specific for the geographic position of each deposit.

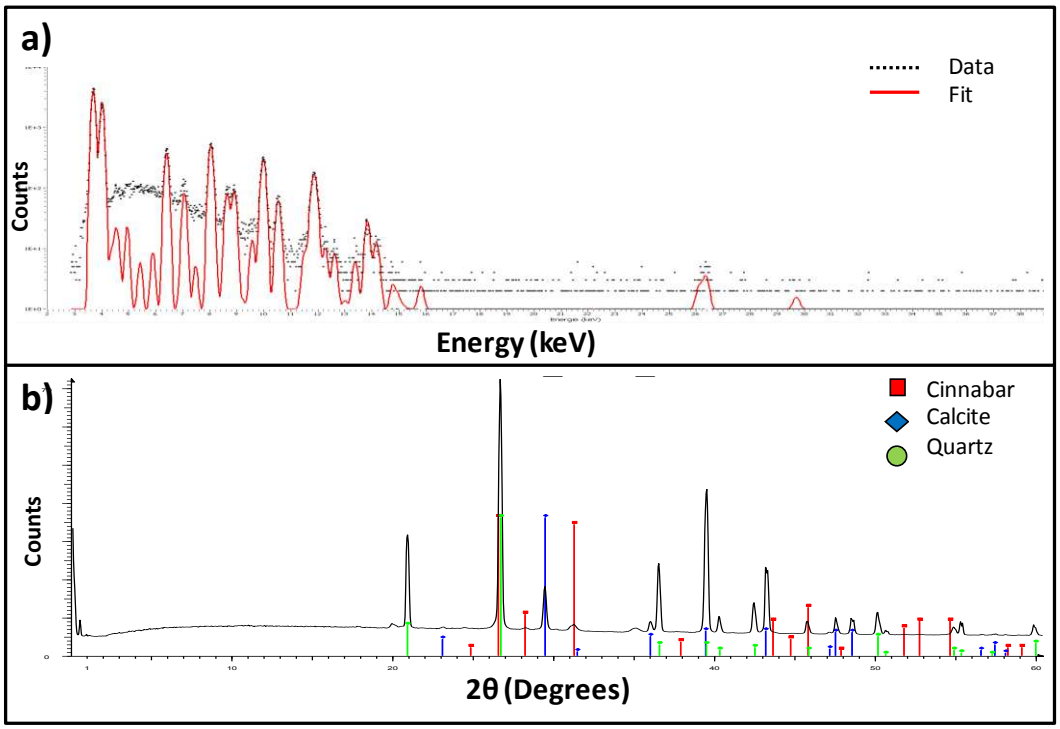

Figure C.1.: *Examples of results obtained during the study of cinnabar ores:* ***a)*** *spectrum obtained by PIXE performed on the white gangue of the sample n°7791 from Huitzuco, Guerrero in Mexico;* ***b)*** *Diffractogram acquired on the same sample.*

Europe

Table C.5.: *Summary of the results obtained by analyzing the gangue of each ore from Europe by PIXE-PIGE giving major and trace elements (cited by decreasing proportion) and the whole ore by XRD giving the present phases.*

Provenance	Elements (PIXE-PIGE)		Phases (XRD)	Reference number	
	Majors	Traces			
Spain, Almaden (El Entredicho)	**X**	**X**	Quartz, jarosite, cinnabar	Cin_alm_1	
Spain, Almaden (El Entredicho)	**X**	**X**	Quartz, cinnabar	Cin_alm_2	
Italy, Tuscany (Monte Amiata, Montalcino, Siena)	**X**	**X**	Cinnabar	Cin_monteamiata_1	
Italy, Tuscany (Monte Amiata, Montalcino, Siena)	Si, Al, Hg, K, S, P, Mg, Na, Cl	Ti, Ca, Fe, Cr, Sr, Zr, Y, Rb, Cu	Cinnabar, quartz, gypsum, anhydrite, dolomite	Black	27960
Germany, Rhineland-Palatinate (Wolfstein, Zweibrücken)	Fe, Hg, Si, Na, S, Al, Ca, Mg, Cl, K	Sb, As, Ti, Mo, Ni, Sr, Zn Cu	Cinnabar, hematite, barite	Black	27935
Germany, Rhineland-Palatinate (Wolfstein, Zweibrücken)	**X**	**X**	Cinnabar, quartz, pyrite, goethite	428	
Germany, Saxe-Anhalt (Mansfeld, Halle)	Ca, Mg, Fe, S, Si, Al	Hg, Mn, Sr, Cl, V, Pb, Cu, As, Zn	Cinnabar, quartz, dolomite, calcite	Black	7825
Slovenia, Idrija	Si, Al, Mg, S, K, Na	Fe, Hg, Ca, Ti, U, V, Sr, Zr, Cu, Mo, Cr, Zn, Mn, Y, Ni, As	Cinnabar, quartz	Black	Cin_Idrija_1
Slovenia, Podljubelj	**X**	**X**	**X**	Cin_podljubelj_1	
Slovenia, Podljubelj	**X**	**X**	**X**	Cin_podljubelj_2	
Slovenia, Podljubelj	**X**	**X**	**X**	Cin_podljubelj_3	
Slovenia, Podljubelj	**X**	**X**	**X**	Cin_podljubelj_4	
Slovenia, Podljubelj	**X**	**X**	**X**	Cin_podljubelj_5	
Austria, Carinthia (Loibl pass)	Si, Al, K, Ti, Na, Fe, Mg, Ca, S	Zr, Hg, Mn, Rb, As, Cu, Sr, Zn	Cinnabar, quartz, albite	Grey	7807
	Ca, Fe, Mg, Mn, Si, Al, Na, S, Cl	Hg, Sr, Cr, As, Zn, Cu		White	

America

Table C.6.: *Summary of the results obtained by analyzing the gangue of each ore from America by PIXE-PIGE giving major and trace elements (cited by decreasing proportion) and the whole ore by XRD giving the present phases. Cross indicate that analysis was not possible.*

Provenance	Elements (PIXE-PIGE)		Phases (XRD)	Reference number	
	Majors	Traces			
USA, California (Altoona, Trinity City, Trinity Co)	Hg, S, Si, Fe, Al, K, Ca, Na, P, Mg, Cl	Ti, Zr, Cu, Cr, Ni	Cinnabar, quartz, gypsum, jarosite	Grey	27951
USA, California (Redington, Knoxville, Napa Co)	Si, Hg, S, Al, Mg, Cl	Fe, Ni, Ca, Na, Cu	Cinnabar, quartz, pyrite, opal	Black	7834
USA, California (Napa Co)	Si, S, Na, Al, Mg	Fe, Ni, K, Hg, Cr, Ca, Sr, As, Zn	Cinnabar, pyrite, opal	Grey	420
	Si, S, Al, Mg, Na	Fe, K, Ni, Cr, Hg, Sr, As		White	
USA, California (Napa Co)	**X**	**X**	Cinnabar, quartz, opal	7801	
USA, California (New Almaden, Santa Clara (Co))	**X**	**X**	Cinnabar, quartz, magnesite	7794	
USA, Nevada (Lovelock, Churchill (Co))	**X**	**X**	Cinnabar	39641	
USA, Arkansas (Pike Co)	Si, Al, K, Ca, S, Ti, Mg	Fe, Hg, Na, Zn, Cr, Sr, Zr, Rb	Cinnabar, quartz	White	27948
USA, Alaska (Red Devil mine, Kuskokwim (Co))	Si, Al, K, Ti, Mg, Fe, Na, S, Cl, Ca	Hg, As, Rb, Cu, Cr, Zr,Sr, Ni, Zn	Cinnabar, quartz, stibinite	Black	43041
	Si, Al, K, S	Hg, As		White	
	Sb, S, Si, Al, Mg, Na, Ti, K, Fe	Hg, As, Mo, Cu, Zn		Grey	
Mexico, San Louis Potosi (Charcas)	Ca, Mg	Sr, Fe, Mn	Calcite, quartz	White	27951
Mexico, San Louis Potosi (Guadalcazar)	Si, Al, Hg, S, Na	Fe, Ca, Cl, Ti, K, Zr, Pb, Zn, Cu, Y, As, Ni	Cinnabar, quartz, kaolinite	White	7790
Mexico, Guerrero (Huitzuco)	Ca, Si, Al	Hg, Cu, Fe, As, Mn, Zn	Cinnabar, quartz, calcite	Black	7791
	Si, Ca, Al, K, S, Mg	Hg, Cu, Fe, As, Zn		White	
Mexico, Guerrero (Huitzuco)	**X**	**X**	Cinnabar, stibiconite	Black	8066
Mexico, Jalisco (Puerto de Ledesma)	**X**	**X**	Cinnabar	27950	
Mexico, Guanajuato (Victoria, Atarjea)	Al, S, Hg, K, Si, Cl, Na	Ca, Sr, Fe, Rb, Pb, Cu	Cinnabar, quartz, cristobalite, stishovite, alunite	White	7793

	X	**X**	Cinnabar, quartz, metacinnabar, calomel, corderoite	Black	
Chile, Coquimbo (Ovalle)	**X**	**X**	Cinnabar	27940	
Peru, Huancavelica (Santa Barbara, Huancavelica)	As, Mg, Si, S, Na, Ca, P	Fe, Hg, Sr, Cr, Cu, Ni	Quartz, realgar, carlinite	Black	29042
Colombia, Caldas (La Esperanza, Aranzazu)	Si, S, Ca, Al, Mg, Na	Hg, Fe, Zn, Cu	Cinnabar, quartz, pyrite	White	40432
	Si, Ca, Mg, Fe, S, Cl, Na	Mn, Hg, Sr, Cr, Zn, Cu, Y		Black	
Brasil, Minas Gerais (Tripuhy, Ouro Preto)	**X**	**X**	Cinnabar	Yellow	7799

Asia

Table C.7.: *Summary of the results obtained by analyzing the gangue of each ore from Asia by PIXE-PIGE giving major and trace elements (cited by decreasing proportion) and the whole ore by XRD giving the present phases.*

Provenance	**Elements (PIXE-PIGE)**		**Phases (XRD)**	**Reference number and area analyzed**	
	Majors	**Traces**			
China	Ca, Mg, S, Fe, Si, Al	Mo, As, Hg, Sr, Cr, Cu, Zn, Ni	Dolomite, quartz, cinnabar	Grey	Cin_chin_1
	Ca, Mg, S, Si, Al, Cl	Ba, Hg, Ti, Fe, Mn, Sr, Cu		White	
China	**X**	**X**	Cinnabar	Blackened cinnabar	Cin_chin_2

Origin not known

Table C.8.: *Summary of the results obtained by analyzing the gangue of the unknown ore by PIXE-PIGE giving major and trace elements (cited by decreasing proportion) and the whole ore by XRD giving the present phases.*

Provenance	**Elements (PIXE-PIGE)**		**Phases (XRD)**	**Reference number**	
	Majors	**Traces**			
Not known	Si, Al, Hg, Fe, K, Ca, Mg	Ti, Zr, As, Cr, Cu, Ni	Cinnabar, quartz	Black	10196

The major and trace elements and all the phases identified formed the beginning of an interesting database, but it did not seem to show groups specific for a provenance or an area. But as the provenance of the ore could play a role in the kinetic of the alteration, the geographical traceability of cinnabar should be more studied and a database for all deposits should be created and shared.

Abstract

Pigments colour can sometimes evolve, unexpectedly, from the painter's or curator's point of view. The most common degradation of red mercury sulfide (α-HgS), used in a cinnabar natural form or in a vermilion synthetic form, is turning into black or silver-gray. This phenomenon is rather capricious and does not happen systematically. Since Antiquity, cinnabar was often used in paintings, even if it was known to suffer from degradation under the influence of sunlight and humidity.

Analyses of original works of art presenting mercury sulfide in their pictorial layers allowed identifying different degradation compounds, such as calomel (Hg_2Cl_2) and different polymorphous phases of $Hg_3S_2Cl_2$. Furthermore, artificial ageing experiments were used to reproduce the formation of some of these products on model samples and confirm light and chlorine as two necessary parameters to induce the presence of these alteration products. Pourbaix diagrams and simulations obtained from thermodynamics calculation appeared to be consistent with the evolution of the composition of α-HgS model samples during artificial ageing experiments. The chemical characterization of the alteration products was rather challenging mainly because of the micrometric size of the alteration (multi-)layers. Beyond the different analytical techniques available, synchrotron-based micro X-ray diffraction, micro X-ray fluorescence and micro X-ray absorption spectroscopy proved to be very helpful for the identification and localization of both original and altered compounds.

These researches confirmed preliminary hypothesis on factors influencing the alteration of mercury sulfide and explain the conditions in which these degradations occur in order to avoid them in the future.

Keywords: micro X-ray diffraction, micro X-ray absorption spectroscopy, artificial ageing, cinnabar, vermilion, degradation, painting.

Résumé

La couleur des pigments peut parfois évoluer, de façon imprévisible, du point de vue du peintre ou du conservateur. La dégradation la plus commune du sulfure de mercure rouge (α-HgS), utilisé dans sa forme naturelle du cinabre ou synthétique du vermillon, est la coloration en noir ou gris-argenté. Ce phénomène n'apparait pas systématiquement. Depuis l'Antiquité, le cinabre était souvent utilisé dans les peintures, même s'il était connu pour se dégrader sous l'influence de l'irradiation solaire et de l'humidité.

Les analyses réalisées sur des œuvres originales contenant du sulfure de mercure ont permis l'identification de différents composés de dégradation, comme le calomel (Hg_2Cl_2)et différentes phases polymorphes de α-$Hg_3S_2Cl_2$. De plus, des expériences de vieillissements artificiels ont permis de reproduire la formation de calomel et de corderoite à partir d'échantillons modèles de HgS et confirmer que la lumière et le chlore sont deux paramètres essentiels pour former les différents produits d'altération. Les diagrammes de Pourbaix ainsi que les simulations obtenus à partir de calculs thermodynamiques ont semblé corroborer l'évolution de la composition des échantillons modèles de α-HgS observée lors des expériences de vieillissement artificiel. La caractérisation chimique de ces produits d'altération est assez difficile notamment à cause de la taille micrométrique des (multi-)couches d'altération. Au-delà des différentes techniques analytiques disponibles, la micro-diffraction X, la micro-fluorescence X et la micro-spectroscopie d'absorption X avec source synchrotron ont récemment prouvé leur intérêt dans l'identification et la localisation des composants à la fois originaux et altérés.

Ces recherches ont confirmé les hypothèses préliminaires sur les facteurs influençant l'altération du sulfure de mercure et indiquent les conditions dans lesquelles ces dégradations se réalisent dans le but de les éviter dans le futur.

Mots-clefs : micro diffraction des rayons X, micro spectrométrie d'absorption des rayons X, vieillissement artificiel, cinabre, vermillon, dégradation, peinture.